REACTIONS IN COAL ASH MELTS

by

DAVID PETER KALMANOVITCH

October 1983

A thesis submitted for the degree of
Doctor of Philosophy of the University of London
and for the Diploma of Membership of
the Imperial College

Department of Metallurgy & Materials Science
Imperial College of Science & Technology
London SW7

ABSTRACT

The burning of coal in pulverised-fuel-fired boilers is the major source of steam-generated electricity in the United Kingdom. Coal ash, produced as a product of combustion may form deposits on the heat absorbing surfaces of the furnace causing significant reduction in thermal efficiency. The nature of the deposits may range from a dense vitreous mass to a lightly sintered conglomeration. The tendency of an ash to form deposits is called its slagging propensity.

This study has involved the investigation of factors pertinent to the formation of deposits in a boiler. The characterisation of the fusion process in coal ashes and the determination of crystal growth rates in glasses analogous to known lignitic-type ashes have indicated that deposits may approach equilibrium rapidly. The increase in strength (and hence growth) of deposits is known to occur by viscous flow sintering and thus the crystallisation behaviour of an ash melt will be a determining factor in the severity of boiler slagging.

The crystallisation behaviour of compositions in the systems $CaO-Al_2O_3-SiO_2$, $CaO-MgO-Al_2O_3-SiO_2$ and $CaO-Al_2O_3-SiO_2$-iron oxide (in a reducing atmosphere) relevant to coal ash compositions have been studied and compared with the observed devitrification of coal ash melts. The results have shown that crystallisation behaviour of ash melts is well represented by the system $CaO-FeO-Al_2O_3-SiO_2$. The quaternary system has been constructed from literature data as planes of constant FeO content (5-30% at 5% increments). From a model of deposit growth and high temperature phase equilibria

a method has been developed to predict the slagging propensity of a coal ash from the normalised four-component composition. This method has been shown to give more accurate predictions of slagging propensity than the various empirical and theoretical methods used to date.

CONTENTS

		Page
ABSTRACT		2
CHAPTER 1.	INTRODUCTION	12
CHAPTER 2.	LITERATURE SURVEY	
2.1	Coal	21
2.2	Operation of a boiler	22
2.3	Slagging of a boiler	24
2.4	Prediction of formation of boiler deposits	26
2.5	Coal mineral matter	28
2.6	Effect of heat on the major minerals	36
2.7	Mechanism of melting complex mineral mixtures	39
2.8	Formation of boiler deposits	44
2.9	Formation of slag deposits	45
2.10	Laboratory studies of boiler deposits	48
2.11	Models of deposit formation	49
2.12	Prediction of slagging propensity	51
2.13	Prediction of slagging propensity from ash analyses	55
2.14	Calculation of viscosity of slag from ash analyses	57
2.15	High temperature microscopy	61
2.16	Electrical resistance of coal ash	62
2.17	Phase equilibria studies	62
2.18	Ternary phase diagrams relevant to coal ash melts	71
2.19	Crystal growth rates in silicate melts	78
2.20	Summary	83
CHAPTER 3.	EXPERIMENTAL	
3.1	High temperature microscopy of coal ashes	88
	3.1.1 Apparatus	89
	3.1.2 Method	92
3.2	Crystallisation of ash melts	94
	3.2.1 Apparatus	95
	3.2.2 Method	95
	3.2.3 Phase analysis of quenched samples	96
3.3	Fusion of coal ash	97
	3.3.1 Apparatus	97
	3.3.2 Method	98
3.4	Crystal growth rates	102
	3.4.1 Preparation of glasses	103
	3.4.2 Determination of crystal growth rates	105

		Page
3.5	Crystallisation studies of three component glasses	106
	3.5.1 Preparation of glasses	109
	3.5.2 Crystallisation studies	109
3.6	Crystallisation studies of glasses in the system $CaO-MgO-Al_2O_3-SiO_2$	110
	3.6.1 Preparation of glasses	112
	3.6.2 Crystallisation studies	112
3.7	Crystallisation studies of the system $CaO-Al_2O_3-SiO_2$-iron oxide	114
	3.7.1 Preparation of glasses	116
	3.7.2 Apparatus	118
	3.7.3 Crystallisation studies	120
	3.7.4 Analysis of quenched samples	121
3.8	Crystallisation of multicomponent glasses of compositions based on that of a lignitic-type ash	125
	3.8.1 Preparation of glasses	125
	3.8.2 Crystallisation	125
3.9	Crystallisation of a glass of composition based on that of a bituminous-type ash	125
CHAPTER 4.	RESULTS	
4.1	High temperature microscopy	127
4.2	Quenching experiments on ash melts	129
4.3	Ash fusion in a vertical-tube furnace	134
4.4	Ash fusion in an electric muffle furnace	141
4.5	Crystal growth rates	145
4.6	Crystallisation of $CaO-Al_2O_3-SiO_2$ glasses	149
4.7	Crystallisation of $CaO-MgO-Al_2O_3-SiO_2$ glasses	151
4.8	Crystallisation studies of the system $CaO-Al_2O_3-SiO_2$-iron oxide	155
4.9	Crystallisation of model glasses based on a lignitic-type ash composition	165
4.10	Crystallisation of a glass of bituminous-type composition.	167
CHAPTER 5.	DISCUSSION	
5.1	High temperature microscopy	169
5.2	Crystallisation of ash melts	174
5.3	The fusion of coal ash	175

Page

5.4 Crystal growth rates 179

5.5 Correlation of crystallisation of $CaO-Al_2O_3-SiO_2$ glasses with lignitic-type ash melts 190

5.6 Crystallisation of $CaO-MgO-Al_2O_3-SiO_2$ glasses and correlation with the crystallisation of ashes 198

5.7 Crystallisation of $CaO-Al_2O_3-SiO_2$-iron oxide glasses 221

5.7.1 Crystallisation behaviour of glasses F1-F20 containing 5-20 wt % FeO 225

5.8 Crystallisation of multicomponent glasses based on ash composition 242

5.9 Comparison of coal ash melt crystallisation with predictions based on the system $CaO-FeO-Al_2O_3-SiO_2$ 251

5.10 Prediction of slagging propensity 270

CHAPTER 6. CONCLUSIONS AND SUGGESTIONS FOR FURTHER WORK 288

6.1 Conclusions 288

6.2 Suggestions for further work 289

APPENDIX A Components used for preparation of glasses 291

APPENDIX B Determination of oxygen partial pressure for an initial gas mixture of hydrogen and carbon dioxide 292

APPENDIX C Viscosity of coal ash melts 296

REFERENCES 305

ACKNOWLEDGEMENTS 312

LIST OF TABLES

No.		Page
1.1	Common minerals present in coal	15
2.1	Enthalpy of combustion of coal components	22
2.2	Slagging scale	27
2.3	Major minerals observed in coals	30
2.4	Examples of coal mineralogy	34
2.5	Range of component oxides of British coal ashes	35
2.6	Thermal decomposition of kaolin and shale group minerals	37
2.7	Temperature of thermal decomposition of carbonate minerals	40
2.8	Characteristics determined in the standard ash fusion test	53
2.9	Slagging factors calculated from coal ash composition	56
3.1	Chemical composition of LTA's KA, KC and KB	90
3.2	Chemical composition of LTA KD	97
3.3	Composition of glasses used in crystal growth rate studies	104
3.4	Composition of $CaO-Al_2O_3-SiO_2$ glasses	111
3.5	Composition of K series of $CaO-MgO-Al_2O_3-SiO_2$ glasses	111
3.6	Composition of J and I series of $CaO-MgO-Al_2O_3-SiO_2$ glasses	117
3.7	Composition of $CaO-Al_2O_3-SiO_2$-iron oxide glasses	117
3.8	Composition of multicomponent glasses of composition based on that of ash KA	126
3.9	Composition of glass D1 (based on that of ash KB)	126
4.1	High temperature microscopy of low-temperature ashes	128
4.2	Crystallisation of ash melts as determined on the high temperature microscope	130
4.3	Results of crystallisation experiments on ash KA using the quenching technique	131
4.4	Results of crystallisation experiments on ash KC using the quenching technique	131

No.		Page
4.5	Results of crystallisation experiments on ash KB using the quenching technique	132
4.6	Comparison of XRD pattern of an iron spinel sample and the patterns of hercynite and magnetite	133
4.7	Fusion of ash KD in air	135
4.8	Crystallisation behaviour of three component glasses	150
4.9	Crystallisation behaviour of CaO-MgO-Al_2O_3-SiO_2 glasses	153
4.10	Comparison of the XRD pattern of a CaO-MgO-Al_2O_3-SiO_2 melilite with those of the two end members	154
4.11	Results of crystallisation experiments on CaO-Al_2O_3-SiO_2-iron oxide glasses and the Fe^{2+}/total iron ratio determined	158
4.12	Crystallisation behaviour of glasses of the system CaO-Al_2O_3-SiO_2-iron oxide	162
4.13	Comparison of XRD patterns of three melilites observed in CaO-Al_2O_3-SiO_2-iron oxide glasses with that of gehlenite	163
4.14	Comparison of the XRD pattern of an observed iron spinel with those of hercynite and magnetite	164
4.15	Crystallisation of multicomponent glasses based on the composition of ash KA	166
4.16	Crystallisation of glass D1. A composition based on that of a bituminous-type ash	166
4.17	Comparison of XRD patterns of two spinels observed in glass D1 with those of hercynite and magnetite	168
5.1	Fusion of lignitic-type ashes	171
5.2	Comparison of high temperature microscope observations of ash KA	171
5.3	Ash fusion temperatures of a bituminous type ash	172
5.4	Activation energies for crystal growth	184
5.5	Composition of two lignitic type ashes	196
5.6	Composition of residual liquid phases for CaO-MgO-Al_2O_3-SiO_2 glasses	208
5.7	Observed and predicted crystallisation of lignitic ash melts (based on the system CaO-MgO-Al_2O_3-SiO_2)	214
5.8	Crystallisation paths of glass KA	215

No.		Page
5.9	Crystallisation behaviour of glasses of the system $CaO-Al_2O_3-SiO_2$-iron oxide	222
5.10	Composition of residual liquid phase for F series of glasses	233
5.11	Crystallisation behaviour of multicomponent glasses	245
5.12	Composition of residual liquid phase for glass MAT 3 (normalised composition)	246
5.13	Composition of residual liquid phase for glass D1 (normalised composition)	246
5.14	Crystallisation behaviour of bituminous-type melts and predictions based on the system $CaO-FeO-Al_2O_3-SiO_2$	252
5.15	Composition of residual liquid phase of bituminous ash melts	255
5.16	Crystallisation behaviour of lignitic ash melts and predictions based on the system $CaO-FeO-Al_2O_3-SiO_2$	263
5.17	Composition of residual liquid phase of lignitic ash melts	265
5.18	Slagging behaviour of various ashes and predicted crystallisation behaviour	273
5.19	Composition of residual liquid phase for ash melts of known slagging behaviour	276

LIST OF FIGURES

No.		Page
1.1	Diagram of a 600 MW pulverised coal fired boiler	13
2.1	Viscosity-temperature curves of two coal ash slags	59
2.2	Gibbs function/temperature curve for a hypothetical silicate melt	79
2.3	Theoretical curve of crystal growth rate vs. temperature	82
3.1	Detail of thermocouple used in the high temperature microscope	91
3.2	Gas-tight cell of high temperature microscope	91
3.3	High temperature microscope	91
3.4	Vertical-tube furnace used for the study of ash fusion	99
3.5	System $CaO-Al_2O_3-SiO_2$. Ternary compositions studied	108
3.6	Alumina rod assembly used in the study of iron oxide glasses	119
4.1	Graph of surface growth vs. time for MAT 8 glass at 1100^oC	146
4.2	Graph of crystal growth rate vs. temperature for MAT 8 glass	147
4.3	Graph of crystal growth rate vs. temperature for MAT 9 glass	148
5.1	Graph of crystal growth rate vs. temperature for MAT 8 and MAT 9 glasses	180
5.2	Graph of crystal growth rate vs. square-root time for MAT 8 glass at various temperatures	181
5.3	Graph of crystal growth vs. square-root time for MAT 9 glass at various temperatures	182
5.4	Graph of maximum crystal growth rate vs. reciprocal temperature for MAT 8 glass	185
5.5	Graph of maximum crystal growth rate vs. reciprocal temperature for MAT 9 glass	186

No.		Page
5.6	Graph of viscosity (calculated) vs. reciprocal temperature for MAT 8 glass	188
5.7	Graph of viscosity (measured) vs. reciprocal temperature for MAT 9 glass	189
5.8	System $CaO-Al_2O_3-SiO_2$. Crystallisation of ternary melts	197
5.9	System $CaO-MgO-Al_2O_3-SiO_2$, 5% MgO plane. Compositions studied	199
5.10	System $CaO-MgO-Al_2O_3-SiO_2$, 10% MgO plane. Compositions studied.	200
5.11	System $CaO-MgO-Al_2O_3-SiO_2$, 15% MgO plane	201
Crystallisation of K series of glasses		
5.12	System $CaO-MgO-Al_2O_3-SiO_2$, 5% MgO plane	209
5.13	System $CaO-MgO-Al_2O_3-SiO_2$, 10% MgO plane	210
5.14	System $CaO-MgO-Al_2O_3-SiO_2$, 15% MgO plane	211
5.15	Plot of liquidus temperature vs. MgO for a series of $CaO-Al_2O_3-SiO_2$ compositions to which MgO has been added	213
Crystallisation of lignitic-ash melts		
5.16	System $CaO-MgO-Al_2O_3-SiO_2$, 5% MgO plane	218
5.17	System $CaO-MgO-Al_2O_3-SiO_2$, 10% MgO plane	219
5.18	System $CaO-MgO-Al_2O_3-SiO_2$, 15% MgO plane	220
Crystallisation of F series of glasses		
5.19	System $CaO-FeO-Al_2O_3-SiO_2$, 5% FeO plane	235
5.20	System $CaO-FeO-Al_2O_3-SiO_2$, 10% FeO plane	236
5.21	System $CaO-FeO-Al_2O_3-SiO_2$, 15% FeO plane	237
5.22	System $CaO-FeO-Al_2O_3-SiO_2$, 20% FeO plane	238
5.23	System $CaO-FeO-Al_2O_3-SiO_2$, 25% FeO plane	239
5.24	System $CaO-FeO-Al_2O_3-SiO_2$, 30% FeO plane	240
5.25	System $CaO-FeO-Al_2O_3-SiO_2$, 50% FeO plane	241
Crystallisation of multicomponent glasses		
5.26	System $CaO-FeO-Al_2O_3-SiO_2$, 5% FeO plane	247
5.27	System $CaO-FeO-Al_2O_3-SiO_2$, 10% FeO plane	248
5.28	System $CaO-FeO-Al_2O_3-SiO_2$, 15% FeO plane	249
5.29	System $CaO-FeO-Al_2O_3-SiO_2$, 20% FeO plane	250

No.		Page
Crystallisation of bituminous ash melts		
5.29a.	System $CaO-FeO-Al_2O_3-SiO_2$, 5% FeO plane	256
5.30	System $CaO-FeO-Al_2O_3-SiO_2$, 10% FeO plane	257
5.31	System $CaO-FeO-Al_2O_3-SiO_2$, 15% FeO plane	258
5.31a	System $CaO-FeO-Al_2O_3-SiO_2$, 20% FeO plane	259
5.32	System $CaO-FeO-Al_2O_3-SiO_2$, 25% FeO plane	260
5.33	System $CaO-FeO-Al_2O_3-SiO_2$, 30% FeO plane	261
Crystallisation of lignitic ash melts		
5.34	System $CaO-FeO-Al_2O_3-SiO_2$, 5% FeO plane	266
5.35	System $CaO-FeO-Al_2O_3-SiO_2$, 10% FeO plane	267
5.36	System $CaO-FeO-Al_2O_3-SiO_2$, 15% FeO plane	268
5.37	System $CaO-FeO-Al_2O_3-SiO_2$, 20% FeO plane	269
Crystallisation of slagging and non slagging melts		
5.38	System $CaO-FeO-Al_2O_3-SiO_2$, 5% FeO plane	278
5.39	System $CaO-FeO-Al_2O_3-SiO_2$, 10% FeO plane	279
5.40	System $CaO-FeO-Al_2O_3-SiO_2$, 15% FeO plane	280
5.41	System $CaO-FeO-Al_2O_3-SiO_2$, 20% FeO plane	281
5.42	System $CaO-FeO-Al_2O_3-SiO_2$, 25% FeO plane	282
5.43	System $CaO-FeO-Al_2O_3-SiO_2$, 30% FeO plane	283

PLATES

Page

Photomicrographs of roasted ash samples treated at 1450°C in air for various times

Plate		
1	R6 (15s)	137
2	R6 (15s)	137
3	R6 (15s)	137
4	R6 (15s)	139
5	R6 (15s)	139
6	R6 (15s)	139
7	R6 (15s)	140
8	R6 (15s)	140
9	R2 (60s)	140
10	R2 (60s)	142
11	R2 (60s)	142
12	R2 (60s)	142

Plates 13-15	Photomicrographs of raw LTA treated at 1450°C in air for 15s.	143
Plates 16-18	Electronmicrographs of raw LTA treated at 1450°C in air for 15s	144

CHAPTER 1

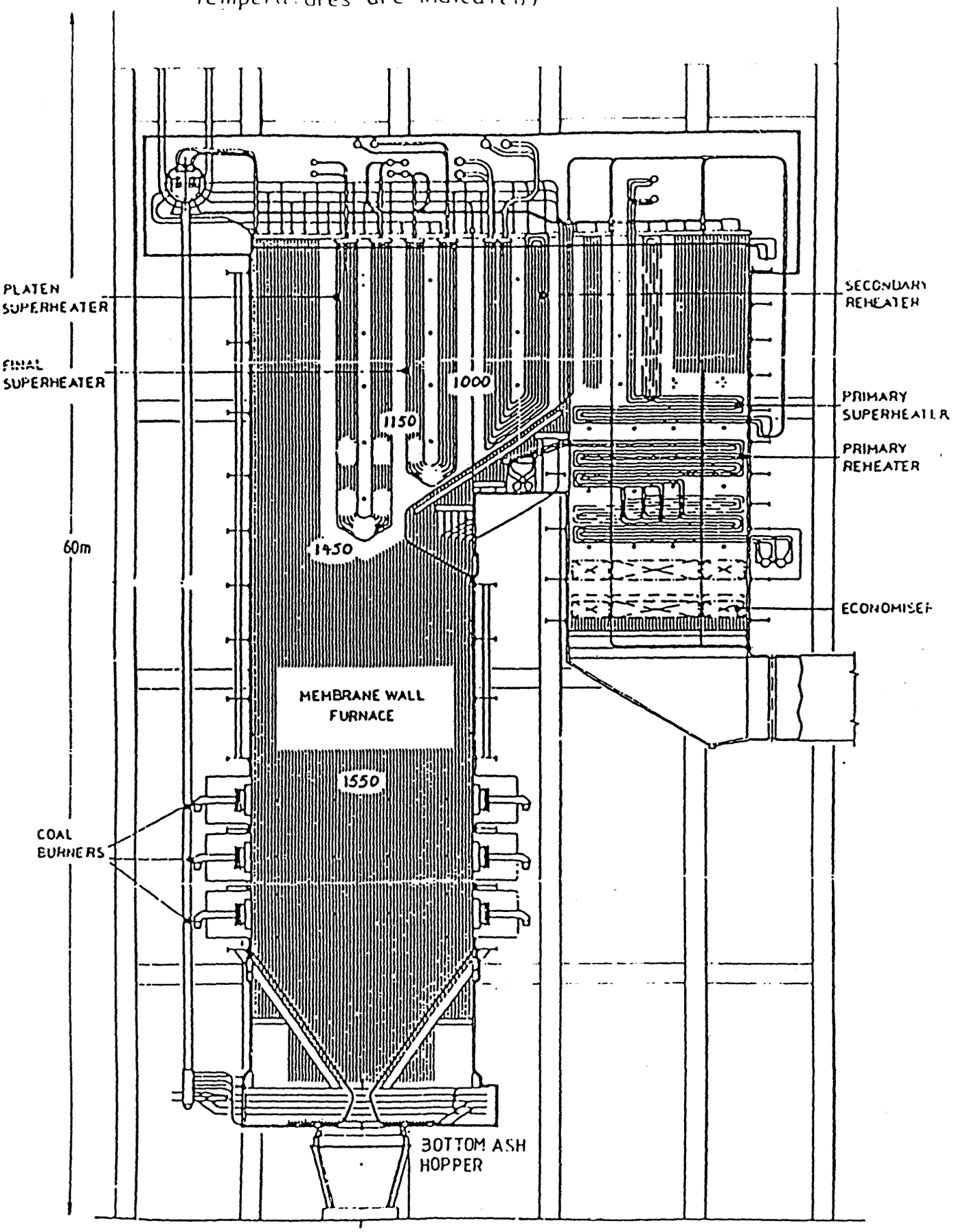
INTRODUCTION

The combustion of coal is the major source of electrical power in the United Kingdom. The high relative cost of oil and the capital investment involved in nuclear power generation ensures that coal will remain the primary energy source for electricity in the United Kingdom.

Modern coal-fired boilers as used in the United Kingdom by the Central Electricity Generating Board use pulverised fuel and the rating of the most efficient boilers is over 500 MW. While the boilers are specifically designed for a given coal or range of coals to be fired, the overall characteristics of the boiler are generally the same. A typical pulverised-fuel boiler of 600 MW designed by Babcock Power Ltd is illustrated in Fig.1.1. Coal is fed to the burners with preheated primary air after being pulverised to particles of about 50 μm in diameter. In the burner zone the carbonaceous material present in the coal burns leaving a residue called ash. The temperatures produced in the burner zone may range from 1500 °C to 1600 °C. The boiler walls which contain superheat steam at 420 °C to 430 °C are designed to absorb the radiant heat. The superheater and reheater regions in the convective zone cool the outgoing gases and at the same time improve the thermal efficiency of the boiler. The approximate gas temperatures within various parts of the boiler are indicated in Fig.1.1.

Coal is a fossil fuel formed by sedimentary processes and is a dirty fuel compared to oil, that is there may be a significant

Fig.1.1 Diagram of a 600MW pulverised coal fired boiler (Designed by Babcock Power Ltd Approximate gas temperatures are indicated)



amount of mineral phases present in the coal which may be closely associated with the carbonaceous matter. It is the presence of the minerals that leads to formation of ash when a coal is burnt. The major mineral groups present in coal are alumino-silicates, such as kaolinite, carbonates, such as dolomite, and iron sulphides, usually pyrite. Quartz (SiO_2) may also be present in significant proportions. The various minerals commonly observed in coals have been compiled in Table 1.1. The accessory group minerals are those usually observed in association with alumino-silicate group minerals. Both the specific and relative amounts of minerals present in coal vary between mining regions and within a given coal seam.

When a coal is burnt the nature of the ash formed will depend primarily on the reaction between the mineral particles. Within a pulverised fuel-fired boiler the gas temperatures which the mineral particles will experience vary from about 300 °C to 1600 °C, while the total residence time of the particles within the main body of the boiler (Fig.1.1) is designed to be about 1-2 seconds.

There have been relatively few quantitative studies of the mineral phases present in coal. The standard practice is to determine only the chemical composition of a laboratory produced ash (coal is air roasted at 750°-800 °C). The composition of an ash will be determined by the original coal mineral matter and usually consists of silica, alumina, iron oxide, lime, magnesia, soda, potash, titania and the oxides of phosphorus and sulphur. The major component oxides are silica and alumina. Iron oxide or lime may be the third major component. Coal ashes are classified as bituminous-type when the iron oxide content is greater than the sum of lime and magnesia contents, and as

TABLE 1.1

Common minerals present in coal

Group	Species	Formula
Shale *	muscovite, hydro-muscovite, illite, bravaisite, montmorillonite	$(K,Na,H_3O,Ca)_2$ $(Al,Mg,Fe,Ti)_4$ $(Al,Si)_8\ O_{20}(OH,F)_4$
Kaolin/clay *	kaolinite, livesite, metahalloysite	$Al_2(Si_2O_5)(OH)_4$
Sulphide	pyrites, marcasite	FeS_2
Carbonate	ankerite, ankeritic calcite, ankeritic-dolomite, ankeritic chalybite	$(Ca,Mg,Fe,Mn)CO_3$
Chloride	sylvite, halite	KCl, NaCl
Accessory	quartz	SiO_2
	felspar	$(K,Na)_2O.Al_2O_3.6SiO_2$
	garnet	$3CaO.Al_2O_3.3SiO_2$
	hornblende	$CaO.3FeO.4SiO_2$
	gypsum	$CaSO_4.2H_2O$
	apatite	$9CaO.3P_2O_5.CaF_2$
	zircon	$ZrSiO_4$
	epidote	$4CaO.3Al_2O_3.6SiO_2.H_2O$
	biotite	$K_2O.MgO.Al_2O_3.3SiO_2.H_2O$
	augite	$CaO.MgO.2SiO_2$
	prochlorite	$2FeO.2MgO.Al_2O_3.2SiO_2.2H_2O$
	diaspore	$Al_2O_3.H_2O$
	lepidocrocite	$Fe_2O_3.H_2O$
	magnetite	Fe_3O_4
	kyanite	$Al_2O_3.SiO_2$
	staurolite	$2FeO.5Al_2O_3.4SiO_2.H_2O$
	topaz	$Al_2(SiO_4)(OH,F)_2$
	tourmaline	$MgAl_3(BOH)_2Si_4O_{19}$
	penninite	$5MgO.Al_2O_3.3SiO_2.2H_2O$

* also referred to as aluminosilicates.

lignitic-type when the sum of lime and magnesia contents is greater than the iron oxide content.

The formation and presence of coal ash in a boiler present many problems with its design and the attainment of optimum operating efficiency. Particles of ash may fall into the ash hopper or be carried through the body of the boiler by convection forces to be precipitated in the flyash hopper. As coal may contain up to 40 wt % ash sufficient provision must be made in the design of the boiler for the presence of ash.

The thermal efficiency of a boiler may be drastically reduced by the formation of deposits, from ash particles on the heat-absorbing surfaces. In severe circumstances the boiler may have to be shut down for cleaning. There are two types of deposit, the most serious of which is the glassy or semivitreous type, called slag formed on tubes in the region of the boiler receiving radiant heat. Fouling deposits are formed in the convection passages and are sintered in nature and are generally less troublesome.

The designers of a boiler may incorporate various features both to reduce the formation and growth of deposits and to remove any deposit formed during normal operation. The methods used at present to predict the likelihood of a given coal ash forming a deposit give misleading results or are limited over the range of coal ash compositions to which they apply. The most common method is that of the determination of the temperatures at which a cone of laboratory prepared ash undergoes various degrees of deformation when heated due to the presence of a liquid phase. Other methods involve calculation of slag viscosities from empirically derived equations or determination of various slagging parameters

calculated from the chemical analysis of the ash.

The methods of predicting the slagging propensity of a coal ash do not take into account the mechanism of deposit formation and growth. In a pulverised-fuel fired boiler the coal minerals are completely fused, with the exception of some quartz in some circumstances, within the burner zone despite very short residence times. Studies of boiler deposits, usually of slag type, have shown that the major crystalline phases present were not those which would be expected from the individual thermal decomposition of the mineral phases present in the coal and had clearly crystallised from a melt. The growth of a deposit will depend on the behaviour of fused ash particles, namely the adhesion of the particles to any deposit already present. A model previously developed, based on sintering mechanisms, indicates that the mechanism of growth of a deposit is sintering by viscous flow. The model further indicates that the rate of growth is dependent primarily on the reciprocal of the viscosity of the liquid phase present at a given temperature. For the predominantly glassy slag deposits in which there is significant liquid phase (usually of low viscosity) the rate of growth, that is the rate of capture and assimilation of the fused ash particles, will be greater than that of the fouling deposits formed at lower temperatures where a liquid phase present would have a respectively higher viscosity.

The viscosity of a coal ash melt has been shown to be dependent on the chemical composition and oxygen potential of the local atmosphere for a given temperature. For boiler deposits crystallisation may occur in the ash particles before significant sintering or assimilation has taken place by viscous flow. Both

the degree of crystallisation and the composition of the crystalline phase or phases have an effect on the viscosity of the residual liquid phase within a fused ash particle or deposit.

The novel approach used in this study has been the use of relevant high temperature phase equilibria data to model the crystallisation behaviour of coal ash melts. Phase equilibrium diagrams can predict both the fusion and/or crystallisation behaviour, under equilibrium conditions of a composition defined by the diagram. The crystallisation path of a melt cooled below its liquid temperature indicates the change in chemical composition of the residual liquid phase with crystallisation and can also indicate the amount of crystalline phase or phases present at a given temperature under equilibrium conditions. Thus, phase equilibria data should be able to provide the information necessary to predict the slagging propensity of a coal ash based on the model of rate of growth of coal ash deposits.

The chemical composition of ash may contain eleven component oxides and for such systems the determination and representation of phase equilibria data would be complex and limited. Fortunately there are three or four major component oxides present in coal ash, namely silica, alumina, iron oxide or/and lime which may constitute more than 90 wt % of the ash content. Using the approximation that the minor components have limited effect on the phase equilibria compared to the effect of the major components the composition can be normalised to three or four components.

Before phase equilibria can be applied to the prediction of slagging propensities of coal ashes various kinetic factors must be determined. Though there is significant evidence of the rapid fusion of ash in the boiler there have been relatively few studies

of the rate of ash fusion. It was an aim of this project to determine the phase changes in a sample of coal ash treated at temperatures similar to those observed in a boiler for various times. A further aim was the determination of crystal growth rates in glasses of compositions analagous to known coal ashes. Thus with the knowledge of the rate of ash fusion and the rate at which crystallisation occurs in ash melts an indication of the rate at which ash particles approach equilibrium in a boiler may be obtained.

It was the main aim of this project to obtain detailed crystallisation behaviour of coal ash melts and to correlate the behaviour with crystallisation of model three and four component mixtures. The ternary system studied was that of $CaO-Al_2O_3-SiO_2$ which may be pertinent to lignitic-type ashes. Quaternary systems would be expected to give closer correlation with the crystallisation behaviour of ash melts and therefore the systems $CaO-MgO-Al_2O_3-SiO_2$ and $CaO-Al_2O_3-SiO_2$-iron oxide were studied in regions of the system relevant to lignitic-type and bituminous-type ash melts respectively. The variable oxidation state of iron necessitated the study of the latter system in a controlled atmosphere (mildly reducing).

The crystallisation behaviour of coal ash melts has been found to be dominated by the quaternary system $CaO-FeO-Al_2O_3-SiO_2$ including those of lignitic-type compositions. A method has been devised using phase equilibria data of the quaternary system to predict the slagging propensity of a coal ash based on the mechanism of rate of growth of boiler deposits from the normalised four component composition of the ash. The predictions obtained for a number of coal ashes (of a wide range of compositions) of known slagging behaviour have been found to be more accurate than

the predictions obtained from the various techniques presently used by boiler designers and operators.

CHAPTER 2

LITERATURE SURVEY

2.1 COAL

Coal is a fossil fuel formed by the anaerobic decomposition of plant material. The burning of coal in steam generating boilers is the major primary source of energy for power generation in the United Kingdom. In 1982, 85% of the UK's electricity supply was produced from coal[1]-fired boilers. The World Coal Study[2] has indicated that coal was planned to be the predominant fossil fuel for steam generated electricity up to the year 2000. The increasing cost of oil and the high capital cost of nuclear power stations has increased the importance of coal as a primary energy source.

Designers of coal-fired boilers have endeavoured to increase thermal efficiency by increasing boiler size and increasing the gas temperatures[3]. While these design parameters have a theoretical basis problems have been found to occur in many new boilers due to the characteristics of the ash. The ash is the inorganic residue remaining after combustion of the carbonaceous matrix in which many minerals are intimately mixed. The major ash related problem is reduced heat transfer caused by formation of deposits.

The mineral matter in coal can vary widely in terms of content and composition between one source and another. Large power stations such as the CEGB Ferrybridge 'C' in South Yorkshire, UK, take coals from up to 60 different collieries, which leads to problems in relating thermal efficiency to the coal being burned at a given time.

2.2 OPERATION OF A BOILER

Coal is comprised mainly of a carbonaceous matrix containing predominantly carbon, with some hydrogen and sulphur, which were the major elements, apart from oxygen, present in the original plant material. These three elements are the major components of coal which undergo combustion. The possible reactions are listed in Table 2.1 along with the enthalpy of combustion (ΔH_c).

TABLE 2.1

Reaction			ΔH_c/kJ mol^{-1}	
$C(graphite) + \frac{1}{2}O_2(g)$	$\rightleftharpoons$	$CO(g)$	-106.43	(1)
$CO(g) + \frac{1}{2}O_2(g)$	$\rightleftharpoons$	$CO_2(g)$	-286.14	(2)
$H_2(g) + \frac{1}{2}O_2(g)$	$\rightleftharpoons$	$H_2O(g)$	-238.54	(3)
$S(rh) + O_2(g)$	$\rightleftharpoons$	$SO_2(g)$	-297.57	(4)

A coal-fired boiler is designed to burn the fuel efficiently and to raise the temperature of steam for turbine generators. As can be seen from reactions (1) and (2) the partial combustion of carbon to carbon monoxide severely reduces the heat produced. Thus a major operational parameter must be the supply of excess oxygen to ensure complete combustion.

There are three basic designs of coal-fired boilers, namely stoker, cyclone and pulverised coal-fired boilers. The choice of design will depend on the properties of the coal and the ash, The properties will determine other design parameters such as

furnace geometry, heat flux and combustion conditions. Further details of design criteria can be found elsewhere.[4] Pulverised coal-fired combustion has been the preferred design in recent years as it can be used for a wider range of coals and will be the only method discussed here.

In a pulverised coal-fired furnace the coal is fed from hoppers with preheated primary air to a pulveriser which grinds the coal to a fine powder (particles about 50 μm in diameter). The coal-air mixture is then fed to a number of burners where it is mixed with the required amount of secondary air. The carbonaceous and volatile matter will burn rapidly in the flame according to the reactions (1) and (2) above. Hydrogen and sulphur also react with oxygen as outlined above. The gas temperatures in the burner zone, produced by the combustion, range from 1500 °C to 1600 °C. The inorganic material present in the coal is released from the carbonaceous matrix and is taken up by the convection currents present in the boiler; the velocity and paths taken by the individual ash particles will depend on their size, shape and density. The residence time for ash particles between the burner zone and the major convection surfaces is about 1-2 seconds.[5]

A schematic representation of a pulverised fuel fired boiler is given in Fig.1.1 and is based on a design of a Babcock Power Ltd boiler. The walls of the furnace and the banks of superheaters and economisers are made up of tubes which carry superheated water at 420-430 °C. The major proportion of steam is raised by radiation from the burner zone to the adjacent walls of the furnace. The superheaters and economisers are used to absorb the remaining heat from the hot

gases; the temperature of the gases leaving the boiler is designed to be approximately 300 °C and this heat is used to raise the temperature of the primary air supply. The thermal efficiency of a boiler under ideal conditions may be greater than 70%.

The predicted gas temperatures within the furnace have been indicated in Fig.1.1. The maximum temperature in the burner zone is in the range 1500-1600 °C with the gas temperatures in the superheater region ranging from 1450 °C to about 1150 °C. The temperatures of clean walls is designed to be 420-430 °C and maintained at this temperature by the cooling effect of the superheated steam.[5]

2.3 SLAGGING OF A BOILER

The inorganic material associated with coal will behave differently from the combustible matter. The temperatures in the burner zone are sufficiently high to cause significant decomposition and chemical reaction of the coal mineral matter. The product of the high temperature reactions is called ash. A 600 MW boiler burns approximately 270 tonnes of coal per hour; assuming an average ash content of 15 wt %, 40 tonnes of ash will be produced. The boiler is designed to remove the ash, both in the bottom ash hopper (Fig.1.1) and in the fly ash hopper. Ash particles may be relatively molten within the major body of the boiler, and their behaviour will depend on their physical and chemical characteristics and on furnace conditions. Some ash may be deposited on the heat absorbing surfaces of the boiler. The deposits are usually divided into three main types:

1. Fused slag deposits which are formed on furnace walls and other surfaces exposed to predominantly radiant heat.
2. High temperature bonded deposits which form on convection heating surfaces, e.g. superheaters and reheaters.
3. Low temperature deposits which form on air heaters and economisers.

Slag deposits are formed by the deposition of molten or tacky particles from the gas stream. As the major proportion of steam is raised from radiant heat transfer the thermal efficiency is seriously reduced by the formation of a slag layer on the tubes of the furnace. The thermal conductivity of a fused deposit at 1000 °C has been given as about 0.294 Wm^{-1} K^{-1} [6] compared to iron at 1000 °C of about 29 Wm^{-1} K^{-1}. [7] The reduction of heat absorbed by the boiler tubes increases the gas temperature and may thus lead to the formation of high temperature bonded deposits with subsequent further heat losses. The slag deposit may be difficult to remove due to its glassy nature and thus the formation of such a slag has a very serious effect on boiler efficiency.

The formation of high temperature bonded deposits on the convection heating surfaces is usually called fouling. The mechanism of fouling is usually thought to be via the formation on the convection tubes of an alkali matrix layer which has a sufficiently low-melting point that it traps passing fly ash particles. Further build-up is due to sintering of the attached particles. Serious fouling causes blockages of the gas passages which results in higher exit gas temperatures and problems in air updraft which in turn leads to incomplete combustion. The build-up of fouling deposits can be reduced by soot or steam

blowing from lances strategically placed and used either intermittently or continuously.

The presence of low temperature deposits is less troublesome than slag or fouling deposits and is easily removed.

The cost of the reduced efficiency of coal fired boilers due to the presence of deposits has been estimated to be about $500 M dollars per annum[5] in the United States.

2.4 PREDICTION OF FORMATION OF BOILER DEPOSITS

The tendency of a coal ash to form a fused slag deposit is usually referred to as its slagging propensity. The degree of slagging is a subjective term and thus it is very difficult to quantify. Sanyal and Coleman[8] have recently outlined the problems of defining a slagging scale and put forward a suggested scale. The requirements for a scale are:-

(a) it must be easily understood by the boiler operators;
(b) it must quantify a subjective observation;
(c) it must not rely on specialised equipment;
(d) it must be an exact indication of the furnace conditions;
(e) it must be able to allow comparison between different furnaces.

The authors devised the following arbitrary scale of slagging propensity (P_s) based on the factor F_e which is the fraction of heat absorbed compared to that theoretically possible (Table 2.2).

TABLE 2.2

F_e	P_s	Operational comment
1.0	0	Unobtainable with coal-fired plant
0.9	1	Cleanest possible condition with coal
0.8	2	Initial increase of attemperation
0.7	3	Further increase of attemperation
0.6	4	Dirtiest condition that can be tolerated without operational changes, e.g. application of high excess air
0.5	5	Initial increase of excess air and attemperation
0.4	6	Further increase of excess air and attemperation
0.3	7	Dirtiest possible condition at which boiler can be fired at full load
0.2	8	Reduce load
0.1	9	Completely slagged up furnace

The boiler operator monitors mainly the amount of steam being raised, the temperature of the exit gases and the carbon monoxide content of the flue gases. The amount of steam being raised is important as any variation may affect the running of the turbines. The increase in exit gas temperature indicates decreasing thermal efficiency and the carbon monoxide content indicates the degree of combustion in the boiler. From the measurements the operator can observe the onset of slagging and can take the necessary precautions against a slag build-up by attemperation (the blowing of cooler gases into slagging regions) and then by increasing the excess air. If slagging continues the operator has to reduce load by reducing the amount of coal being burnt which results in a derating of the steam output. In severe circumstances, if the boiler is heavily slagged, it may have to be shut down for cleaning.

Thus the scale devised by Sanyal and Coleman can be readily and accurately used by operators and comparisons made between boilers. The scale is based on operating observations and can not be applied to the prediction of slagging propensity. There are a number of empirical tests and factors based on the chemical composition of coal ash to predict the likelihood of slag formation by a given coal ash. These will be discussed in detail subsequently and shown to be misleading in the predictions of slagging propensity due mainly to the lack of insight into the actual mechanism of deposit formation.

2.5 COAL MINERAL MATTER

The study of coal minerals at temperatures analogous to those found in a burner zone of a pulverised-fuel-fired boiler will assist the assessment of the effect of varying mineral matter on the formation of deposits.

Coal is found as seams between various types of sedimentary rock strata. Lessing[9], from detailed petrological study, distinguished between two types of mineral matter; inherent, where the mineral matter is closely associated with the carbonaceous particles, and adventitious material where the minerals are not closely associated with the coal particles.

The specific minerals present and their relative abundance in a coal will be governed by the original plant material and the local geology.

There have been many investigations of coal mineralogy, a recent comprehensive review has been that of Gluskoter.[10] Though many different distinct mineral phases have been observed in coals

the majority of the minerals are in one of four groups: aluminosilicates, sulphides, carbonates and silica (quartz). The minerals commonly observed in coals are listed in Table 2.3 with their chemical formulae.

The aluminosilicates are clay minerals and are usually the most common mineral constituent of coals and of the surrounding rock strata. The most common clay minerals associated with coals are illite, kaolinite and mixed-layer illite-montmorillonite. Of the few detailed studies, Rao and Gluskoter[11] determined the mean value of the clay content in the mineral matter of Illinois Basin coals to be 52 wt %.

Iron sulphide (FeS_2) is the most common sulphide mineral observed in coal and is an inherent mineral. There are two forms of iron sulphide: pyrite with a cubic structure and marcasite which has an orthorhombic structure. Pyrite is observed more often than marcasite. Sphalerite (ZnS) and galena (PbS) are the other main sulphide minerals sometimes observed in coals.

The most common carbonate minerals observed in coals are dolomite ($CaCO_3.MgCO_3$) and ankerite ($2CaCO_3.MgCO_3.FeCO_3$), but calcite ($CaCO_3$) and siderite ($FeCO_3$) are also commonly reported.

Silica (SiO_2), in the form of quartz is observed in all coals and is an adventitious mineral. The quartz content depends markedly on the local geology and is associated with the aluminosilicates and silicate minerals.

Quantitative mineralogy is difficult as standard techniques to remove the carbonaceous matter alter the mineral matter.

TABLE 2.3

Major minerals observed in coals

Mineral	Chemical formula
Clay Group	
Montmorillonite	$Al_2Si_4O_{10}(OH)_2.xH_2O$
Illite-sericite	$KAl_2(AlSi_3O_{10})(OH)_2$
Kaolinite	$Al_4Si_4O_{10}(OH)_8$
Halloysite	$Al_4Si_4O_{10}(OH)_8$
Chlorite (prochlorite, penninite)	$Mg_5Al(AlSi_3O_{10})(OH)_8$
Muscovite	$K_2Al_4(Si_6Al_2O_{20})(OH,F)_4$
Sulphide Group	
Pyrite	FeS_2
Marcasite	FeS_2
Sphalerite	ZnS
Galena	PbS
Carbonate Group	
Calcite	$CaCO_3$
Dolomite	$(Ca,Mg)CO_3$
Siderite	$FeCO_3$
Ankerite	$(Ca,Fe,Mg)CO_3$
Sulphate Group	
Barite	$BaSO_4$
Gypsum	$CaSO_4.2H_2O$
Anhydrite	$CaSO_4$

TABLE 2.3 continued

Chloride Group	
Halite	$NaCl$
Sylvite	KCl
Bischofite	$MgCl_2.6H_2O$
Silicate Group	
Quartz	SiO_2
Biotite	$K(Mg,Fe)_3(AlSi_3O_{10})(OH_2)$
Garnet	$(Fe,Ca,Mg)_3(Al,Fe)_2(SiO_4)_3$
Kyanite	Al_2SiO_5
Staurolite	$Al_4FeSi_2O_{10}(OH)_2$
Epidote	$Ca_2(Al,Fe)_3Si_3O_{12}(OH)$
Albite	$NaAlSi_3O_8$
Sanidine	$KAlSi_3O_8$
Orthoclase	$KAlSi_3O_8$
Augite	$Ca(Mg,Fe,Al)(Al,Si)_2O_6$
Hornblende	$NaCa_2(Mg,Fe,Al)_5(Si,Al)_8O_{22}(OH)_2$
Topaz	$Al_2SiO_4(OH,F)_2$
Oxide & Hydroxide Group	
Hematite	Fe_2O_3
Magnetite	Fe_3O_4
Rutile	TiO_2
Phosphate Group	
Apatite	$Ca_5(PO_4)_3(F,Cl,OH)$

Though the adventitious material such as quartz and clays may be separated by fine crushing of the coal followed by float-and-sink separation inherent minerals such as iron sulphides are difficult to separate. The standard technique of ashing finely ground coal by roasting at 800 °C [12] affects nearly all the minerals present, for example, clays lose interstitial water, carbonates decarboxylate and iron sulphides are oxidised. A detailed mineralogical analysis of such an ash would not be a true description of the original mineral content of the coal. A recently developed technique called low-temperature ashing overcomes such difficulties. Finely ground coal is placed in a gas-tight cell which is then filled with oxygen at 133 Pa. A radiofrequency of 450 MHz is passed through the oxygen causing a discharge and the resulting activated oxygen atoms oxidise the carbonaceous matter. The temperature within the cell is reported to be less than 150 °C.[13] The most sensitive mineral to oxidation is pyrite and has been observed to be only slightly affected by this ashing technique.[13] Detailed mineralogy of the low-temperature ash may be obtained by a number of techniques. The most straight-forward and widely used method is that of X-ray diffraction analysis. Gluskoter [14] and O'Gorman and Walker[15] have extensively used X-ray diffraction analysis to determine the detailed mineralogical contents of coals.

Other techniques of evaluating coal minerals using low temperature ash which have been utilized are infra-red spectroscopy[16] and electron microscopy.[17,18]

Huggins et al.[19] have used ^{57}Fe Mossbauer spectroscopy and scanning electron microscopy with automatic image analysis of finely ground coal to obtain quantitative determination of the

minerals present in various American coals. The method does not rely on any coal or ash preparation techniques as it determines coal minerals in situ. The results of the study have been listed in Table 2.4 and illustrate the wide variation in coal mineralogy between different coal seams.

Neither qualitative nor quantitative determination of the mineralogical contents of coals fired in power stations are normally undertaken. Operators of coal-fired boilers are concerned primarily with the calorific value, moisture content, ash content and fusion temperatures of the coals supplied. The chemical composition of the coal ash is determined as it is used to evaluate various deposit forming factors. The analysis is given in terms of the weight percent of oxides and the particular chemical composition will of course depend on the original minerals present in the coal. The major inorganic oxides present in coal and the coal ash are silica, alumina, iron oxide, lime and magnesia, and minor oxides are soda, potash, titania, sulphur (expressed as sulphur trioxide), manganese oxide and phosphorus (expressed as phosphorus pentoxide). The range of the component oxides observed in British coals is listed in Table 2.5.[12] The major variation between chemical compositions of coal ashes is the relative amount of lime and magnesia contents compared to the iron oxide content. Ashes with a total lime plus magnesia content greater than the iron oxide content are called lignitic-type. Bituminous-type ashes are those with an iron oxide content greater than the lime plus magnesia content. The distinction between the two types of ashes is used to determine which deposit-forming factors are valid in assessing a coal's suitability for firing.

TABLE 2.4

Examples of coal mineralogies[19]

Crystalline phases given in weight % of ash

Mineral	Formula	B seam, Colorado	Pittsburgh seam, Penn.	Anthracite Mass
Quartz	SiO_2	30 ± 5	15 ± 3	32 ± 6
Kaolinite	$Al_2Si_2O_5(OH)_4$	21 ± 5	16 ± 3	trace
Illite	$K(Al,Fe)_4(Si,Al)_8O_2(OH)_4$*	trace	9 ± 2	24 ± 4
Chlorite	$(Fe,Mg,Al)_6(Si,Al)_4O_{10}(OH)_8$*	-	-	8 ± 2
Montmorillonite	$(Ca,Na)(Al,Mg)_4(Si,Al)_8O_2(OH)_4$*	12 ± 3	1 ± 1	trace
Mixed silicates	n.d.	21 ± 4	6 ± 2	9 ± 2
Pyrite	FeS_2	trace	34 ± 7	3 ± 2
Siderite	$FeCO_3$	5 ± 3	trace	1 ± 1
Calcite	$CaCO_3$	5 ± 2	9 ± 3	7 ± 3
Ankerite	$Ca(Fe,Mg)(CO_3)_2$	trace	-	9 ± 3
Others	n.d.	2 ± 2	5 ± 2	2 ± 2
Unknown	n.d.	4 ± 2	6 ± 2	5 ± 2
Wt % ash		8.8	8.5	18.6

* simplified formula

n.d. = not determined

TABLE 2.5

Compositional range of British coal ashes*

Component	Range/wt %
Silica, SiO_2	15-55
Alumina, Al_2O_3	10-40
Ferric oxide, Fe_2O_3	1-40
Calcium oxide, CaO	1-25
Magnesium oxide, MgO	0.5-5
Sodium oxide, Na_2O	0-8
Potassium oxide, K_2O	0-5
Titanium oxide, TiO_2	0-3
Manganese oxide, Mn_3O_4	0-1
Sulphate, SO_4	0-12
Phosphate, P_2O_5	0-3

* from BS 1016 Part 14:1963.[12]

2.6 EFFECT OF HEAT ON THE MAJOR MINERALS

The thermal breakdown and reactions of the individual minerals present in coal have been extensively reviewed by Watt.[20]

The major mineral groups present in coal are the clays, shales and sulphides. The general decomposition of the kaolinite (a specific form of clay) group and three major shale group minerals, illite, muscovite and biotite are listed in Table 2.6. Kaolinite ($Al_2(Si_2O_5)(OH)_4$) when heated to 500 °C loses the hydroxyl groups. At 925 °C the three dimensional silicate layer crystal structure characteristic of clays is broken with the loss of amorphous silica to form a silicon spinel ($2Al_2O_3.3SiO_2$). Further heating to 1100 °C loses SiO_2 from the spinel to form mullite ($3Al_2O_3.2SiO_2$) a very refractory mineral which is stable up to 1800 °C.

The crystal lattice of illite ($KAl_2(AlSi_3O_{10})(OH)_2$) breaks down when heated at 950 °C to produce an amorphous glass, formed from the alkali oxide and silica from the outer layer of the lattice, spinel ($MgO.Al_2O_3$) formed from the alumina and magnesia from the middle layers of the lattice, and silica in the low temperature polymorph of quartz. Further heating to 1300 °C produces mullite and the mineral is completely liquid above 1400 °C.

Biotite ($K(MgFe)_3(AlSi_3O_{10})(OH)_2$) is stable up to 1100 °C at which temperature the crystal lattice is destroyed forming a spinel, magnetite (Fe_3O_4) or magnesioferrite ($MgO.Fe_2O_3$), leucite ($K_2O.Al_2O_3.4SiO_2$) and mullite. At 1200 °C a liquid is formed and at 1500 °C both glass and olivine [$2(CaO,FeO),SiO_2$] are observed.

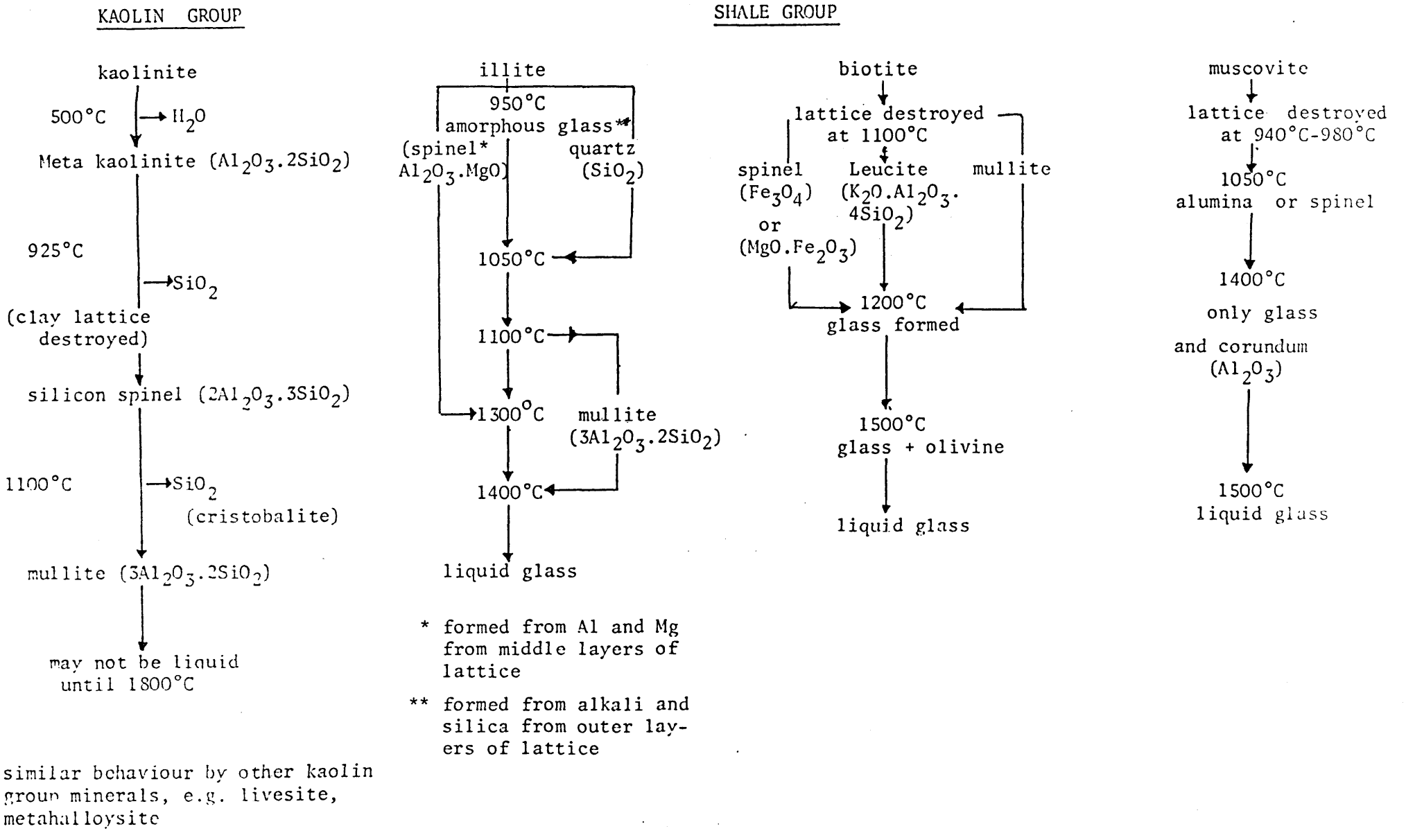


TABLE 2.6

Thermal decomposition of kaolin and shale group minerals

The crystal lattice of muscovite is destroyed between 940 °C and 980 °C. On further heating to 1050 °C alumina (Al_2O_3) or spinel ($MgO.Al_2O_3$) is formed from the amorphous mineral. At 1400 °C only liquid and corundum (Al_2O_3) is present and above 1500 °C only liquid glass is observed.

The thermal reactions of iron sulphides (FeS_2) depends mainly on the atmosphere. The most common products of roasting pyrite in air are wustite (FeO), pyrrhotite(FeS), magnetite ($FeO.Fe_2O_3$) and iron(III) sulphate $Fe_2(SO_4)_3$, S_n (polymeric sulphur, n = 2-8), sulphur dioxide (SO_2) and sulphur trioxide (SO_3). Schwab and Phillinis[21] studied the reaction in excess air at temperatures in the range 400 °C - 500 °C and the following reactions were found to be taking place:

$$FeS_2 + {}^5/_4O_2 \rightarrow \tfrac{1}{2}Fe_2O_3 + SO_2 \qquad (1)$$

$$FeS + {}^7/_2O_2 \rightarrow \tfrac{1}{2}Fe_2(SO_4)_3 + \tfrac{1}{2}SO_2 \qquad (2)$$

The oxidation was found to be predominantly by reaction (1) with 80% Fe_2O_3 being present at 400 °C with decreasing amounts of $Fe_2(SO_4)_3$ with increasing temperature. The rate of reaction was found to be mainly dependent on the rate of diffusion of oxygen through the sulphate/oxide layer.

Studies by Flint and Copson[22] have shown that the thermal decomposition of pyrite in air begins at about 370 °C with a stable complex formed between hematite (Fe_2O_3) and iron(II) sulphate ($FeSO_4$) over the range 440 °C - 600 °C. At higher temperatures the products were Fe_2O_3, FeO or Fe_3O_4 depending on the oxygen potential of the atmosphere used. The products at 1000 °C were exclusively Fe_2O_3 and SO_2.

The carbonate minerals are the only other major mineral group present in coal which undergo significant chemical changes on heating. The minerals decompose according to the general reaction

$$MCO_3 \rightleftharpoons MO + CO_2$$

All the products are stable with respect to further decomposition except for siderite, $FeCO_3$ where the product FeO is sensitive to oxidation. The temperatures at which decomposition takes place for the carbonate minerals as observed by differential thermal analysis are listed in Table 2.7.

2.7 MECHANISM OF MELTING COMPLEX MINERAL MIXTURES

The minerals present in a coal may not be isolated and are usually intimately mixed. The processes involved in melting mixtures are solid phase reaction, sintering and formation of a liquid phase.

Solid phase reaction occurs as a result of vacancies in the lattices of the reacting species permitting diffusion of atoms and/or ions between adjacent crystal lattices. The solid state reactions, according to Kohn[28] are kinetically controlled with the reactions proceeding exothermically until one of the reactants is used up. There are five possible mechanisms in the rate determining step:[29] (i) chemical reaction (ii) diffusion (iii) sublimation (iv) fusion and (v) crystallisation.

Sintering can be considered as the formation of solid products of reaction of contiguous particles but also occurs between particles of the same composition. The driving force

TABLE 2.7

Temperature of thermal decomposition of carbonate minerals

Mineral	Formula	Temperature/°C	Ref.
Calcite	$CaCO_3$	810-920	23
Magnesite	$MgCO_3$	580-630	24
Dolomite	$MgCO_3.CaCO_3$	745-870	25
Siderite	$FeCO_3$	500-585	26
Ankerite	$(Ca(Mg,Fe)(CO_3)_2)$	variable	27

in the sintering process is the reduction in surface energy by decreasing the surface area.

There are four possible sintering mechanisms, vapo risation and condensation, surface diffusion, volume diffusion and viscous flow. Mass transfer by viscous flow is the predominant mechanism and is the one pertinent to this study. Viscous flow is influenced by surface tension which varies with the curvature of the surface, bringing about transfer of material from regions of high pressure (convex surfaces) to regions of low pressure (concave surfaces).[30] The rate of transfer will depend on the temperature, surface tension and coefficient of viscosity of the liquid. The liquid phase may be formed by a solid state reaction in which the product is a low-melting-point compound.

If the temperature at which the mineral mixture is subjected to is high enough, viscous flow will continue and a liquid phase will be the major component. The rate of formation of a homogeneous liquid will depend on the viscosity, surface tension, atmosphere (in some cases) and the miscibility of the remaining phases.

Watt and Wilkins[31] studied the rate of assimilation of coal minerals within ash melts using mixtures of muscovite, kaolinite, pyrite and quartz. The investigators found that when the mixtures were heated, the first phase observed to melt was pyrite which flowed freely into the kaolinite where it was found to oxidise and then solidify as magnetite ($FeO.Fe_2O_3$). The next phase to melt, at about 1300 °C, was muscovite which was found to assimilate initially the kaolinite, then the calcium oxide (which was presumably an impurity present in muscovite) followed by the

magnetite with quartz being the most resilient to melting. The study has been useful in giving a qualitative understanding of the processes involved in the melting of ash.

A recent study by Mitchell and Gluskoter[32] determined the mineralogical content of several low temperature ashes obtained from American coals and the effect of temperature on the minerals. The ash was heated at 100 °C intervals in the range 400 °C - 1400 °C for half an hour. The crystalline phases present in the heated ash were qualitatively determined by X-ray diffraction techniques. The investigators found evidence of significant reactions between minerals. Reaction products such as gehlenite ($2CaO.Al_2O_3.SiO_2$) and anorthite ($CaO.Al_2O_3.2SiO_2$) were observed at about 800 °C for some coal ashes. In all cases where an iron oxide crystalline phase formed as the initial product it was found to be hematite (Fe_2O_3) while magnetite ($FeO.Fe_2O_3$) formed at higher temperatures (1300 °C - 1400 °C). The phases observed at temperatures above 1400 °C were magnetite, gehlenite or anorthite and glass with no original coal mineral being present. This would have also been the case at lower temperatures ($\sim$900 °C) if it were not for the persistence of the coal mineral quartz (SiO_2).

Padia[33] has studied the combustion of coal under simulated combustion conditions. By adjusting the rate of fuel supply, various flame temperatures could be achieved. He observed that at all temperatures above 1227 °C the ash was nearly completely fused even though the particles had a calculated residence time of about 1 second. Padia also observed that the ash particles had formed hollow spheres (cenospheres). These are formed from the gases such as sulphur dioxide and carbon dioxide from the thermal break-down of various minerals expanding into a viscous melt.

Thus it is feasible to suggest that the minerals present as a mixture in coal are nearly completely fused within the burner zone of a boiler. Quartz is the most resistant to dissolution. Cooper[34] has shown that the rate of dissolution of quartz spheres in a sodium silicate melt is governed, under forced convection conditions, by the diffusion through the boundary layer. The radii of quartz spheres in a sodium silicate glass (nominally 60% SiO_2) at 950 °C were measured after a given time. The plot of radius against time indicated that the value of the diffusion coefficient for the dissolution of quartz in the melt was 3.3×10^{-6} cm^2 s^{-1}. The rate of dissolution was approximately linear for spheres of 10 to 5 mm radius at 1.3 μm s^{-1} but increased to a value of about 2 μm s^{-1} for a sphere of radius 2 mm.

For quartz crystals in a complex liquid such as molten coal ash, the dissolution rate will depend on the diffusion coefficient and the original quartz particle size. The diffusion coefficient is dependent mainly on the chemical composition of the melt local to the crystal and the temperature. There has been no investigation of the rate of dissolution of quartz in coal ash melts and it is apparent that the values obtained would vary considerably with the chemical composition. The presence of undissolved quartz will affect significantly the chemical composition of the liquid phase formed within the burner zone.

2.8 FORMATION OF BOILER DEPOSITS

Deposits are formed in p.f. fired boiler due to the adhesion of fused or partially fired ash particles to the exposed surfaces of the boiler. These surfaces may be clean tubes or that of deposits already present. The most troublesome deposits are the hard-bonded glassy slags on the furnace walls as they markedly affect the thermal efficiency of the boiler. Fouling deposits cause less reduction in boiler efficiency as they are formed on convection surfaces. Studies of the mechanisms of deposit formation have involved full-scale investigations and laboratory studies which have led to various models of slagging and fouling being proposed.

Pulverised-fuel (p.f.) fired boilers were developed to overcome the severe slagging and fouling problems experienced with stoker-fired boilers. The burner zone temperatures in p.f. boilers are a few hundred degrees less than those observed in the fuel bed of a stoker-fired boiler and thus p.f. boilers were not expected to experience deposit formation. In 1946 no significant slagging and fouling of p.f. fired boilers operating in Britain was reported[35] but by 1947 a number of British boilers were reported to be suffering from slagging problems.

A number of studies in the 1950's attempted to ascertain the cause of the formation of the hard bonded deposits found in the superheater region of boilers during this period. An early study by Carlile[36] observed that deposits removed from fifty British power stations contained high proportions of alkali sulphates and pyrosulphates. A chemical analysis of a sample showed an alkali content of about 25% whereas the coal ash

contained only 1% alkali. Other studies confirmed that alkali oxide volatilisation was the initial step in the formation of some types of deposits.[37,38,39] The accepted mechanism was that sodium and potassium oxides volatilised from the coal and ash particles within the burner zone. On reaching the boiler tubes (containing steam at about 420 °C) the oxides would condense possibly reacting with the sulphur oxide gases (SO_2 and SO_3) forming an alkali matrix. The alkali matrix traps the high melting point ash particles forming the actual deposit.

Other deposits reported[40] were observed to have been formed by the initial presence of a calcium sulphate matrix. As calcium sulphate has a relatively high melting point (1300 °C), the presence was considered to be due to the formation of calcium chloride (b.p. > 1600 °C) in the burner zone which condensed on the boiler tubes and reacted with the sulphur oxides.

2.9 FORMATION OF SLAG DEPOSITS

While there have been many studies of fouling deposits, formed initially by an alkali or calcium sulphate sticky-matrix there have been few detailed investigations of the formation of slagging deposits. A slag is defined, albeit qualitatively, as a glassy or semi-vitreous deposit formed on surfaces of the boiler receiving radiant heat.

In 1964, Watt[41] reviewed the mineralogy of coal-ash slags and found that no detailed description of slags was available. Most of the data presented was that obtained from blast furance slags!

Two recent reports by Hanusch and Grimshaw[42,43] gave a detailed analysis of boiler deposits removed from a South African boiler burning coal with a lignitic-type ash. The gas temperatures were determined at the various sampling points and the deposits removed manually after a boiler shutdown. The deposits were observed to be predominantly homogeneous with no evidence of alkali or calcium matrix deposits. Apart from calcium sulphate and quartz being present the crystalline phases determined by quantitative X-ray diffraction techniques appeared to have crystallised from a vitreous melt. The predominant crystalline phase was anorthite ($CaO.Al_2O_3.2SiO_2$) with anhydrite ($CaSO_4$) and magnetite ($FeO.Fe_2O_3$) as the most dominant of the minor crystalline phases present. The glass content was determined to be dependent on the gas temperature in the region of the sample, the proportion of glass decreasing with decreasing temperature. The evidence indicated that the ash had been completely fused within the burner-zone of the boiler.

A full scale study on the influence of coal mineral matter on slagging of utility boiler was undertaken by the Battelle Institute for the Electric Power Research Institute (EPRI)[44] of the United States. The investigation involved the study of slags removed from five American boilers. No evidence of alkali or calcium matrix was observed but many samples removed showed significant viscous flow between particles. Phase analysis was not undertaken but electron micrographs showed that crystallisation within the vitreous deposit had taken place. The authors could not determine any correlation between mineral matter and furnace slagging.

Friedrich et al.[45] have studied the deposits formed by two different Canadian coals with lignitic-type ashes in a pilot scale

boiler. The deposits formed were vitreous slags and no evidence was observed for the alkali matrix nor the calcium sulphate deposits. Crystalline phase analysis by petrological microscopy and powder X-ray diffraction showed that the only original coal ash mineral in the deposit was that of quartz. The other crystalline phase observed in the deposit of one type of coal was mullite ($3Al_2O_3.2SiO_2$) whereas the other phase present with the quartz in the deposit of the other coal was anorthite ($CaO.Al_2O_3.2SiO_2$) with some evidence of hercynite ($FeO.Al_2O_3$), all of which had crystallised from a vitreous melt.

Livingston, Sanyal and Williamson[46] have used petrological microscopy, scanning electron microscopy and electron microprobe analysis to obtain detailed morphological and mineralogical analysis of a number of slag deposits removed from a U.K. and a Finnish power station. The crystalline phases observed, excluding quartz, had grown from a vitreous melt. Anorthite, mullite and hercynite were determined in varying proportions in a glassy matrix for the deposit removed from the Finnish power station. The study led to a detailed description of a complete slag deposit. Livingston, Sanyal and Williamson distinguished between three different regions of the deposits by the degree of crystallinity. The region nearest the boiler tube was observed to be predominantly glassy. The outer region of the deposit was a mass of sintered material with some particles partially assimilated into a predominantly crystalline matrix. The intermediate region had an increasing amount of crystallinity between the glassy inner region and the crystalline outer layer.

2.10 LABORATORY STUDIES OF BOILER DEPOSITS

The alkali sulphate/pyrosulphate or calcium sulphate matrix mechanism only accounts for the initial capture of fly ash by the sticky deposit. The growth of the deposit will depend on the local temperature, and the factors which affect the rate of sintering and viscous flow properties. Smith[47] studied the sintering of fly ash and observed that the temperature at which sintering begins varies with particle size, iron content and alkali oxide content. The variation with particle size would be expected from the theory of sintering processes; the author observing the lowest sintering temperatures for particles 17-27 μm in diameter. The behaviour of iron oxide on sintering in air was found to be complex. For some coal ashes studied, addition of 10 wt % iron oxide was found to decrease the sintering temperature but on addition of 29% iron oxide the sintering temperature was observed to increase, indicating that the properties of iron oxide had become the determining factor. The effect of alkali oxide content was determined by washing different samples of fly ash and determining the sintering temperature. All the samples had higher sintering temperatures after the removal of the water soluble alkali content.

Raask[48] studied the fusion of silicate particles in a vertical tube furnace. He observed that coal mineral particles such as quartz and muscovite were completely transformed to spherical particles at 1600 K (1327 °C) for up to 0.5 s. The transformation of an irregularly shaped particle at a given temperature for a given time was dependent on the radius, viscosity and surface tension. The viscosity required for the

transformation was calculated to be several orders of magnitude greater than that required for viscous flow under gravity (25 Ns m^{-2}). Scanning electron microscopy of fly ash particles showed that all the mineral particles had been transformed to spheres; cenospheres (hollow) and plerospheres (spheres containing other spheres).

Recent studies by Moza and Austin[49] have illustrated the adhesion of fused ash to various steel alloys at 550 °C. The strength of the adhesion was dependent on both the chemical composition of the ash melt and the alloy. This adhesion of molten ash to wall tubes must be a possible mechanism for the initial formation of a slag deposit. Crystalline phases were observed in the region of the deposit furthest away from the glass-alloy interface which is analogous to the observations of true slags by Livingston et al.[46]

2.11 MODELS OF DEPOSIT FORMATION

While there seem to be different mechanisms for the initial adhesion of fly ash particles on heat absorbing surfaces, the differences between slags and fouling deposits is the degree of sintering by viscous flow.

Raask[48] used the following relationship derived by Frenkel to describe the coalescence of deposited particles by viscous flow:

$$\left(\frac{x}{r}\right)^2 = \frac{3\gamma t}{2\eta r}$$

where x is the radius of neck growth between the spherical

particles of radius r, γ is the surface tension, η the viscosity and t is the time. The term $(x/r)^2$ is a parameter of degree of sintering and could be related to the strength of the boiler deposit after time t, given by

$$s = k(x/r)^2$$

substituting for $(x/r)^2$

$$s = k.\frac{3\gamma t}{2\eta r}$$

where k is a constant, and differentiating with respect to t

$$\frac{ds}{dt} = \frac{3k\gamma}{2\eta r}$$

which is the rate of building of a slag deposit. Therefore both the strength and the rate of build-up of a deposit are proportional to the radius of the original particle and the viscosity. The surface tension and the radius of the particle do not vary in magnitude compared to that of viscosity.[48] Thus the rate of growth of a deposit is dependent predominantly on the viscosity of the liquid phase. As viscosity is dependent on the chemical composition and temperature the rate of growth of a deposit must be a function of these two variables. Lauf[50] has shown the dependence of viscosity on the formation of fly ash cenospheres. The viscosity was calculated by two different empirically derived methods[51,52] from the chemical composition. It was observed that for an ash with a viscosity of greater than $\log_{10}$ 4.11 at 1260 °C, all the ash was converted to cenospheres and had passed through the boiler. At lower viscosities, cenosphere formation was rapidly reduced with increased deposit formation. These results fit the model developed by Raask, that is, with an increase in viscosity both the strength and the rate of build-up of deposit will decrease. Furthermore there must be a critical value of η when ds/dt and s

approach zero. In the case of slag deposits, Livingston et al.[46] have observed varying degrees of viscous flow in the outer region of slags. The rate of growth of the slag will depend on the rate of assimilation of the fly ash particles into the slag proper. Significant crystallisation of the fly ash particles was observed which would affect the viscosity of the residual liquid phase. The actual effect will depend on the degree of crystallisation, the crystalline phases and their morphology and the chemical composition of the ash particles. The crystallisation characteristics of a vitreous melt of a given composition are primarily temperature dependent. Therefore all the variables in the model developed by Raask for a given coal ash chemical composition are dependent on the temperature.

2.12 PREDICTION OF SLAGGING PROPENSITY

Slagging propensity is the term used by boiler engineers to describe the ability of a coal and hence its ash to form a deposit when burnt in a power station. There are empirical and theoretical methods used to evaluate the slagging propensity of a coal to determine its suitability for firing. The major empirical test used is the measurement of ash fusibility, under standard conditions. The theoretical methods are factors calculated from the chemical composition of the ash.

There are two standard fusibility tests in use: one British[53] and the other American.[54] Both are similar in principle and design but the British test is more rigidly defined. In the British Standard test, ash is produced from the coal by roasting in air to 800 °C. The ash is ground to pass through a

163 μm B.S. mesh and is then formed into a trilateral pyramid by means of a mould with rigidly defined dimensions. The pyramid or cone, as it is referred to, is placed on a refractory tile and placed in a furnace at 900 °C. The tile and ash-cone are left for ten minutes, then the temperature is increased at the rate of 10 °C per minute. The sample is viewed through a telescope in which a ruled graticule is incorporated which is used to determine the degree of deformation of the cone while being heated. Three deformation temperatures are recorded in the British standard and four in the American standard. The definitions and tolerances of each of the deformation temperatures are listed in Table 2.8. The tests are carried out both in air and in a reducing atmosphere (H_2:CO_2, 1:1 initial volumes in the British standard). With reference to Table 2.8, the difference in the temperatures between the fluid flow and the deformation temperature is generally taken to be the range of temperatures within which the ash will be sticky or viscous.

The ash fusion temperatures of a coal ash are used both to decide the coal's suitability for firing and as parameters in boiler design. Generally if the coal ash has low fusion temperatures it would be expected to have a higher slagging propensity than a coal ash with high ash fusion temperatures. If a boiler is to be designed the engineers require the fusion temperatures of the ashes of the coals which are to be fired. The engineers can incorporate various features in the design, such as reduced gas temperatures and facilities for soot blowers if the fusion temperatures are relatively low. Conversely if the fusion temperatures are high, the designer can utilise higher gas temperatures without fear of significant slagging problems.

TABLE 2.8

Characteristics determined in the standard ash fusion tests

Characteristic temperature	Observation of cone	Tolerance/°C between operators
British Standard 1016		
Deformation	First rounding of tip of cone	80
Hemisphere	Height = ½ width of base	50
Flow	Height = ⅓ height at hemisphere temperature	80
ASTM D-1857		
Initial deformation (DT)	First rounding of tip of cone	70
Softening (ST)	Height = width	55
Hemispherical (HT)	Height = ½ width	55
Fluid (FT)	Profile becomes flat layer, maximum height 2.5 mm	85

While the results from ash fusion tests are used extensively it has been well known that the results do not represent the true behaviour of coal ash in a boiler.[55] The determination of the degree of deformation is a subjective test, hence the large tolerance allowed (Table 2.8). Ash particles in a boiler have totally different temperature-time histories than the ash cone in the standard tests. Recent experiments by Huffman et al.[56] have illustrated that the assumptions inherent in the ash fusion tests were incorrect. After determining the ash fusion temperatures (according to ASTM-D1857) ash cylinders were prepared and treated at the fusion temperatures for a given time in a constant atmosphere. The quenched samples were studied by ^{57}Fe Mossbauer spectroscopy and scanning electron microscopy with automatic image analysis and X-ray diffraction techniques. The results showed that the initial deformation temperature is not the temperature at which the liquid phase first appears. Analysis of samples treated at their respective initial deformation temperature (IDT) showed that there was a significant amount of liquid phase present; all samples left at their IDT's for up to 45 minutes appeared to be at the fluid temperature. All the phases observed in the quenched ash samples, except that of quartz, were due to high temperature transformation and interaction of the mineral phases present in the original high temperature ash.

Though the fusion test is patently unreliable on both theoretical and experimental grounds it is used, and will continue to be, until a more accurate, reliable and straightforward method is devised and accepted by the power generation industry.

2.13 PREDICTION OF SLAGGING PROPENSITY FROM ASH ANALYSES

The chemical analyses of coal ashes, in terms of oxides, are used to give an indication of slagging propensity by the calculation of various factors. They have been extensively reviewed by Winegartner.[57] For simplicity only the most commonly used factors have been tabulated in Table 2.9 along with known parameters and limitations. The detailed study by EPRI[44] on the slagging of American utility boilers also involved the correlation of some of the factors and the results have been included in this Table.

The various factors outlined have been developed from very small data bases and are extremely inaccurate for coal ashes not lying within the ranges originally studied. As seen in Table 2.9 no factor has been derived for coals with lignitic type ashes and thus slagging propensity predictions can only be based on ash fusion tests. The factors give very little insight to the actual slagging mechanism according to the model developed by Raask (section 2.11) except that they can give a qualitative indication of viscosity. Sage and McIlroy[58] have correlated base to acid ratio to coal ash viscosity and ash melting. Generally the higher the value of the ratio the lower the viscosity and hence the higher the likelihood of deposit formation. Attig and Duzy[59] developed the slagging factor R_s empirically. While the base to acid ratio gives an indication of viscosity the coefficient λ is intended to indicate the viscous plastic range of the ash. The fouling factor R_f, also developed empirically by Attig and Duzy, was based on the alkali matrix bonding model but correlates well with the observations of Smith.[47]

$$\lambda = \frac{\%\text{sulphur}}{}$$

TABLE 2.9

Slagging factors calculated from coal ash composition

Parameter	Definition	Suggested values	Correlation
Base to acid ratio =	$(CaO + MgO + Fe_2O_3 + K_2O + Na_2O) \div (Al_2O_3 + SiO_2) = B/S$	None	moderate slagging for a unit which experienced severe slagging
Silica percentage = SP	$SiO_2 + Fe_2O_3 + CaO + Al_2O_3 + MgO = 100$ $SP = SiO_2/(Al_2O_3 + Fe_2O_3 + CaO + MgO)$	None	Low slagging for a unit which experienced severe slagging
Slagging factor = R_s	$R_s = (B/S) \times \%$ sulphur	<0.6 low 0.6-2.0 medium 2.0-2.6 high >2.6 severe	moderate slagging for a unit which experienced severe slagging
Fouling factor = R_f	$R_f = (B/S) \times \% Na_2O$	<0.2 low 0.2-0.5 medium 0.5-1.0 high >1.0 severe	n.d.

2.14 CALCULATION OF VISCOSITY OF SLAGS FROM ASH ANALYSES

In the model of slagging developed by Raask[48] the strength and rate of build-up of a slag are given by the two relations:

$$\text{strength of deposit} = s = \frac{3\gamma t}{2\eta r}.k$$

$$\text{rate of build-up of slag} = \frac{ds}{dt} = \frac{3\gamma k}{2\eta r}$$

It is possible to calculate the viscosity from the ash analysis using a number of methods. The two methods in use are:

(a) Nicholls and Reid[60]

The silica percentage is calculated as given in Table 2.8 and the viscosity interpolated using curves of viscosity-temperature-silica percentage derived experimentally.

(b) Watt and Fereday[52]

The composition is normalised so that % SiO_2 + % Al_2O_3 + % Fe_2O_3 + % CaO + % MgO = 100

$$\log_{10}\eta = \frac{10^7 \times M}{(T-150)^2} + C$$

[M = 0.00835 x % SiO_2 + 0.00601 x % Al_2O_3 - 0.109

C = 0.0415 x % SiO_2 + 0.0192 x % Al_2O_3 + 0.0276 x % Fe_2O_3 + 0.16 x % CaO - 4.92]

Where T is the temperature in °C and η is the viscosity (Pas).

These methods are used as viscometric determinations are extremely time-consuming and expensive, but are only valid over the fluid Newtonian range. That is, the methods only determine the viscosity when the ash is completely molten whereas deposits may be formed at temperatures well below the liquidus temperature. The viscosity of coal ash melts have been studied

by a number of workers, notably Reid,[61] Nicholls and Reid,[60] Reid and Cohen,[62] and Watt and Fereday.[52] The log viscosity/temperature curves for two coal ash melts have been reproduced from Reid and Cohen's studies[62] with conversion of temperature to degrees Celsius in Fig 2.1. As can be seen for both curves there is a temperature above which the curve is linear, i.e. the flow of the melt is Newtonian. Below the particular temperature called the temperature of critical viscosity (T_{cv}) the viscosity becomes non-Newtonian or plastic. This is due to crystalline phases present in the melt causing significant drag; the actual effect will depend on the volume fraction of crystalline material and the aspect ratio. At lower temperatures the viscosity is so great that the ash is effectively frozen.

The temperature of critical viscosity has been considered an important indication of slagging propensity. Generally, the higher the value of T_{cv} the lower the slagging propensity. With reference to Fig.2.1, ash Y would be less likely to form a slag deposit than ash X. Hoy, Roberts and Wilkins[63] have developed the following relation to calculate the temperature of critical viscosity.

The ash composition is normalised so that

$$\% SiO_2 + \% Al_2O_3 + \% Fe_2O_3 + \% CaO + \% MgO = 100$$

and, using the normalised values

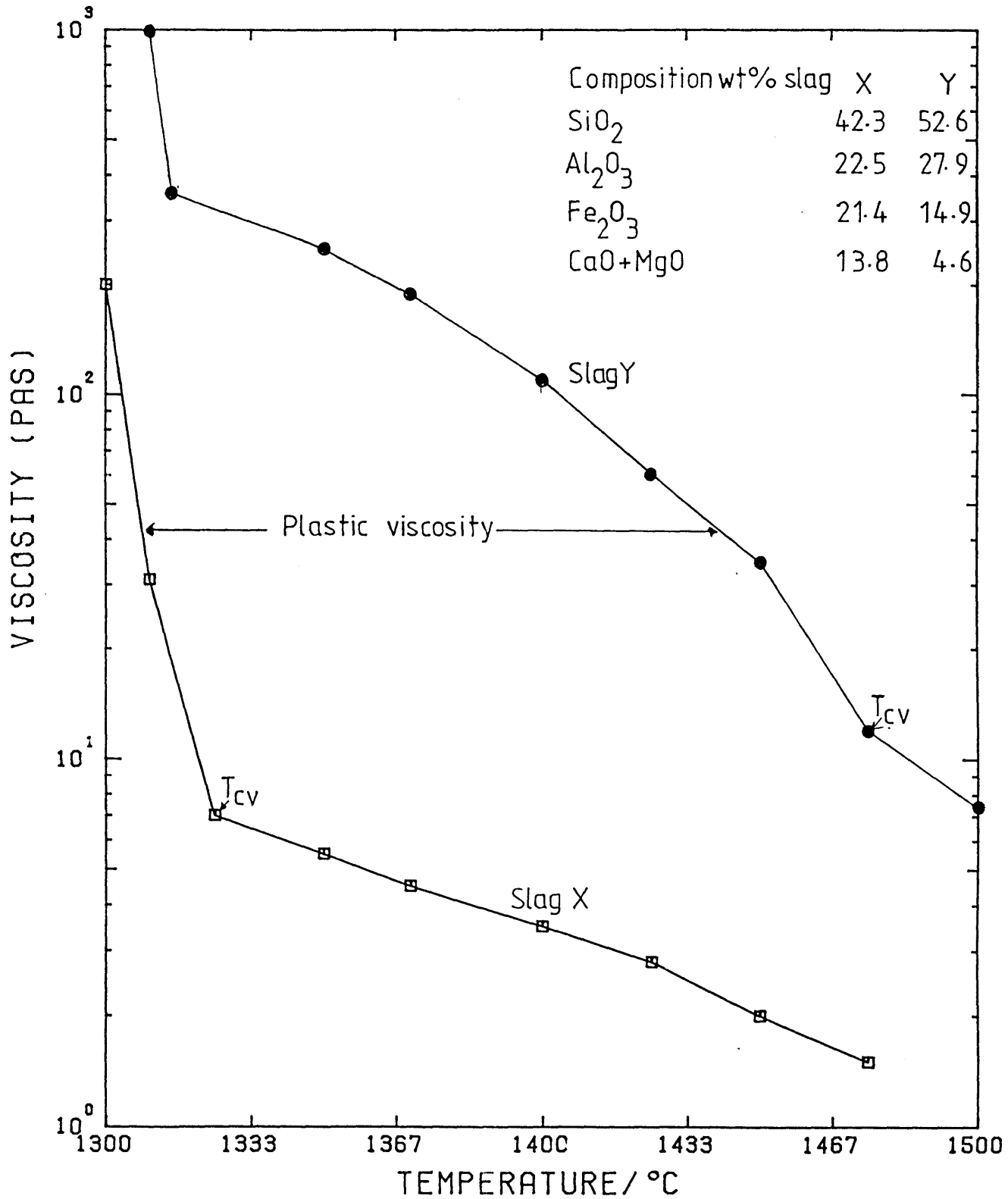
$$T_{cv}/°C = 2990 - 1470 \times \left(\frac{\% SiO_2}{\% Al_2O_3}\right) + 360 \times \left(\frac{\% SiO_2}{\% Al_2O_3}\right)^2$$

$$- 14.7 \times (\% Fe_2O_3 + \% CaO + \% MgO)$$

$$+ 0.15 \times (\% Fe_2O_3 + \% CaO + \% MgO)^2.$$

Not all coal ash melts experience a temperature of critical

Fig 2.1. Viscosity-temperature curves of two coal-ash slags.
(From the data of Reid and Cohen[62].)



viscosity nor does the value give any indication of the viscosity at or below T_{cv}. The slagging model is dependent on the viscosity, along with the surface tension and radius of the particles, of the liquid phase after crystallisation. The temperature of critical viscosity can only give a qualitative indication of slagging propensity.

Gibb[64] has recently developed a more accurate yet semi-quantitative method for determining slagging propensity from coal ash viscosity studies. The author measured the viscosity/temperature relationship of nine British coal ash slags using both heating and cooling cycles. The log of viscosity against temperature curves showed a distinct difference between the "heating" and "cooling" results which the author discussed in terms of supercooling of the melt. (The degree to which melts can remain relatively fluid below their apparent melting points.) On heating some supercooled melts rapid devitrification was observed and the samples did not exhibit fluid flow over a relatively large temperature range (~300 °C), which according to the author was due to heterogeneous crystallisation of the melt. The general observation reported was that the ease of crystallisation, i.e. the reluctance to form a supercooled liquid, increases with the base-to-acid ratio (therefore increasing slagging propensity) and this could explain in part the devitrification observed in the "heating" cycle curves.

Gibb arbitrarily chose the temperature at which the melt had a viscosity of 10^6 Ns m^{-2} as a slagging index and designated it as $T_v(6)$. The general observation reported for the slags studied was that the lower the $T_v(6)$ values, the more likely the slag to form a

supercooled glass and hence the lower the slagging propensity.

The difficulty with the Gibb method is that it relies on the determination of $T_v(6)$, though a value could be calculated by using the relationship derived by Watt and Fereday[52] (p.57). The small number of ash melts studied limits the extension of the slagging index $T_v(6)$ to a wide range of coals.

2.15 HIGH TEMPERATURE MICROSCOPY

The standard ash fusion tests though extensively used are not the only methods that can be used to observe the fusion characteristics of coal ash. Various techniques have been developed and used to heat an ash sample while observing the changes through a microscope. The most highly accurate technique is that developed by Welch[65] after Ordway[66] using a heated thermocouple tip.

Initial high temperature microscopy studies attempted to correlate the observations with the standard ash fusion temperatures. The method did not give a good correlation as the principles involved are completely different, the fusion tests observes the effect of a liquid phase present in the sample whereas the microscopic method can observe directly the softening of ash particles and the presence of a liquid phase. Jones et al.[67] and Vasser[68] found that microscopic observations gave closer correlation to full scale boiler ash behaviour than the corresponding standard ash fusion observations.

A recent laboratory study of the coal minerals by Nolan et al.[69] made use of the high-temperature microscope. Two low temperature lignitic ashes with different lime contents were studied on the instrument, showing different fusion characteristics (though their respective ash fusion temperatures were very similar). The crystallisation behaviour of the two ashes were also studied on the high temperature microscope by heating a sample of the ash to 1550 °C for 10-15 minutes to ensure a homogeneous melt, and then decreasing the temperature of the thermocouple by several hundred degrees to a predetermined temperature and so induce crystallisation. The crystalline phases produced in the melt were determined by microscopic observation (both on the "hot" in situ and quenched samples) and electron microprobe analysis. The results showed greatly differing crystallisation behaviour between the two ashes studied, which correlated very well with the prediction made from the high temperature phase diagram of the system $CaO-Al_2O_3-SiO_2$ when the normalised compositions of the ashes (% CaO + % Al_2O_3 + % SiO_2 = 100) were considered and the crystallisation paths determined. The authors observed that the liquidus temperatures of the ashes were about 150 °C less than the those predicted from the three component phase diagrams attributed to the fluxing properties of the other oxides.

High temperature microscopy, though not often used for studying the thermal behaviour of coal ash appears to be a more accurate technique than the cone fusion tests. By studying the fusion of low temperature ash a more realistic indication of the processes involved in ash fusion may be achieved. The in situ crystallisation of coal ashes by high temperature microscopy is restricted to those of lignitic-type, i.e. low iron oxide content

(less than 6 wt % Fe_2O_3). The observations of the temperature at which a liquid phase first appears, the apparent liquidus temperature and the crystalline phases present in subsequently cooled melts are all important in the prediction of slagging propensity.

2.16 ELECTRICAL RESISTANCE OF COAL ASH

A recent paper by Cumming[70] has indicated that the fusibility of ash can be observed by the measurement of the D.C. resistance of an ash sample. The author worked on the assumption that finely ground and tightly packed coal ash would act as a semiconductor with regard to its resistance-temperature characteristics, i.e. $\log \rho \propto \frac{1}{T}$. Thus the formation of a small amount of a liquid phase between the electrodes would affect the solid-state characteristics of the ash increasing the conductivity of the sample.

2.17 PHASE EQUILIBRIA STUDIES

Coal ash contains up to eleven oxides, the relative proportions of which may vary considerably between various coals. This section deals with the study of the interactions between the major oxide components and the correlations with true ash fusion behaviour. Phase diagrams of relevance to coal ash compositions are introduced and the methods used to determine the phase equilibria reviewed. The valuable data obtainable from phase diagrams for studying coal ash melts is described.

Of particular interest to this study has been the correlation of the ash fusion test results to the high temperature chemistry of the coal ash. An early study by Thiessen et al.[71] showed the influence of eutectic (minimum melting) compositions on the thermal behaviour of the ash-cones which was similar to the behaviour of pure inorganic oxides. The authors suggested that the coal ash should be considered in terms of fusion as a mixture of inorganic oxides as given by the standard chemical analysis. After comparing the fusion characteristics of four component mixtures and coal ashes (with added alumina) the authors came to the conclusion that the initial deformation was comparable to the melting of the lowest fusing material. Later studies by Gould and Brunges[72] supported this conclusion. The subsequent fusion temperatures will be dependent on the viscosity, chemical reactions, and the thermal decomposition and rate of dissolution of the remaining crystalline phases in the liquid phase.

In two detailed studies of coal ash fusion temperatures Estep et al.[73,74] determined that the fusion characteristics of coal ash were dominated by the major four components, i.e. the proportions of silica, alumina, ferric oxide and lime. The authors produced curves of ash fusion temperatures against composition which were used to make predictions of the fusion temperatures of coal ashes which were found to be within the tolerance of the experimental method. The fusion temperatures of four-component mixtures of the major oxides based on known coal ash compositions were generally the same as the true ash fusion temperatures which agreed with Thiessen et al.[71]. The authors also studied the effect of addition of lime, magnesia or sodium oxide on the fusion temperatures of a number of ashes and synthetic mixtures based on

coal ash compositions. The effects observed were that lime, magnesia and sodium oxide all acted as fluxes until, for lime and magnesia only a certain level of additive was reached (characteristic of the original composition) when the addition of more lime or magnesia increased the fusion temperatures.

An early review by Barrett[75] discussed the chemical background to the fusion and flow properties of coal ash. The author showed that, theoretically for a simple two-component system which had a single eutectic composition, the curve of fusion temperature against composition would follow closely the liquidus curve for the binary system. The locus of the softening temperatures of FeO, SiO_2 mixtures was shown to follow closely the liquidus curve of the system. The author emphasised that synthetic ash mixtures had to be heated at about 850 °C for a significant time before initial deformation temperatures should be determined. The treatment increases the rate at which the liquid phase could be formed in the sample presumably by solid state reactions.

Rieke[76] made the assumption that coal ash was just impure kaolin and studied the system kaolin-FeO. Barrett plotted Rieke's results of initial deformation temperatures on the phase diagram of the binary system FeO-SiO_2, but the curve did not correspond with the liquidus. This could have been due to the presence of alumina (a major component of kaolin) but may also have been due to the correlation of the behaviour of minerals to that of pure oxides with a method which would not decompose the mineral matter into the component oxides.

Barrett came to the conclusion that the fusion characteristics of coal ashes were related to their respective chemical composition

and not the mineralogical content. The limited amount of relevant phase equilibrium data available at the time of the review (1945) prevented the author from more detailed correlations and discussion.

A number of quantitative correlations between ash fusibility and chemical composition were reported and discussed by Barrett. The earliest attempt at correlation was by Prost[77] who derived the following refractory quotient, Q,

$$Q = \frac{\text{O in } Al_2O_3}{\text{O in CaO} + \text{O in } Fe_2O_3 + \text{O in MgO}} \div \frac{\text{O in } SiO_2}{\text{O in } Al_2O_3}$$

The fusion temperatures were found to increase with increasing values of Q but high iron oxide content caused anomalies.

Nicholls and Selvig[78] plotted the ratio

$$R = \frac{Al_2O_3 + SiO_2}{Fe_2O_3 + CaO + MgO + Na_2O + K_2O}$$

against the softening temperature for some U.S. coals which gave a reasonably average curve (but with some points 150 °C out).

Barrett plotted the compositions of coal ashes studied by Nicholls and Selvig on the compositional diagrams of Estep et al.[73] and observed that the predictions of softening temperatures obtained were more reliable than an actual laboratory determination. The results confirmed that the coal ash, in terms of fusibility, can be regarded as a four-component mixture of the major oxides with closer correlations obtained by taking an empirical account of the effect of the minor constituents present in the ash. Of the minor component oxides, the most prominent are magnesia, potassium oxide, and sodium oxide, with minor presence of titania and

phosphorus pentoxide. The empirical effects of these oxides have been evaluated; titania and phosphorus pentoxide can be regarded as equivalent to silica, the alkali oxides and magnesia can be regarded in a general sense as having an effect similar to lime.

Schaefer and Demorest[79] assumed that over the composition ranges of most coal ashes the liquidus curves for the systems involved may be approximated by straight lines. By making the further assumption that the fluxing action of lime (and thus, equivalently, of MgO, K_2O and Na_2O) was six tenths that of FeO, they derived the following relation for the softening temperature (ST).

$$ST = f(Al_2O_3/SiO_2) \times \left(\frac{SiO_2 + Al_2O_3}{FeO + 0.6(CaO + MgO + K_2O + Na_2O}\right)$$

A curve was obtained by plotting the softening temperature of 98 coal ashes against the relationship in brackets. The average error was within the accuracy of the experimental method but Barrett[75] believed that the good agreement was due to the small number of ashes studied.

Jones and Butler[80] assumed that the fluxing action of FeO, CaO, MgO, Na_2O and K_2O were all equivalent and used a curve based on chemical analysis and softening temperatures to determine the reduction of the liquidus temperature from the phase diagram of the system Al_2O_3-SiO_2.

The fusion characteristics of a number of Indian coal ashes, and their corresponding four-component synthetic mixtures were determined by Dutta et al., both in air[81] and in a mildly reducing atmosphere.[82] The effects of additions of lime, magnesia, iron

oxide and sodium oxide on the softening temperatures were studied in greater detail than the Estep et al. investigations[73,74] with larger additions of the oxides.

The effect of addition of lime was observed to be more complex than that determined by Estep et al.. While the initial addition of lime caused reduction of softening temperature the plot of softening temperature against percent lime indicated that the effect of increased lime content was dependent on the original coal ash composition. A similar effect was observed for the addition of magnesia to the two ashes studied whereas the addition of sodium oxide was observed to decrease the softening temperature linearly over the range of additions.

The effect of additions of iron oxide on the softening temperature as determined in air was observed to be more complex. Low levels of iron oxide (less than 10 wt %) caused reductions in the softening temperature with a fluxing effectof 15-16 °C per wt % Fe_2O_3. Further addition of iron oxide decreased the fluxing effect and in some cases the softening temperature was observed to increase. The authors attempted to correlate the effects observed to the lime content and silica to alumina ratio but without success; the softening temperatures for all the coal ashes studied were observed to reach a maximum value in the range 1370 - 1395 °C at about 44 wt % Fe_2O_3.

The effect of the iron oxide additions on the softening temperature as determined in a mildly reducing atmosphere (1:1 hydrogen:steam mixture) was generally observed to lower the value for all the samples studied. The authors referred to the iron oxide present as Fe_2O_3 but, under the conditions used, some FeO

would be expected to be present in the sample and would account for the lower softening temperatures observed as FeO is a better flux than Fe_2O_3.

The authors also plotted the softening temperatures determined for the series of lime additions against the lime content of the ternary system $CaO-Al_2O_3-SiO_2$ for various silica to alumina ratios. The curves obtained followed the liquidus curve quite closely indicating that the observations of the effect of the addition of lime on the softening temperature was governed by the three major components, that is, lime, silica and alumina.

Winegartner and Rhodes[83] used the concept of basic and acidic oxides (p.**56**) contained in coal ash to calculate the ash softening temperature using a regression analysis computer programme. The results of the predictions of the softening temperatures obtained were within the tolerance of the experimental determination.

Recent studies on the behaviour of coal ash at high temperature, both in a reducing atmosphere and in air, by Huffman et al[84] have shown that the assumption inherent in the theory of the ash fusibility tests were incorrect. The fusion temperatures were determined for a number of coal ashes of different chemical compositions according to the latest ASTM method. The results were then used in a series of quenching experiments where a cylinder of ash was treated at one of its previously determined fusion temperatures for a given time in a constant atmosphere. The heat-treated cylinder was then quenched in air. The phases present in the sample were determined by ^{57}Fe Mössbauer spectroscopy, scanning electron microscopy with automatic image analysis, and powder X-ray diffraction. Mössbauer spectroscopy is a powerful

instrument in the study of iron in compounds and can distinguish between the iron in glass, tetrahedral sites or octahedral sites. This study was the first detailed phase analysis of the ash treated in the fusion tests. The results showed that the initial deformation temperature (IDT) was not the temperature at which a liquid phase first appears. The analysis of the samples treated at their respective IDT showed that there was a significant amount of a liquid phase present. All samples left at their IDT's for up to 45 minutes appeared to be at their fluid temperature. This observation confirms the results of the high temperature microscopy of coal ash, a technique which observes the presence of a liquid phase not the effect of the liquid phase on the shape of the cone.

The crystalline phases in the quenched samples, except for that of quartz, were products of the high temperature reactions of the collective mixture of the mineral phases present in the ash.

Huggins et al.[85] used three coal ashes from the study by Huffman et al and added iron oxide, calcium oxide (as $CaCO_3$) and potassium oxide (as K_2CO_3) to each of the ashes respectively, keeping the same silica to alumina ratio. The ash fusion temperatures (AFT's) of the resulting mixtures were then determined and correlated with the relevant phase equilibria diagram (Al_2O_3-SiO_2-XO, where X = Fe, Ca or K_2). The authors plotted the liquidus temperature against percentage XO for a constant SiO_2: Al_2O_3 ratio and, on the same graph, plotted the AFT's for the ash-XO mixtures. The curves of the AFT's followed the curve of the liquidus quite closely. Therefore, though the ash fusion temperatures are non-equilibrium values, the fusion of the ash is governed by the relative proportions of the major component oxides and not the original coal minerals. The behaviour of coal ash at

high temperatures may be governed by the corresponding ternary phase diagram when the major three oxide components constitute more than 90 wt % of the ash composition.

The curves obtained for the AFT's of ashes with added lime were similar in shape to those reported by Dutta et al.[81]. However, the analogous curves of the addition of potassium oxide showed less fluxing effect than the curves obtained for sodium oxide additions as reported by the Indian workers. This may be due to the different chemical compositions and silica to alumina ratios of the ashes studied in the two investigations.

2.18 TERNARY PHASE DIAGRAMS RELEVANT TO COAL ASH MELTS

The attempts to correlate ash fusion temperatures with chemical composition have necessitated the introduction of equilibrium phase diagrams. Phase diagrams can represent the phases present under equilibrium conditions at a particular temperature for a given chemical composition. The basis of the diagram is the interrelation between the number of phases (P), and the degrees of freedom (F) to the number of components (C) given by the Gibbs phase rule:[86]

$$P + F = C + 2$$

The oxides present in coal ash have negligible vapour pressure at the temperatures of interest and therefore the condensed phase rule

$$P + F = C + 1$$

is used.

The phase diagrams are defined by the number of components. The simplest correlation of coal ash behaviour at high temperatures with that of phase equilibria data is the use of ternary phase diagrams of relevant oxide systems, e.g. $CaO-Al_2O_3-SiO_2$ and $FeO-Al_2O_3-SiO_2$. Coal ash sometimes only contains three oxides in major proportions (i.e. $\sum_{i=1}^{i=3}$ wt % > 90) with the remaining oxides having a very minor presence. Though this is not a general observation for the chemical composition of coal ashes, some samples may be chosen which fall within these compositional limits.

The importance of ternary phase diagrams in this context necessitates a discussion of the experimental techniques and the representation of the data obtained, including how they may be used to describe the melting and crystallisation behaviour of condensed ternary oxide mixtures. The earliest detailed study of the system $CaO-Al_2O_3-SiO_2$ was that by Rankin and Wright[87]. The authors developed the quench technique which has become a basic standard method for condensed oxide systems. A sample of known composition was prepared from pure oxides and a homogeneous glass produced by fusion at an appropriate temperature from the mixture. A small amount of glass was finely ground and contained in a small platinum envelope which was placed in a vertical drop-tube furnace set at the desired temperature and left for a given time. Subsequently the sample was quenched by melting the supporting wire causing the sample to drop into a pool of mercury immediately below the furnace. The phases present in the sample were determined by microscopic observation only, but of course modern techniques of phase analysis include X-ray diffraction techniques and electron probe microanalysis. Equilibrium was ensured by increasing the time of heat treatment until no further phase changes were observed

in successive samples. The authors determined the liquidus temperature, primary, secondary and tertiary crystalline phases and ternary eutectics and peritectics by this method.

The usual method of representing ternary condensed systems is as an equilateral triangle with each apex representing 100 % (wt or mole) of each component. Liquidus temperatures are represented by isotherms (locus of all points of equal temperature), regions of univariance (F =1) as boundaries between primary crystalline phases and regions of invariance (F = 0) by points at which three primary crystalline fields meet. The direction of falling temperature is indicated by arrows along the boundaries; the points of invariance where all the arrows converge are eutectic compositions, if only two arrows converge the point is called a peritectic.

Compatability triangles are drawn on the diagram by connecting the composition points of the primary phases. The connecting lines are called Alkemade lines and the point where they intersect the boundaries between two primary phases is a local temperature maximum. The triangles are useful as by definition there will be only one eutectic within each triangle and hence only a single phase assemblage at the solidus temperature, which is determined by the compositions of the primary phases.

The ternary phase diagram can fully describe the crystallisation of a liquid of a composition defined by the three components under equilibrium conditions. At the liquidus temperature the respective crystalline phase will begin to exsolve, on further cooling more primary phase will be precipitated and the residual liquid phase will become richer in the components which are not present or in

minor proportions in the primary crystalline phase. The crystallisation path is defined by the projection of the line between the composition of the primary crystalline phase and the composition of the melt to the temperature of interest within the primary field defined by the liquidus isotherm. The path represents the change in composition of the residual liquid phase with temperature. If the temperature of the melt is reduced still further a boundary will be reached, at this point the melt is saturated with the respective secondary phase (i.e. the adjacent primary crystalline phase), and will begin to precipitate. On further cooling both crystalline phases will continue to exsolve as indicated by the arrows along the boundary until a point of invariance is reached where the three adjacent crystalline phases are in equilibrium with a liquid phase. If the invariant point is a peritectic, further cooling will cause dissolution of the primary crystalline phase and subsequent precipitation of the respective secondary and tertiary phases along the boundary until a eutectic point is reached. At a eutectic point three crystalline phases are in equilibrium with a liquid phase but below the eutectic temperature, also called the solidus, no liquid phase is present.

The phase diagram can also describe the fusion behaviour of a solid mixture of chemical composition defined by the three components under equilibrium conditions by reversing the method detailed above. The first appearance of a liquid phase will be at the corresponding eutectic temperature and the sample will not be completely liquid until the liquidus temperature is reached.

Quantitative predictions of relative amounts of the phases present at a given temperature under equilibrium conditions may be achieved. The usual method is that of the lever rule. A full

description of the methods may be found elsewhere.[88]

While the ternary phase diagrams can describe fully the melting and/or crystallising behaviour under equilibrium conditions of any corresponding three-component mixture, for the diagrams to be applied to many component mixtures such as coal ash, certain assumptions have to be made. As already discussed (p.**67**) some workers have assumed various equivalences such as TiO_2 being directly equivalent to silica, magnesia to lime, etc., and thus the complete chemical composition of the coal ash can be converted to a ternary mixture by using the various equivalences. Another method, suitable for lignitic-type ashes when the composition has only three major components (CaO, Al_2O_3 and SiO_2) is that of "normalisation". The minor components are assumed to have negligible effect on the major components and the composition is converted by proportionation to a three-component mixture. While arguments may be raised against either method, the latter is the more satisfactory within the stated limitations. The equivalence method has to be used with much care and no detailed comparison using this method has been made.

Sanyal et al.[89] have used the phase diagram of the ternary system $CaO-Al_2O_3-SiO_2$ in a study of two lignitic low temperature ashes using the corresponding normalised three-component composition of the ashes. The ashes studied showed very different melting and crystallising behaviour which could be directly attributed to their respective normalised compositions when plotted on the phase diagram. The liquidus temperatures for both ashes were observed to be less than that predicted due, according to the authors, to the effect of the minor components such as Na_2O and K_2O being present. The fusion of the ash samples was studied by

high temperature microscopy and the first appearance of a liquid phase was observed at a temperature approximately 150 °C below the corresponding eutectic temperature for both samples. The primary crystalline phases observed after melting the samples and inducing crystallisation by reducing the temperature were those expected from the ternary phase diagram. The authors also predicted the slagging propensities of the ashes by analysing their respective crystallisation paths. Despite having similar ash fusion test characteristics the two compositions had different crystallisation paths. One ash whose composition lay in the primary field of anorthite ($CaO.Al_2O_3.2SiO_2$) had a high liquidus temperature and a crystallisation path which indicated an increasingly viscous residual liquid phase with decreasing temperature and was predicted to have a low slagging propensity. The other ash had a normalised composition within the primary crystalline field of gehlenite ($2CaO.Al_2O_3.SiO_2$), a relatively low liquidus temperature and a crystallisation path which indicated a fluid residual liquid phase. The ash was predicted to have a high slagging propensity. A coal with an ash of a composition similar to that of the former when fired in a full scale p.f. boiler was observed not to form deposits.[5]

Though the above study only dealt with two ashes, the results show that the relevant ternary phase diagrams may give a qualitative indication of the fusion and subsequent crystallisation of coal ash in a boiler. With reference to the models of slagging devised by Raask (p.**49**) the rate at which slag will build up is approximately inversely proportional to the viscosity of the ash melt. The viscosity itself is dependent on chemical composition and temperature. The phase diagram can indicate the liquidus temperature and the change in composition of the residual liquid

phase, as determined by the crystallisation path with temperature. Detailed studies of the viscosity of melts in the system (CaO-Al_2O_3-SiO_2) by Machin and Yee[90] have shown that the viscosity, at a given temperature, increases markedly with increasing silica content, and generally decreases with lime content. The effect of alumina on the viscosity was observed to depend on the silica and lime content, reflecting the amphoteric nature of the oxide. Thus the knowledge of the viscosity of silicate melts along with the data available from a phase diagram may be applied to the Raask model and a more authentic indication of slagging propensity may be obtained.

Although the system CaO-Al_2O_3-SiO_2 can be used for the predictions of the fusion and crystallisation and hence slagging propensity of certain lignitic-type ashes, the analogous system Fe_2O_3-Al_2O_3-SiO_2 cannot be employed in the same manner for bituminous-type ashes as the phase diagram has not been determined. Iron can exist in three oxidation states (metallic Fe^0, ferrous Fe^{2+} and ferric Fe^{3+}), the relative amounts of which depend on temperature and chemical environment, including the oxygen potential of the atmosphere. The atmosphere in a pulverised fuel-fired boiler is designed to be oxidising except in the burner zone and thus no metallic iron would be expected in a deposit. The fusion of bituminous ashes may therefore be correlated with the quaternary system, FeO-Fe_2O_3-Al_2O_3-SiO_2. It would be expected that the greater the number of components of the equilibrium system the closer will be the correlation of fusion and crystallisation of that system with the behaviour of a given coal ash composition.

The quaternary system CaO-MgO-Al_2O_3-SiO_2 may be used to give a better correlation of the fusion and crystallisation behaviour of

lignitic-type ashes of low iron oxide content and thus it can be seen that relevant quaternary systems should give far more accurate fusion and crystallisation predictions, and subsequently indications of slagging propensities, than the corresponding ternary systems.

Unfortunately quaternary oxide systems are more complex than ternary systems, both in their representation and the analysis of the high temperature behaviur of a composition. The true representation of a quaternary condensed oxide system is a regular tetrahedron with each apex representing 100% (wt or mole) of each component. Liquidus isotherms are plotted within the volume; primary crystalline regions are represented by volumes, and the boundaries of adjacent primary volumes are areas of divariance, lines which represent three adjacent primary crystalline phases in equilibrium with a liquid phase, and the peritectic and eutectics are the points at which four primary volumes meet. The crystallisation path is in three dimensions and thus it is difficult to plot and assess the change in composition of the residual liquid phase of a melt with falling temperature. The tetrahedron representation is rarely used and the published quaternary systems are usually plotted as planes through the tetrahedron. There is very little data at present available in the form of relevant quaternary systems applicable to coal ash slagging phenomena.

2.19 CRYSTAL GROWTH RATES IN SILICATE MELTS

The assumption that the minerals present in coal are completely fused, with the exception of very large quartz grains, within the burner zone of a boiler has been shown to valid.

Relevant phase diagrams, though limited in use at present, have predicted the liquidus temperature and the primary crystalline phase of two coal ash melts, and a knowledge of the crystallisation path have enabled slagging propensity predictions to be made. Phase diagrams represent equilibrium conditions and do not indicate the rate at which equilibrium is reached. The crystallisation path, when drawn on the phase diagram, is only valid when the required crystallisation takes place within the ash melt.

Thus a knowledge of crystal growth rates may give an indication of the extent to which relevant phase diagrams may be used to determine slagging propensity of a coal ash.

The thermodynamic driving force for crystallisation from a homogeneous melt is the lower Gibbs function of the crystalline state compared to that of the supercooled liquid and glassy states.

Fig. 2.2. Gibbs function/temperature curve for a hypothetical silicate melt.

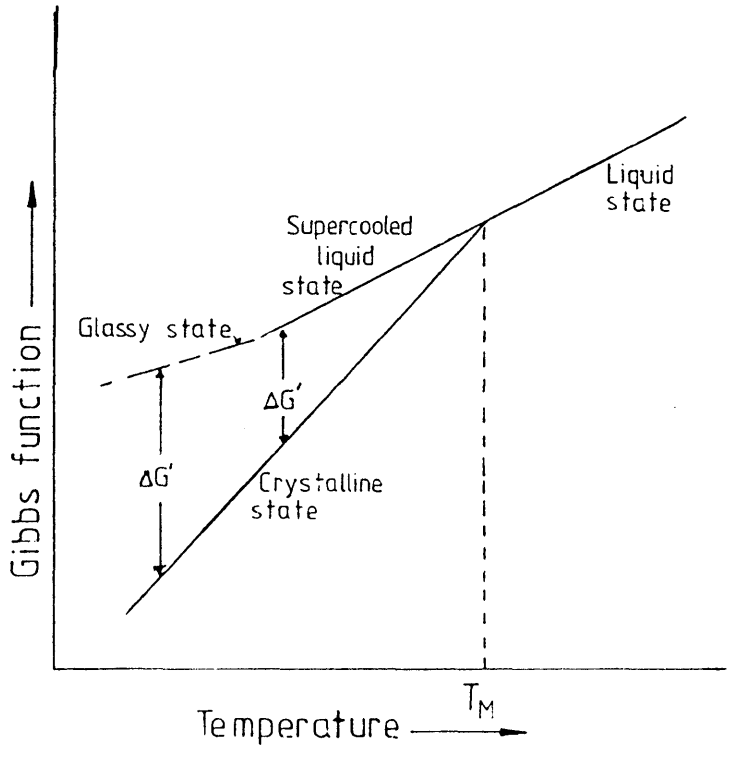


Figure 2.2 is a representation of the Gibbs function of the various states of a hypothetical melt. Below the liquidus temperature, T_M, the crystalline state becomes increasingly stable compared to that of the supercooled liquid state and at greater undercoolings more stable than the corresponding glassy state. The difference in Gibbs functions of the supercooled or glassy state and the crystalline state at any given temperature is indicated by $\Delta G'$.

Thermodynamics therefore predicts an increasing tendency to crystallisation with undercooling below T_M but cannot predict the rate at which crystals grow from a melt.

There are three factors which may determine the rate of crystal growth. They are molecular/ionic diffusion in the melt, flow of latent heat away from the crystal/melt interface, or reactions at the crystal melt interface.

According to Cahn,[91] in rapidly cooled lava flows or in devitrifying ash flow tuffs (hard volcanic rock containing fragments of lava) long-range diffusion is expected to be the rate-controlling crystal growth mechanism. The high cooling rates of ash melts in a boiler compared to normal geological mineral forming cooling rates suggests that the rate controlling mechanism will be long-range diffusion.

For diffusion controlled crystal growth, the rate, U, is given by[92]

$$U = k(D/t)^{\frac{1}{2}}$$

where k is a constant involving concentration terms, D is the diffusion coefficient of the rate determining species, and t is the time. It is apparent that the factors which affect the diffusion coefficient, D, of the crystal forming ions or molecules

through the melt to the interface will affect the crystal growth rate. The major factor is the viscosity of the liquid at the interface.

At small undercoolings below the liquidus temperature the rate of crystal growth rate will be dependent mainly on the value of $\Delta G'$, if the viscosity is sufficiently low. At larger undercoolings the value of $\Delta G'$ and the viscosity of the melt would become increasingly dominant until a maximum growth rate would be observed at a particular temperature. Below this temperature the crystal growth rate will decrease due to the increased viscosity and therefore decreasing diffusion rates. For a crystalline phase not of the same composition as the melt (for example anorthite precipitating from a coal ash melt) the interface becomes increasingly depleted of the ions necessary for crystal growth. The depleted interface increases the effect of viscosity on the diffusion. Williamson et al.[93] studied the rate of anorthite growth in a CaO, MgO, Al_2O_3 and SiO_2 glass with added iron oxide. Higher crystal growth rates were observed when the glass had a high ferrous/total iron ratio than when the predominant oxidation state of iron was ferric. The authors postulated that the observed effect was due to the ferrous ions being rejected from the crystal face resulting in a relative lowering of the viscosity at the interface. In other circumstances the interface may have a higher viscosity than the bulk which may have a significant effect on the crystal growth rate.

A hypothetical plot of crystal growth rate against temperature for a crystalline phase precipitating from a homogeneous melt when the rate determining step is long-range diffusion is illustrated in Fig.2.3 The curve represents the effect of both the thermodynamic

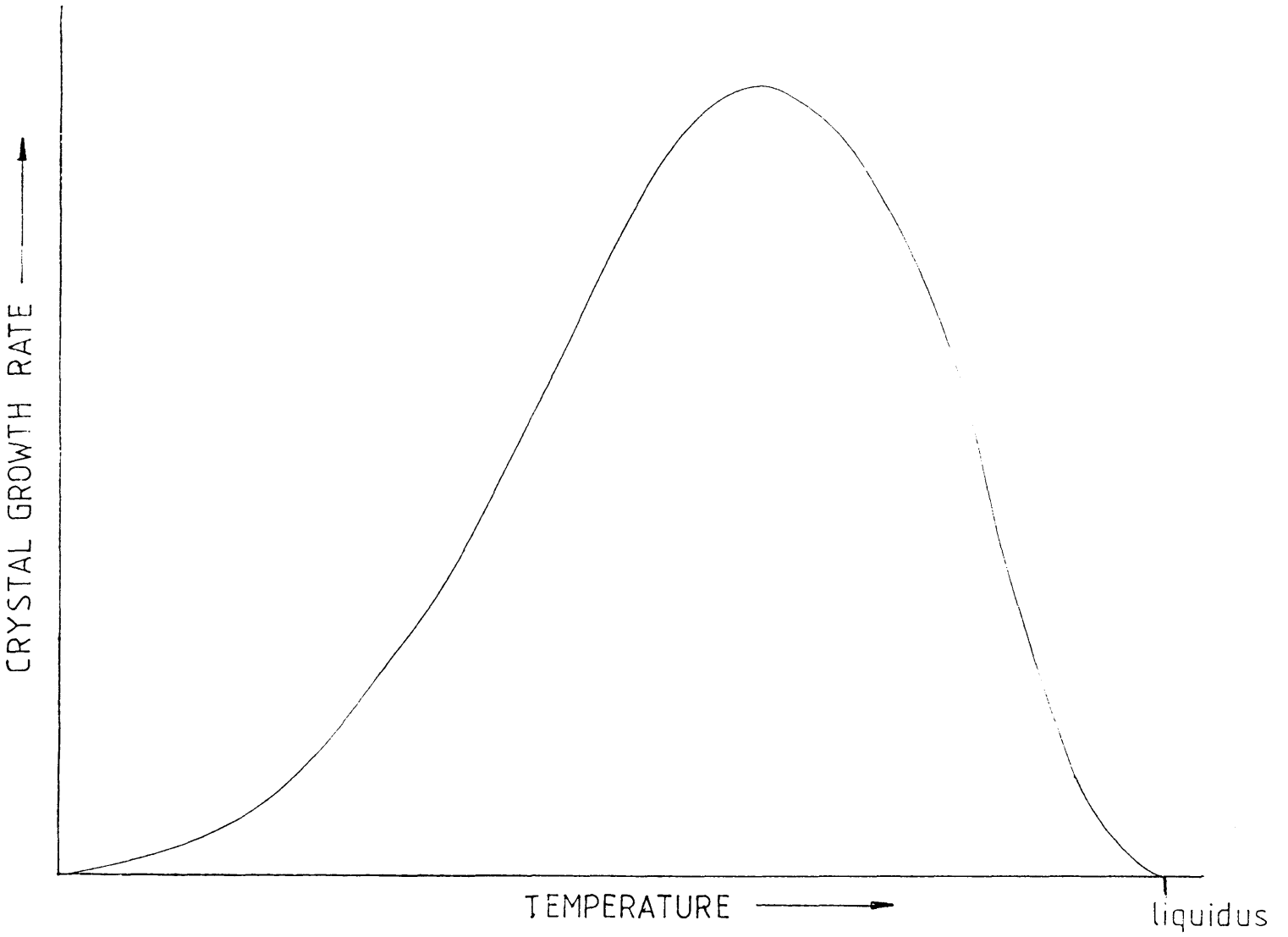


Fig. 2.3. Theoretical curve of crystal growth rate vs. temperature.

driving force and kinetic effects such as viscosity on the crystal growth rates.

Both the crystal growth rate and the growth rate/temperature relationship are difficult to predict and have to be determined experimentally. There have been no determinations of crystal growth rates in ash melts despite the detailed study of ash viscosities and the effect of simultaneous crystallisation.

2.20 SUMMARY

Coal is a fossil fuel formed by sedimentary processes. The mineral phases present in coal are varied and complex and are dependent on the local geology. In a pulverised fuel fired boiler the coal mineral matter is usually, with the exception of some quartz, completely fused within the burner zone (gas temperature 1500 - 1600 °C) forming ash particles. The mineralogical analysis of coal is rarely undertaken; the standard technique is to determine the chemical analysis of a laboratory prepared ash (air roasted at 750 - 800 °C) and the chemical composition (usually comprising eleven component oxides) obtained will be dependent primarily on the original minerals present. The major mineral group present in coal is that of the aluminosilicates and therefore silica and alumina are usually the most dominant oxides present in the ash. Coal ash is usually classified by the major third component, if the iron oxide content is greater than the lime plus magnesia it is bituminous-type and if vice versa it is lignitic-type. The remaining oxides comprise soda, potash, titania, sulphur oxides and phosphorus pentoxide.

Pulverised fuel fired boilers are designed to burn coal to produce steam for electricity generation. The thermal efficiency of a boiler may be drastically reduced by the formation of ash deposits on the heat-absorbing surfaces of the boiler. The most serious deposits are predominantly glassy in nature and called slags and are formed in regions of the boiler receiving radiant heat from the flame. Fouling deposits are usually less troublesome as they can be removed by mechanical means, being generally sintered in nature. The ability of a coal ash to form deposits in a boiler is called its slagging propensity.

There are various methods used at present to predict the slagging propensity of a coal ash. The most common method is the study of the fusion characteristics of a laboratory prepared ash when heated in both air and a mildly reducing atmosphere. The method is subjective and may be inaccurate, and the data obtained may be misleading. The same data may be used for the determination of a coal's suitability for firing and also as design parameters of a boiler. Other methods in general use include the calculation of the viscosity from empirically derived equations using the chemical analysis and the determination of various slagging parameters based on the chemical composition of the ash.

The major criticism of the predictive techniques is that they are not based on mechanisms of growth of boiler deposits. Though there have been various mechanisms proposed for the initial adhesion of ash particles to the heat-absorbing surfaces of the boiler the general mechanism for the rate at which a boiler deposit will grow has been shown to be governed by sintering by viscous flow as developed by Raask.[48] The rate of growth (ds/dt)

at a given temperature is given by:

$$\frac{ds}{dt} = \frac{3\gamma}{2\eta r}k \qquad (k = \text{constant})$$

where γ is the surface tension, r is the radius of the original ash particle and η is the viscosity. Variations in the surface tension and the particle radius are relatively small compared to the viscosity of the ash. Thus the factors which affect the viscosity of the viscous phase at a given temperature will affect the rate of growth of boiler deposits. The viscosity of a homogeneous ash melt will be dependent primarily on the chemical composition and the oxygen potential. For a melt which is partially crystallised the viscosity at a given temperature will be dependent on the composition of the residual liquid phase, the degree of crystallisation and to a lesser extent on the morphology of the crystalline phase or phases present.

Phase diagrams of relevant equilibria systems have been shown to be able to supply the necessary data for accurate predictions of slagging propensity based on the mechanism of deposit growth. The phase diagram of the system $CaO-Al_2O_3-SiO_2$ has been used by Sanyal et al. to predict the slagging propensity of two lignitic-type ashes of low iron oxide contents. The liquidus temperature and the crystallisation path were determined for each normalised (% CaO + % Al_2O_3 + % SiO_2 = 100) composition. The liquidus temperature is the temperature above which the melt, defined by the composition, is wholly liquid under equilibrium conditions. The crystallisation path indicates the change in composition of the residual liquid phase on crystallisation of the primary and subsequent crystalline phases on cooling the melt below the liquidus. A combination of the liquidus temperature, the

crystallisation path, the degree of crystallinity and the change in viscosity of the residual liquid as crystallisation proceeds may all be used to assess the slagging propensity of a coal ash using the Raask model for the formation of a deposit.

Coal ash contains up to eleven component oxides, and phase diagrams of the complete system would be too complex and limited for slagging propensity predictions. The ternary system $CaO-Al_2O_3-SiO_2$ would be expected to be relevant only to coal ashes with low magnesia and iron oxide contents, but the quaternary systems $CaO-MgO-Al_2O_3-SiO_2$ and $CaO-Al_2O_3-SiO_2$-iron oxide should provide pertinent data for lignitic-type and bituminous-type ashes respectively. The effect of the minor components such as the alkali oxides on the phase equilibria of the major components must be taken into account, usually in terms of a lowering of liquidus temperatures, viscosity and eutectic temperatures. The contribution made by the minor components in lowering the liquidus temperature and change in viscosity may be determined from a comparison of the fusion behaviour of low temperature ash and that predicted from the phase equilibria diagram system at thermal equilibrium. The rate at which equilibrium is reached for complex systems such as coal ash melts at temperatures at which boiler deposits are formed will determine the relevance of the use of phase equilibria data. Assuming that coal ash is completely fused in the burner zone of the boiler the rate at which equilibrium is reached at temperatures below the liquidus will depend on the crystal growth rates of the crystalline phases expected to precipitate from the melt as determined from the respective crystallisation path. The mechanism of crystal growth in such complex systems as coal ash, though not determined to date, is expected to be long-range diffusion which is

controlled primarily by the viscosity at a given temperature of the crystal/melt interface.

Thus the factors pertinent to the determination of slagging propensity of coal ashes are the fusion characteristics, the rate of crystallisation and the crystallisation behaviour of coal ash melts.

CHAPTER 3

EXPERIMENTAL

3.1 HIGH TEMPERATURE MICROSCOPY OF COAL ASHES

High temperature microscopy as discussed in the literature survey, is a powerful instrument for the observation of the fusion process of a coal ash. Early investigation involved the study of the fusion characteristics of high temperature ashes, that is ashes derived from coals by air roasting at 800 °C. The thermal behaviour of the minerals present in the high temperature ash as studied by high temperature microscopy and standard ash fusion tests may not correspond to the behaviour of the original mineral matter in the coal. Nolan et al.[69] were the first to use low temperature ash (LTA) in an investigation of ash fusion and crystallisation phenomena by high temperature microscopy. The LTA is produced in an oxygen plasma furnace where the temperature usually does not exceed 150 °C and the minerals present in the ash correspond very closely to the original coal mineral matter.

It was intended that the high temperature microscope be used to investigate the fusion, and to a lesser extent the crystallisation behaviour of three samples of LTA. The three samples of ash were supplied by Babcock Power Ltd Research Centre, Renfrew, Scotland. Two (KA and KC) were of lignitic-type derived from coals burnt at Matla Power Station, South Africa. The bituminous-type ash (KB) was obtained from a coal fired at the CEGB Drax power station. The chemical compositions of the ashes KA and KB were determined by electron probe

microanalysis of glasses prepared from the fusion of a sample of ash at 1550 °C. The composition of the ash KC was determined by standard chemical analytical techniques and supplied by Babcock Power Ltd. The compositions of all the ashes are listed in Table 3.1.

3.1.1 Apparatus

The high temperature microscope used in this study was made by Allison Engineering Limited, Great Yarmouth, Norfolk, UK. The apparatus comprises a thermocouple assembly mounted in a gas-tight cell. The thermocouple (5% Rh/Pt - 20% Rh/Pt wire 0.5 mm in diameter) is connected to a power supply fitted with a 2 kHz oscillator. The choice of alloys ensured sensitive temperature measurement in the region of interest (i.e. 800 °C - 1600 °C). The e.m.f. is negligible at room temperature for this junction removing the need for a cold junction correction. The gas-tight cell contains glass windows above and below the thermocouple junction. When the thermocouple assembly is fitted gas or gas mixtures may be passed through the cell by means of connecting tubes. The cell is fixed to the stage of a transmitting optical microscope orientated so that the resulting optical bench is horizontal with the thermocouple junction suspended vertically at the focal point of the microscope. The thermcouple assembly, gas-tight cell and complete microscope apparatus are illustrated in Figs 3.1, 3.2 and 3.3 respectively.

The power supply/oscillator device to which the thermocouple is connected has two functions; heating of the sample and temperature measurement. For half a cycle of the

TABLE 3.1

Chemical Composition of Low Temperature Ashes KA, KC and KB

	Wt %		
	KA+	KC+	KB*
SiO_2	43.1	51.2	54.5
Al_2O_3	27.8	29.0	26.4
Fe_2O_3	5.1	4.8	9.4
CaO	17.3	9.5	1.5
MgO	3.8	2.6	1.6
Na_2O	0.7	0.6	1.2
K_2O	0.3	1.0	4.2
TiO_2	1.9	1.3	1.1

+Lignitic-type

*Bituminous-type

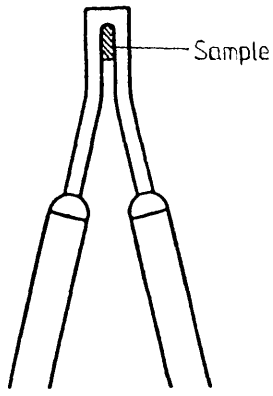


Fig.3.1. Detail of thermocouple used in the high-temperature microscope.

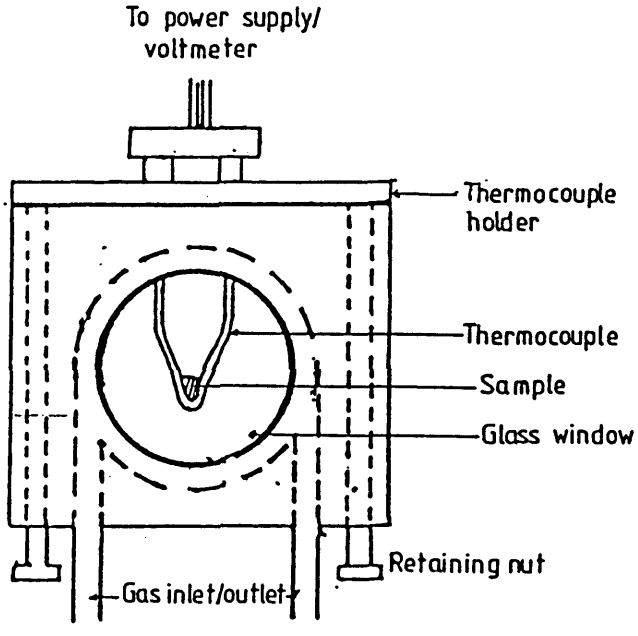


Fig. 3.2. Gas-tight cell of high-temperature microscope.

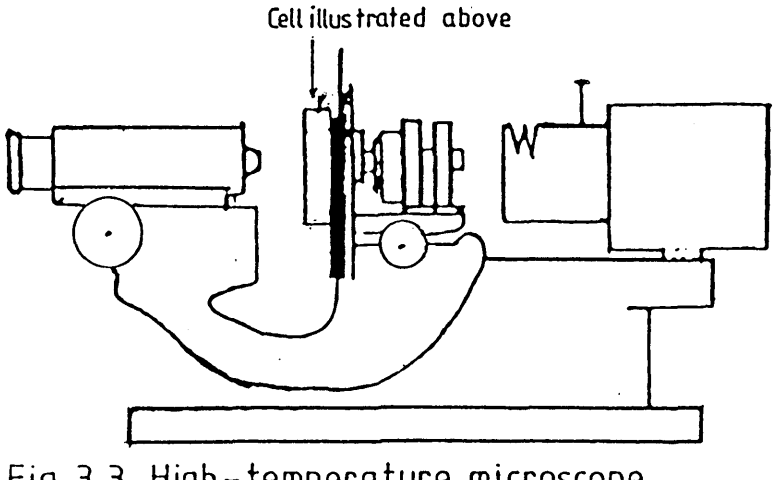


Fig. 3.3. High-temperature microscope

alternating current power is supplied to the thermocouple which acts as a resistance heater. The other half of the cycle us used to measure the resulting e.m.f. at the thermocouple junction. Heating or cooling can be controlled by adjusting potentiometers and the e.m.f. converted into °C by a direct temperature reading milli-voltmeter connected to the device. The accuracy of the instrument when properly callibrated has been reported to be ±2 °C.[94] The apparatus also incorporates a chill switch, which when depressed will thereby terminate the power supply to the thermocouple, quenching the sample very rapidly.

3.1.2 Method

Each thermocouple used was checked for accurate temperature determination by observing the melting behaviour of potassium sulphate (K_2SO_4) which has a distinct melting point (1072 °C). A sample (∿2 mg) of a sample of LTA was finely ground and pressed into the space between the wires at the junction of the thermocouple (Fig.3.1). To obtain sufficient adhesion the temperature of the thermocouple was increased until red hot for just a few seconds to sinter the ash to the Pt wires. The thermocouple was then placed in the gas-tight cell; a gas atmosphere could be passed through the cell to reduce the condensation of volatilised components on the glass windows which obscures the view and/or to control the oxidation state of iron in part of the study of the bituminous-type ash (KB).

The high magnification obtainable (180x) enabled the observation of the rounding of ash particles due to the presence of a small amount of a liquid phase. The temperature

range over which coalescence of adjacent particles began and continued were noted along with the temperature at which a single drop of liquid formed at the junction. No detailed heating rates were used, the temperature was gradually increased from room temperature and when a change in the sample was observed the sample left at that temperature for 15 - 30 s to determine any other changes and to note the observations.

On obtaining a single drop of liquid at the junction, the sample was left for about 1 minute and then the chill switch was depressed forming a vitreous bead. The fused sample was removed from the thermocouple by crushing the bead carefully between two microscope slides. The crushed sample was then taken to a conventional polarising microscope where any evidence of crystallisation was noted.

The liquidus temperature of the lignitic-type ashes were difficult to determine in situ due to the iron oxide content of the ashes. The liquidus temperature was only determined accurately for ash KC by repeating the fusion process with increasing maximum temperature until no evidence of crystallisation was observed in the quenched samples. The highest temperature used (1500 °C) in the high temperature micoscope was observed not to melt the bituminous-type ash KB completely though a single drop of liquid was formed. The fusion of the KB ash was studied both with the cell open to the atmosphere and with dried nitrogen gas being passed through. In a few experiments the oxidation of residual mineral particles in the LTA caused bubbles of gas to form in the sample when the cell was open to the atmosphere. The temperature at which the bubbles evolved, if observed, was noted along with the normal fusion characteristics.

The high temperature microscope was also used in crystallisation studies of the ash samples. A charge of finely ground LTA was pressed into the thermocouple junction and fused at 1500 - 1550 °C for 10 - 15 minutes (with the cell open to the atmosphere) to ensure homogeneity. The temperature was then rapidly reduced to a predetermined level below the liquidus temperature to induce crystallisation and left for a given time. Crystallisation in situ could be observed in some circumstances by crossing the polars of the microscope as the crystalline phases were birefringent. With the remaining cases the samples were quenched and the beads removed for analysis under a conventional polarising microscope. The crystalline phases observed in the samples were noted along with their respective crystallisation treatment. The quenched samples were too small to enable the crystalline phases to be confirmed by X-ray diffraction techniques.

3.2 CRYSTALLISATION OF ASH MELTS

While the high temperature microscopy techniques may give valuable information on the fusion characteristics of coal ash and the initial crystallisation behaviour of an ash melt, the method is impracticable for the determination of the crystallisation behaviour of an ash melt for longer periods of time and at lower temperature where more than one crystalline phase would be expected. Therefore the crystallisation behaviour of each of the ashes (KA, KB, KC) studied originally by high temperature microscopy was determined in an electric muffle furnace. The main advantages were that the samples could be left for longer periods of time (up to a number of days) and

that there would be enough material for phase analysis by optical microscopy and X-ray diffraction techniques.

3.2.1 Apparatus

The samples were contained in small platinum envelopes. The envelope was made by folding 0.0025 mm Pt foil so that it measured approximately 0.8 cm high x 0.5 cm long. Initial trials indicated that the residual carbonaceous particles along with carbonates in the LTA caused frothing with significant loss of sample due to formation of carbon dioxide when treated at temperatures above about 1000 °C. To negate this effect about 1 g of each of the ashes was roasted overnight at 750 °C in a fireclay boat. A sample of the roasted ash was packed into an envelope which could contain about 20 mg. The treatment of the samples was undertaken in a conventional electric muffle furnace with the control thermocouple (Pt/13% Rh-Pt) in the same region of the furnace where the samples would lie. The control thermocouple could also be connected to a digital millivoltmeter for accurate temperature determination. The thermocouple and controller were checked regularly by comparison of temperature with an independent thermocouple.

3.2.2 Method

The envelope containing the roasted ash sample was placed in a depression made in a small alumina refractory brick. The brick was then placed in the furnace set at 1500 or 1550 °C in the proximity of the control thermocouple. After a given time ($\frac{1}{2}$ - 1 hr to ensure homogeneity) the temperature was reduced to a given temperature and left for a given time to induce

crystallisation and to attain thermodynamic equilibrium. The sample was then removed and quenched by dipping the Pt envelope carefully into a bowl of water. After the sample was removed from the envelope the phases present were determined by microscopic and powder X-ray diffraction techniques. The crystallisation treatment was repeated for longer times and at different temperatures to obtain detailed crystallisation behaviour of the ash melt.

3.2.3 Phase analysis of quenched samples

For the preparation of the samples for microscopic observation a portion of each sample was placed on a microscope slide. The sample was fixed on the slide by a thermoplastic resin (Lakeside 70C) and a thin section of the sample was then prepared by grinding and polishing using SiC discs of successively finer grades (up to 800) until the sample was approximately 30 μm thick.

The slide was mounted on the stage of a conventional polarising microscope and the phases present in the sample observed.

The crystalline phases in the quenched samples were confirmed by powder X-ray diffraction using a Guinier de Wolff diffraction camera (cobalt K_α radiation, wavelength 1.79 Å). The resulting pattern was matched to standard powder diffraction patterns.[95]

3.3 FUSION OF COAL ASH

Though high temperature microscopy can determine the fusion characteristics of an ash under controlled heating conditions the technique does not indicate the rate of fusion of the ash at temperatures pertinent to that experienced by coal ash in the burner-zone of a boiler. The purpose of these experiments was to study the fusion characteristics of an ash at 1450 °C and 1550 °C in air.

A low temperature ash (KD) was supplied by Babcock Power Research Centre and the chemical composition is listed in Table 3.2. The ash was from the same mine as that of the lignitic-type ashes KA and KC. The ash had a slightly different chemical composition from the ash KA and therefore a check was made on the mineralogical content of the coal ashes by comparing the X-ray diffraction pattern of ashes KA and KD using the Guinier de Wolff camera. No detectable difference between the two ashes was observed.

TABLE 3.2
Chemical composition of LTA KD[5]

SiO_2	Al_2O_3	CaO	Fe_2O_3	MgO	Na_2O	K_2O	TiO_2	P_2O_5	SO_3
39.5	26.3	14.7	5.1	2.8	0.8	0.7	1.6	0.9	7.6

3.3.1 Apparatus

There were two types of experiments carried out; one using a roasted sample of ash in a vertical tube furnace and the other using raw LTD in an electric muffle furnace. The vertical tube furnace was used so as to obtain a reasonably fast quench.

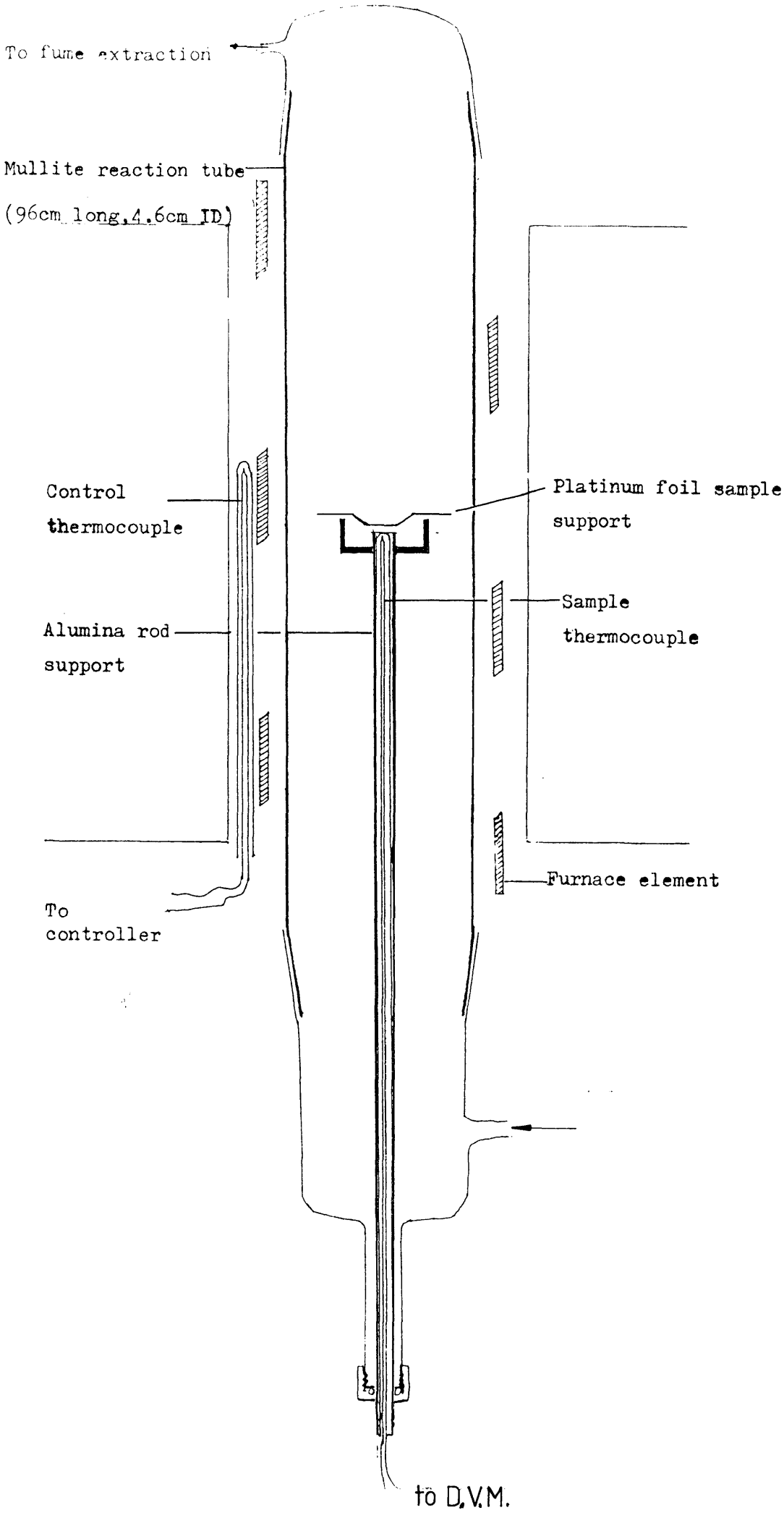
The vertical tube furnace and sample support are illustrated in Fig. 3.4. The apparatus illustrated comprises a platinum foil (~ 1 mm thick) sample holder, an alumina rod support held in a mullite reaction tube. The reaction tube was supported in the centre of a Morganite Electroheat Ltd SiC Crusilite element (type MF). Temperature was controlled by a 40A Eurotherm to which the control thermocouple was connected. The temperature at which the sample was treated was confirmed by the use of the sample thermocouple (Pt 13% Rh/Pt) connected to a DVM. The ends of the reaction tube were ground so that standard Pyrex quick-fit B55 cones could be fitted. The cones were modified as indicated in Fig. 3.4 so as, in the case of the bottom cone, to act as a guide and support for the alumina rod and also to allow the reaction tube to be open to the atmosphere. The top cone was modified to allow the exit of gases to the atmosphere via the laboratory fume extraction.

The second type of fusion experiments was undertaken in the electric muffle used for the study of ash melt crystallisation behaviour (Section 3.2).

3.3.2 Method

Initial experiments in the vertical tube furnace undertaken in air using raw LTA caused significant problems due to the violent oxidation of residual carbonaceous particles in the ash. This necessitated the use of roasted (in air overnight at 750 °C) ash KD for the experiments. The furnace was set at the desired temperature (1450 °C or 1550 °C) and the position at which the sample would experience the temperature when in the hot zone of the

Fig. 3.4. Vertical tube furnace used for the study of ash fusion.



furnace was marked on the alumina support at an appropriate position. The hot zone was checked for temperature variation 1 cm above and below the position at which the sample would be held. A sample of the roasted ash was placed on the Pt foil (∿ 50 mg) and the platform raised manually to the desired position. After a given time the rod was lowered rapidly to a cooler part of the furnace (temperature about 300 °C) and the sample subsequently removed. The process was repeated for a range of times at both temperatures.

For the experiments carried out in the electric muffle furnace a charge of approximately 1 g of raw LTA (KD) was placed in a 70 ml Pt/5% Au crucible. The furnace was set at 1450 °C and allowed to reach equilibrium. The crucible was then placed in the furnace as near to the control thermocouple as possible. After 15 seconds the crucible was removed and quenched by dipping it into a bowl of water. The process was repeated only once for a time of 60 seconds.

Phase analysis of the quenched samples produced in the vertical-tube furnace was performed by optical microscopy of thin or polished sections. The method used to prepare thin sections has already been recounted (Section 3.2.3). Polished sections were prepared by mounting a portion of a sample on a microscope slide using Araldite "Rapid" epoxy resin. The sample was then ground and polished using SiC discs as with the thin sections. Further polishing was achieved by using diamond lapping compounds from 6 μm to 1 μm grades.

For the thin sections, transmitted light microscopy techniques were used for the determination of the phases present using both plane and crossed polarised light, whereas reflected light was used to study the polished sections. To enhance the observation of the crystalline phases present in some of the polished sections the samples were etched in a 2% HF solution for 20 seconds.

Initial phase analysis of the samples prepared in the electric muffle furnace was by powder X-ray diffractometry using Cu Kα radiation (1.54 Å). The instrument was a Philips vertical wide range goniometer with a standard ratemeter. The peaks of the diffractometer recording were converted to 'd' spacings and relative intensities determined to enable analysis of the pattern using the standard powder diffraction patterns. Polished sections were prepared for both samples by mounting in Bakelite, a thermo-setting resin using a 1 inch mould. Samples were polished using

initially 800 grade SiC discs with subsequent diamond polishing to a 1 μm finish. The sections were then studied under a polarising microscope using reflected light and subsequently etched using the 2% HF solution as above and returned to the microscope for further study. The polished sections were carbon coated and then studied by scanning electron microscopy using a JEOL T200 instrument with EDAX (energy dispersive analysis of X-rays) with qualitative analysis facilities. This enabled the composition of the crystalline phases present to be confirmed qualitatively as well as the observation of crystalline morphology at high magnification.

3.4 CRYSTAL GROWTH RATES

The studies of the crystallisation behaviour of coal ashes has involved the determination of the crystalline phases present in samples treated for a considerable time. The premise for this study was that the factors which determine the slagging propensity of a coal ash would be governed by the relevant equilibrium phase diagrams. Therefore the rate at which an ash melt will reach thermodynamic equilibrium will determine the extent to which relevant phase equilibrium diagrams can be applied to the phenomena of boiler deposit formation. The major factor relating to the attainment of equilibrium, assuming that a homogeneous melt is formed, is the rate of crystal growth of the species from the melt.

The great variation in the chemical composition of coal ashes precluded the systematic study of crystal growth rates

for a range of compositions. Two coal ash compositions of lignitic-type were chosen for the study. The composition Mat 8 corresponded to that of the ash KA used in high temperature microscopy and crystallisation experiments, and the composition Mat 9 corresponded to an ash derived from a coal mined in the same region as ash KA but with a relatively higher lime content and would be expected to exhibit significantly different crystallisation behaviour to that of ash KA. The compositions have been listed in Table 3.3.

3.4.1 Preparation of glasses

The raw materials used for the preparation of the glasses of composition Mat 8 and Mat 9 respectively are listed in Appendix A along with the supplier / source and drying temperature; iron(III) oxide was used as the source of iron oxide.

A total of 200 g of each glass was prepared by mixing the correct amounts of raw materials and fusing in an electric muffle furnace at 1550 °C for 1 hr. The total charge was too large for the 70 ml Pt/5% Au crucible so only a portion of the mixture was fused (for 1 hr) at a time, poured out onto a brass plate, left to cool and then crushed in a percussion mortar. The process was continued until all the glass had been used and crushed and then ground to a fine powder in a Tema mill. The glass powder was mixed together and then refused in the same manner with intermittent crushing and grinding twice more to produce a homogeneous glass. On the final melting half the powder was fused at 1550 °C for 1 hr and then the crucible removed and the glass

TABLE 3.3

Composition of glasses used in crystal growth rate studies

Oxide	Mat 8	Mat 9
SiO_2	43.1	33.7
Al_2O_3	27.8	23.0
Fe_2O_3	5.1	2.4
CaO	17.3	34.8
MgO	3.8	4.4
Na_2O	0.7	0.2
K_2O	0.3	0.0
TiO_2	1.9	1.5
	100.0	100.0

poured out into a rectangular mould on a brass plate. The resulting tile was placed on an alumina brick and annealed from 800 °C overnight in an electric muffle furnace. The process was repeated for the remaining portion of the glass powders.

The resulting glass tiles were suitably annealed, i.e. the internal stresses had been removed leaving a glass stable towards mechanical shock. Each tile was then cut into approximately cubic pieces (1 cm^3) using a diamond saw.

3.4.2 Determination of crystal growth rates

The electric muffle furnace previously described (section 3.2.1) was used in the determination of the crystal growth rates of the two glasses. A sample of each glass was placed in the furnace set at a given temperature close to the control thermocouple. After a given time (15 s to 10 minutes) the sample was removed and allowed to cool to room temperature. The sample was then coated in molten Lakeside 70C resin until it was completely covered and then removed. The coating of resin was necessary to ensure that the edges of the samples were not chipped away by subsequent grinding. A side of the sample was then removed on a diamond lap to reveal growth normal to the surface. The exposed face was then polished using SiC discs up to 800 grade. The depth of the surface growth was determined by optical microscopy using reflected light, the eyepiece of the microscope incorporated a previously cal ibrated graticule. The growth was observed to be generally homogeneous but the average of six measurements of the depth of the surface

growth, determined in different parts of the sample was taken as the value of the growth. In some cases the sample was reground to expose a new face and the measurement of surface growth repeated. There was no discernable difference in growth with respect to the orientation of the sample in the furnace. There was also no detectable difference in surface growth between that from the smooth surfaces and that from the rougher surfaces produced by the diamond saw for the same sample.

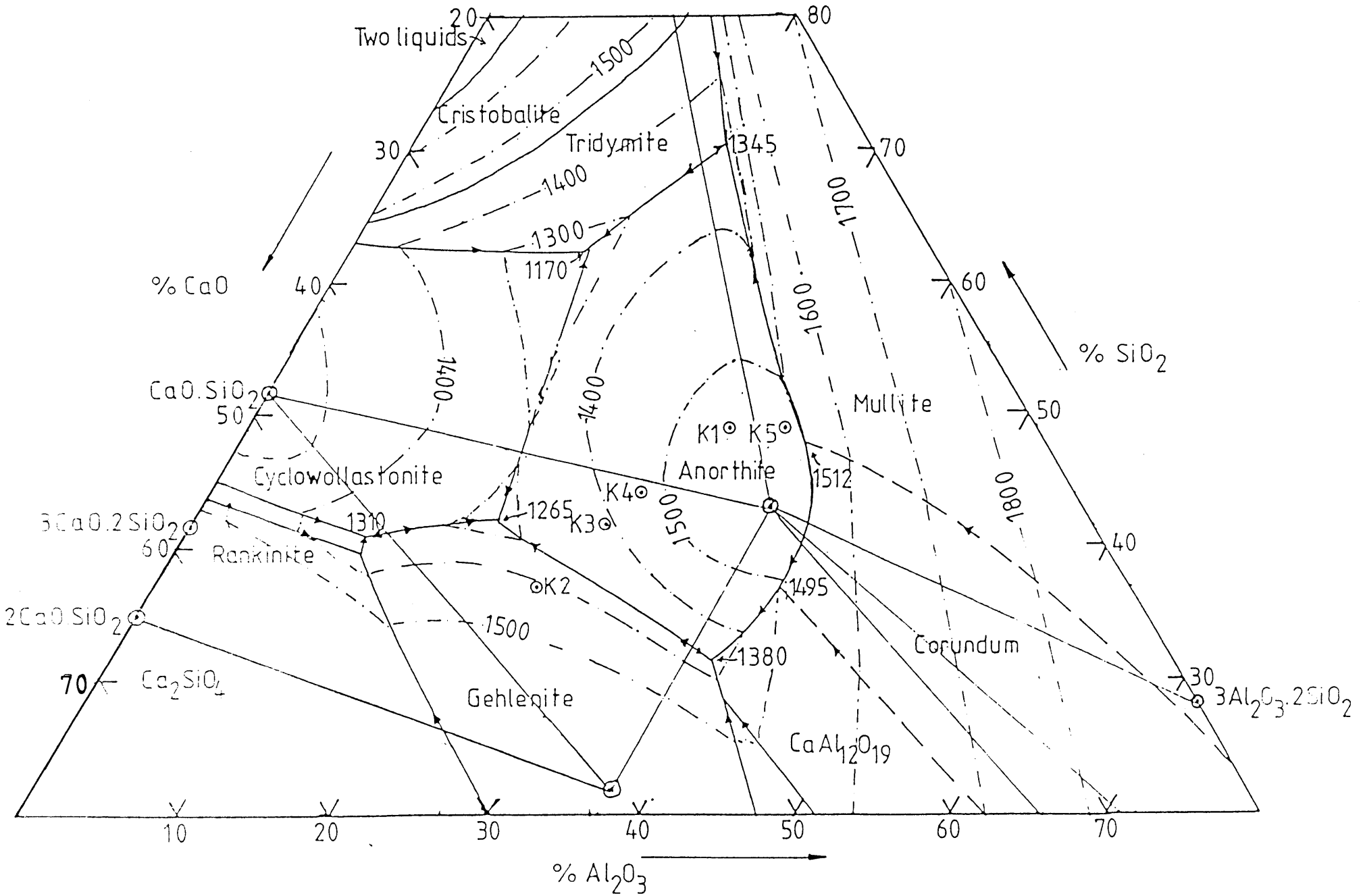
The experiments were repeated for each glass over a range of times at a given temperature until a determination of the maximum growth rate could be obtained. Maximum crystal growth rates were obtained in an analogous manner at various temperatures for each glass until a maximum crystal growth rate/temperature curve was obtained.

3.5 CRYSTALLISATION STUDIES OF THREE COMPONENT GLASSES

The crystallisation behaviour of coal ash melts and to a lesser extent the fusion characteristics of the ash may be governed by the major components. The study by Sanyal and Williamson[89] showed the close correlation between the fusion and crystallisation behaviour of two lignitic-type ashes and that predicted from their corresponding normalised three component composition (% CaO + % Al_2O_3 + % SiO_2 = 100) when plotted on the corresponding ternary phase diagram. As the fusion and crystallisation behaviour of a number of ashes has been studied it was necessary to study the crystallisation behaviour of three component glasses of CaO, Al_2O_3 and SiO_2 of compositions relevant to coal ashes of lignitic-type.

Five ternary compositions were chosen for the study, it was not relevant to study the fusion characteristics of the ternary mixtures in an analogous manner to the high temperature microscopy studies of the coal ashes as the pure components will have significantly different interactions than the mineral components of coal ash at temperatures below the liquidus. Two compositions, K1 and K2, correspond to the three component normalised compositions of the known lignitic-type ashes, K1 corresponds to the ash KA1 (composition listed in Table 3.1) and K2 corresponds to the ash of high lime content, used as the basis of the glass Mat 9 in the crystal growth studies, Table 3.3. The compositions K3, K4 and K5 were chosen so as to have different crystallisation behaviour but to be within the compositional region of lignitic-type coal ashes. The compositions K1 and K2 were plotted on the ternary phase diagram of the system $CaO-Al_2O_3-SiO_2$ (Fig.3.6) and a line drawn between the two compositions. All the compositions on the line will have an equal silica to alumina ratio. Compositions K3 and K4 were chosen to lie in the primary crystalline field of anorthite ($CaOAl_2O_3.2SiO_2$) as well as being on the line K1-K2 and in the compatibility triangle of cyclo-wollastonite ($\alpha CaO.SiO_2$), anorthite and gehlenite ($2CaO.Al_2O_3.SiO_2$), the same as that of composition K2. The composition K5 was chosen so as to have the same silica content and to be in the same primary crystalline field (anorthite) as K1 but to be in the compatibility triangle anorthite, mullite ($3Al_2O_3.2SiO_2$), tridymite. All the compositions have been plotted on the ternary phase diagram (Fig.3.5) and listed in Table 3.4.

Fig.3.5. System $CaO-Al_2O_3-SiO_2$, ternary compositions studied.



3.5.1 Preparation of glasses

For each of the compositions the correct proportion of the raw materials (source and drying temperature are listed in Appendix A) to provide 50 g of glass were carefully weighed out (±0.01 g) and mixed together. A glass was prepared by initial fusing of each mixture (contained in a 70 ml Pt/5% Au crucible) at 1550 °C for 1 hr in an electric muffle furnace. Homogeneity of each glass was ensured by crushing the quenched glass with a porcelain mortar and pestle and remelting the glass twice more for 1 hr at 1550 °C. After the final fusion the quenched glass was crushed to a fine powder with the mortar and pestle.

3.5.2 Crystallisation studies

A small charge of each glass (∿ 1 g) was placed in a 5 ml Pt/5% Au crucible. The crucible was then placed in the electric muffle furnace used for the ash crystallisation studies and set at a given temperature. After a given time the crucible was removed and the sample quenched. In some cases the time of temperature treatment was increased to determine any change in crystallisation with time and if any discrepancy was observed the time increased further until two successive treatments gave the same phase assemblage present. The crystallisation experiments were completed for all five glasses over a range of temperatures. The liquidus temperatures of the glasses were not determined as the relevant data for compositions in the region of interest have been fully published. Phase analysis of the quenched samples was by thin-section microscopy and powder X-ray diffraction. The method of the preparation of thin sections

has previously been described. The phases present in the thin-sections were determined by optical microscopy using transmitted plane and/orcrossedpolarised light. The composition of the crystalline phases present in the quenched samples was determined by powder X-ray diffraction using a Guinier camera.

3.6 CRYSTALLISATION STUDIES OF GLASSES IN THE SYSTEM $CaO-MgO-Al_2O_3-SiO_2$

Lignitic-type ashes have a relatively low iron oxide content by definition and thus the major four components of a typical ash may be silica, alumina, lime and magnesia. The quaternary equilibrium system $CaO-MgO-Al_2O_3-SiO_2$ may give better correlation to the fusion and crystallisation of lignitic-type ash than the corresponding ternary system $CaO-Al_2O_3-SiO_2$. Quaternary phase diagrams are complex both in their representation and the interpretation of the data compared to ternary phase diagrams. The approach in this study was to take the ternary compositions of CaO, Al_2O_3 and SiO_2 previously studied (compositions K1, K2, K3, K4 and K5) and investigate the effect of the addition of 5 and 10 wt % magnesia on the liquidus temperature and the crystallisation behaviour of corresponding glasses. The two series of compositions with 5 and 10 wt % MgO contents based on the ternary compositions K1 to K5 studied are listed in Table 3.5 along with the ternary compositions on which they were based.

A review of the literature of the system $CaO-MgO-Al_2O_3-SiO_2$ indicated that there was a lack of liquidus temperature

TABLE 3.4

Composition of $CaO-Al_2O_3-SiO_2$ glasses

Glass	Composition wt %		
	SiO_2	Al_2O_3	CaO
K1	49.0	31.5	19.5
K2	37.0	25.0	38.0
K3	41.5	27.0	31.5
K4	44.0	28.5	27.5
K5	49.0	35.0	16.0

TABLE 3.5

Composition of the K series of $CaO-MgO-Al_2O_3-SiO_2$ glasses

Glass	Composition wt %				Ternary Composition*
	SiO_2	Al_2O_3	CaO	MgO	
K17	47.0	30.0	18.0	5.0	K1
K18	35.0	24.0	36.0	5.0	K2
K19	39.0	26.0	30.0	5.0	K3
K20	42.0	27.0	26.0	5.0	K4
K21	47.0	33.0	15.0	5.0	K5
K22	44.1	28.4	17.5	10.0	K1
K23	33.3	22.5	34.2	10.0	K2
K24	37.6	24.3	28.3	10.0	K3
K25	49.6	25.6	24.8	10.0	K4
K26	44.1	31.5	14.4	10.0	K5

* the composition of the corresponding $CaO-Al_2O_3-SiO_2$ glass was normalised to 95 and 90% for the series K17-K21 and K22-K26 respectively.

and primary crystalline phase data in the region of the system of interest to this study. Thus a number of compositions were chosen to establish liquidus temperatures and primary crystalline phases; the compositions are listed in Table 3.6. The J series of compositions contained 10 wt % magnesia and the I series contained 5 wt % magnesia.

3.6.1 Preparation of glasses

The correct proportions of quartz, alumina, calcium carbonate (as the source of lime) and magnesia (source and drying temperature, Appendix A) were carefully weighed out (±0.01 g) for each composition to produce 50 g of glass for the compositions based on the ternary compositions and 25 g of glass for the I and J series of compositions. The procedure for the fusion of the inorganic mixture to produce a homogeneous glass for each composition was the same as that for the three-component glasses (section 3.5.1).

3.6.2 Crystallisation studies

The quench technique, as used for the crystallisation studies of the three component glasses, and to a lesser extent high temperature microscopy, was used to determine the liquidus temperature and crystallisation behaviour of the four-component glasses.

Liquidus temperature determination by high temperature microscopy was as follows: a small amount of each glass was finely ground and pressed into the thermocouple junction (previously calibrated with potassium sulphate), the cell was open to the atmosphere. The sample was fused at 1550 °C and

the primary crystalline phase was observed in situ. The liquidus temperature was then determined by increasing the temperature of the thermocouple slowly until only a single crystal was just visible in the melt as observed using crossed polarised light when the primary phase was birefringent or plane polarised light when isotropic.

It was found difficult to observe the crystallisation behaviour of the glasses at temperatures substantially below the liquidus temperature (> 150 °C). The presence of significant proportions of crystalline phase or phases present in the sample precluded in situ determination of the distinct phases. The size of the samples produced in the high temperature microscope was insufficient for determination of the crystalline phases by X-ray diffraction techniques.

The crystallisation behaviour was determined for all the glass compositions by the quench technique. A charge of approximately 1 g of a glass was contained in a 5 ml Pt/5% Au crucible and placed in the electric muffle furnace, used in the previous studies, set at a given temperature, near the control thermocouple. After a given time the crucible was removed and quenched. The sample was removed and used for phase analysis. Liquidus temperature of each of the glasses was determined using this technique by crystallising a sample of the glass in the furnace at a temperature well below the expected liquidus. The temperature of the furnace was then increased to a given value and the sample reintroduced into the furnace for a given time (at least 1 hr). This procedure was repeated

until phase analysis of a quenched sample showed no crystalline phases present when the previous sample, treated at a temperature 10 °C lower was partially crystalline. The temperature at which this occurred was taken as the liquidus temperature with an accuracy of ±10 °C.

The crystallisation behaviour of the glasses using the quench technique, especially those compositions based on the three-component glasses, was determined in an analogous manner to that used for the study of the crystallisation behaviour of the three component glasses.

Phase analysis of the quenched samples was by optical microscopy of thin-sections and powder X-ray diffraction.

3.7 CRYSTALLISATION STUDIES OF THE SYSTEM $CaO-Al_2O_3-SiO_2$-IRON OXIDE

The quaternary system $CaO-MgO-Al_2O_3-SiO_2$ was expected to give a better correlation with the crystallisation behaviour of lignitic-type ashes than the corresponding ternary system $CaO-Al_2O_3-SiO_2$. For bituminous-type ashes the three major components are silica, alumina and iron oxide, and it would be expected that the system $Al_2O_3-SiO_2$-iron oxide may be used to correlate with the crystallisation of the ashes. As some lignitic ashes have an iron oxide content (usually expressed as Fe_2O_3) comparable to or greater than the magnesia content it was considered to be more relevant to study the system $CaO-Al_2O_3-SiO_2$-iron oxide.

Iron can exist in three oxidation states: metallic Fe^0, ferrous Fe^{2+} and ferric Fe^{3+}. The relative proportions

present in
of the different states\a melt containing iron under equilibrium conditions will depend on the temperature, chemical composition and the local oxygen partial pressure. In a pulverised fuel fired boiler the atmospheric condition is usually oxidising and no metallic iron would be expected to be present in the coal ash. For the study of the crystallisation of glasses containing iron oxide a controlled atmosphere was chosen, which was the same as that used in the mildly reducing mode of the British standard ash fusion test.[53] The atmosphere is an initial mixture of dried carbon dioxide and hydrogen in the ratio by volume, 1:1, and is supposed to represent that experienced by ash particles within the burner zone of the boiler[96] but there seems to be no published evidence for this. The reducing effect is due to the reaction of carbon dioxide and hydrogen at high temperature to produce carbon monoxide and water vapour:

$$CO_2 + H_2 \rightleftharpoons CO + H_2O$$

It can be shown (Appendix B) that the oxygen partial pressure obtained from the ratio of partial pressures of $CO:CO_2$ for an initial ratio of $H_2:CO_2$ of 1:1 is markedly dependent on temperature. The reducing effect decreases with increasing temperature from a partial pressure of oxygen of about 10^{-21} bars at 1000 °C to about 10^{-7} bar at 1550 °C. A change in the choice of atmosphere would have caused significant problems with the correlation of experimental results.

The approach used in this section was the same as that with the study of the crystallisation of glasses in the system CaO-MgO-Al_2O_3-SiO_2. That is, the effect of the addition of fixed amounts of iron oxide on the crystallisation behaviour of the series of

ternary (CaO, Al_2O_3, SiO_2) compositions K1, K2, K3, K4 and K5. The wide range of iron oxide contents present in coal ashes necessitated the study of the addition of up to 20% equivalent iron(II) oxide (FeO). Two series of compositions based on the five ternary compositions with 5 and 10 wt % iron(II) oxide contents (series F1-F5 and F6-F10 respectively). Only the ternary compositions K1, K2 and K5 were used as the basis for the compositions containing 15 and 20 wt % iron(II) oxide contents (compositions F11, F12, F15 and F16, F17, F20 respectively). The compositions have been listed in Table 3.7.

3.7.1 Preparation of glasses

The correct proportions of quartz, alumina, calcium carbonate (as the source of lime), iron(II) oxalate ($FeC_2O_4.2H_2O$, as the source of iron(II) oxide) were weighed out (±0.01 g) to produce 50 g of each glass. The source and drying conditions of the materials used have been listed in Appendix A. After mixing of the component oxides the powders were fused at 1550 °C in an electric muffle furnace. As there is a large amount of carbon dioxide and water vapour produced when calcium carbonate and iron(II) oxalate are heated above 1000 °C the following procedure was undertaken for all the compositions to reduce any loss of components during the melting process due to the gases percolating through the mixture. A charge of about 5 g of a mixture was placed in a 70 ml Pt/5% Au crucible and introduced into an electric muffle furnace set at 1100 °C. After about ½ hr the crucible was removed and a further amount was placed in the crucible and

TABLE 3.6

Composition of J and I series of $CaO-MgO-Al_2O_3-SiO_2$ glasses

Glass	Composition wt %			
	SiO_2	Al_2O_3	CaO	MgO
J1	53.3	29.5	12.2	5.0
J2	45.7	35.0	14.3	5.0
J3	38.6	27.1	29.3	5.0
J4	41.0	21.4	32.6	5.0
J5	38.6	24.8	31.6	5.0
J6	41.0	31.9	22.1	5.0
I1	44.1	17.5	28.4	10.0
I2	43.0	20.0	27.0	10.0
I3	44.1	26.6	19.3	10.0
I4	50.5	28.9	10.6	10.0
I5	53.5	29.0	7.5	10.0
I6	38.0	19.3	32.7	10.0
I7	33.2	20.9	35.9	10.0

TABLE 3.7

Composition of $CaO-Al_2O_3-SiO_2$ iron oxide glasses

Glass	Composition wt %			
	SiO_2	Al_2O_3	CaO	FeO*
F1	47.0	30.0	18.0	5.0
F2	35.0	24.0	36.0	5.0
F3	39.0	26.0	30.0	5.0
F4	42.0	27.0	26.0	5.0
F5	47.0	33.0	15.0	5.0
F6	44.0	28.4	17.6	10.0
F7	33.3	22.4	34.3	10.0
F8	37.4	24.2	28.4	10.0
F9	39.5	25.6	24.8	10.0
F10	44.0	31.6	14.4	10.0
F11	41.6	26.8	16.6	15.0
F12	31.5	21.2	32.3	15.0
F15	41.6	29.8	13.6	15.0
F16	39.2	25.2	15.6	20.0
F17	29.6	20.0	30.4	20.0
F20	39.2	28.0	12.8	20.0

* equivalent FeO

returned to the furnace for ½ hr. The process was repeated until all the mixture had been introduced at 1100 °C. The temperature of the furnace was then raised to 1550 °C and the crucible left for 1 hr to produce complete fusion of the mixture. The crucible was then removed and the melt poured onto a brass plate and allowed to cool to room temperature. The glass was crushed in a percussion mortar and ground to a fine powder in a Tema mill. The powder was replaced in the crucible and remelted at 1550 °C for a further hour. The process was repeated once more to obtain a homogeneous glass which was subsequently crushed and ground to a powder using a Tema mill.

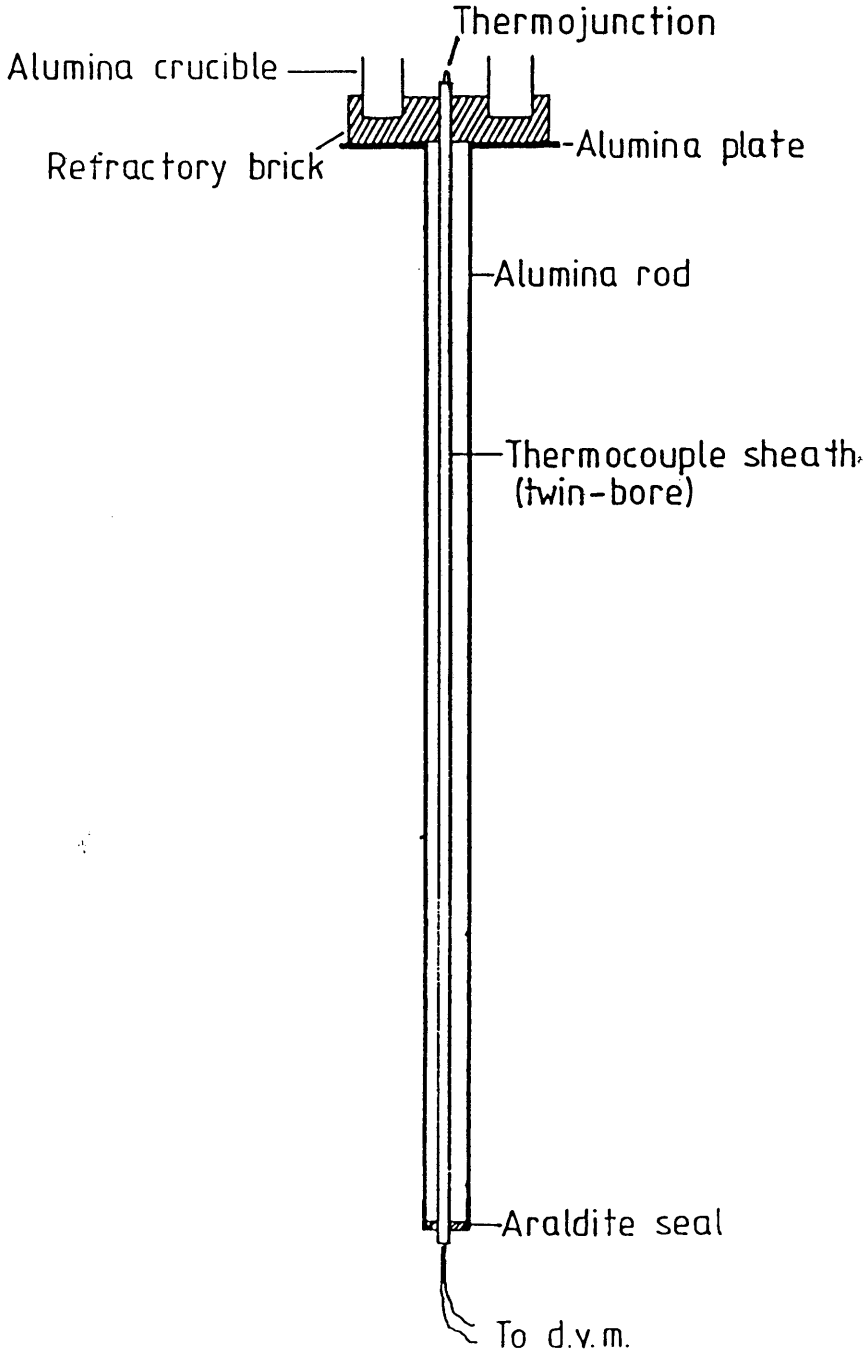
The same procedure was used to prepare homogeneous glasses for all the compositions to be studied. There was no evidence of attack of the platinum crucible by the iron due, presumably, to the oxidising conditions (air atmosphere) present in the furnace (iron II is known to alloy with platinum).

3.7.2 Apparatus

The apparatus used for the determination of the crystallisation behaviour of the glasses was the vertical tube furnace used for the investigation of ash fusion (Section 3.3) and illustrated in Fig.3.5. The apparatus was connected to a gas train which supplied the mildly reducing atmosphere. The gas train comprised two calibrated capillary flow meters, connected to cylinders of hydrogen and carbon dioxide via drying columns of magnesium perchlorate/silica gel. The outlet from each of the flow meters was connected to the base of a mixing vessel containing 3 mm glass balls. The mixed gas was fed to the bottom pyrex cone illustrated in Fig.3.5 Exit gases were passed

from the top pyrex cone through a steam trap to collect condensing water vapour (a product of the high temperature reaction between CO_2 and H_2) then to the atmosphere via the laboratory fume extraction.

Fig.3.6. Alumina rod assembly used in the study of iron oxide glasses.



The reducing conditions to be used precluded the use of platinum or platinum alloys to contain the samples. Recrystallised alumina crucibles(supplied by Thermal Syndicate Ltd, Wallsend, UK) measuring 1 cm high, 0.5 cm I.D. were used as sample containers. The alumina rod assembly used in the ash fusion investigation was unsuitable for the support of the alumina crucible. The support was modified so as to hold up to four crucibles at a time with the junction of the sample thermocouple in a position to determine the mean temperature at which the samples were treated.

The alumina rod assembly used as the sample support is illustrated in Fig.3.6.

3.7.3 Crystallisation studies

A small charge ($\sim$ 1 g) of each glass was placed in an alumina crucible which was then put on the platform of the alumina support. The temperature of the furnace was set at a given value and the gas train connected, the valves opened and the flow adjusted. The support was pushed up manually to a pre-determined position for the samples to experience the desired temperature (confirmed by using the sample thermocouple). After a given time the platform was lowered to a much cooler region of the reaction tube ($\sim$ 300 °C) and the gas flow stopped. The crucible was then removed and allowed to cool to room temperature. In some circumstances the samples had shrunk considerably and could be removed easily. For the samples of a more vitreous nature wetting of the crucible necessitated the crushing of the crucible to remove the samples.

The determination of liquidus temperatures for the compositions using this technique was not undertaken for three reasons: firstly, that the alumina crucibles were attacked by the fluid melt at temperatures near the liquidus; secondly, the determination would take a disproportionate amount of experimental time compared to that for the determination of crystallisation behaviour; and thirdly, as the oxygen potential of the atmosphere used in the study varied with temperature the liquidus data obtained would be of limited value.

The crystallisation behaviour of each of the glasses was determined by repeating the quenching experiments over a range of temperatures. In some cases equilibrium was established by increasing the time of treatment at a particular temperature until two successive samples had the same assemblage of phases as determined by phase analysis.

3.7.4 Analysis of quenched samples

The phases present in the quenched samples were determined by optical microscopy of thin and polished sections, and powder X-ray diffraction.

The relative proportions of iron(II) oxide and iron(III) oxide present in the quenched samples was of interest to this study. Iron(II) oxide is known to have a greater fluxing effect than iron(III) oxide and thus the relative proportions will have an effect on the crystallisation behaviour of the melts.

The method used to determine the ferrous iron(II) content was based on that of Hey[97] using iodine monochloride as the oxidising agent.

A stock solution of ICl was prepared by dissolving 3.22 g KIO_3 (BDH, Analar) in 37.5 ml distilled water, adding 5.00 g of potassium iodate (BDH, Analar) and the solution made up to 100 ml with 9 M hydrochloric acid. A 25 ml aliquot of this solution was taken and diluted to 250 ml with 9 M hydrochloric acid in a volumetric flask. To the solution a few ml of carbon tetrachloride was added which formed a non-aqueous layer at the bottom of the flask.

A small amount of each sample (20 - 50 mg) was finely ground and carefully weighed out (±0.0001 g) into a 250 ml conical flask (to which a stopper could be fitted). To the powder a 10 ml aliquot of the dilute ICl solution, 50 ml of 9 M hydrochloric acid and a few ml of carbon tetrachloride were added. The flask was then stoppered and shaken for ten minutes to dissolve the sample. The solution was then titrated with 0.0005 M potassium iodate solution with intermittent shaking until the iodine in the CCl_4 layer was removed.

The chemical reactions of the titration are:

$$2Fe^{2+} + 2ICl + 2H^{+} = 2Fe^{3+} + 2HCl + I_2$$

$$2I_2 + KIO_3 + 6HCl = KCl + 5ICl + 3H_2O$$

Therefore, for every mole of iodate solution used there must be four moles of ferrous iron present. Thus 1 ml of 0.0005 M KIO_3 solution was equivalent to 0.1117 $_{mg}Fe^{2+}$. A check was made to determine if any Fe^{2+} was oxidised during the solution step by any other means than that by the iodine monochloride. A known amount of iron(II) oxalate in the acid/ICl solution was titrated, with KIO_3 solution and the oxidation of the ferrous ion appeared to be by the iodine monochloride only.

In all cases the dilute ICl solution was "balanced" before an aliquot was taken from the flask for the dissolution/oxidation step of the titration. That is, if iodine was present in the CCl_4 layer dilute KIO_3 solution was added dropwise with intermittent shaking until the iodine was removed or if it was not present a few drops of very dilute KI solution was added to produce a small amount of iodine which was removed with the dilute KIO_3 solution. This was to ensure that all the ferrous ions present in the sample would produce the stoichiometric amount of iodine during dissolution.

In some cases a blank run was prepared at the same time as the true solution containing ground sample to determine if the solution decomposed to produce iodine while the titration of the true solution was being performed. There was no evidence for this occurring but care was taken to keep to the same schedule for all the titrations.

Total iron content of the quenched samples was determined by atomic absorption spectrophotometry using a Perkin Elmer 2280 instrument in the absorption mode. To the flask containing the dissolved sample and the titrated solution, 100 ml of distilled water was added. The flask was stoppered and shaken thoroughly and a portion of the aqueous layer was decanted into a 100 ml volumetric flask, care being taken not to transfer any of the CCl_4 layer.

Four standard solutions were prepared by dissolving various masses of iron(II) oxalate in the same solution as the quenched samples and then diluted to known volumes with distilled water. The absorption of the solutions was determined under standard

conditions and a graph of iron concentration (p.p.m.) against absorption drawn. The absorption of each of the solutions containing dissolved sample was then recorded under the same conditions and the iron concentration determined from the calibration curve. The ferrous/total iron ratio was then calculated for each of the titrated solutions. The ratio was determined for all the quenched samples and the original glasses.

3.8 CRYSTALLISATION OF MULTICOMPONENT GLASSES OF COMPOSITIONS BASED ON THAT OF A LIGNITIC-TYPE ASH

The process of normalising the chemical composition of an ash to the major components used in this study is open to the criticism that no account is taken of the individual effects of the minor components. For example, components such as the alkali oxides are known to have significant fluxing effect on the ash fusion characteristics of an ash. It was an aim of this project to determine the crystallisation behaviour of a series of glasses based on the composition of a lignitic-type ash with increasing number of the metallic oxide components, the final glass to include all the component oxides. The ash chosen for study was that of KA and was normalised to five, seven, and eight components to include the magnesia, alkali oxides (Na_2O and K_2O), and titania contents respectively. The compositions were designated Mat 3 , Mat 4 , Mat 5, respectively and are listed in Table 3.8 with the composition of the ash KA.

3.8.1 Preparation of glasses

The components necessary to produce 50 g of each glass were carefully weighed out (source and drying conditions of the materials listed in Appendix A) and mixed together. Iron(III) oxide was used as the source of iron.

The mixtures were fused at 1550 °C to produce a homogeneous glass in the same manner as that for the three-component glasses (section 3.4) and subsequently ground to a fine powder in a Tema mill.

3.8.2 Crystallisation studies

A small charge of each glass (∿ 50 mg) was placed in a platinum envelope which was supported on an alumina refractory brick. The sample was then introduced into an electric muffle furnace which was set at a given temperature, and after a given time removed and quenched. The sample was then used for phase analysis, the techniques of which have previously been described. The crystallisation behaviour was determined by repeating the crystallisation treatment for the glasses over a range of temperatures for a range of times. No attempt was made to determine the liquidus temperature of the glasses.

3.9 CRYSTALLISATION OF A GLASS OF COMPOSITION BASED ON THAT OF A BITUMINOUS-TYPE ASH

A glass was prepared with the same composition as the bituminous-type ash KB using iron(III) oxide as the source of iron oxide. The composition of the glass D1 has been

listed in Table 3.9. The procedures used for the preparation of the glass and determination of the crystallisation behaviour were the same as that for the glasses based on the lignitic-type ash composition. Phase analysis of quenched samples was achieved by optical microscopy of thin or polished sections and by X-ray diffractometry.

TABLE 3.8

Compositions of Multicomponent Glasses based on the Composition of Ash KA

GLASS	COMPOSITION Wt %							
	SiO_2	Al_2O_3	CaO	Fe_2O_3	MgO	Na_2O	K_2O	TiO_2
KA (ASH)	43.1	27.8	17.3	5.1	3.8	0.7	0.3	1.9
MAT 3	44.4	28.6	17.8	5.3	3.9	0.0	0.0	0.0
MAT 4	43.9	28.3	17.7	5.2	3.9	0.7	0.3	0.0
MAT 5	43.1	27.8	17.3	5.1	3.8	0.7	0.3	1.9

TABLE 3.9

Composition (wt %) of Glass D1 (based on that of Ash KB)

SiO_2	Al_2O_3	Fe_2O_3	CaO	MgO	Na_2O	K_2O	TiO_2
54.5	26.4	9.4	1.5	1.6	1.2	4.2	1.1

CHAPTER 4

RESULTS

4.1 HIGH TEMPERATURE MICROSCOPY

The high temperature microscope was used to observe the fusion characteristics of three low temperature ashes. The instrument was also used to a lesser extent to determine the crystallisation behaviour of the ash melts. Ashes KA and KC were of lignitic-type whereas ash KB was of bituminous-type. The fusion characteristics observed for the three ashes are listed in Table 4.1; the data for each ash being the accumulation of three separate determinations. Initial observation was the coalescence of the ash particles. This was characterised by a rounding of the particles due to the formation of a small amount of a liquid phase. Coalescence was observed to increase with increasing temperature until there was a significant quantity of a liquid phase present. For the ash KA carbon dioxide was observed to evolve at 1270 °C. Fusion was considered to be complete when the sample appeared to be a single drop of liquid. All the ashes were studied with the cell open to the atmosphere; the fusion of ash KB was also studied with dried nitrogen gas being passed through the cell.

Examination of the quenched samples from the highest fusion temperatures, using a conventional polarising microscope confirmed that fusion was complete for the ash KA (treated at 1450 °C). The presence of a few lath-like crystals characteristic of anorthite ($CaO.Al_2O_3.2SiO_2$) in the quenched sample of KC (treated at 1360 °C) indicated that

TABLE 4.1

High-temperature microscopy of low-temperature ashes

ASH KA (in air)

Temperature/°C	Observations
980	Ash coalesced slightly
1270	Liquid flowed and CO_2 evolved
1330	Single drop of liquid formed
1450	No changes

ASH KB (in air)

Temperature/°C	Observations
1000 - 1250	No change
1250 - 1350	Ash particle lost some sharp edges and coalesced slightly
1400	Melting commenced
1450	Single drop formed

ASH KB (in nitrogen)

Temperature/°C	Observations
1000 - 1150	No change
1150 - 1250	Ash particles coalesced
1250 - 1400	Coalescence increases
1400	Single drop formed

ASH KC (in air)

Temperature/°C	Observations
1000 - 1200	No change
1200	Coalescence began
1200 - 1300	Appreciable amount of liquid phase present
1300	Single drop formed
1300 - 1360	No further change observed

the liquidus temperature had almost been achieved. The quenched sample of KB (treated at 1450 °C in air) was predominantly crystalline with acicular (needle-like) crystals indicative of mullite ($3Al_2O_3.2SiO_2$) indicating that the liquidus temperature had not been attained.

The crystallisation behaviour of the lignitic-type ashes KA and KC were determined by high-temperature microscopy. The crystallisation treatment and the phases observed in the subsequently quenched samples have been listed in Table 4.2. The only crystalline phase observed in the samples was anorthite characterised by its lath-like morphology and low birefringence.

4.2 QUENCHING EXPERIMENT ON ASH MELTS

The crystallisation behaviour of ashes KA, KB and KC was determined by a series of quenching experiments using an electric muffle furnace. Phases present in the samples were analysed by microscopic and X-ray powder diffraction techniques. The crystallisation treatment and the crystalline phases present in the samples have been listed in Tables 4.3, 4.4 and 4.5 for the ashes KA, KC, and KB respectively.

Ashes KA and KC contained only anorthite in the quenched samples. The X-ray pattern matched that of the standard pattern (No 10-379). The primary crystalline phase observed in quenched samples of ash KB was mullite and was present as a mass of fine crystals in a glass matrix. The XRD pattern matched that of the standard No 15-776. The hematite (αFe_2O_3, pattern No 13-534) determined in various samples was observed to be at the surfaces of the sample only, and not

TABLE 4.2

Crystallisation of ash melts as determined on the high-temperature microscope

	Crystallisation treatment		Crystalline phases
	Temp/°C	Time/mins	
ASH KA	1400	10	anorthite
	1350	10	anorthite
	1200	10	anorthite
	1100	10	anorthite
ASH KC	1300	15	anorthite
	1200	15	anorthite
	1100	15	anorthite

TABLE 4.3

Results of crystallisation experiments on ash KA using the quenching technique

Run No	Crystallisation temperature/°C*	Time/hrs	Crystalli phases observed
KA15	1390	80.0	glass †
KA12	1150	24.0	anorthite
KA21	1150	180.0	anorthite
KA18	1100	15.0	anorthite
KA19	1100	42.0	anorthite
KA10	1050	0.5	anorthite
KA20	1050	22.0	anorthite
KA9	1000	24.0	anorthite
KA7	950	24.0	anorthite
KA22	950	80.0	anorthite
KA4	940	1.5	anorthite
KA6	900	24.0	anorthite

* temperature of crystallisation following fusion of the sample at 1450 °C for 0.5 hrs

† no crystalline phases observed in the sample

TABLE 4.4

Results of crystallisation experiments on ash KC using the quenching technique

Run No	Crystallisation temperature/°C*	Time/hrs	Crystalline phases observed
KC1	1300	1.0	anorthite
KC2	1200	10.0	anorthite
KC3	1100	24.0	anorthite
KC4	1000	15.0	anorthite

* crystallisation treatment after fusion at 1450 °C for 1 hr

TABLE 4.5

Results of crystallisation experiments on ash KB using the quench technique

Run	Crystallisation*		Crystalline phases
	Temp/°C	Time/hrs	
KB6	1400	1.0	mullite
KB7	1400	2.0	mullite
KB15	1400	18.0	mullite
KB8	1350	2.0	mullite
KB9	1250	2.0	mullite
KB14	1250	20.0	mullite + hematite
KB18	1200	40.0	mullite + iron spinel
KB17	1170	20.0	mullite + iron spinel
KB10	1150	2.0	mullite + iron spinel
KB16	1150	4.0	mullite + iron spinel
KB19	1100	26.0	mullite + iron spinel
KB11	1050	2.0	mullite + hematite
KB12	950	14.0	mullite + hematite

* after fusion at 1550 °C for 1 hr

TABLE 4.6

Comparison of XRD pattern of an iron spinel sample and the patterns of hercynite and magnetite

$FeO.Al_2O_3$ Hercynite (No 3-894)		KB10 Measured spinel pattern (treated 1150 °C 2 hrs)		$FeO.Fe_2O_3$ Magnetite (No 19-629)	
d/A°	Int	d/A°	Int	d/A°	Int
4.69	20	4.75	vw	4.852	8
2.87	60	2.90	m	2.967	30
2.45	100	2.48	s	2.532	100
2.02	80	2.05	ms	2.099	20
1.64	16	1.88	vw	1.72	10
1.56	40	1.58	m	1.62	30

within the mullite/glass matrix. The spinel phase present in the samples quenched from temperatures in the range 1100 °C - 1170 °C was a member of the solid solution series hercynite ($FeO.Al_2O_3$) - magnetite ($FeO.Fe_2O_3$). The pattern of the sample KB10 (excluding lines assigned to mullite) has been compared with those of the two end members of the solid solution series in Table 4.6. Detailed lattice parameter determination by X-ray diffraction techniques to enable a composition to be assigned to the phase from known data was not undertaken. The pattern listed in Table 4.6 indicates that the spinel phase was hercynite rich. Microscopic observations of thin sections containing the spinel phase revealed tiny cubic crystals ($\sim$ 4 μm) in a mullite matrix. The spinel crystals were opaque both in plane and cross polarised light. In the sample KB10 the phase was observed to be a local collection of single crystals with a dendritic morphology whereas in the other samples the crystals appeared uniformly as discreet particles throughout the sample.

4.3 ASH FUSION IN A VERTICAL-TUBE FURNACE

The fusion of ashes KD (previously roasted in air at 750 °C over night) was studied in a vertical-tube furnace at 1450 °C and 1550 °C in air. The fusion treatment and the macroscopic and microscopic observations of the quenched samples have been listed in Table 4.7. The smallness of the sample necessitated that only a section of the sample could be examined and the observations may therefore not be characteristic of the whole sample.

TABLE 4.7

Fusion of ash KD in air

Sample	Treatment		Shape of sample	Optical observations
	Temp/°C	Time/s		
R6	1450	15	Spherical	Quartz present mainly around outer rim, some cubic crystals (iron-rich spinel). Interior contains anorthite crystals and pores in an unhomogeneous glass.
R1	1450	30	Spherical	Quartz grains still at surface - anorthite crystals nucleated and grown from the surface and pores. Glass unhomogeneous.
R2	1450	60	Flat	Trace of quartz, small cubic crystals present. Predominantly crystalline with much anorthite present.
R3	1450	120	Flat	Long anorthite needles (140 μm) in glassy matrix. A few quartz grains observed with a highly siliceous glassy rim.
R5	1450	240	Flat	Homogeneous glass with no quartz observed. Single conglommeration of iron-rich cubic crystals present.
S2	1550	30	Flat	Unhomogeneous glass with a few pores and a number of quartz grains.
S3	1550	45	Flat	Unhomogeneous glass, quartz grains and pores.
S4	1550	60	Flat	Unhomogeneous glass, quartz grains and pores.
S6	1550	75	Flat	Unhomogeneous glass, no quartz observed.
S7	1550	90	Flat	Unhomogeneous glass with large quartz grains.
S5	1550	120	Flat	Homogeneous glass with a few pores and only a few large quartz grains.

Sample R6 (treated at 1450 °C for 15 s) was a single spherical drop when removed from the furnace. Microscopic observation of the polished section revealed that the sample was predominantly crystalline with quartz, iron spinel, hematite and anorthite crystals present in a glassy matrix containing many pores. Plates 1 - 8 are optical micrographs of the various features observed in R6. Plate 1 shows an iron-rich area (bright region - top left hand corner), pores (black spheres), quartz crystals (bright grains), and a glassy region between the various features. The photomicrograph was taken under partial crossed polars and shows the characteristic high birefringence of quartz and differing composition of the iron spinel crystals (different reflectivities). Plate 2 is of approximately the same region of R6 as Plate 1 but was taken under plane polarised light. The quartz grains appear speckled and the spinel crystals seem to have the same reflectivities. The anorthite crystals are clearly evident being the dark grey needles in a light grey matrix. Plate 3 is of the same region as Plate 2 but under full crossed polars, note the triangular particle in the quartz grain showing complete extinction which was bright under plane polars (Plate 2). The iron spinel crystals also shows complete extinction characteristic of the phase.

To reveal the crystalline morphology of sample R6 the sample was etched. Plates 4 and 5 are photomicrographs of the etched polished section taken under plane and partial crossed polarised light. Anorthite crystals, quartz grains and glass are clearly evident. Note the large quartz grain (top right hand corner) and the siliceous solution rim around the

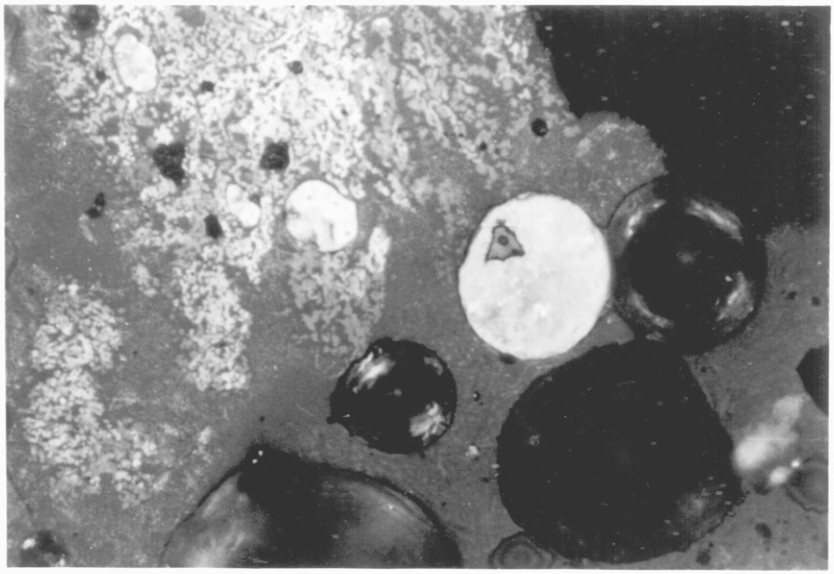


PLATE 1. Sample R6 (1450°C, air, 15s) reflected light (partial crossed polars). Magnification 220x.

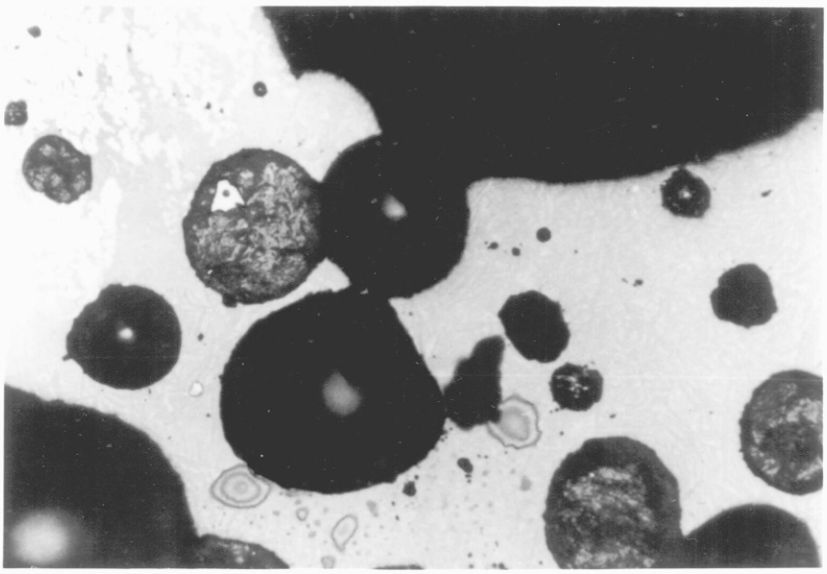


PLATE 2. Sample R6 (1450°C, air, 15s) reflected light (plane polarised). Magnification 220x.

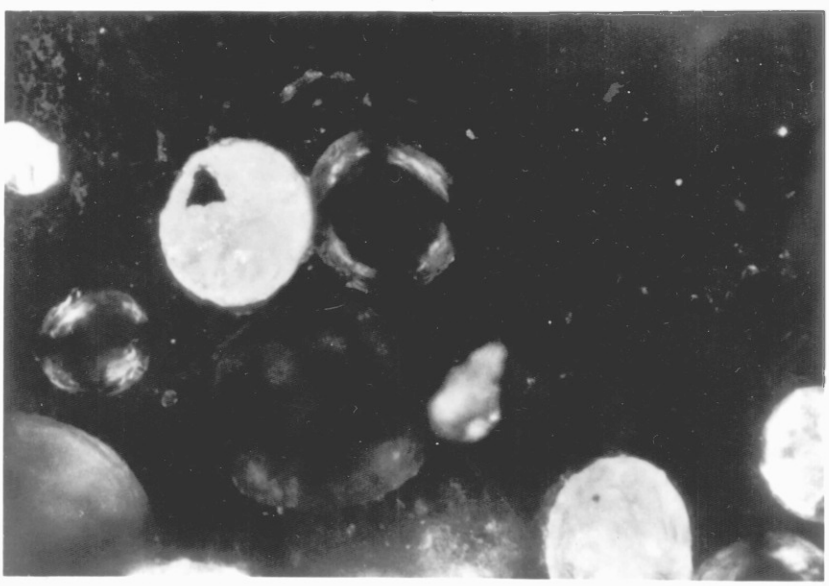


PLATE 3. Sample R6 (1450°C, air, 15s) reflected light (full cross polars). Magnification 220x.

large grain shown in Plate 5. The iron-rich area of the etched sample was observed at higher magnification (Plate 6, plane polars) and showed the different reflectivities of the euhedral spinel crystals and the dendritic morphology of the hematite crystals.

The colour photomicrographs of sample R6 (Plates 7 and 8) taken of the unetched section shows the iron-rich area of the sample. Plate 8 was taken under partialcrossedpolars and shows the different partial extinctions of the iron spinel crystals and the red-colour birefringence of the hematite crystals.

Sample R1 (1450 °C, 30 s) was observed to be a single spherical drop when removed from the furnace. Microscopic observations revealed quartz grains and anorthite crystals, heterogeneity of the glass was indicated by dark streaks in the matrix.

The sample R2 (1450 °C, 60 s) was a flat layer when removed and observation of the thin section revealed a few quartz and iron spinel crystals present. The major crystalline phase was anorthite, observed in an apparently homogeneous glass melt. Plate 9 is a photomicrograph of the anorthite crystals in the glassy region of the sample.

The sample treated at 1450 °C in air for 120 s (R3) was flat when removed from the furnace. The polished section, when etched, revealed long anorthite crystals and quartz crystals in a homogeneous glassy matrix; a few pores were also observed. Plates 10 and 11 show a quartz grain and anorthite crystals in sample R3, the latter photomicrograph was taken

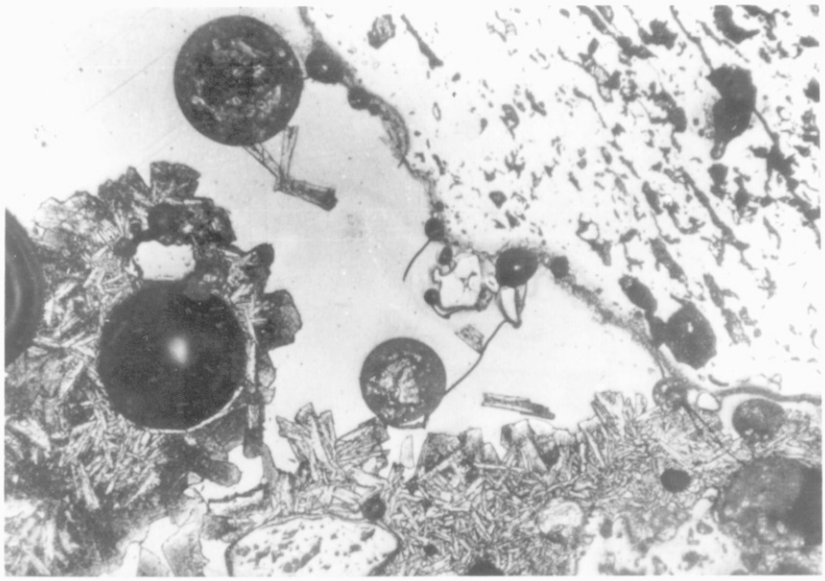


PLATE 4. Sample R6 (1450°C, air, 15s) etched, reflected light (plane polarised). Magnification 165x.

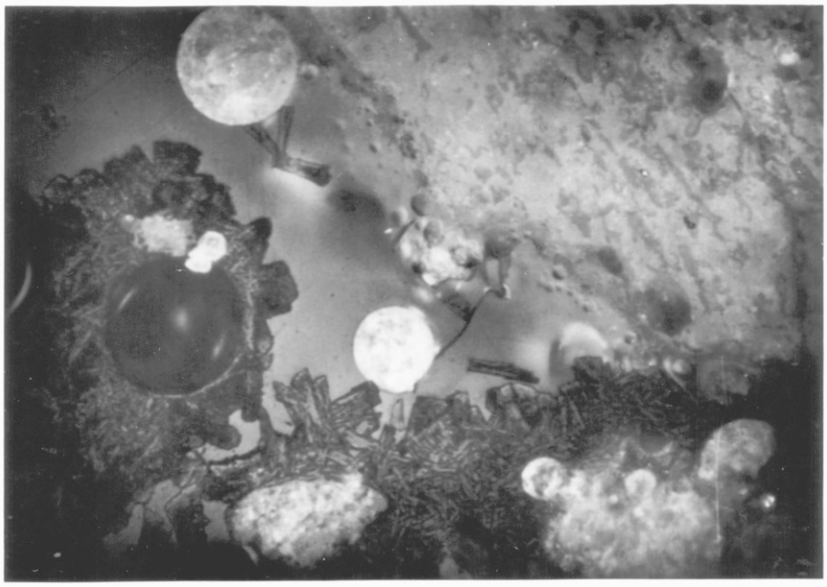


PLATE 5. Sample R6 (1450°C, air 15s) etched, reflected light (partial crossed polars). Magnification 165x.

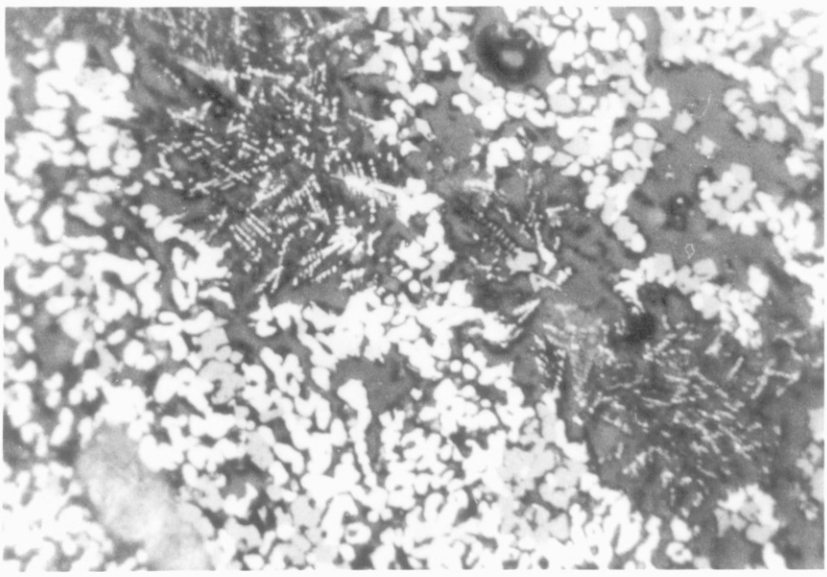


PLATE 6. Sample R6 (1450°C, air, 15s) etched, reflected light (plane polars). Magnification 864x.

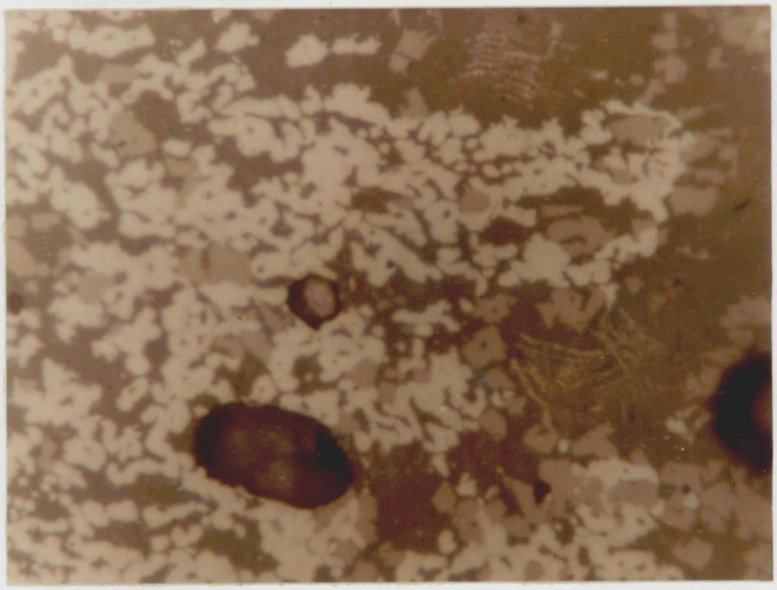


PLATE 7. Sample R6 (1450 °C, air, 15s) reflected light (plane polarised). Magnification 760x.

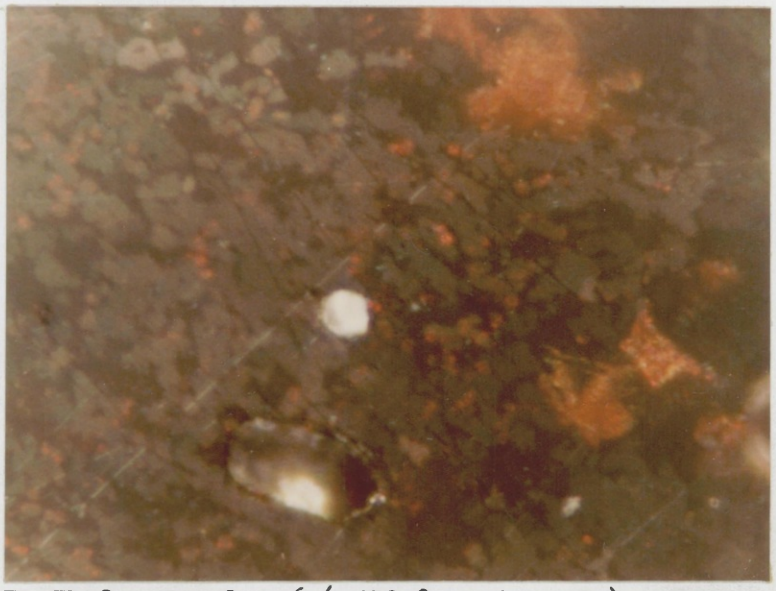


PLATE 8. Sample R6 (1450 °C, air, 15s) reflected light (partial crossed polars). Magnification 760x.

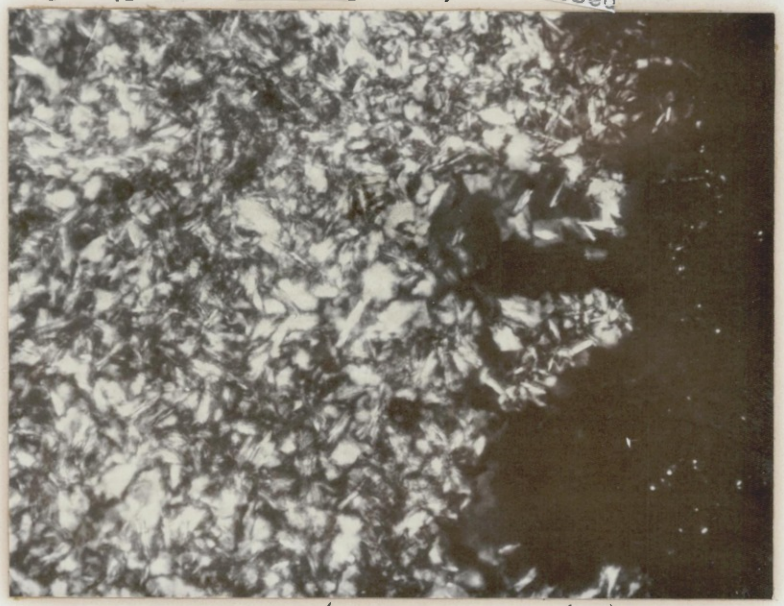


PLATE 9. Sample R2 (1450 °C, air, 60s) transmitted light (fully crossed polars). Magnification 55x.

under partial crossed polars and reveals a solution rim. Plate 12 is of another region of the same sample and shows a conglomeration of quartz crystals in the lower region of the Plate, a few pores and anorthite crystals.

The sample R5 (1450 °C, air, 240 s) was also flat when removed from the furnace. The glass appeared to be homogeneous with no pores or quartz crystals. A single conglomeration ($\sim$ 8 μm) of iron spinel crystals was present in the thin section studied.

All the samples treated at 1550 °C in air were observed to be flat when removed from the furnace. The only crystalline phase observed was that of quartz. Generally the samples appeared to be less porous than the samples treated at 1450 °C in air. The glass phase, as determined from analysis of thin sections, was observed to be nhomogeneous (dark, presumably iron rich, streaks) in all samples except for sample S5 (treated for 120 s).

4.4 ASH FUSION IN AN ELECTRIC MUFFLE FURNACE

Two samples of unroasted LTA (KD) were treated at 1450 °C in an electric muffle furnace for 15 and 60 s, designated Z1 and Z2 respectively. The quenched samples were markedly different as determined by macroscopic and microscopic observations. Sample Z1 was observed to be a collection of spheres slightly fused together (about 1 mm in diameter) when removed from the furnace. Sample Z2 was a single melt and had formed a layer at the bottom of the crucible.

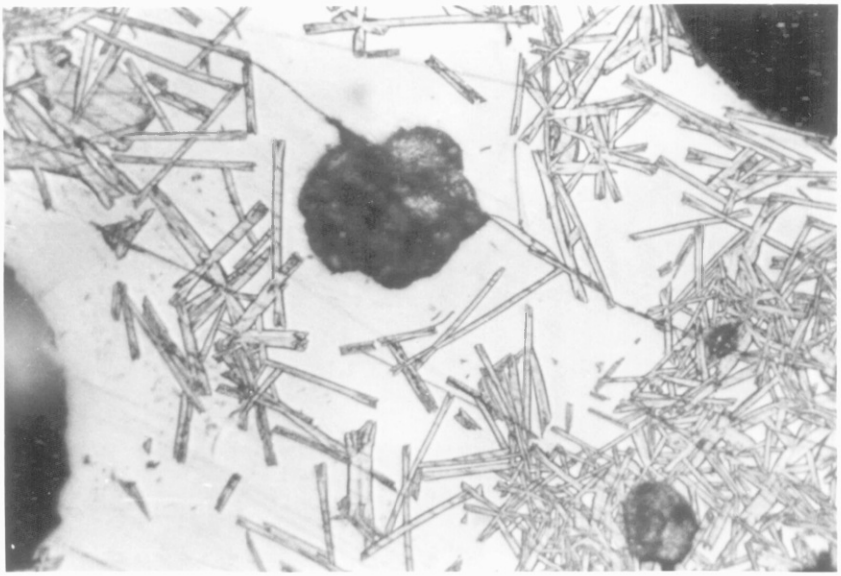


PLATE 10. Sample R2 (1450°C, air, 60s) etched, reflected light (plane polarised). Magnification 170x.

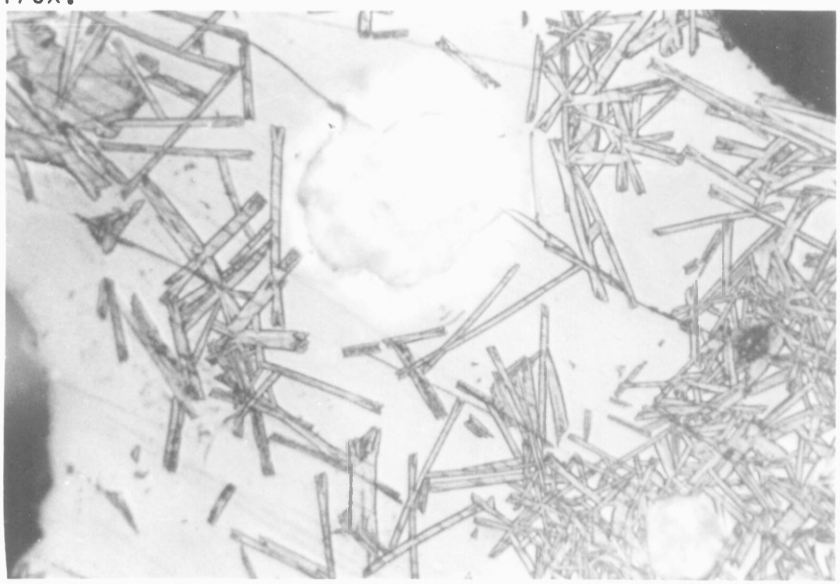


PLATE 11. Sample R2 (1450°C, air, 60s) etched, reflected light (partial crossed polars). Magnification 170x.

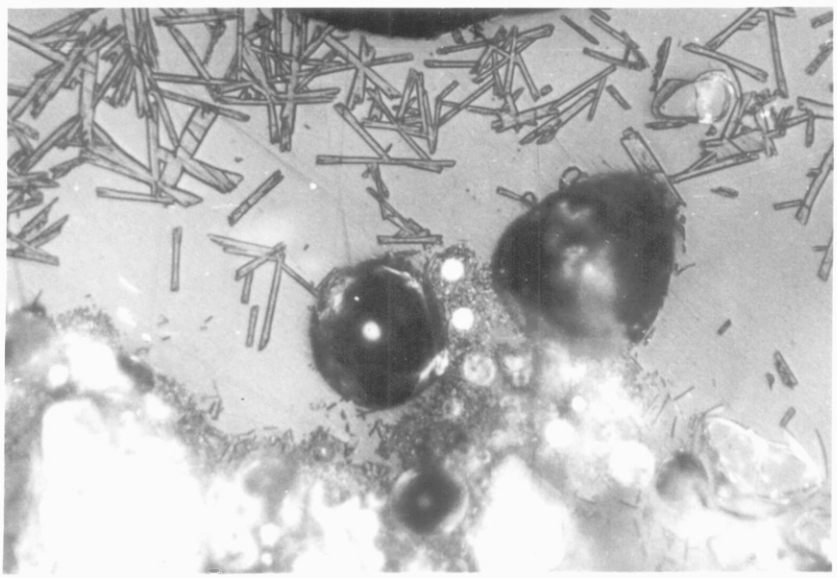


PLATE 12. Sample R2 (1450°C, air, 60s) etched, reflected light (partial crossed polars). Magnification 220x.

Optical microscopy of polished sections revealed coke particles, formed from the residual coal particles present in the LTA and pores, in both samples. Etching of sample Z1 enhanced observation of anorthite crystals, iron spinel regions and quartz grains. Plates 13, 14 and 15 are optical micrographs of sample Z1 (etched) and show the features observed (the light grey area is that of the mounting compound). The Plates 13 and 14 are of the same region of the sample taken under plane and crossed polars. A coke particle is clearly evident in Plate 13 (bright region, bottom left-hand corner) which extinguishes under partial cross-polars (Plate 14). The iron spinel crystals (bright semi-spherical region top right-hand corner, Plate 13) did not extinguish under partial crossed polars (note the clear facets of the crystals in Plate 14). The quartz grains are clearly present in Plate 14 and the morphology of the anorthite crystals can be discerned in Plate 15. Sample Z2 was predominantly glassy with few pores present and a number of large quartz grains.

Scanning electron microscopy of sample Z1 confirmed the optical microscopic observations. Plate 16 is a scanning electron micrograph showing an area of glassy material and a crystalline region; the morphology of the anorthite crystals is clearly evident. Plate 17 is of the same general area as Plate 16 but at a higher magnification in the region of the pore. The crystalline phase was determined to comprise only lime, alumina and silica using qualitative EDAX facilities. A quartz grain is clearly present in the electron micrograph (Plate 18) of sample Z1. The angular features, characteristic of quartz crystals are slightly rounded. The grain was determined to comprise silica only using EDAX facilities.

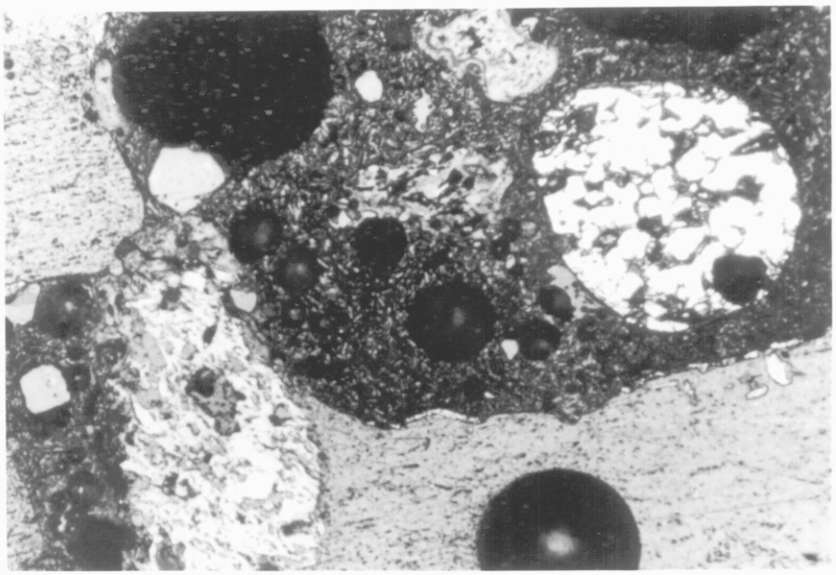


PLATE 13. Sample Z1 (1450°C, air, 15s, raw LTA) etched, reflected light (plane polars). Magnification 240x.

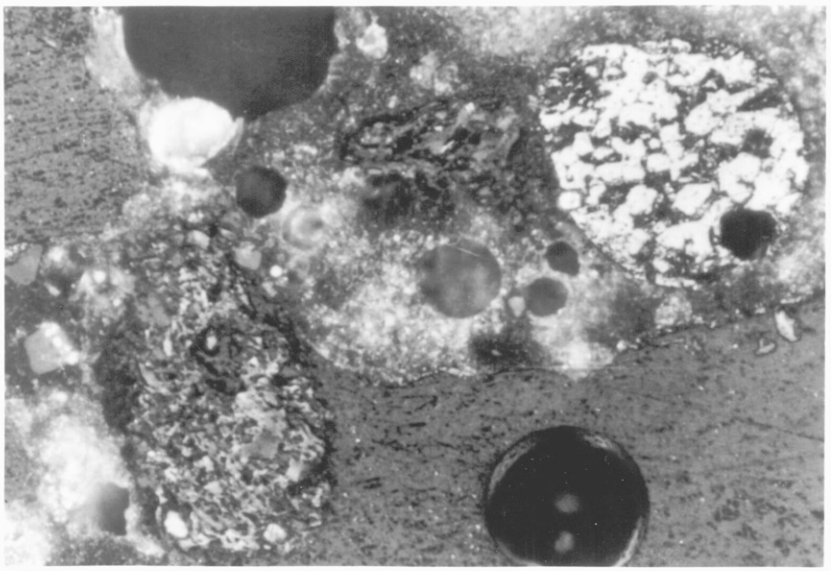


PLATE 14. Sample Z1 (1450°C, air, 15s, raw LTA) etched, reflected light (partial crossed-polars). Magnification 240x.

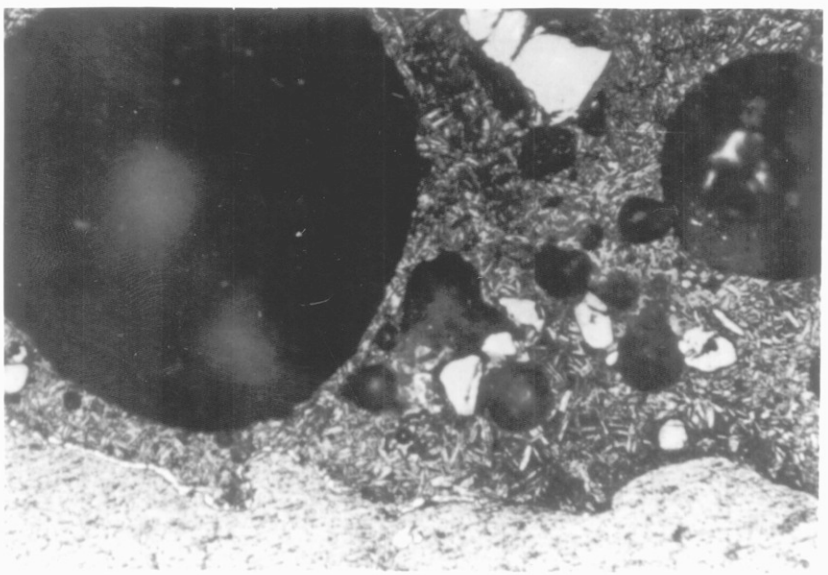


PLATE 15. Sample Z1 (1450°C, air, 15s, raw LTA) etched, reflected light (plane polars). Magnification 640x.

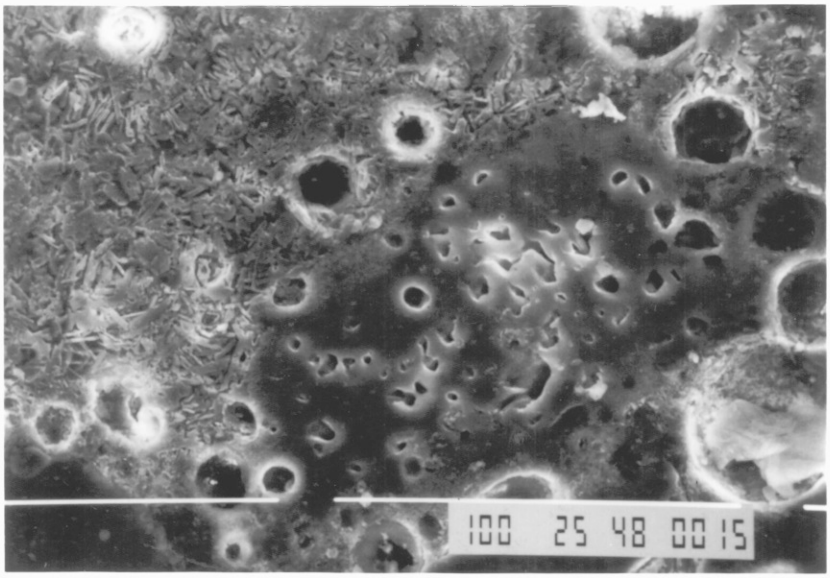


PLATE 16. Sample Z1 (etched). Glassy and crystalline region (white bar = 100 µm).

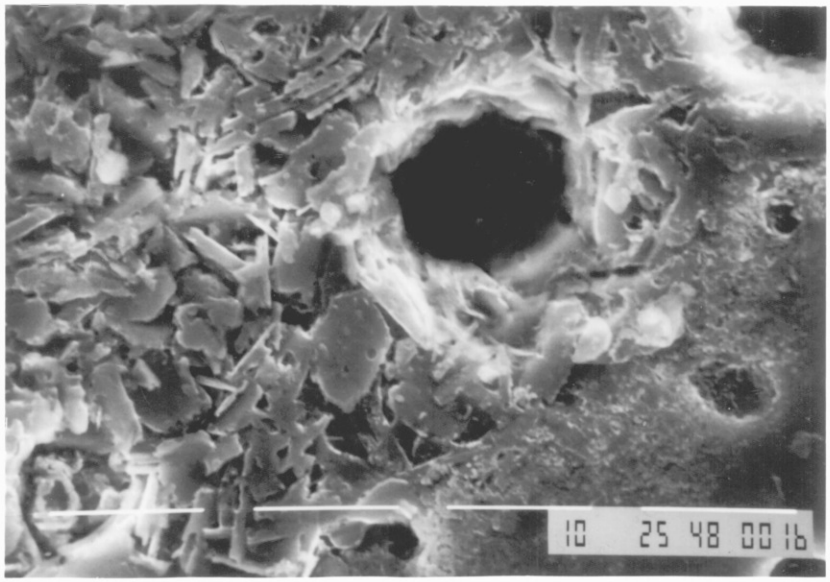


PLATE 17. Sample Z1 (etched). Crystalline area around pore, glassy region bottom right corner (white bar = 10 µm).

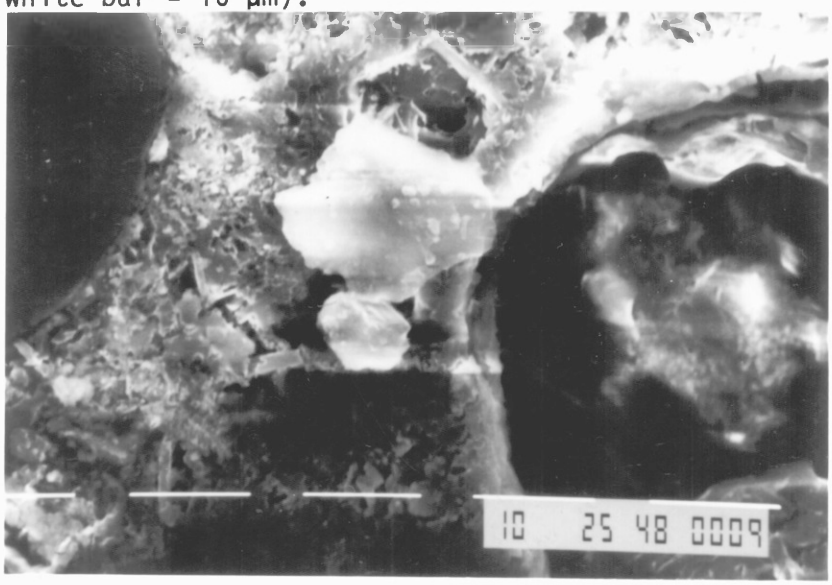


PLATE 18. Sample Z1 (etched). Crystalline area between two pores and quartz grains (centre) (white bar = 10 µm).

The XRD analysis of both samples showed that Z1 contained anorthite and quartz whereas quartz was the only phase to report for sample Z2.

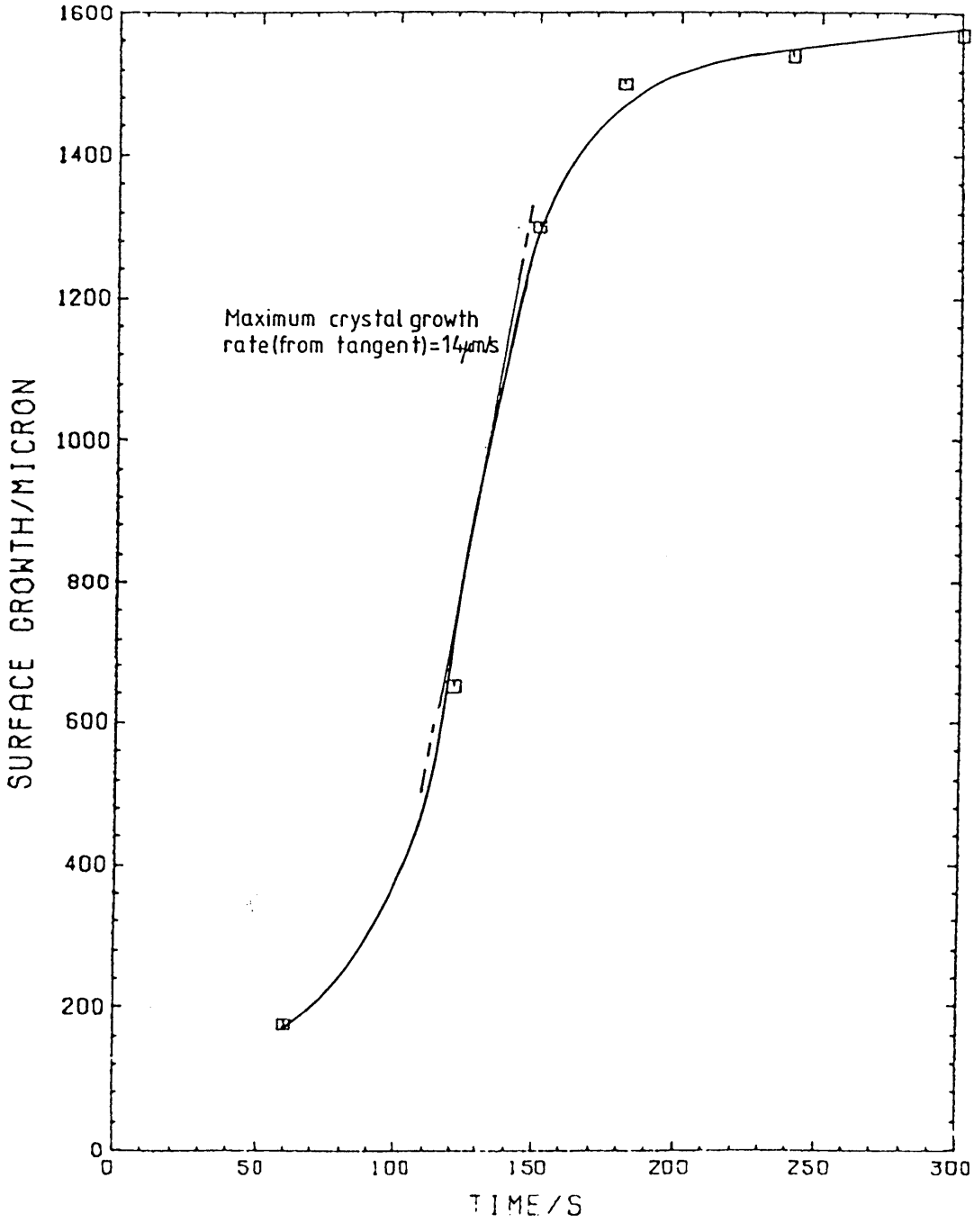
4.5 CRYSTAL GROWTH RATES

Two glasses were prepared based on the chemical composition of two known lignitic-type ashes. The glass Mat 8 was of the same composition as the ash KA and the glass Mat 9 was of the same as that of an ash of significantly higher lime content studied previously by Nolan et al.[69]

For both glasses studied the crystal growth was from the surface of the sample and was linear. For the glass Mat 8, the crystalline phase was anorthite and for the glass Mat 9 the phase was a melilite (composition not confirmed) as determined by the morphology of the crystals at the interface. For each glass the thickness of surface growth was plotted against time at each temperature of treatment. The graph of surface growth against time for Mat 8 glass at 1100 °C has been reproduced in Fig.4.1. The maximum growth rate for each temperature of treatment was determined by calculating the gradient of the tangent to the curve at the region of maximum growth as indicated in Fig.4.1.

The maximum crystal growth rates for the Mat 9 glass at temperatures above 1200 °C were difficult to determine. This was due to the residual liquid phase of the sample

Fig.4.1. Graph of surface growth vs. time for MAT8 glass at 1100 °C.



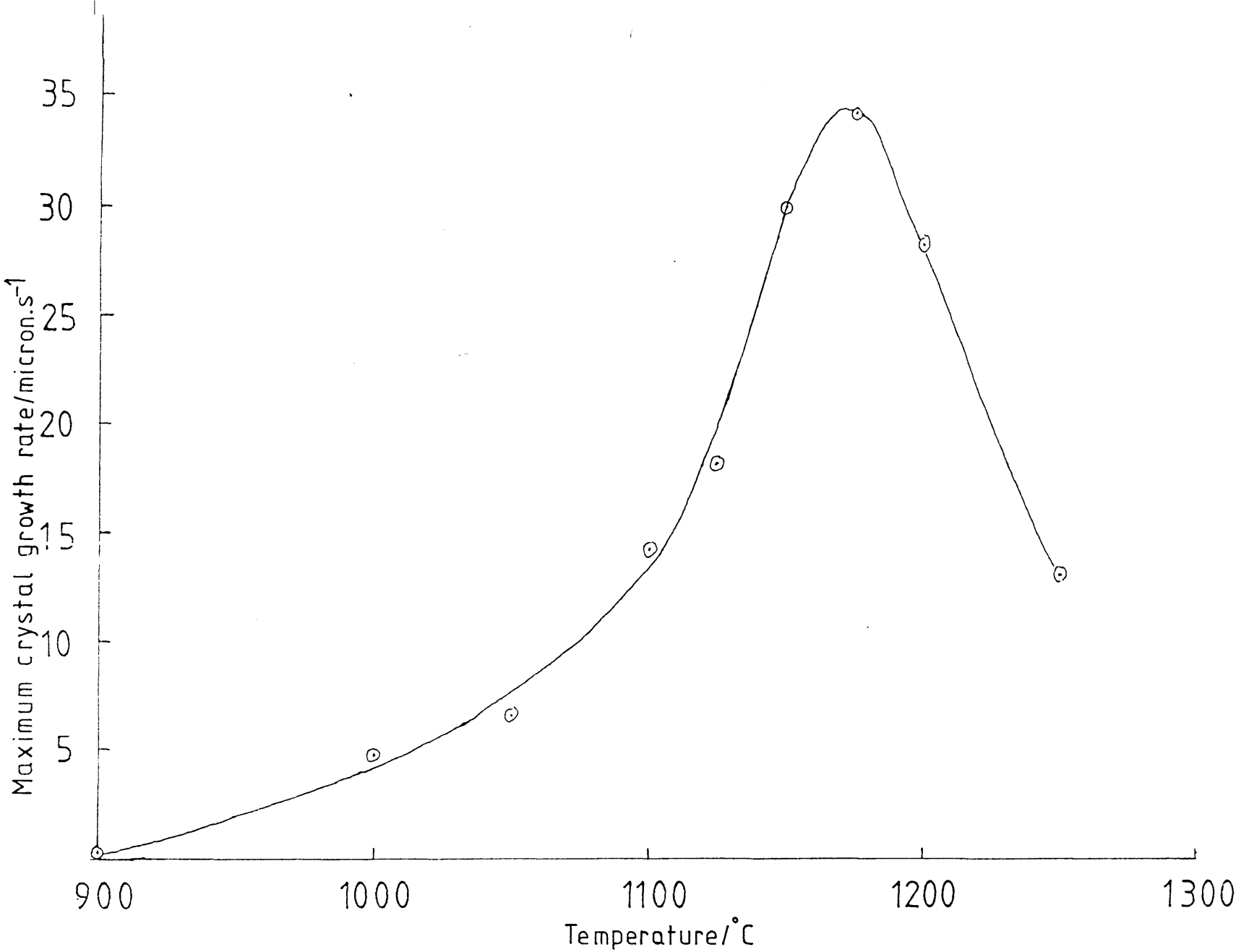


Fig.4.2. Graph of crystal growth rate vs. temperature for MAT8 glass.

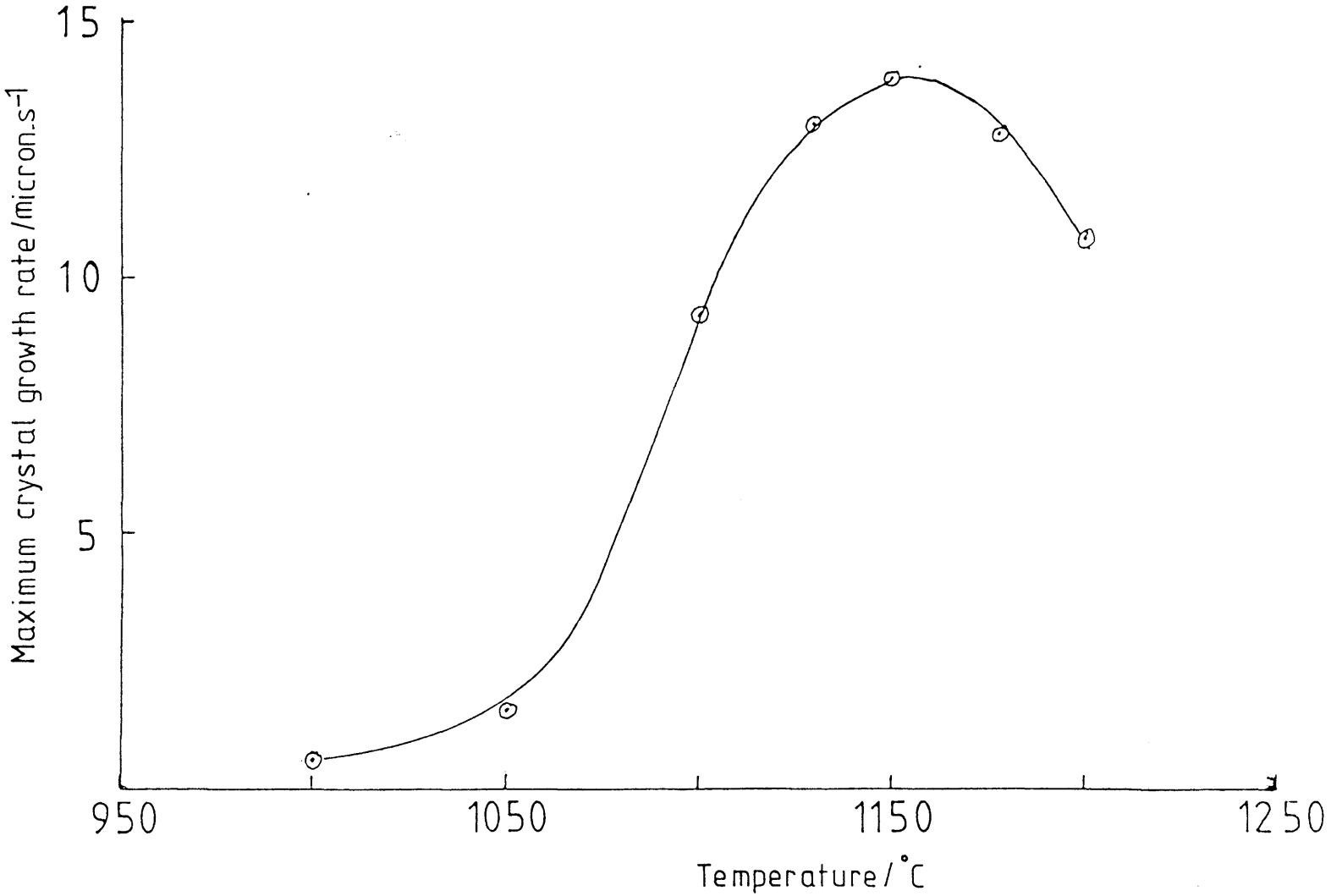


Fig. 4.3. Graph of crystal growth rate vs. temperature for MAT9 glass.

being very fluid and flowing away from the upper-most surface leading to gross deformation of the sample. The maximum growth rates obtained for the glasses Mat 8 and Mat 9 have been plotted against the temperature of treatment in Figs 4.2 and 4.3.

4.6 CRYSTALLISATION OF $CaO-Al_2O_3-SiO_2$ GLASSES

The crystallisation behaviour of the five three-component glasses of CaO, Al_2O_3 and SiO_2 was studied using quenching experiments in an electric muffle furnace. The results of the study have been compiled in Table 4.8. The value of the liquidus temperature given is taken from the phase diagram for the ternary system (Fig.3.6). The temperature of appearance of the secondary and tertiary phases included in Table 4.8 is that of the highest temperature and longest treatment at which the quenched sample contained the respective phase. For the glasses where the secondary or tertiary phase was not observed, the longest treatment of the glass at temperatures expected to induce the required crystallisation have been included.

The primary crystalline phase for the glasses K1, K3, K4 and K5 was anorthite and for the glass K2 was gehlenite ($2CaO.Al_2O_3.SiO_2$). Gehlenite was characterised by its dendritic morphology and birefringence. Secondary and tertiary phases were determined by X-ray diffraction. Only the glass K2 was observed to crystallise fully to three crystalline components (gehlenite, anorthite, and cyclo-wollastonite ($\alpha CaO.SiO_2$)).

TABLE 4.8

Crystallisation behaviour of three component glasses

Glass	Composition wt %			Liquidus temp	Primary phase	Appearance of secondary phase		Secondary phase	Appearance of tertiary phase		Tertiary phase
	SiO_2	Al_2O_3	CaO			Temp/°C	Time/hrs		Temp/°C	Time/hrs	
K1	49.0	31.5	19.5	1520	anorthite	1100	76	n.o.	-	60	n.o.
K2	37.0	25.0	38.0	1450	gehlenite	1200	60	anorthite	1200		cyclowollastonite
K3	41.5	27.0	31.5	1390	anorthite	1100	72	n.o.	-		n.o.
K4	44.0	28.5	27.5	1460	anorthite	1100	105	n.o.	-		n.o.
K5	49.0	35.0	16.0	1510	anorthite	1100	72	n.o.	-		n.o.

n.o. = not observed. No crystallisation of secondary or tertiary phases occurred with the heat treatment listed.

4.7 CRYSTALLISATION OF $CaO-MgO-Al_2O_3-SiO_2$ GLASSES

The crystallisation behaviour of the four component glasses containing CaO, Al_2O_3, SiO_2 and with 5 or 10 wt % MgO was again determined by quenching experiments and to a lesser extent by high temperature microscopy.

The results of the study have been compiled in Table 4.9. The series of glasses K17 - K21 and K22 - K26 were based on the ternary glass compositions K1 - K5 with 5 and 10 wt % MgO respectively. The J and I series of glasses also contained 5 and 10 wt % MgO respectively and were chosen to determine primarily the primary crystalline phases of compositions on the corresponding planes of the quaternary system.

The liquidus temperatures of the K series of glasses were determined accurately (± 5 °C) by high temperature microscopy with which the primary crystalline phase could be observed in situ. Confirmation of the liquidus temperature was obtained from quenching experiments. For the J and I series of glasses the liquidus temperatures were not determined to the same degree of accuracy; the temperatures given in Table 4.9 indicate the highest value at which the glass was treated to induce crystallisation. Thus the greater (>) or less than (<) sign indicates whether the primary crystalline phase was present or not respectively at the heat treatment temperature. The approximate sign ($\sim$) used in some cases indicates that only a very few crystals were observed in the sample treated at the indicated temperature and thus was very close to the true liquidus temperature.

The primary crystalline phases were readily determined by microscopic observation. Anorthite was characterised by its lath-like morphology; melilite, a solid solution series between gehlenite ($2CaO.Al_2O_3.SiO_2$) and akermanite ($2CaO.MgO.2SiO_2$) by its dendritic morphology (like feathers) and a wide range of birefringent colours; spinel ($MgO.Al_2O_3$) crystals were observed as discrete transparent regular octahedra ($\sim$ 10 μm) of slightly higher refractive index than the glass matrix and extinguished under cross polars due to the isotropic nature of the phase. Cordierite ($2MgO.2Al_2O_3.5SiO_2$) was only determined as a primary phase for the glass I5 and was observed as transparent colourless crystals of rectangular cross section with weak birefringence.

The temperature of appearance of the secondary and tertiary crystalline phases given in Table 4.9 is the highest value at which the respective phase was observed in the quenched sample. The time of the treatments have not been included, the results tabulated were checked by increasing the length of heat treatment or from quenching experiments above and below the recorded temperature. Crystalline phases were determined by X-ray diffraction, the patterns of the phases anorthite, spinel, cordierite and diopside ($CaO.MgO.2SiO_2$) corresponded to the respective standard patterns. Melilite was determined to be present by comparing the pattern obtained, after excluding the lines attributed to other phases present with the patterns of the two end members of the solid solution series. The detailed composition was not determined. The melilite pattern obtained for a sample of glass K23 treated at 1400 °C for 2 hours has been compared with the two end members in Table 4.10 .

TABLE 4.9

Crystallisation behaviour of $CaO-MgO-Al_2O_3-SiO_2$ glasses

Glass	composition wt % SiO_2	Al_2O_3	CaO	MgO	Liquidus Temperature	Primary Crystalline Phase	Temperature of appearance of 2° phase/°C	Secondary Crystalline Phase	Temperature of appearance of 3° phase/°C	Tertiary Crystalline phase
K17	47.0	30.0	18.0	5.0	1450	Anorthite	-	n.o	-	n.o
K18	35.0	24.0	36.0	5.0	1420	Melilite	1300	Anorthite	1200	Spinel
K19	39.0	26.0	30.0	5.0	1350	Anorthite	1300	Melilite	1200	Spinel
K20	42.0	27.0	26.0	5.0	1410	Anorthite	-	n.o	-	n.o
K21	47.0	33.0	15.0	5.0	1470	Anorthite	1350	Spinel	1200	Cordierite
K22	44.1	28.4	17.5	10.0	1420	Anorthite	1360	Spinel	1300	Melilite
K23	33.3	22.5	34.2	10.0	1460	Spinel	1300	Melilite	-	n.o
K24	37.4	24.3	28.3	10.0	1450	Spinel	1200	Anorthite	1200	Melilite
K25	39.6	25.6	24.8	10.0	1440	Spinel	1350	Anorthite	1200	Melilite
K26	44.1	31.5	14.4	10.0	1455	Spinel	1400	Anorthite	-	n.o
J1	53.3	29.5	12.2	5.0	>1450	Anorthite	1300	Cordierite	n.d	n.d
J2	45.7	35.0	14.3	5.0	>1400	Anorthite	1350	Melilite	1300	Spinel
J3	38.6	27.1	29.3	5.0	<1400	Anorthite	1320	Melilite	n.d.	n.d
J4	41.0	21.4	32.6	5.0	<1400	Anorthite	1250	Melilite	n.d	n.d
J5	38.6	24.8	31.6	5.0	~1360	Melilite	1300	Anorthite	1200	Spinel
J6	41.0	31.9	22.1	5.0	~1430	Anorthite	1400	Spinel	1200	Melilite
I1	44.1	17.5	28.4	10.0	~1240	Melilite	1200	Anorthite	1150	Pyroxene*
I2	43.0	20.0	27.0	10.0	~1300	Anorthite	1200	Melilite	1200	Pyroxene*
I3	44.1	26.6	19.3	10.0	~1400	Anorthite	1200	Spinel	1200	Pyroxene*
I4	50.5	28.9	10.6	10.0	<1400	Anorthite	1300	Cordierite	n.d	n.d
I5	53.5	29.0	7.5	10.0	~1350	Cordierite	1300	Anorthite	1300	Cordierite
I6	38.0	19.3	32.7	10.0	~1350	Melilite	1300	Spinel	1200	Pyroxene*
I7	33.2	20.9	35.9	10.0	1445	Melilite	1400	Spinel	n.d	n.d

n.o = not observed

n.d = not determined

*Pyroxene observed as diopside ($CaO.MgO.2SiO_2$) only.

TABLE 4.10

Comparison of the XRD pattern of a $CaO-MgO-Al_2O_3-SiO_2$ melilite with those of the two end members

$2CaO.Al_2O_3.SiO_2$ Gehlenite (No.20-199)		K23.4 (Treated at 1430°C ½hr)		$2CaO.MgO.2SiO_2$ Akermanite (No.10-391)	
d/Å	Int.	d/Å	Int.	d/Å	Int.
5.46	6	5.45	w	5.55	12
5.08	6	5.10	w	4.22	10
4.22	4	4.20	vw	3.91	6
3.71	20	3.70	m	3.73	14
3.43	2	3.45	vw	3.51	6
3.07	25	3.07	m	3.09	30
2.85	100	2.85	s	2.87	100
2.72	6	2.72	w	2.78	4
2.535	8	2.53	w	2.488	18
2.435	20	2.44	m	2.391	10
2.404	25	2.40	m	2.039	20
2.29	14	2.29	w	1.959	6
2.195	2	n.d.	-	1.905	8
2.126	2	n.d.	-	1.854	10
2.043	16	2.03	m	1.764	30
1.967	2	1.97	vw	1.673	4
1.924	8	1.92	w	1.643	4
1.864	6	1.865	w	1.602	6
1.812	10	1.815	w	1.510	8
1.754	35	1.75	m	1.471	4
1.723	8	1.72	w	1.435	8
1.632	2	1.64	vw	1.398	10
1.616	4	1.62	w		
1.519	16	1.52	m		

n.d. = not determined

For the K series of glasses, where a secondary and/or tertiary phase was not observed (Table 4.9) the results were checked by increasing the time of crystallisation treatment at various temperatures down to 1000 °C. For example glass K20 was treated at 1200 °C for 16 hours and the quenched sample contained only anorthite. In the case of the I and J series of glasses the data of interest was the primary crystalline phase and not the detailed crystallisation behaviour, as determined for the K series of glasses.

4.8 CRYSTALLISATION STUDIES OF THE SYSTEM CaO-Al_2O_3-SiO_2-IRON OXIDE

The results of the crystallisation studies of the F series of glasses (compositions based on the ternary glasses K1 - K5) in a mildly reducing atmosphere have been listed in Table 4.11, compositions are given in Table 4.12. The crystalline phases were determined predominantly by X-ray diffraction especially for the glasses treated at temperatures substantially below the liquidus. This was because at these temperatures the samples were predominantly lightly sintered masses of low mechanical strength and the crystalline particles were too small for microscopic observation.

The results have been listed in descending order of crystallisation temperature and increasing length of treatment. The $Fe^{2+}/\Sigma Fe$ ratio determined for each of the quenched samples has been recorded as a percentage. The $Fe^{2+}/\Sigma Fe$ ratio obtained for the original glasses have also been included. The partial pressure of oxygen at the

treatment temperature (obtained from the data in Appendix B) is also listed in the Table. The accuracy of the method used is ±20% due mainly to the small amount of sample taken or available for analysis.

Clear trends were not observed in the $Fe^{2+}/\Sigma Fe$ ratios determined in the quenched samples, it would be expected that the ratio would increase with decreasing temperature of treatment. The major observation is that the crystallisation of the glass affects the values substantially. The general trends observed are that the ratios decrease with crystallisation of calcium silicate phase (wollastonite solid solution or cyclowollastonite) and olivine (specifically $CaO.FeO.SiO_2$), and increase with decreasing temperature and with crystallisation of melilite, iron spinel, and fayalite ($2FeO.SiO_2$). The $Fe^{2+}/\Sigma Fe$ ratios in calcium sodium silicate glasses have been shown by Paul[98] to be dependent on the glass composition. While there has been no previous investigation of the effect of crystallisation on the $Fe^{2+}/\Sigma Fe$ ratios it would be expected that the change in the composition of the residual liquid phase with devitrification would affect the values. In this context the original composition of the glass and the crystallising phases would also be determining factors.

The results listed in Table 4.11 have been used to compile the crystallisation behaviour of each of the glasses in Table 4.12. The compositions of the glasses have also been included with the iron oxide content given as equivalent FeO. Liquidus temperatures are indicated by greater than (>) or less than (<) signs depending on whether a crystalline phase was present in the quenched sample treated at that temperature or not respectively. The temperature of the appearance of secondary, tertiary and quaternary phase is the

highest temperature at which the respective phase was observed.

The melilite phase observed in the quenched samples was found by X-ray diffraction to correspond closely to that of gehlenite ($2CaO.Al_2O_3.SiO_2$). The patterns attributed to melilite for samples F2.4, F12.1, F7.10 have been compared with the standard pattern of gehlenite in Table 4.13. There was no evidence of solid solution in the series gehlenite-iron akermanite ($2CaO.FeO.2SiO_2$).

The term spinel was used to designate a member of the solid solution series hercynite-magnetite. The spinel observed in all the quenched samples corresponded in composition with that of hercynite. The XRD pattern of the spinel phase of sample F15.2 has been compared with those of the two end members in Table 4.14 .

The tertiary phase observed for the glass F2 was cyclo-wollastonite ($\alpha CaO.SiO_2$) in the quenched samples treated at 1200 °C and 900 °C. At other temperatures the tertiary phase present was wollastonite ($\beta CaO.SiO_2$), the low temperature polymorph of calcium metasilicate.

Cyclowollastonite was determined to be present as the tertiary phase in the sample F3.8 (treated at 1200 °C) whereas at other temperatures wollastonite was observed.

For the glasses F12 and F17, iron-wollastonite ($(CaO,FeO)SiO_2$) was observed to be present in quenched samples as the secondary phase. In the case of the glass F17 both melilite and iron wollastonite were present in the sample

TABLE 4.11

Results of crystallisation experiments on $CaO-Al_2O_3-SiO_2$-iron oxide glasses and the Fe^{2+}/total iron ratio determined

Run	Crystallisation Temp/°C	Crystallisation Time/hrs	Crystalline phases	$(\frac{Fe^{2+}}{\Sigma Fe}) \times 100$	$\log_{10} p_{O_2}$
F1	-	-	AN	28	-
F1.9	1480	2.0	AN	67	- 8.4
F1.5	1450	1.5	AN	59	- 8.6
F1.6	1450	3.0	AN	33	- 8.6
F1.8	1450	20.0	AN	38	- 8.6
F1.3	1400	1.5	AN	52	- 9.2
F1.7	1300	4.5	AN	72	-10.2
F1.13	1200	24.0	AN	50	-11.5
F1.11	1100	10.5	AN	72	-13.0
F1.10	1000	6.0	AN	55	-14.4
F1.12	900	13.0	AN	57	-16.2
F2	-	-	-	27	-
F2.4	1300	6.0	MEL	79	-10.2
F2.6	1200	12.0	MEL,AN,αCS	72	-11.5
F2.5	1100	13.0	MEL,AN,CS	36	-13.0
F2.3	1000	6.0	MEL,AN,CS	21	-14.4
F2.7	900	13.0	MEL,AN	68	-16.2
F2.13	900	22.0	MEL,AN,αCS	24	-16.2
F2.8	800	20.0	MEL	86	-18.5
F2.9	700	20.0	MEL	75	-21.0
F3	-	-	-	7	-
F3.2	1450	1.5	AN	31	- 8.7
F3.13	1410	14.5	AN	38	- 9.0
F3.12	1390	7.0	AN	55	- 9.2
F3.6	1350	8.5	AN	37	- 9.8
F3.3	1300	3.0	AN	47	-10.2
F3.5	1300	4.5	AN	46	-10.2
F3.7	1200	2.5	AN,MEL	17	-11.5
F3.8	1200	5.0	AN,MEL,αCS	25	-11.5
F3.14	1100	5.0	AN,MEL,CS	24	-13.0
F3.17	1100	20.0	AN,MEL,CS	34	-13.0
F3.16	1000	28.0	AN,MEL,CS	38	-14.4
F3.15	900	13.0	AN,MEL,CS	57	-16.2
F4	-	-	-	23	-
F4.4	1400	1.0	AN	57	- 9.2

Run	Crystallisation Temp/°C	Crystallisation Time/hrs	Crystalline phases	$(\frac{Fe^{2+}}{\Sigma Fe}) \times 100$	$\log_{10}P_{O_2}$
F4.6	1350	8.5	AN	65	- 9.8
F4.5	1300	4.5	AN	67	-10.2
F4.8	1200	2.5	AN	52	-11.5
F4.9	1200	5.0	AN,MEL	68	-11.5
F4.13	1200	24.0	AN,MEL	73	-11.5
F4.10	1100	5.0	AN,MEL,CS	61	-13.0
F4.12	1000	28.0	AN,MEL,CS	60	-14.5
F4.11	900	13.0	AN,MEL,CS	54	16.2
F5	-	-	-	35	-
F5.13	1500	4.0	glass	44	- 8.2
F5.4	1400	2.5	AN	55	- 9.2
F5.8	1400	20.0	AN	66	- 9.2
F5.7	1350	8.5	AN	72	- 9.8
F5.9	1350	24.0	AN	48	- 9.8
F5.10	1300	3.0	AN	44	-10.2
F5.6	1300	4.5	AN	44	-10.2
F5.7	1200	24.0	AN,SP	35	-11.5
F5.16	1100	20.0	AN,SP	56	-13.0
F5.15	1000	28.0	AN,SP	53	-14.4
F5.14	900	14.0	AN,SP	71	-16.2
F6	-	-	-	36	-
F6.10	1480	20.0	glass	74	- 8.3
F6.3	1400	20.0	AN	94	- 9.2
F6.4	1350	24.0	AN	95	- 9.8
F6.7	1300	5.0	AN	69	-10.2
F6.6	1200	5.0	AN	61	-11.5
F6.5	1100	9.0	AN	72	-13.0
F6.9	1000	28.0	AN,FAY	75	-14.4
F6.8	900	14.0	AN,FAY	74	-16.3
F7	-	-	-	20	-
F7.11	1420	23.0	MEL	48	- 9.0
F7.10	1325	18.0	MEL	42	-10.0
F7.3	1200	0.5	MEL,AN	44	-11.5
F7.6	1200	12.0	MEL,AN	48	-11.5
F7.4	1100	3.0	MEL,AN,CS	43	-13.0
F7.5	1000	6.0	MEL,AN,CS	38	-14.4
F7.7	900	14.0	MEL,AN	69	-16.3
F7.8	800	20.0	MEL,AN,CS	51	-18.5

Run	Crystallisation Temp/°C	Time/hrs	Crystalline phases	$(\frac{Fe^{2+}}{\Sigma Fe}) \times 100$	$\log_{10} P_{O_2}$
F8	-	-	-	24	-
F8.7	1420	23.0	glass	38	- 9.0
F8.3	1300	6.0	AN	20	-10.2
F8.2	1200	5.0	AN,MEL	51	-11.5
F8.5	1100	9.0	AN,MEL,SP	71	-13.0
F8.4	1000	12.0	AN,MEL,SP,OLIV	49	-14.4
F8.6	900	14.0	AN,MEL,SP	69	-16.3
F9	-	-	-	29	-
F9.9	1424	23.0	AN	28	- 9.0
F9.5	1350	3.0	AN	64	- 9.8
F9.4	1300	6.0	AN,MEL	51	-10.2
F9.3	1200	5.0	AN,MEL	66	-11.5
F9.8	1100	20.0	AN,MEL	74	-13.0
F9.6	1000	12.0	AN,MEL,OLIV	66	-14.4
F9.7	900	25.0	AN,MEL,OLIV	83	-16.3
F10	-	-	-	45	-
F10.9	1400	5.0	AN	47	- 9.2
F10.2	1350	3.0	AN	72	- 9.8
F10.6	1300	5.0	AN	78	-10.2
F10.5	1200	5.0	AN,SP	86	-11.5
F10.8	1100	20.0	AN,SP	54	-13.0
F10.3	1000	12.0	AN,SP,FAY	75	-14.4
F10.7	900	25.0	AN,SP,FAY	81	-16.3
F11	-	-	-	40	-
F11.3	1400	24.0	AN,FAY	59	- 9.2
F11.2	1300	24.0	AN,FAY	50	-10.2
F11.1	1200	6.0	AN,FAY	55	-11.5
F11.7	1100	6.0	AN,FAY	79	-13.0
F11.6	1000	20.0	AN,FAY	79	-14.4
F12	-	-	-	9	-
F12.2	1300	6.0	MEL,CFS	57	-10.2
F12.1	1200	5.0	MEL,CFS	25	-11.5
F12.8	1140	21.0	MEL	61	-12.3
F12.9	1100	28.0	MEL,AN,CFS	58	-13.0
F12.10	1000	20.0	MEL,AN,CFS,SP	14	-14.4
F12.3	900	25.0	MEL,AN,CFS,SP	42	-16.3

Run	Crystallisation Temp/°C	Time/hrs	Crystalline phases	$(\frac{Fe^{2+}}{\Sigma Fe}) \times 100$	$\log_{10} p_{O_2}$
F12.4	800	20.0	MEL,AN,CFS,SP	63	-18.5
F12.5	700	18.0	MEL,AN,CFS,SP	63	-21.0
F15	-	-	-	24	-
F15.5	1350	12.0	AN	55	- 9.8
F15.4	1300	6.0	AN	65	-10.2
F15.3	1200	16.0	AN	55	-11.5
F15.2	1100	6.0	AN,SP	51	-13.0
F15.6	1000	20.0	AN,SP,FAY	69	-14.4
F16	-	-	-	22	-
F16.5	1350	12.0	glass	55	- 9.8
F16.4	1300	6.0	AN,FAY	50	-10.2
F16.3	1200	16.0	AN,FAY	60	-11.5
F16.2	1100	6.0	AN,FAY	69	-13.0
F16.1	1000	20.0	AN,FAY	87	-14.4
F17	-	-	-	6	-
F17.3	1300	10.0	MEL,CFS	56	-10.2
F17.9	1200	23.0	MEL,CFS	46	-11.5
F17.2	1100	5.0	MEL,CFS	67	-13.0
F17.1	1000	5.0	MEL,AN,OLIV	66	-14.4
F17.4	900	25.0	MEL,AN,OLIV	67	-16.3
F20	-	-	-	22	
F20.8	1450	5.0	AN	59	- 8.7
F20.7	1400	5.0	AN,FAY	50	- 9.2
F20.4	1385	6.0	AN,FAY	68	- 9.4
F20.5	1300	10.0	AN,FAY,SP	66	-10.2
F20.3	1200	7.0	AN,FAY,SP	54	-11.5
F20.2	1100	5.0	AN,FAY,SP	78	-13.0
F20.1	1000	5.0	AN,FAY,SP	65	-14.4
F20.6	900	14.0	AN,FAY,SP	59	-16.3

Key:

AN = anorthite $CaO.Al_2O_3.2SiO_2$

MEL = melilite $2CaO.Al_2O_3.SiO_2$ - $2CaO.FeO.2SiO_2$

αCS = cyclowollastonite $\alpha CaO.SiO_2$

CS = wollastonite $\beta CaO.SiO_2$

SP = hercynite-magnetite ($FeO.Al_2O_3$ - $FeO.Fe_2O_3$)

FAY = fayalite $2FeO.SiO_2$

OLIV = olivine $2(CaO.FeO)SiO_2$

CFS = iron wollastonite $(CaO,FeO)SiO_2$

TABLE 4.12

Crystallisation behaviour of glasses of the system $CaO-Al_2O_3-SiO_2$-iron oxide

Glass	composition wt % SiO_2	Al_2O_3	CaO	FeO	Liquidus temp/°C	Primary phase	Temp.of appearance of 2° phase	Secondary phase	Temp.of appearance of 3° phase	Tertiary phase	Temp.of appearance of 4° phase	Quaternary phase
F1	47.0	30.0	18.0	5.0	>1480	anorthite	-	n.o.	-	n.o.	-	n.o.
F2	35.0	24.0	36.0	5.0	>1300	melilite	1200	anorthite	1200	calcium + silicate	-	n.o.
F3	39.0	26.0	30.0	5.0	>1450	anorthite	1200	melilite	1100	calcium + silicate	-	n.o.
F4	42.0	27.0	26.0	5.0	>1400	anorthite	1200	melilite	1100	calcium + silicate	-	n.o.
F5	47.0	33.0	15.0	5.0	<1500	anorthite	1200	iron spinel	-	n.o.	-	n.o.
F6	44.0	28.4	17.6	10.0	<1480	anorthte	1000	fayalite	-	n.o.	-	n.o.
F7	33.3	22.4	34.3	10.0	>1420	melilite	1200	anorthite	1100	calcium + silicate	-	n.o.
F8	37.4	24.2	28.4	10.0	<1420	anorthite	1200	melilite	1100	iron spinel	1000	olivine
F9	39.6	25.6	24.8	10.0	>1420	anorthite	1300	melilite	1000	olivine	-	n.o.
F10	44.0	31.6	14.4	10.0	>1400	anorthite	1200	iron spinel	1000	fayalite	-	n.o.
F11	41.6	26.8	16.6	15.0	>1400	anorthite	1400	fayalite	-	n.o.	-	n.o.
F12	31.5	21.2	32.2	15.0	>1300	melilite	1300	iron wollastonite	900	anorthite	900	iron spinel
F15	41.6	29.8	13.6	15.0	>1350	anorthite	1100	iron spinel	1000	fayalite	-	n.o.
F16	39.2	25.2	15.6	20.0	<1350	anorthite	1300	fayalite*	-	n.o.	-	n.o.
F17+	29.6	20.0	30.4	20.0	>1300	melilite	1300	iron + wollastonite	-	-	-	n.o.
F20	39.2	28.0	12.8	20.0	<1450	anorthite	1400	fayalite	1300	spinel	-	n.o.

+ see text

* determined as the secondary crystalline phase from the analysis of intensities of XRD pattern

n.o. not observed

TABLE 4.13

Comparison of XRD patterns of three melilites observed in $CaO-Al_2O_3-SiO_2$-iron oxide glasses with that of gehlenite

$2CaO.Al_2O_3.SiO_2$ gehlenite (No 20-199)		F2.4 treated at 1300 °C, 6 hrs		F7.10 treated at 1325 °C, 18 hrs	F12.1 treated at 1200 °C, 5 hrs
d/Å	Int	d/Å	Int*	d/Å	d/Å
5.08	6	5.04	vw	5.04	n.d.
4.22	4	n.d.		n.d.	n.d.
3.71	20	3.70	w	3.71	3.70
3.43	2	3.43	vvw	n.d.	n.d.
3.07	25	3.06	w	3.07	3.07
2.85	100	2.85	s	2.86	2.85
2.72	6	2.71	vw	2.71	n.d.
2.535	8	2.53	vw	2.53	2.53
2.435	20	2.43	w	2.44	2.43
2.404	25	2.40	w	2.40	2.40
2.29	14	2.29	w	2.29	2.29
2.195	2	2.19	vvw	n.d.	n.d.
2.126	2	n.d.		n.d.	n.d.
2.043	16	2.045	w	2.04	2.04
1.967	2	1.963	vw	1.97	1.97
1.924	8	1.92	vw	1.93	1.93
1.864	6	1.86	vw	1.86	n.d.
1.812	10	1.814	vw	n.d.	n.d.
1.754	35	1.753	m	1.76	1.76

n.d. = not determined. * intensity observed for all three samples

TABLE 4.14

Comparison of the XRD pattern of an observed iron spinel with those of hercynite and magnetite

$FeO.Al_2O_3$ Hercynite (No 3-894)		F.15.2 measured spinel pattern (treated 1100 °C, 6 hrs)		$FeO.Fe_2O_3$ Magnetite (No 19-629)	
d/Å	Int	d/Å	Int	d/Å	Int
4.69	20	4.70	w	4.852	8
2.87	60	2.88	m	2.967	30
2.45	100	2.45	s	2.532	100
2.02	80	2.02	m	2.099	20
1.64	16	1.64	vw	1.72	10
1.56	40	1.565	w	1.62	30

treated at the highest temperature (1300 °C). Analysis of the XRD pattern indicated that melilite was the primary crystalline phase. There is no standard pattern for the phase iron-wollastonite, comparison of the pattern obtained with that of $(CaO,FeO,MgO)SiO_2$ (9.82%FeO,8.0%MgO) showed a close correlation.

At lower crystallisation temperatures for glass F17 (1000 °C and 900 °C) only melilite, anorthite and olivine were observed with no evidence of a wollastonite phase. The samples quenched at lower temperatures did not contain olivine, the crystalline phases present at the sample treated at 800 °C were melilite, anorthite, wollastonite and spinel.

Quaternary phases were observed for the glasses F8, F12 and F17 only.

4.9 CRYSTALLISATION OF MODEL GLASSES BASED ON A LIGNITIC-TYPE ASH COMPOSITION

The results of the crystallisation study of the series of multicomponent glasses based on the composition of the lignitic-type ash KA have been listed in Table 4.15. The glass Mat 3 corresponded to the normalised five component composition of the ash (SiO_2, Al_2O_3, CaO, Fe_2O_3 and MgO). Glasses Mat 4 and Mat 5 corresponded to the normalised compositions seven and eight component compositions to include the sodium and potassium oxide contents and titania content respectively. The composition of each glass is listed in Table 4.15.

Crystalline phases present in the quenched samples were determined predominantly by X-ray diffraction. The

TABLE 4.15

Crystallisation of multicomponent glasses based on the composition of ash KA

Run	Crystallisation treatment* Temp/°C	Time/hrs	Crystalline phases
Mat 3.4	1400	13.0	anorthite + magnetite
Mat 3.3	1300	1.5	anorthite + magnetite
Mat 3.6	1300	3.0	anorthite + magnetite
Mat 3.2	1200	16.0	anorthite + magnetite
Mat 3.7	1100	3.0	anorthite
Mat 3.5	1100	7.0	anorthite + magnetite
Mat 3.1	1000	12.0	anorthite
Mat 4.5	1450	2.0	(glass only)
Mat 4.3	1400	1.0	anorthite
Mat 4.3	1300	3.0	anorthite
Mat 4.7	1200	16.0	anorthite + iron wollastonite
Mat 4.1	1200	18.0	anorthite + iron wollastonite
Mat 4.4	1100	20.0	anorthite + iron wollastonite
Mat 4.6	1000	20.0	anorthite + iron wollastonite
Mat 5.4	1400	5.0	anorthite
Mat 5.2	1300	4.0	anorthite
Mat 5.3	1200	4.0	anorthite
Mat 5.1	1000	15.0	anorthite

*after remelting at 1500 °C for 1 hour.

COMPOSITION OF GLASSES

Glass	composition wt %							
	SiO_2	Al_2O_3	CaO	Fe_2O_3	MgO	Na_2O	K_2O	TiO_2
MAT 3	44.4	28.6	17.8	5.3	3.9	0.0	0.0	0.0
MAT 4	43.9	28.3	17.7	5.2	3.9	0.7	0.3	0.0
MAT 5	43.1	27.8	17.3	5.1	3.8	0.7	0.3	1.9

primary phase for all three glasses studied was anorthite. Magnetite was observed as the secondary crystalline phase for glass Mat 3, the XRD pattern matching that of the standard. The phase iron-wollastonite [$(CaO,FeO)SiO_2$] was determined to be the secondary crystalline phase for glass Mat 4. Only anorthite was observed for the glass Mat 5.

4.10 CRYSTALLISATION OF A GLASS OF BITUMINOUS-TYPE COMPOSITION

The glass D1 was prepared based on the composition of the bituminous-type ash KB. The results of the crystallisation study of the glass has been listed in Table 4.16 along with the chemical composition. Mullite was observed to be the primary phase with iron spinel as a secondary phase. The XRD analysis of the quenched samples containing the iron spinel phase indicated that the composition lay close to the hercynite end member of the hercynite-magnetite solid solution series. The spinel patterns for samples D1.4 and D1.5 have been compared with those of the two end members in Table 4.17.

The hematite observed was determined to be at the surface of the sample only and not in the bulk of the sample as with the iron spinel phase.

TABLE 4.16

Crystallisation of glass D1. A composition based on that of a bituminous-type ash

Run	Crystallisation treatment*		Crystalline phases
	Temp/°C	Time/hrs	
D1.10	1400	18	mullite + hematite
D1.5	1300	48	mullite + hematite
D1.4	1200	18	mullite + iron spinel + hematite
D1.2	1180	40	mullite + iron spinel
D1.8	1150	18	mullite + iron spinel
D1.9	1130	48	mullite + iron spinel
D1.6	1100	16	mullite + iron spinel
D1.7	1000	60	mullite + iron spinel

* after remelting at 1550 °C for 1 hour

Composition wt %

SiO_2	Al_2O_3	Fe_2O_3	CaO	MgO	Na_2O	K_2O	TiO_2
54.5	26.4	9.4	1.5	1.6	1.2	4.2	1.1

TABLE 4.17

Comparison of XRD patterns of two spinels observed in glass D1 with those of hercynite and magnetite

$FeO.Al_2O_3$ Hercynite (No.3-894)		D1.4 measured pattern		D1.7 measured pattern	$FeO.Fe_2O_3$ Magnetite (No.19-629)	
d/Å	Int.	d/Å	Int.	d/Å	d/Å	Int.
4.69	20	4.74	vw	4.75	4.852	8
2.87	60	2.90	m	2.90	2.967	30
2.45	100	2.49	s	2.48	2.532	100
2.02	80	2.06	ms	2.05	2.099	20
1.64	16	1.89	vw	1.89	1.72	10
1.56	40	1.59	m	1.58	1.62	30

CHAPTER 5

DISCUSSION

The earlier chapters have outlined many of the problems relating to the deposition of furnace slags in p.f. boilers and in particular the prediction of the slagging propensity of coal. The experimental programme was designed to throw new light on the reactions which occur between coal minerals as they pass through the flame and subsequently cool. The cooling ash particles either pass through the furnace or are retained on the furnace walls. The rate of fusion of coal ash, the rate of crystallisation of the silicate melt and high temperature phase equilibria studies have been used to help elucidate many of the problems encountered by both the designers and operators of coal-fired furnaces. The following discussion has been divided in a number of sections to analyse the data obtained using the various experimental techniques and concludes by comparing the known slagging propensity of a number of coals with the prediction which can now be made as the result of the present study.

5.1 HIGH TEMPERATURE MICROSCOPY

The fusion characteristics of low temperature ashes from two lignitic and a bituminous coal were determined by high temperature microscopy. The fusion properties of lignitic-type ashes KA and KC are compared with the results of the BS fusion test in Table 5.1. The characteristic temperatures observed for the lignitic-type ashes were generally lower than the standard ash fusion temperatures as determined by Babcock Power Ltd. The first

appearance of a liquid phase, characterised by coalescence of ash particles was observed for ashes KA and KC to be 290°C and 110°C respectively lower than the initial deformation temperature. The temperature at which a single drop of liquid was formed did not correspond to the fluid temperature for ash KC but was within experimental limits for ash KA.

Ash KA was previously studied by high temperature microscopy by Nolan et al.[69] and the results compare favourably with the observations of this study. The two sets of results are compared in Table 5.2.

The fusion properties of ash KB was observed to be different in air than in an inert atmosphere (nitrogen). The ash contained 9.6% iron oxide (expressed as Fe_2O_3) and it would be expected that the iron-bearing minerals (e.g. pyrite, FeS_2) would not be oxidised in the nitrogen atmosphere. Thus the iron present would be predominantly in the ferrous state. Ferrous oxide is known to be a better flux than ferric oxide and the lower fusion characteristics determined in nitrogen are consistent with the fluxing action. The effect is comparable to that observed in the standard ash fusion test between the values determined in air and in a reducing atmosphere. Though the standard fusion data was not obtained for the ash KB, the results of an ash of similar iron oxide content have been listed in Table 5.3 and show a difference of 70 °C for the IDT and 40 °C for the FT.

It is difficult to correlate the high temperature microscope observations with the ash fusion temperatures as discussed in the literature survey. The standard test is used to determine the fluid range of a coal ash melt and from the values obtained a

TABLE 5.1

Fusion of lignitic-type ashes

Ash KA

High-temperature Microscopy+		B.S. Test*[69]	
Temperature/°C	Observation	Temp./°C	Characteristic
980	Ash coalesced slightly	1270	I.D.T.
1270	Liquid flowed & gas evolved	1340	H.T.
1330	Single drop of liquid formed	1370	F.T.
1450	No changes	-	-

Ash KC

High-temperature microscopy+		B.S. Test*[5]	
Temperature/°C	Observation	Temp./°C	Characteristic
1000-1200	No change	1310	I.D.T.
1200	Coalescence began	1350	H.T.
1200-1300	Appreciable amount of liquid present	1410	F.T.
1300	Single drop formed		
1300-1360	No further change		

+in air *mildly-reducing conditions

TABLE 5.2

Comparison of high-temperature microscope observations of ash KA

This study		Nolan et al.[69]	
Temperature/°C	Observation	Temp./°C	Observation
980	Ash coalesced slightly	1020	Ash began to shrink
1270	Liquid flowed & gas evolved	1310	Large amount of liquid formed & gas evolved. Single drop formed.
1330	Single drop of liquid formed		
1450	No changes		

TABLE 5.3

Ash Fusion Temperatures of a Bituminous-type Ash*

	Temperature/^{o}C	
	AIR	REDUCING
IDT	1270	1200
HEMISPHERE	1300	1240
FLOW	1350	1310

Ash Analysis, Composition Wt%

SiO_2	Al_2O_3	Fe_2O_3	CaO	MgO	Na_2O	K_2O	TiO_2
47.2	20.1	10.2	7.0	3.9	1.2	0.9	2.4

*Polish coal-fired in Hanasaari boiler, Finland.

predicted slagging propensity may be made. The study of the fusion of LTA, which contains the original coal mineral matter, would be expected to give more accurate indications of the temperature range at which a liquid phase will be present than the standard fusion tests which use roasted ash. The phases present in roasted ash may be significantly different from those present in the LTA and thus the interactions between the minerals during a heat treatment will be different.

The only crystalline phase observed for the lignitic-type ashes KA and KC was anorthite. The bituminous-type ash KB was observed to crystallise mullite only, but not from a homogeneous liquid as with ashes KA and KC.

While the high temperature microscope gave the fusion characteristics of ashes the instrument is limited in use for the full characterisation of an ash. The observations, as with the standard fusion test, are subjective and different operators may record different behaviour. This is reflected in Table 5.2 where the observations of this study and that of Nolan et al.[69] for the same ash are compared. Although the effect of different heating rates on the fusion characteristics of the ashes was not investigated it is feasible that this could well affect the observations. It should be noted that the standard fusion test is undertaken at a heating rate of 5 °C per minute. Ideally the heating rate should be as slow as possible to allow the system to approach or reach equilibrium at each stage. Since this is impractical for laboratory/industrial practice a compromise rate must be used.

With respect to the direct observation of the crystallisation behaviour of ash melts on the high temperature microscope the technique may present problems. The small amounts of iron oxide in the lignitic-type ashes precluded observation of the crystalline phases in the melt, nor can lengthy crystallisation treatment analogous to the residence time of ash particles in a boiler be performed.

Thus in conclusion, the high temperature microscope was found to be useful in determining the fusion characteristics and the crystallisation behaviour of ash melts. Generally the instrument gives lower temperatures at which the liquid phase first appears than the BS test. The observations for the bituminous-type ash in an inert atmosphere were consistent with the standard fusion characteristics determined in a mildly reducing atmosphere

due to the greater fluxing effect of ferrous ions than ferric ions. The method, as with the standard fusion test does not subject the ash to the same time temperature history that ash particles experience in a coal-fired boiler and thus on its own is limited in terms of assessment of slagging propensity.

5.2 CRYSTALLISATION OF ASH MELTS

Only anorthite was observed to crystallise in the series of quenching experiments for the ashes KA and KC. The reluctance of other phases to crystallise was surprising, with extensive treatments failing to produce further crystallisation. According to the phase rule more than one crystalline phase would be expected to crystallise for a multicomponent system such as coal ash. The observed behaviour confirms the observations of Hanusch and Grimshaw[42] who studied the phases present in boiler deposits formed from coal ashes of similar composition. The authors reported anorthite as the major crystalline phase, other crystalline phases present (in minor proportions) included calcium sulphate, hematite and magnetite.

In the case of the bituminous-type ash KB, mullite and an iron spinel phase were observed. There is no data available yet on the mineralogical content of deposits formed (if any) by coals of similar ash composition in boilers (e.g. Drax, Yorkshire).

The crystallisation behaviour of the ashes will be discussed in detail in context with further data in a subsequent section.

5.3 THE FUSION OF COAL ASH

The study of the fusion of coal ash in air and 1550 °C indicated that the physical and chemical processes involving both the formation of a liquid phase and crystallisation are quite rapid.

The formation of spherical drops, after 15 s at 1450 °C for both the roasted and raw LTA samples was a significant observation. An appreciable amount of liquid phase must be formed and be of sufficiently high viscosity to form spheres. This, because the expanding gases, (from the decomposition of various minerals) must be trapped within a viscous liquid phase. The presence of a permeable mineral within the wall of the sphere would cause collapse of the structure. It should be noted that no attempt was made to compact the samples before treatment. The samples were placed loosely on or in the sample holder and the formation of the spherical particles must have been due to large surface tension forces within the liquid phase. The particles were similar in morphology to fly ash particles formed in boilers reported by various investigators including Raask[48] and Lauf.[50]

The presence of anorthite crystals in the samples treated for 15 s at 1450 °C was surprising. According to Nolan et al.[69] the major mineral phase of an ash of similar composition to that studied (derived from the same coal source) was kaolinite with minor amounts of calcite, quartz, dolomite and pyrite also present. For anorthite to form so rapidly both the kaolinite and calcite and/or dolomite must have fused and reacted.

Iron spinel and hematite crystals were observed for the roasted LTA sample treated at 1450 °C for 15 s whereas for the analogous raw LTA sample only iron spinel crystals were present. The presence of hematite may have been due to the roasting treatment during which the pyrite would be oxidised. The clear euhedral morphology of the spinel crystals indicates that the phase had crystallised from a melt. Similar spinel crystals have been observed in bituminous-type slags by Livingston et al.[46] and Kiss et al.[110]. The different reflectivities of the crystals observed for the roasted LTA sample was a feature also reported by Livingston et al.. Watt and Wilkins[31] observed that when mixtures of kaolinite and pyrite were heated, pyrite initially melted and flowed between the kaolinite lattice, and subsequently crystallised as magnetite. A similar mechanism may occur for true ash compositions with the melted pyrite reacting with components such as alumina in the liquid phase. This would explain the different reflectivities of the spinel crystals observed. Spinel crystals generally have higher melting points than plagioclase minerals such as anorthite (e.g. hercynite $FeO.Al_2O_3$ m.p.1743°C, anorthite m.p. 1550 °C) and thus once formed would be more resistant to melting. This may account for the observation of a small group of spinel crystals in a sample treated for 4 minutes at 1450 °C (sample R5).

The samples R2 and Z2 treated for 60 s at 1450 °C were significantly different. The sample R2 was formed from roasted LTA whereas Z2 was formed from raw LTA. Sample R2 contained a significant amount of anorthite whereas sample Z2 was predominantly glass with quartz grains and coke particles with no anorthite observed. This may have been due to some combustion of coal particles within the LTA for sample Z2 causing an increase in ash bed temperature. The sample within the muffle furnace received

radiant heat (sample Z2) while the sample R2 was shielded from the furnace element and thus the sample Z2 may have experienced a higher temperature than R2.

The reluctance of quartz to dissolve in the liquid phase confirmed observations of various investigators such as Livingston et al.[46] and Friedrich et al.[45] who have observed quartz grains in slag deposits. As discussed in Chapter 2 the rate of solution of quartz is controlled by the diffusion coefficient of SiO_2 at the quartz/melt interface and will be dependent on the viscosity, composition and temperature of the melt. Quartz is a very stable refractory mineral, being composed of SiO_2 tetrahedra, the bonding of which is predominantly covalent. To dissolve quartz the strong covalent bonds of silica must be broken. The photomicrograph (Plate 11) shows clearly a solution rim around a quartz grain. The solution rim will have a viscosity gradient ranging from infinity for the solid quartz grain to the viscosity of the bulk liquid phase. Silica is well known to increase the viscosity of melts[90] and thus it would be expected that the larger quartz grains would be the most resistant to dissolution. This has been observed in studies by Livingston[99] who found that while the mean linear intercept of quartz grains on the outer sintered region of a slag deposit was about 10 μm, the value within the glassy and crystalline region was about 40 μm. This confirms the observations of this study that while small quartz particles were observed for samples treated for 15 s at 1450 °C only large quartz grains were present in samples treated for longer than 1 minute at 1450 °C and in all samples treated at 1550 °C.

The samples treated at 1550 °C were predominantly glassy with some residual quartz, although not observed in all samples. Analysis of thin sections revealed the glass to be unhomogeneous with dark, presumably iron-rich, streaks in samples treated for less than 120 s. Thus the temperature was above the liquidus for the ash.

In conclusion the fusion processes of the coal ash studied occur very rapidly. Quartz was the only coal mineral found not to dissolve at 1450 and 1550 °C despite treatments of up to 2 minutes. There was no significant difference in fusion behaviour between LTA and roasted ash except for the presence of iron spinel and hematite crystals being present in the samples of the latter. The crystallisation of anorthite within the sample indicates that the melt approaches equilibrium rapidly. That is, there was probably an incubation period between the sample being introduced into the furnace and the sample reaching the set temperature. During this incubation period a liquid phase forms and dissolves the other mineral phases, with crystallisation of anorthite occurring simultaneously. It was only in the sample treated for longer than 120 s at 1450 °C (vertical tube furnace) that no anorthite was present indicating a delay of the same order of time. The samples treated for short times (1450 °C for 15 s and 30 s) resembled fly ash particles being similar in morphology to those studied in other investigations. Samples treated for longer times resembled slag deposits. The presence of quartz in all the samples was expected from glass-forming studies and mineralogical investigations of slag deposits. All the other minerals had melted and fused within a short period of time.

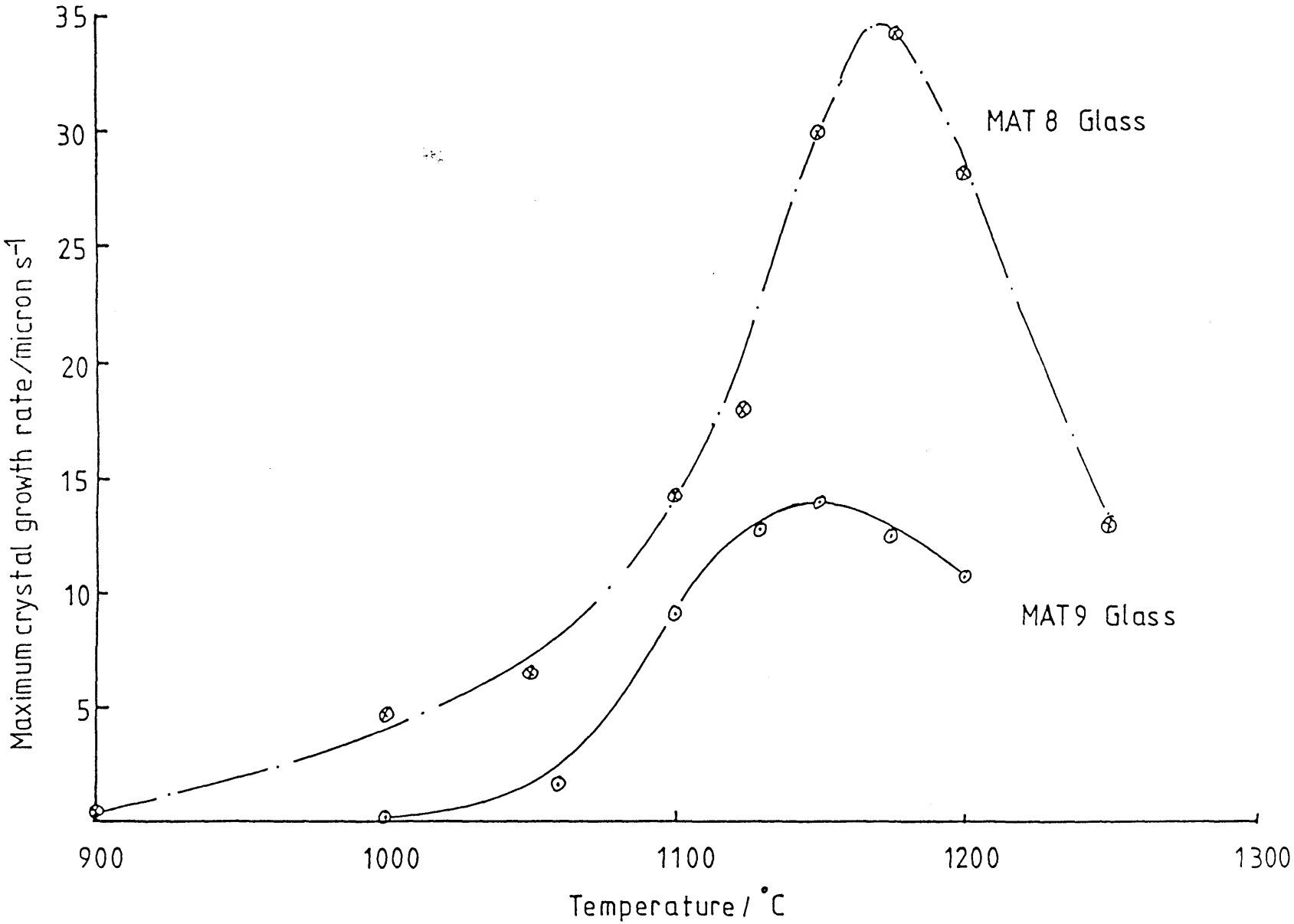
5.4 CRYSTAL GROWTH RATE

The maximum crystal growth rates/temperature curves obtained for the two glasses, Mat 8 and Mat 9, have been reproduced in Fig.5.1. The glass Mat 8 corresponded in composition to the ash KA and the composition of glass Mat 9 was based on a high-lime ash from the same region as ash KA. The values of the growth rates of both glasses are surprisingly high, especially that of Mat 8 glass. Crystal growth rates have not previously been measured in coal ash systems.

Investigators at Imperial College have followed the crystallisation processes in iron-making slag systems and glass-ceramic materials. The maximum crystal growth rate observed for anorthite/wollastonite crystallising from the surface was 5.6×10^{-2} μm s^{-1} at 968 °C in a glass of composition 50.4% SiO_2, 14.3% Al_2O_3, 28.5% CaO, 1.9% MgO, 2.5% FeO and 2.4% Fe_2O_3 by Williamson et al.[93] Keyworth[100] determined the surface growth rate of anorthite/wollastonite from a $CaO-Al_2O_3-SiO_2$ glass. A maximum value was observed of 1.1 μm s^{-1} at 1200 °C for a glass of composition 53% SiO_2, 15% Al_2O_3 and 30% CaO. These values compare with the maximum growth rates determined in this study of 34 μm s^{-1} for glass Mat 8 and 13.8 μm s^{-1} for glass Mat 9 (crystallising phases anorthite and melilite respectively).

The crystal growth observed for glasses Mat 8 and Mat 9 at various temperatures have been plotted against square root time in Figs 5.2 and 5.3. The curves are linear for all the samples which shows that the rate of growth is long-range diffusion (see p.80). Thus the high growth rates observed in

Fig. 5.1. Graph of crystal growth rate against temperature for MAT 8 and MAT 9 glasses.



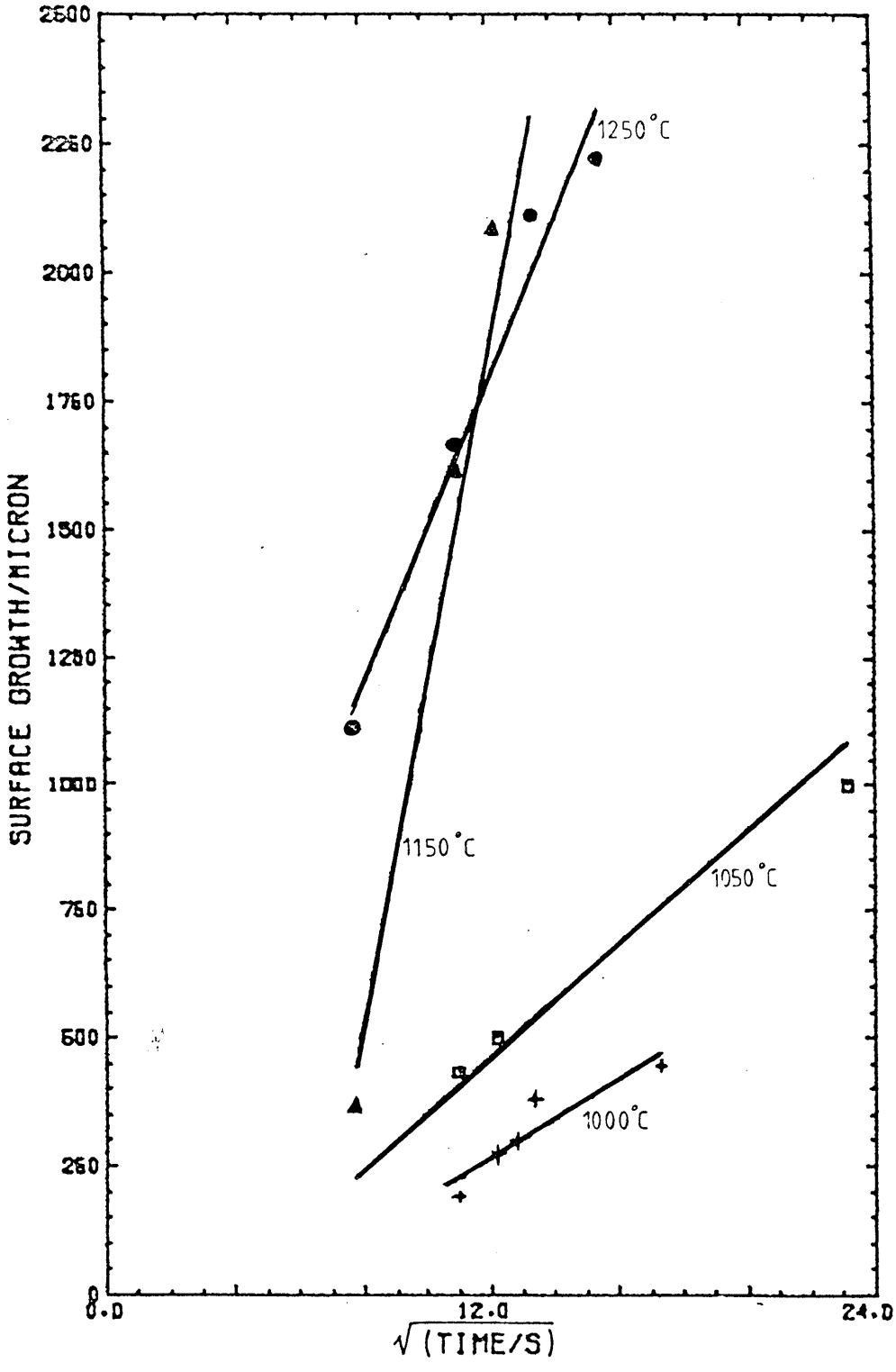


Fig.5.2. Graph of crystal growth vs. square-root time for MAT8 glass at various temperatures.

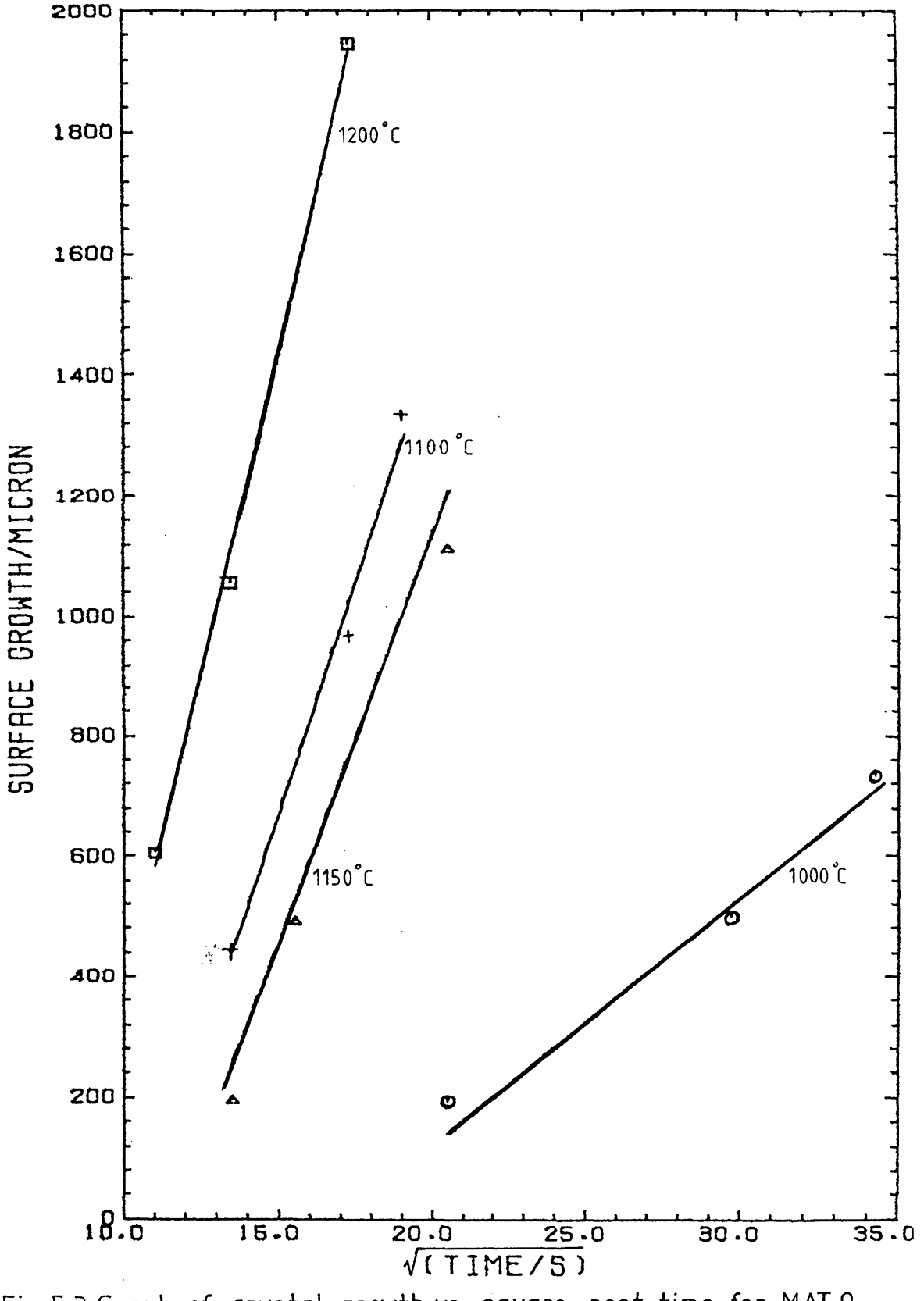


Fig.5.3. Graph of crystal growth vs. square-root time for MAT 9 glass at various temperatures.

study may be due to the decrease in viscosity at the melt/crystal interface. That is as anorthite crystallises from the surface the interface will become enriched in the ions not involved in the formation of the crystal lattice, i.e. iron, sodium, potassium, magnesium and titanium. Iron oxide, soda, magnesia and potash are all known to reduce the viscosity of glass melts and thus the lower the viscosity at the interface the higher will be the rate of diffusion of CaO, Al_2O_3 and SiO_2 to the crystal front. Williamson et al have observed increasing crystal growth rates of anorthite/wollastonite in glasses with increasing amounts of iron(II) oxide as opposed to iron(III) oxide, due to the greater fluxing effect of the former.

The high rate of crystal growth of anorthite in the Mat 8 glass corresponded to the observations of the growth of anorthite in the ash fusion samples. For example, crystals of 140 μm length were observed in a sample treated at 1450 °C for 120 s which is a rate of 1.0 μm s^{-1}. Though the systems are not directly comparable the value obtained is about the same as the maximum growth rate observed by Keyworth and if the time of incubation and other processes is taken into account the growth rates may be of the same order as that observed for glass Mat 8. The observation explains the rapid devitrification of the ash fusion samples as they must have passed through a stage in the treatment at which the system was at a temperature suitable for crystal growth.

The relatively lower maximum crystal growth rate of melilite in the Mat 9 glass was initially unexpected. The lower silica and higher lime content was expected to lead to a lower viscosity of the glass and hence higher diffusion rates. The activation energy

for crystal growth for the Mat 8 and Mat 9 glasses were determined by plotting the natural logarithm of the rate against reciprocal absolute temperature in Figs 5.4 and 5.5. The slope of the curve is equal to the activation energy divided by the gas constant (R). The values obtained have been indicated on the respective graphs and show that the activation energy for maximum growth (Ea) for Mat 8 glass (250 kJ mol^{-1}) is less than half the value of the Mat 9 glass (515 kJ mol^{-1}). The values of activation energy of this study have been compared with those of Williamson et al[93] and Keyworth[100] in Table 5.4. Williamson et al. observed that the activation energy for viscous flow for the glasses studied was of the same order of magnitude as the activation energy for crystal growth. This would be expected on theoretical grounds (see Rawson[101]) in that the energy needed to break the intermolecular bonds in a glass for the formation of a crystalline phase must be comparable to the energy required to break the bonds so that the melt will flow.

TABLE 5.4

Activation energies for crystal growth

Glass composition wt %									Ea/kJ mol^{-1}	Ref.
SiO_2	Al_2O_3	CaO	MgO	Fe_2O_3	FeO	Na_2O	K_2O	TiO_2		
43.1	27.8	17.3	3.8	5.1	0.0	0.7	0.3	1.9	250	a
33.7	23.0	34.8	4.4	2.4	0.0	0.2	0.0	1.5	515	b
53	15	32	0	0.0	0.0	0.0	0.0	0.0	416	c
50.3	14.2	28.5	2.0	2.5	2.5	0.0	0.0	0.0	559	d

a this study glass Mat 8

b this study glass Mat 9

c Williamson et al.[93]

d Keyworth[100]

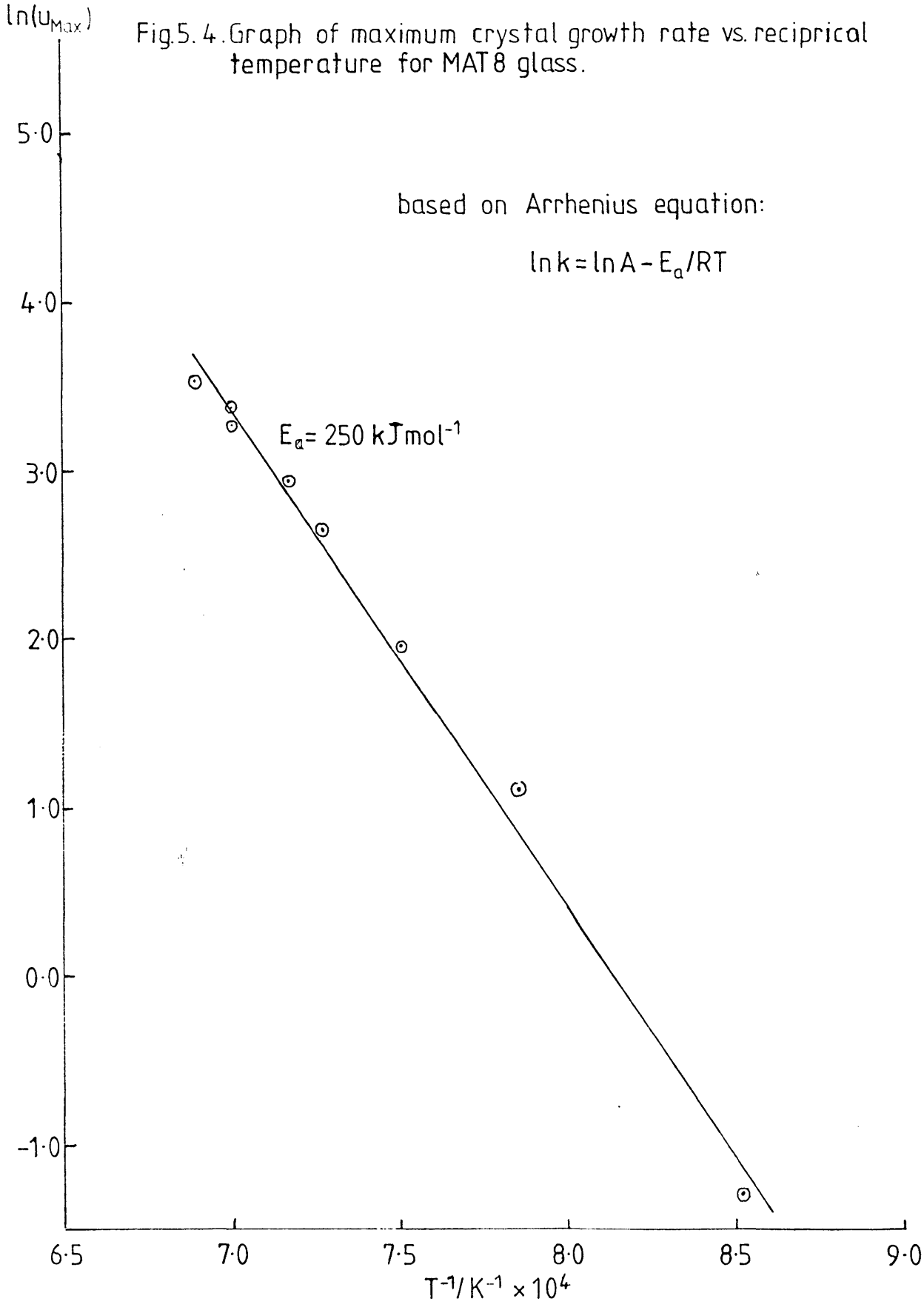
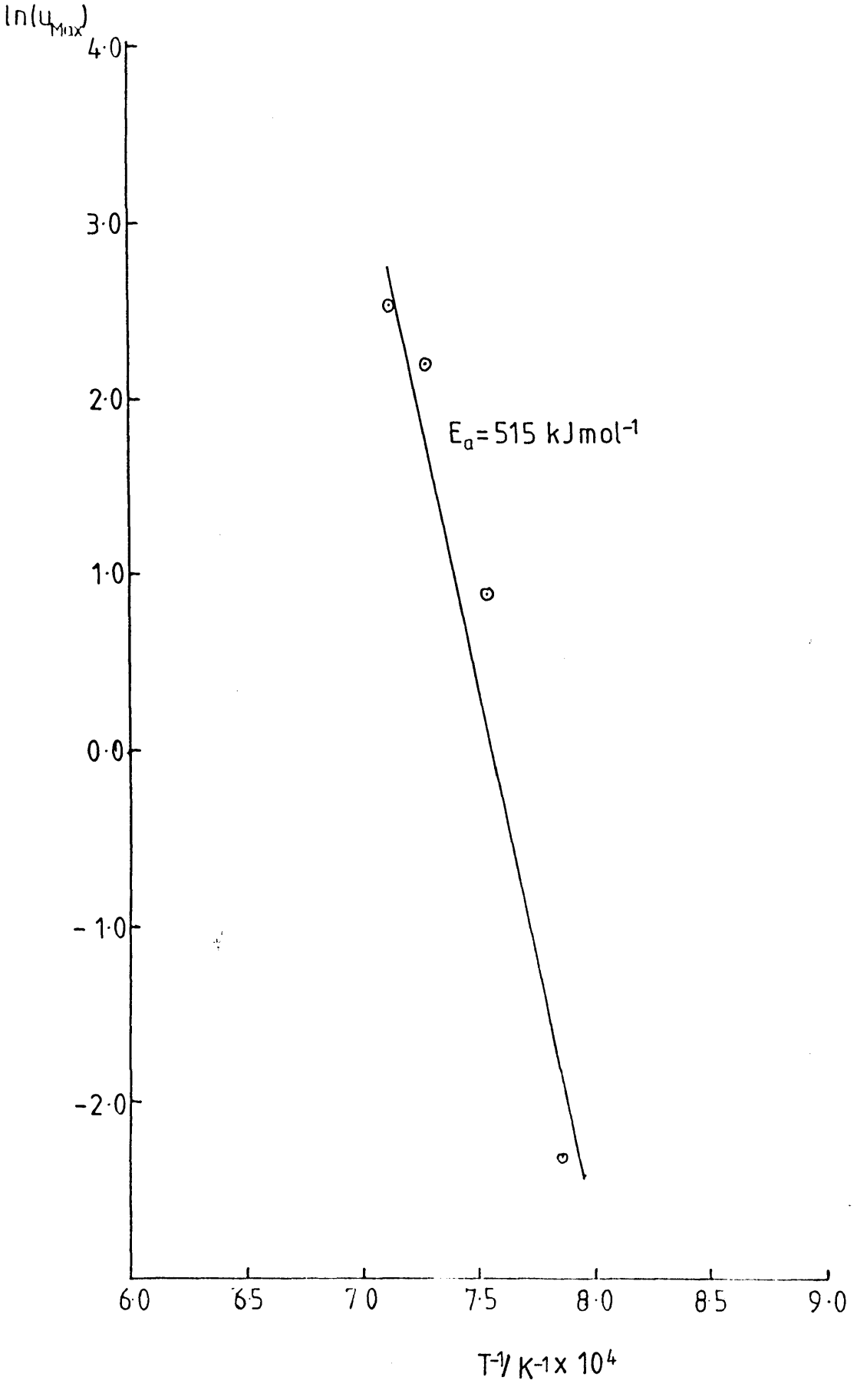


Fig.5.4. Graph of maximum crystal growth rate vs. reciprical temperature for MAT8 glass.

Fig.5.5. Graph of maximum crystal growth rate vs. reciprical temperature for MAT 9 glass.



The activation energy for viscous flow has been determined for glasses Mat 8 and Mat 9 from the Arrhenius plots of natural log viscosity against $^1/T(K)$ (Figs 5.6 and 5.7). The viscosity values for glass Mat 8 were determined from the equations derived by Urbain et al.,[101a] the method is discussed in detail with relation to coal ash melts in Appendix C. The viscosity data for glass Mat 9 was that of Gibb[102] determined experimentally for a coal ash of the same composition.

The activation energy for viscous flow for Mat 8 glass (226 kJ mol^{-1}) is very close to the value for crystal growth determined (250 kJ mol^{-1}). This confirms the expected mechanism, that of long-range diffusion controlled crystallisation. The value of the activation energy for viscous flow for Mat 9 glass (64 kJ mol^{-1}) which was approximately an order of magnitude less than the activation energy for crystal growth (515 kJ mol^{-1}). The curves of crystal growth versus square root time for glass Mat 9 (Fig.5.3) indicate growth controlled by long-range diffusion. It will be shown that the amount of melilite to crystallise from the glass would be expected to be small and that this might cause the high activation energy observed for crystal growth. That is the interface between the crystal front and the liquid phase containing the ions necessary for crystal growth will increase in size markedly with crystallisation of the primary phase if the amount of the thermodynamically favourable phase to crystallise out is small.

With reference to Fig.5.1 it should be noted that the crystal growth rate for both glasses studied decreased rapidly below the maximum value with decreasing temperature. The lowest maximum

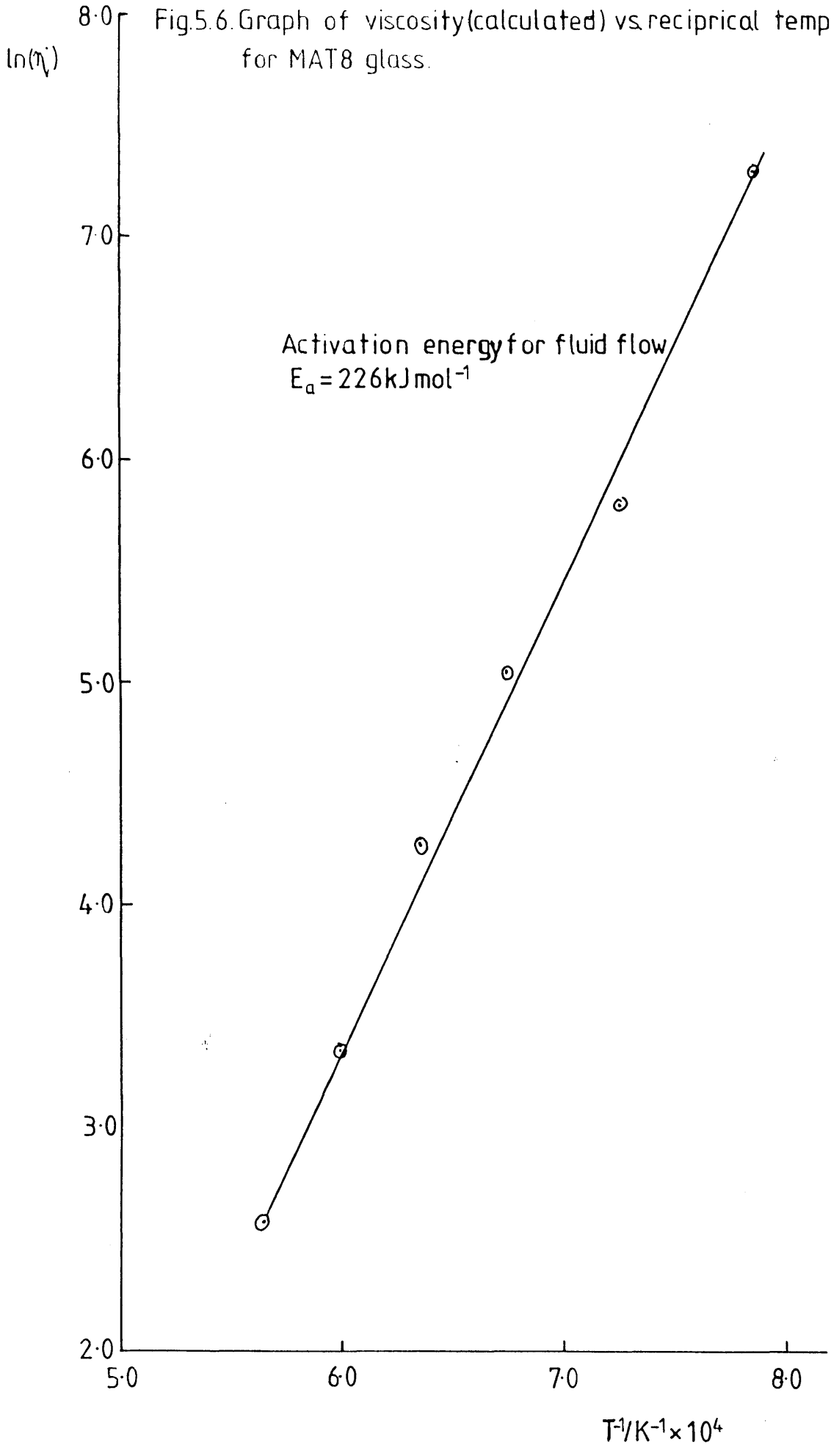
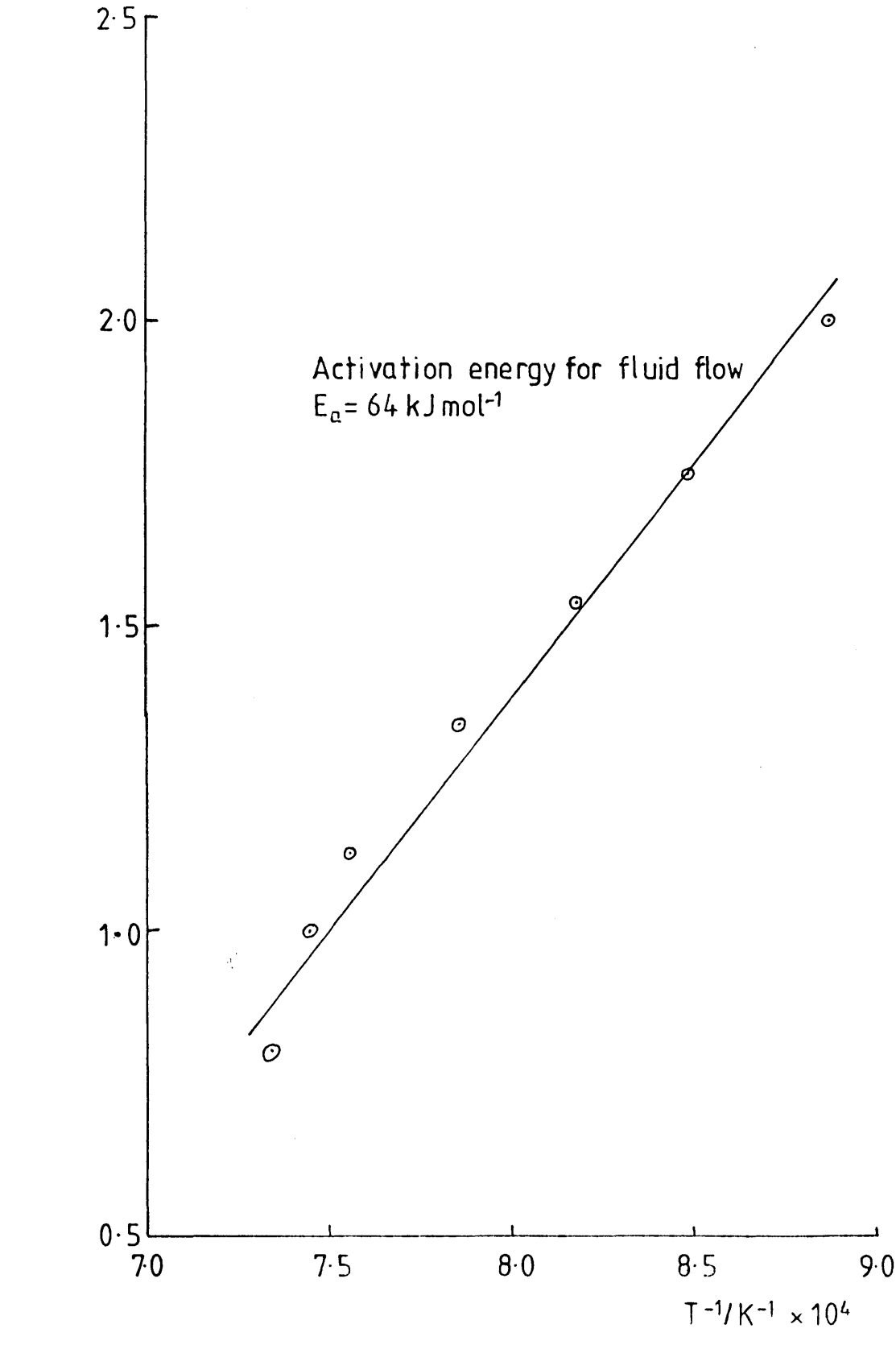


Fig.5.6. Graph of viscosity(calculated) vs. reciprical temperature for MAT8 glass.

Fig.5.7. Graph of viscosity(measured[102]) vs. reciprical temperature for MAT 9 glass.



crystal growth rate observed was 0.9 μm s^{-1} at 900 °C for Mat 8 glass and 0.3 μm s^{-1} for Mat 9 glass at 1000 °C. In the study of bituminous slags Livingston et al.[46] observed a glassy layer with no evidence of crystallisation in the region adjacent to the furnace tubes. The temperatures within the layer must have been lower than that required for crystal growth of anorthite or iron spinel (the major crystalline phases). The authors suggested that the temperatures within the layer ranged from about 420 °C at the furnace wall to about 700 °C at the outer edge. The observations of this study, though not directly comparable, indicate that similar crystal growth phenomena may occur in bituminous slags.

5.5 CORRELATION OF CRYSTALLISATION OF $CaO-Al_2O_3-SiO_2$ GLASSES WITH LIGINITIC-TYPE ASH MELTS

The series of glasses K1 - K5 were chosen to be in the region of the ternary system $CaO-Al_2O_3-SiO_2$ of relevance to lignitic-type ashes. Glasses K1 and K2 were the normalised three component compositions of ash KA and Mat 9 glass (which was based on a high-lime lignitic-type ash). The other compositions were chosen so as to have different crystallisation paths.

The compositions of the glasses have been plotted on the ternary system in Fig.5.8 and the initial crystallisation paths indicated. Glass K1 lies in the compatability triangle anorthite, cyclo-wollastonite and tridymite. Under equilibrium conditions at 1000 °C all three phases would have crystallised. From the crystallisation path it is evident that the residual

liquid phase will become increasingly silica rich and hence more viscous with crystallisation of anorthite. The increased viscosity will decrease the likelihood of further crystallisation as the liquid phase will be more stable towards devitrification. Thus only the primary crystalline phase would be expected for this composition. Glass K5 lies in the compatibility triangle anorthite, mullite, silica and the crystallisation path is towards the mullite boundary. With crystallisation of anorthite the residual liquid phase would be more viscous which would explain the reluctance of mullite to crystallise.

The crystallisation behaviour observed for the glasses K3 and K4 was the same as that for K1 and K5, i.e. only anorthite was observed to crystallise. This was unexpected as the residual liquid phase would become less viscous with crystallisation of anorthite as indicated by the crystallisation paths.

Glass K2 was the only composition to devitrify completely to the three crystalline components expected from the compatibility triangle (gehlenite, anorthite and cyclowollastonite) after treatment at temperatures below the eutectic (1265 °C). This behaviour is presumably due to the lower viscosity of the melt and the residual liquid phase.

The correlation of ash melt behaviour can only be made between the crystallisation behaviour of glass K1 and to a lesser extent glass K2. The glass K1 corresponded to the normalised three component composition of ash KA and the glass K2 with the composition of the glass Mat 9. The ash KA was observed to crystallise anorthite only as with the glass K1. The phase diagram would predict little crystallisation of anorthite at

temperatures below the liquidus from the crystallisation path. Though quantitative mineralogical content was not performed, optical analysis of ash samples showed significant amounts of crystallisation. The glass Mat 8 was based on the full composition of ash KA; observation of the samples subjected to crystal growth treatment also indicated significant crystallisation. In the case of the glass K2 the phase diagram would predict a small amount of gehlenite before crystallisation of anorthite and cyclowollastonite. This explains in part the lower crystal growth rates of melilite observed for Mat 9 glass. As the primary phase grows into the glass a limiting factor to growth must be the amount of the phase allowed by the composition.

Sanyal and Williamson[89] have compared the fusion behaviour of two low temperature ashes with that expected from the normalised three component composition on the $CaO-Al_2O_3-SiO_2$ phase diagram. The initial appearance of a liquid phase was approximately 150 °C below the corresponding eutectic temperature for the two ashes. The ternary composition of ash KC has been plotted on the phase diagram (Fig.5.8). The composition is in the primary field of mullite and the compatibility triangle mullite, anorthite, silica with the corresponding eutectic 1340 °C. The initial appearance of a liquid phase was observed to be at 1200 °C, i.e. 140 °C below the eutectic. The liquidus temperature of the ash was approximately 1360 °C which compares with 1590 °C for the ternary composition, a difference of 230 °C. The ash melt was observed to crystallise as anorthite only which the ternary phase diagram would not predict.

Sanyal and Williamson suggested that the difference in the value of the temperature of appearance of a liquid phase observed for an ash composition and the corresponding eutectic temperature

for the normalised composition was due to the presence of the minor components. With reference to the composition of the ash (Table 3.1) the major three components comprised 9 6 wt % of the total composition (excluding SO_3). The minor components such as magnesia, soda, potash and the iron oxides generally have a fluxing effect when added to silicate melts. Thus the liquidus and eutectic temperatures which the phase diagram predicts must be treated with care. The liquidus temperature of an ash would be expected to be lower than that of the corresponding ternary composition due to the effect of the minor components. The initial appearance of a liquid phase will depend upon the interaction and decomposition of the mineral phases present in the ash and the fluxing effect of the other oxides.

The applicability of ternary phase diagrams to predicting ash fusion characteristics will therefore be limited and qua ternary or multicomponent phase diagrams could give more reliable data.

Within the main body of the boiler the coal minerals experience the flame temperature of ∿1550 °C and subsequently the gas temperatures (1450 - 1000 °C). As has been shown, the fusion processes of the minerals in the lignitic-type ash KD occur rapidly both at 1450 °C and 1550 °C. The importance of high temperature phase equilibrium diagrams is that they can give valuable information on phase changes which will occur as the molten ash cools within the body of the boiler.

Hanusch and Grimshaw[42] have analysed deposits formed from coal ashes of similar mineralogical and chemical composition to ashes KA, KC and KD. Samples removed from the platen superheater (gas temperature ∿1450 °C) which received radiant heat

consist mainly of anorthite in a glassy/amorphous matrix with traces of magnetite detected. Samples removed from regions of lower gas temperatures were glassy with again anorthite as the major crystalline phase and appreciable quantities of anhydrite ($CaSO_4$). Ilmenite ($FeO.TiO_2$) and apatite ($3CaO.P_2O_5$) could have been present, but in trace proportions.

The composition of the sample which had the highest anorthite content has been normalised to the three major components (Table 5.5) and plotted on the ternary diagram (Fig.5.8, point M1). The crystallisation path has also been indicated and shows that for the melt cooled below 1490 °C (the liquidus) the residual liquid phase will become increasingly silica-rich as crystallisation of primary anorthite occurs. The composition is similar to the glass K5 studied and thus only anorthite would be expected in the deposit. All the samples had similar chemical composition except for that which had a high $CaSO_4$ content indicating that the primary crystallisation phase would be anorthite with a viscous residual liquid phase.

The deposits were found not to be troublesome for the boiler operators as they could be easily removed by soot-blowing. Scanning electron microscopic analysis of the samples indicated that only the high temperature deposit was vitreous in nature; the other deposits consisted of loosely sintered particles. This type of microstructure would be expected from the Raask model of deposit growth which states that the rate of increase in deposit strength (ds/dt) is given by:

$$\frac{ds}{dt} = \frac{3\gamma k}{2\eta r} \qquad (k = \text{constant})$$

Thus, assuming that γ and r (surface tension and initial radius of the particles respectively) are constant the values of $^{ds}/_{dt}$ will depend inversely on the viscosity. The phase diagram indicates that the residual liquid phase on crystallisation will become increasingly SiO_2-rich and hence more viscous. Thus, as the degree of crystallinity increases the rate at which the increase in deposit strength increases must fall off if the Raask model is applicable. It is therefore not surprising that the superheater deposits show the observed microstructure. The presence of anhydrite can be explained by the capture of SO_3 by lime in a melt below 1300 °C. The removal of lime from the liquid phase, along with the crystallisation of magnetite, would be expected to increase the viscosity of the liquid phase reducing the rate of growth of a deposit at a given temperature.

Pollman and Albrecht[103] have studied the deposits formed from lignitic-type ash from South African coal (Kriel seam). The deposits contained anorthite with quartz and hematite (as minor components) determined by X-ray diffraction analysis. The structure of the deposits was sintered with significant viscous flow between particles. An optical micrograph showed anorthite lathes in a glassy matrix almost identical to that observed in the present fusion study (see Plate 9). The authors stated that the anorthite was formed by the reaction:

$$Al_2O_3.2SiO_2.2H_2O + CaCO_3 \rightarrow CaO.Al_2O_3.2SiO_2 + CO_2 + H_2O$$

kaolinite calcite anorthite

However, morphology of the crystalline phase clearly indicates that the anorthite formed from a melt and not by direct interaction between coal minerals, as suggested by these authors.

The chemical composition of the ash (given in Table 5.5) has been normalised to three components and plotted on Fig.5.8. As can be seen the composition (KR) lies in the primary field of anorthite and has a liquidus temperature of approximately 1450 °C. The crystallisation path indicates a silica-rich, and hence more viscous, liquid phase. On initial analysis the ash would not be expected to form troublesome deposits. The lower liquidus temperature would increase the liquid content of the slag at a given temperature compared to the composition M1 . The boiler operators reduced the slagging significantly by decreasing the flame temperature resulting in an increased amount of fly ash. Analysis of the fly ash indicated that complete fusion of the ash did not occur in the boiler under these conditions, minerals such as mullite, quartz, hematite and anhydrite being observed.

TABLE 5.5

Composition of Two Lignitic-type Ashes

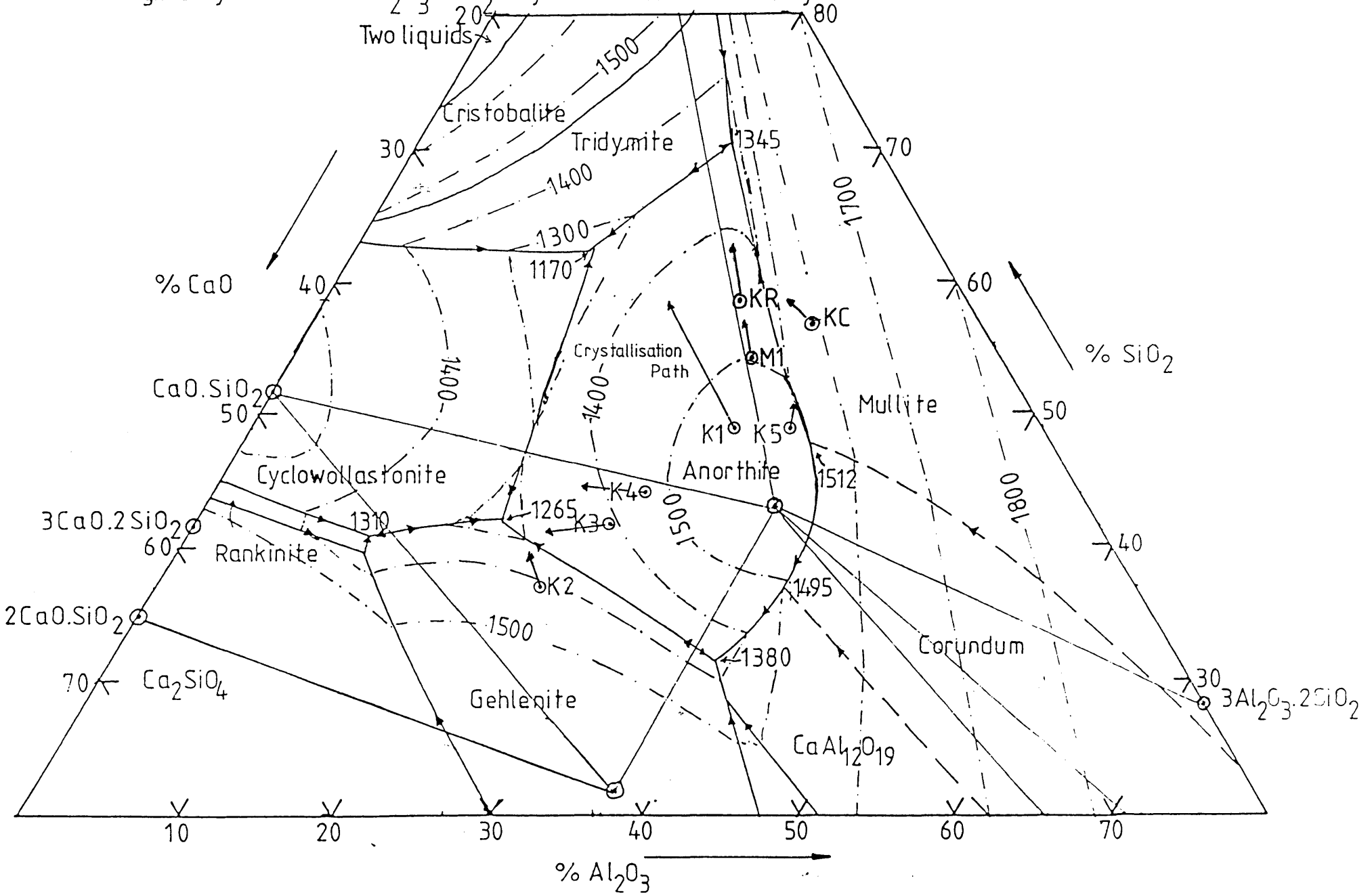
Composition Wt %

ASH	SiO_2	Al_2O_3	Fe_2O_3	CaO	MgO	Na_2O	K_2O	TiO_2
M1[42]	46.7	25.9	6.4	13.8	3.1	0.8	0.4	1.5
KR[103]	51.6	23.7	4.9	13.1	1.7	0.3	0.3	2.2

Normalised Composition Wt %

	SiO_2	Al_2O_3	CaO
M1	54.0	30.0	16.0
KR	58.4	26.8	14.8

Fig.5.8. System $CaO-Al_2O_3-SiO_2$ [88] Crystallisation of ternary melts.



5.6 CRYSTALLISATION OF $CaO-MgO-Al_2O_3-SiO_2$ GLASSES AND CORRELATION WITH THE CRYSTALLISATION OF ASHES

The series of glasses K17 - K21 and K22 - K26 were based on the ternary compositions K1 - K5 with 5 and 10 wt % MgO. The liquidus temperature and the crystallisation behaviour of the glasses have been detailed in Table 4.9.

The method of description of the quaternary system $CaO-MgO-Al_2O_3-SiO_2$ chosen for this study was the use of planes of constant MgO. As the crystallisation paths of four component systems is three dimensional and the primary crystalline fields become volumes not areas as in ternary systems the planes of 5, 10 and 15% of the quaternary system of interest to coal ashes have been reproduced in Figs 5.9, 5.10 and 5.11. Though no compositions containing 15% MgO were studied it is necessary to consider the primary fields present on this plane.

The 5% MgO plane (Fig.5.9) has been constructed from data given by Gutt and Russell[104] and Cavalier et al.[105] The positions of the boundaries between adjacent fields and the liquidus temperatures were checked using compositions K17 - K21 and J1 - J6. Comparison of the data showed good agreement and the diagram has been drawn to conform with the results of the present study. The 10% MgO plane (Fig.5.10) was constructed from the data of Prince[106] and from the liquidus temperatures and primary crystalline phases observed for the series of glasses K22 - K26 and I1 - I7. The 15% MgO plane (Fig.5.11) has been constructed from the data of Cavalier et al..

The series of diagrams shows clearly the effect of magnesia on the crystallisation behaviour of the quaternary glasses.

Fig.5.9. System $CaO-MgO-Al_2O_3-SiO_2$,5%MgO plane. Compositions studied.

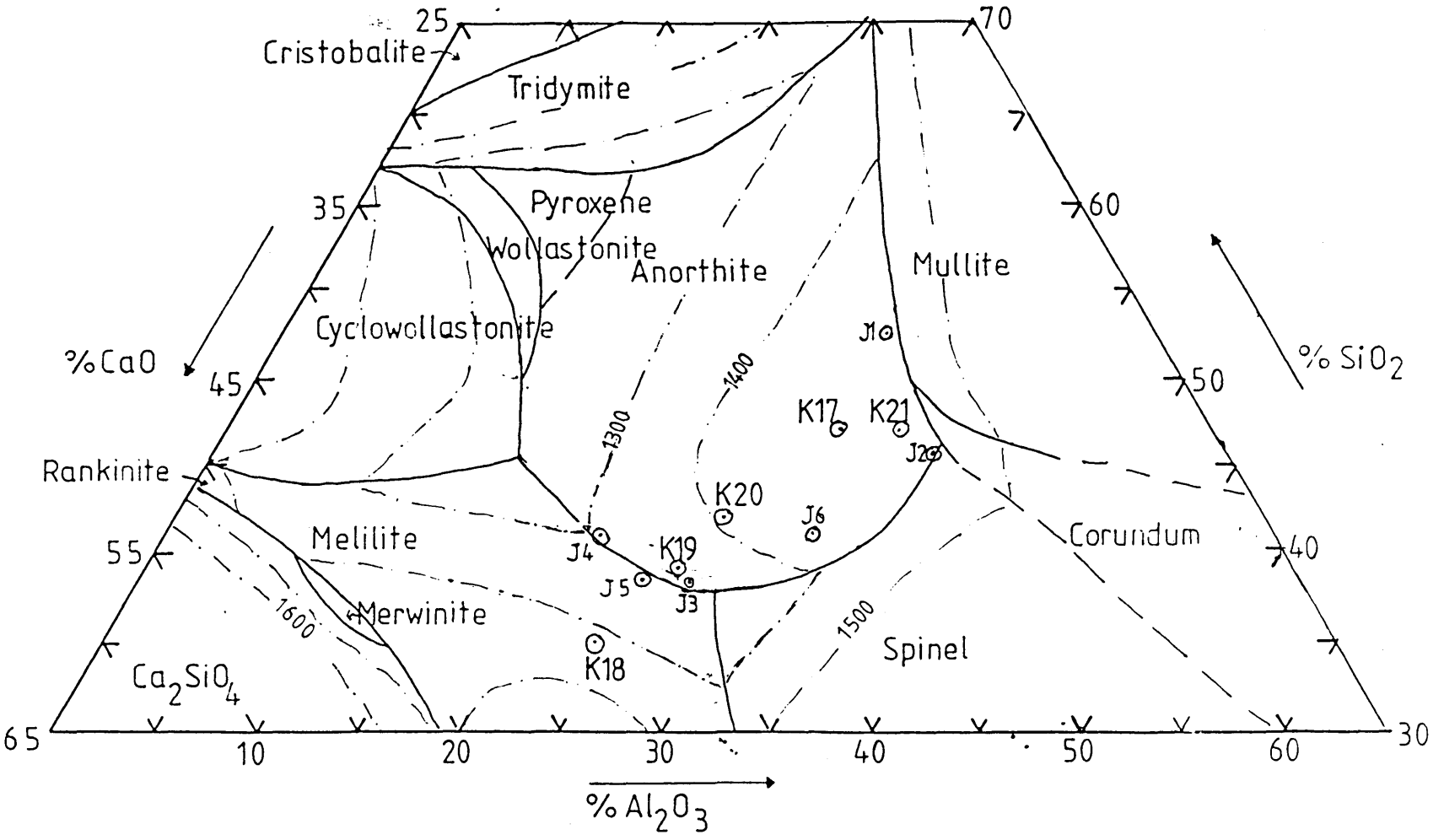


Fig.5.10. System $CaO-MgO-Al_2O_3-SiO_2$, 10% MgO plane. Compositions studied.

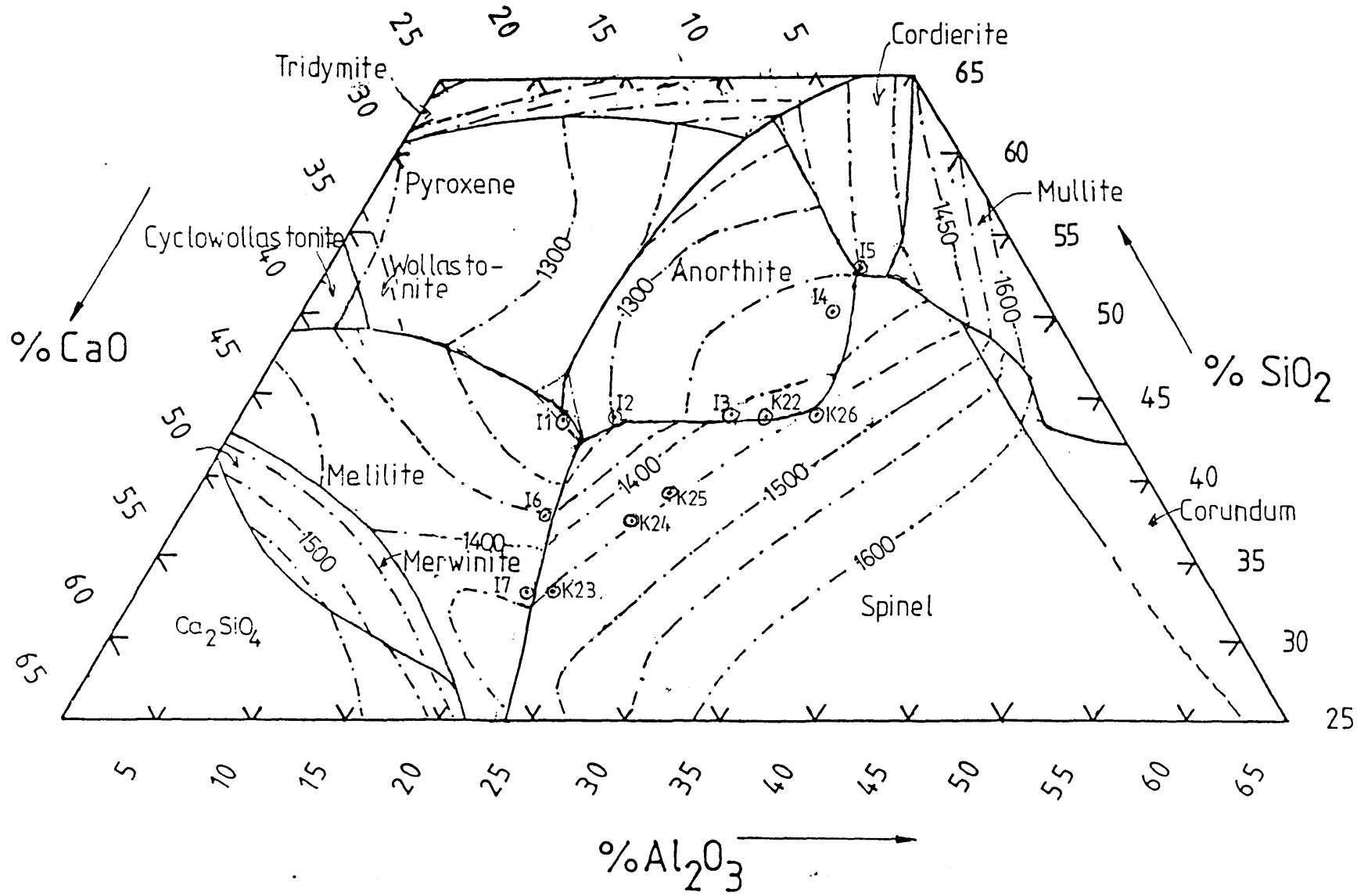
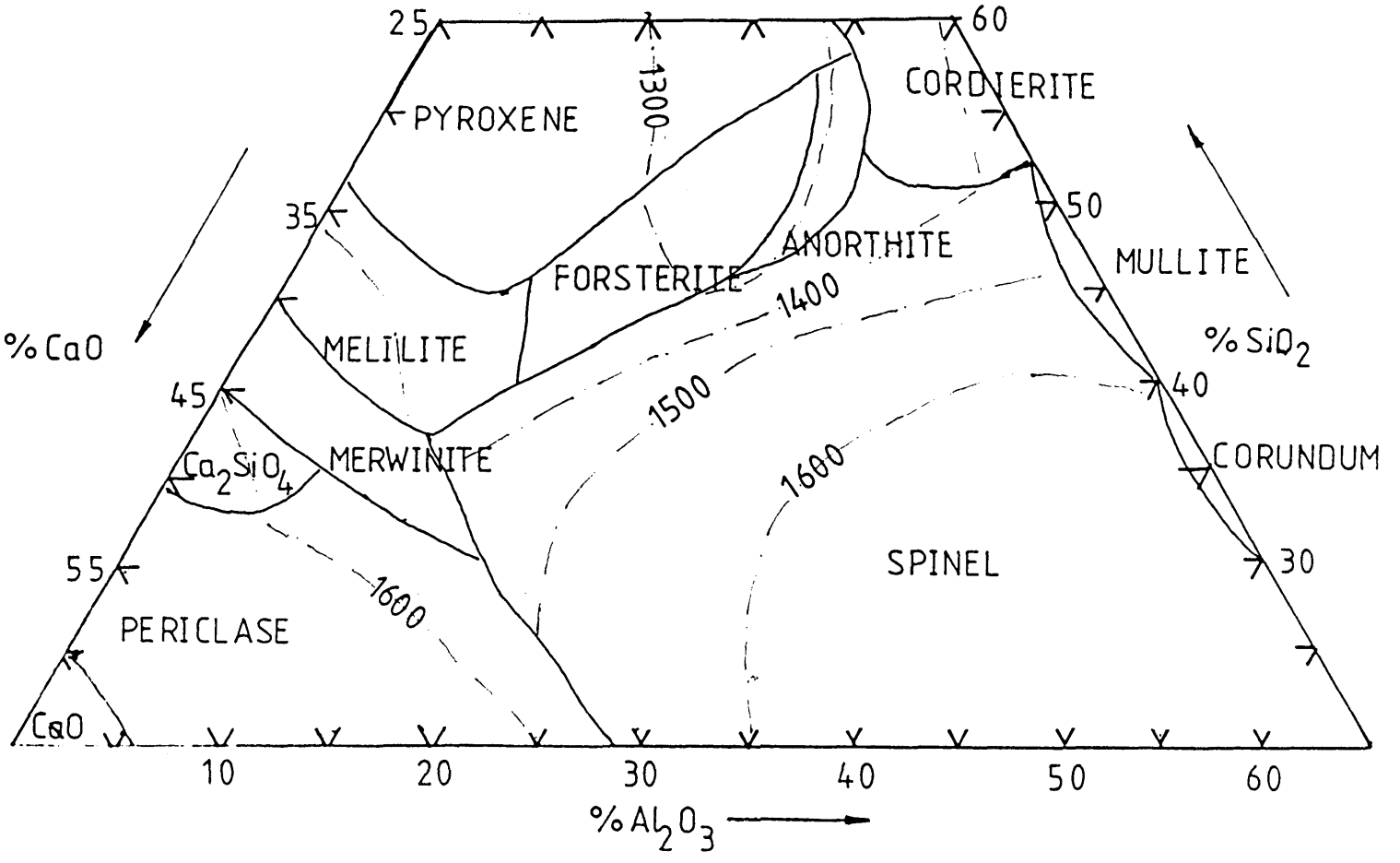


Fig.5.11. System $CaO-MgO-Al_2O_3-SiO_2$, 15 %MgO plane.



While the 5% MgO plane has only the magnesia-containing phases of melilite, spinel and pyroxene (a solid solution series between diopside, $CaO.MgO.2SiO_2$ and clinoenstatite $MgSiO_3$). The 10% MgO plane is dominated by the melilite, spinel ($MgO.Al_2O_3$) and pyroxene primary phase fields. The major phases present on the base ternary system, such as anorthite and mullite are barely present on the 15% MgO plane. Phases such as forsterite (an olivine, $2MgO.SiO_2$), merwinite ($3CaO.MgO.2SiO_2$), cordierite ($2MgO.2Al_2O_3.5SiO_2$) and periclase (MgO) have significant presence at this level, while dominated by the spinel field.

The crystallisation of a quaternary melt is quite complex as indicated by the changes in primary crystalline fields detailed above. If the primary crystalline phase does not contain magnesia then as the phase crystallises the residual liquid phase will become enriched in magnesia. If, on the other hand, the primary phase contains magnesia the residual liquid phase will become depleted in MgO. This behaviour can readily be seen by reference to the behaviour of the series of glasses K17 - K21 and K22 - K26 in Table 4.9. For example, the glass K17 was observed to crystallise anorthite only. Though it is difficult to visualise the crystallisation path it is possible to calculate the composition of the residual liquid phase on the planes above the original composition. It is only possible to do this for compositions which have primary crystalline phases which do not exhibit solid solution. For clarity it will be advantageous to take as an example glass K17. The composition lies on the 5% MgO plane in the primary field of anorthite. Below the liquidus temperature the residual liquid phase will become increasingly enriched in magnesia with crystallisation of anorthite. For a 100 g batch of

composition K17, containing 5 g MgO, it is clear that 50 g of anorthite must crystallise for the residual liquid phase to contain 10% MgO. The mass of the individual components of anorthite removed from the liquid phase are therefore 21.5 g SiO_2, 18.5 g Al_2O_3 and 10 g CaO. Taking these values from the original components the composition of the residual liquid phase is obtained.

	SiO_2/g	Al_2O_3/g	CaO/g	MgO/g	Total/g
K17	47.0	30.0	18.0	5	100
- 50 g anorthite	-21.5	-18.5	-10.0	-0	-50
residual liquid phase	25.5	11.5	8.0	5	50
Normalising to 100					
K17/10	51.0	23.0	16.0	10.0	100

The composition of the residual liquid phase (K17/10) has been plotted on the 10% MgO plane (Fig.5.13) and, as can be seen, lies in the anorthite primary field. Thus further crystallisation of anorthite may occur and the composition of the residual liquid phase on the 15% MgO can be calculated. For the residual liquid phase to contain 15 wt % MgO 66.7% anorthite must crystallise (28.7% SiO_2, 24.7% Al_2O_3, 13.3% CaO).

Again, for a 100 g batch, the residual liquid phase will contain 18.3 g SiO_2, 5.3 g Al_2O_3, 4.7% CaO and 5.0 g MgO, and normalising to 100 g the composition K17/15 is obtained:

	SiO_2/g	Al_2O_3/g	CaO/g	MgO/g	Total/g
K17/15	55.0	15.9	14.1	15.0	100

The composition K17/15 has been plotted on the 15% MgO plane (Fig.5.14) and lies in the primary phase of pyroxene. The crystallisation path can not be determined after the path encounters the boundary between the primary and secondary phase, but it can be seen that significant amounts of anorthite must crystallise out (66.7%) before the secondary phase will appear. This may explain the observation of anorthite only in the crystallisation study of this glass.

The compositions of the residual liquid phases of the series of glasses K17 - K21 have been listed in Table 5.6 along with the original composition. The composition of the primary crystalline phase of glass K18 has been assumed to be gehlenite so that the crystallisation behaviour can be investigated. The compositions of the residual liquid phase have been calculated for the crystallisation paths which have encountered a secondary phase up to the plane containing the secondary phase.

The crystallisation of glass K18 provides an interesting example, the composition of the residual liquid phase on the 10% MgO plane (K18/10) has been plotted on Fig.5.13 and is in the primary phase of pyroxene. The glass was observed to crystallise in the sequence melilite, anorthite, spinel which may be due to solid solution of magnesia in the melilite phase. The removal of magnesia from the residual liquid phase would not cause the crystallisation path to move towards the 10% MgO plane and may be pointed towards the base ternary plane ($CaO.Al_2O_3$-SiO_2) in which anorthite is a dominant field and thus anorthite may be expected to be the secondary phase. The prediction of tertiary crystalline phases from the calculated crystallisation path is not possible with quaternary systems due to the variable crystallisation allowed

along the boundary (area of divariance). From the behaviour observed for glass K18 it appears that on crystallisation of the secondary phase the residual liquid phase becomes enriched in alumina and magnesia with subsequent crystallisation of spinel.

The composition of the residual liquid phase of glass K19 (composition K19/10) on crystallisation of anorthite has been plotted on Fig.5.13. The composition is in the primary phase of melilite and thus the crystallisation path must have encountered the melilite/anorthite boundary. This agrees with the observed crystallisation behaviour (sequence anorthite, melilite and spinel) for glass K19.

The glass K20 was only observed to crystallise anorthite which was unexpected from the crystallisation path (composition K20/10 is in the primary field of melilite). No ready explanation can be offered for this anomalous behaviour other than possible experimental error.

The crystallisation behaviour of glass K21 was observed to be anorthite, spinel followed by cordierite. The compositions of the residual liquid phase (K21/10 and K21/15) have been plotted on the respective MgO plane and confirm the secondary phase of spinel. It appears that the crystallisation of more than 50% anorthite is required before the anorthite/spinel boundary is encountered, with the residual liquid phase becoming enriched in alumina, silica and magnesia. Crystallisation of cordierite as the tertiary phase indicates that the crystallisation of spinel does not reduce the magnesia content of the residual liquid significantly causing subsequent crystallisation of cordierite ($2MgO.2SiO_2.5SiO_2$) at lower temperatures.

Only the glass K22 of the compositions on the 10% MgO plane did not lie in the primary phase of spinel. The proximity of K22 to the anorthite/spinel boundary on the 10% MgO plane and the dominance of the spinel primary field on the 15% MgO plane indicates that spinel would crystallise as the secondary phase (as observed).

As with the K17 - K21 series of glasses it is possible to calculate the composition of the residual liquid phase. The glasses K23 - K26 are all in the primary field of spinel and as the composition point is on the $MgO-Al_2O_3$ binary system at 28% MgO, 72% Al_2O_3 the crystallisation path for compositions lying on the 10% MgO plane must be initially towards the 5% plane. That is with crystallisation of spinel the residual liquid phase will become depleted in magnesia. The method to calculate the composition on the 5% plane is somewhat different from that for crystallisation of anorthite. The method is best illustrated with reference to glass K23. If, for a 100 g batch, 21.6 g crystallises as spinel, the residual liquid phase will lose 6.1 g MgO and 15.5 g Al_2O_3. The compositions will be:

	SiO_2/g	Al_2O_3/g	CaO/g	MgO/g	Total/g
K23	33.3	22.5	34.2	10.0	100
-21.6 g spinel	- 0.0	- 15.5	-0.0	-6.1	-21.6
	33.3	7.0	34.2	3.9	78.4
and normalising to 100					
K23/5	42.5	9.0	43.6	5.0	100

The composition of the residual liquid phase on the 5% MgO plane is obtained. The process has been repeated for the glasses K24 -

K26 on the 5% plane have been listed in Table 5.6 along with the original compositions.

The secondary phase observed for the glass K23 was melilite. The composition K23/5 plotted on the 5% MgO plane (Fig.5.12) lies in the melilite primary field which explains the observed behaviour.

The secondary and tertiary crystalline phases for the glass K24 were not distinguished, both anorthite and melilite being observed in samples treated at 1200 °C. The composition K24/5 lies in the primary crystalline field of cyclowollastonite which suggests that the crystallisation path must have encountered a boundary (anorthite/spinel or melilite/spinel) prior to reaching the 5% MgO plane.

The glass K25 was observed to crystallise in the sequence spinel, anorthite and melilite. The composition K25/5 lies in the primary phase of anorthite and thus matches the observations. Only the secondary phase of anorthite was observed for the glass K26 which would be expected from the composition of the residual liquid phase K25/5 on the 5% plane.

The liquidus temperatures of compositions K1 - K5 and with 5 and 10 wt % additions of MgO have been plotted against MgO contents in Fig.5.15. As can be seen the effect of the magnesia is initially as a flux except for the K2 - K18 - K23 series, reducing the liquidus temperatures. An increase in liquidus temperature was observed for all the series of compositions except for those of K1 - K17 - K22 and K5 - K21 - K26. The increase would be expected from the liquidus isotherms on the planes of the quaternary system and from the study of ternary systems such as $CaO-Al_2O_3-SiO_2$. The observations were similar to those of Estep

TABLE 5.6

Composition of Residual Liquid Phases for $CaO-MgO-Al_2O_3-SiO_2$ Glasses

Glass	Composition Wt %				Primary Field
	SiO_2	Al_2O_3	CaO	MgO	
K17	47.0	30.0	18.0	5.0	Anorthite
K17/10	51.0	23.0	16.0	10.0	Anorthite
K17/15	55.0	15.9	14.1	15.0	Pyroxene
K18	35.0	24.0	36.0	5.0	Gehlenite
K18/10	48.0	11.0	31.0	10.0	Pyroxene
K19	39.0	26.0	30.0	5.0	Anorthite
K19/10	35.0	15.0	40.0	10.0	Melilite
K20	42.0	27.0	26.0	5.0	Anorthite
K20/10	41.0	17.0	32.0	10.0	Melilite
K21	47.0	33.0	15.0	5.0	Anorthite
K21/10	51.0	29.0	10.0	10.0	Anorthite/Spinel
K23	33.3	22.5	34.2	10.0	Spinel
K23/5	42.4	9.0	43.6	5.0	Melilite
K24	37.4	24.3	28.3	10.0	Spinel
K24/5	47.6	11.3	36.1	5.0	Cyclowollastonite
K25	39.6	25.6	24.8	10.0	Spinel
K25/5	50.4	13.0	31.6	5.0	Anorthite
K26	44.1	31.5	14.4	10.0	Spinel
K26/5	56.2	20.5	18.3	5.0	Anorthite

Key: Example K17 represents original composition with 5% MgO, K17/10 represents the composition of the residual melt after sufficient anorthite was crystallised to give a residue containing 10% MgO. In this way the change in composition in terms of CaO, Al_2O_3 and SiO_2 may be followed as the primary phase crystallises.

Fig.5.12. System $CaO-MgO-Al_2O_3-SiO_2$, 5% MgO plane. Crystallisation of K series of glasses.

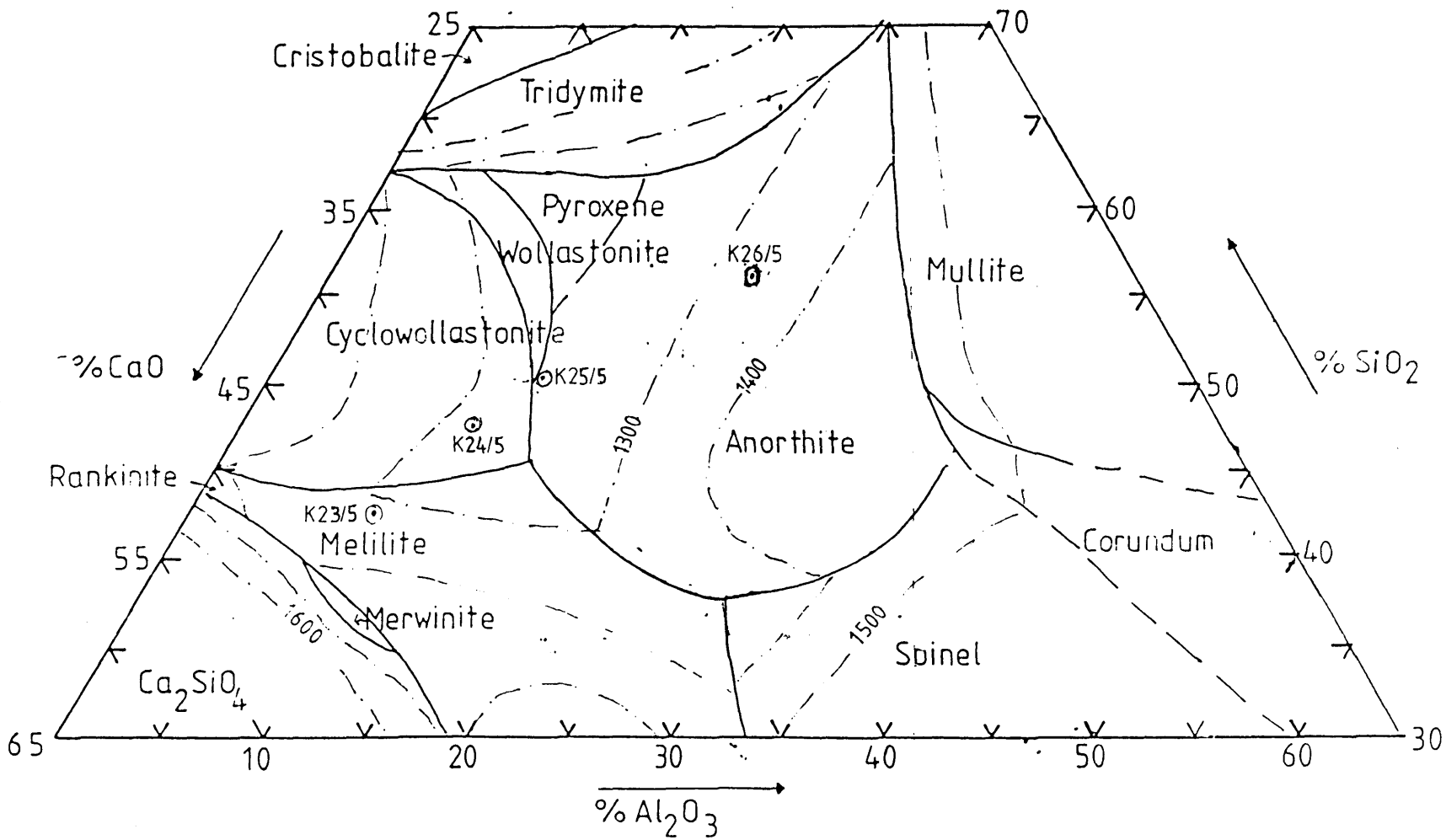


Fig.5.13. System $CaO-MgO-Al_2O_3-SiO_2$, 10% MgO plane. Crystallisation of K series of glasses.

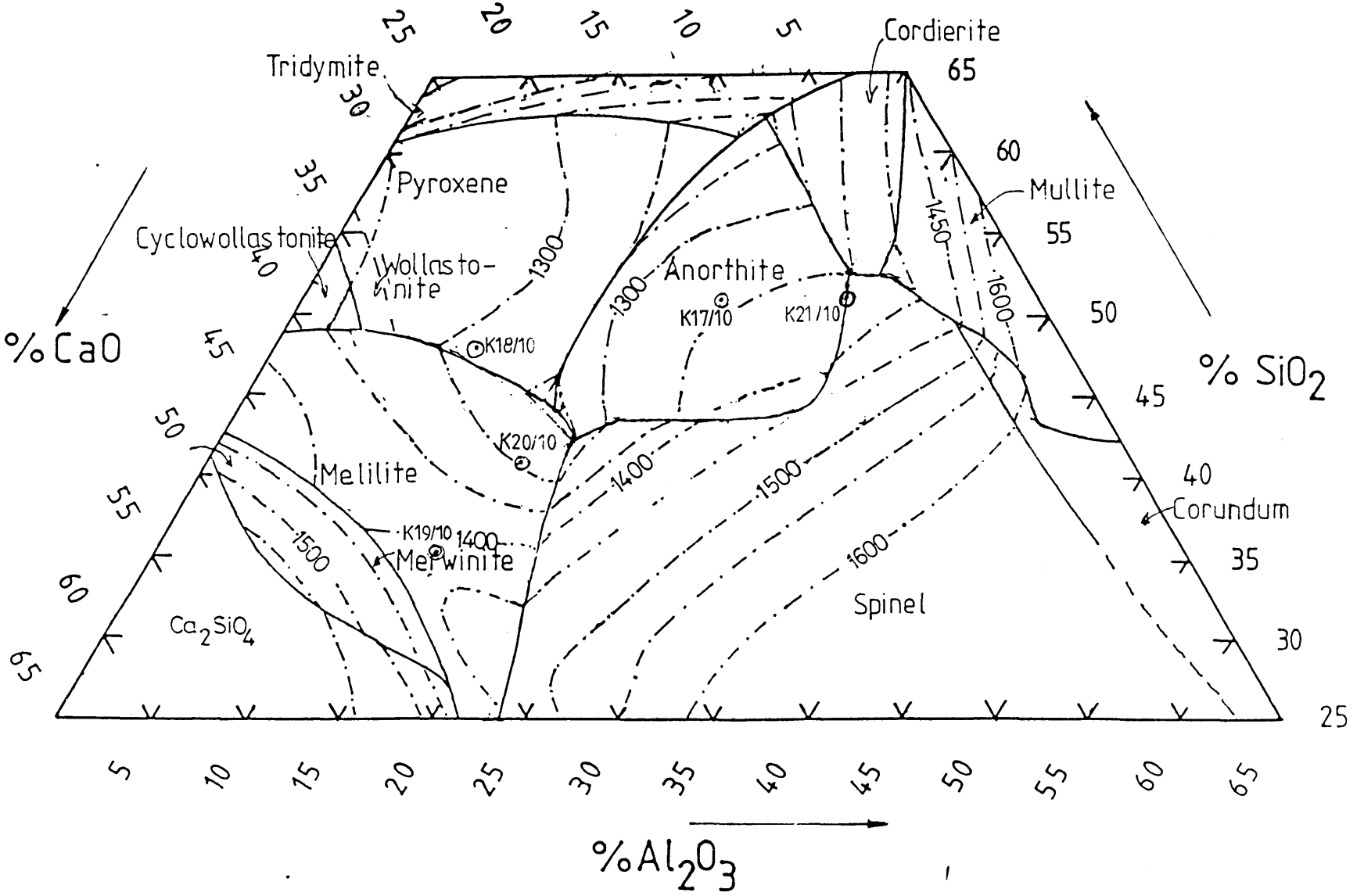
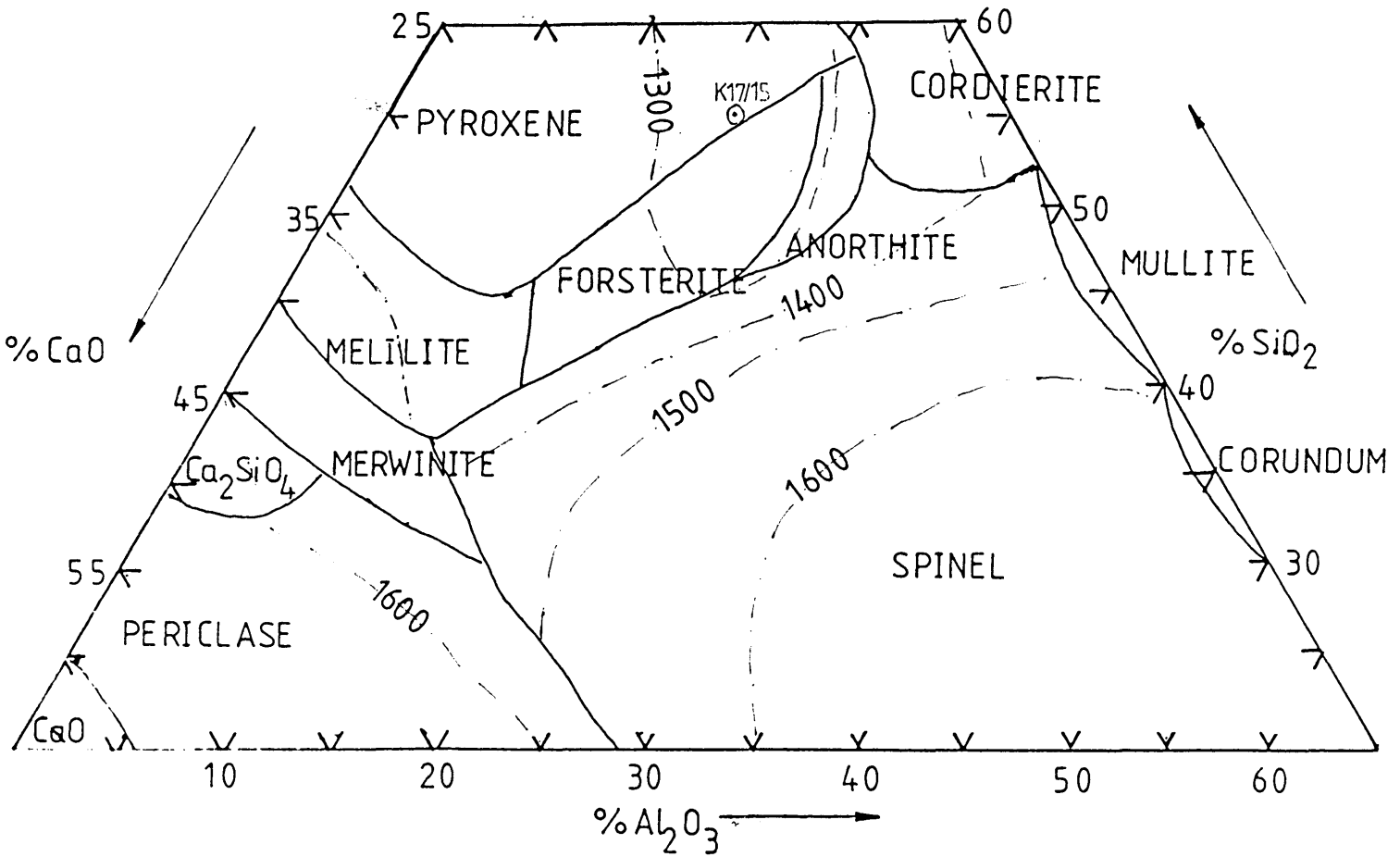


Fig. 5.14. System $CaO-MgO-Al_2O_3-SiO_2$, 15 % MgO plane. Crystallisation of K series of glasses.



et al.[74] who studied the effect of addition of magnesia and lime on the ash fusion temperatures of coal ashes. Though the observations are not directly comparable to those of this study, the addition of magnesia initially caused lowering of fusion temperatures with local minima observed and subsequently increasing fusion temperature with increased magnesia contents. It is clear from the quaternary system that the effect of magnesia as a flux will be dependent primarily on the original composition and thus the prediction of the degree to which a magnesia addition will reduce the liquidus temperature of a melt must be approached with care.

The relevance of the quaternary system $CaO-MgO-Al_2O_3-SiO_2$ to the crystallisation of lignitic-type ash melts can only be verified by comparing the predictions of the phase diagram with the phases observed in deposits. The crystallisation behaviour of the ashes KA and KC and the results of other studies have been listed in Table 5.7. Included in the Table is the chemical compositions, normalised ($CaO-MgO-Al_2O_3-SiO_2$) composition and the primary crystalline phases, predicted from the diagram for each of the samples. (The normalised compositions have been plotted on the 5% MgO plane, Fig.5.16, using the silica and alumina contents.)

Of the eight ash compositions only five predicted primary phases corresponding to the observed major phase. The primary crystalline phase predicted for ash KC was mullite whereas anorthite was observed. The composition of the residual liquid phase for KA on the planes above the original composition have been listed in Table 5.8 and plotted on the corresponding plane of the tetrahedron.

Fig.5.15.Plot of liquidus temperature vs. MgO for a series of $CaO-Al_2O_3-SiO_2$ compositions to which MgO has been added.

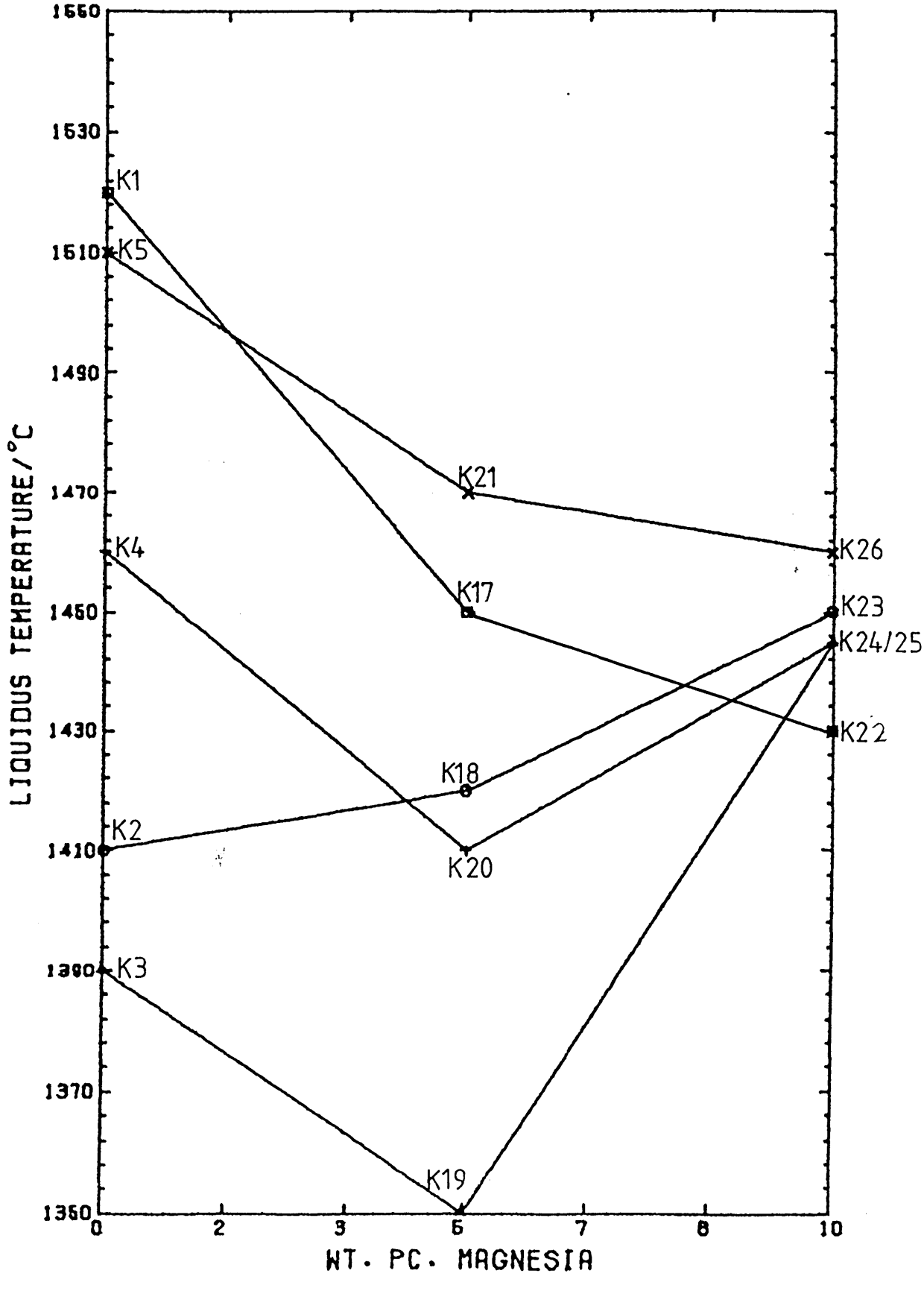


TABLE 5.7

Observed and predicted crystallisation of lignitic ash melts (based on the system $CaO-MgO-Al_2O_3-SiO_2$)

Ash	Composition Wt %									Crystalline Phases Observed	Normalised composition wt %				Primary Phase
	SiO_2	Al_2O_3	Fe_2O_3	CaO	MgO	Na_2O	K_2O	TiO_2	MnO		SiO_2	Al_2O_3	CaO	MgO	
KA	43.1	27.8	5.1	17.3	3.8	0.7	0.3	1.9	n.d	Anorthite	46.8	30.2	18.8	4.2	Anorthite
KC	51.2	29.0	4.8	9.5	2.6	0.6	1.0	1.3	n.d	Anorthite	55.5	31.4	10.3	2.8	Mullite
HG1[42]	46.7	25.9	6.4	13.8	3.1	0.8	0.4	1.5	n.d	Anorthite Magnetite $CaSO_4$	52.2	28.9	15.4	3.5	Anorthite
HG2[43]	47.7	30.1	5.2	10.6	2.5	0.5	0.6	1.8	n.d	Anorthite. Cordierite Cristobalite	52.5	33.1	11.7	2.7	Mullite
PA[103]	51.6	23.7	4.9	13.1	1.7	0.3	0.3	2.2	n.d	Anorthite	57.3	26.3	14.5	1.9	Anorthite
SR[107]	41.8	13.0	11.5	20.1	5.2	n.d	n.d	0.5	9.4	Melilite	52.3	16.2	25.1	6.5	Anorthite
TH[107]	28.5	11.5	16.4	34.8	1.9	n.d	n.d	0.2	0.1	Hercynite Anorthite Melilite	37.1	15.0	45.3	2.5	Melilite
PB[107]	27.0	9.8	4.1	52.4	2.4	n.d	n.d	0.2	0.1	Ca_2SiO_4	29.5	10.7	57.2	2.6	Ca_2SiO_4

n.d = not determined.

TABLE 5.8

Crystallisation path of glass KA

	SiO_2	Al_2O_3	CaO	MgO	Primary crystalline phase
KA	46.8	30.2	18.8	4.2	anorthite
KA/5	47.5	28.9	18.6	5.0	anorthite
KA/10	52.1	20.8	15.1	10.0	anorthite
KA/15	56.4	12.9	17.7	15.0	pyroxene

The crystallisation path for glass KA is similar to that observed for glass K17 for which only anorthite was observed to crystallise. This behaviour was identical to that of coal ash melt KA. Hanusch and Grimshaw[42] investigated the mineralogy of the deposit (HG1) formed from an ash similar to KA and KC (from the same coal source). Anorthite was determined to comprise 45% of the deposit which had formed in the superheater region (gas temperature about 1450 °C). The minor phases observed were magnetite and anhydrite and the remainder of the deposit was glass or amorphous material. The quaternary phase diagram predicts correctly the primary phase for the 4-component composition HG1. The composition of the residual liquid phase on the 5% MgO plane has been calculated (HG 1/5) and also lies in the primary field of anorthite. The composition on the residual liquid phase on the 10% plane is outside the limits of the diagram but the crystallisation path is towards the region of high silica content. The system does not account for the crystallisation of magnetite nor anhydrite, the latter being formed by the capture of SO_3 by CaO. In a subsequent study, Hanusch and Grimshaw[43] observed significant proportions of cordierite and cristobalite in a deposit from the same region of the boiler. The major phase for the deposit (HG2) was anorthite

but the normalised composition on the 5% MgO plane would predict mullite. It could well be that on the 2.7% MgO plane of the quaternary system the composition lies in the anorthite field. The crystallisation of cristobalite and cordierite was unexpected by the authors but with reference to the glass K21 studied (p.205) cordierite ($2MgO.2Al_2O_3.5SiO_2$) can crystallise from glasses containing only 5% MgO. Detailed observation of the MgO planes indicates that there may be a peritectic point between the 5 and 10% MgO levels at which mullite redissolves and cordierite then forms. This is indicated by the relative size of the mullite field and those of anorthite and cordierite. The boundary between anorthite and cordierite on the 10% and 15% MgO plane shows that the two phases can exist in equilibrium whereas mullite is only in equilibrium with spinel and to a very limited extent with cordierite. Thus with the proposed presence of a quaternary peritectic where mullite redissolves, the crystallisation of anorthite and cordierite can be explained. Cristobalite is known to crystallise from siliceous melts in preference to tridymite and with reference to the magnesia levels where the anorthite/cordierite boundaries exist indicate a very siliceous residual liquid phase the crystallisation would be expected. The authors suggested that the deposit had a relatively long residence time at the soaking temperature which would account for the presence of cristobalite and cordierite.

The crystalline phase observed for the composition PA was the same as that which would be predicted from the quaternary composition. The deposit was studied by Pollman and Albrecht[103] and has previously been discussed in relation to the ternary system $CaO-Al_2O_3-SiO_2$ (see p.195). The composition of the residual liquid

phase on the 5% MgO plane (80.6% SiO_2, 8.9% Al_2O_3, 5.5% CaO) is outside the silica content of the diagram but indicates a highly siliceous residual liquid phase. This behaviour was predicted from the ternary composition KR on the ternary phase diagram but is also confirmed, albeit qualitatively, by the four component composition.

The mineralogy of the slags SR, TH and PB removed from German slag-tap furnaces was determined by Rost and Ney[107] using petrological techniques. The authors only reported the phase or phases observed optically and the phases included in Table 5.7 may not be representative of the whole sample. The iron oxide contents for all the samples were significantly greater than the magnesia content and the quaternary system correctly predicted the phase for sample PB only (that of dicalcium silicate). The phase melilite was reported for sample SR whereas anorthite would have been predicted from the quaternary phase diagram (see point SR, Fig.5.16). Of interest to note is the exceedingly high manganese oxide content (9.4%) which may account, with the iron oxide content, for the observed behaviour.

The quaternary system correctly predicted the formation of melilite in the slag TH but would be unable to account for the presence of hercynite.

A study of the quaternary system CaO-MgO-Al_2O_3-SiO_2 provides a useful insight into the behaviour of lignitic coal ash melts. Sufficient examples have been given to show that the predicted crystallisation behaviour may correspond well with experimental observations. However relatively few detailed studies have been conducted on the microstructure of coal ash slags. The use of this system is severely handicapped if the ash contains an

Fig.5.16. System $CaO-MgO-Al_2O_3-SiO_2$,5% MgO plane. Crystallisation of lignitic ash melts.

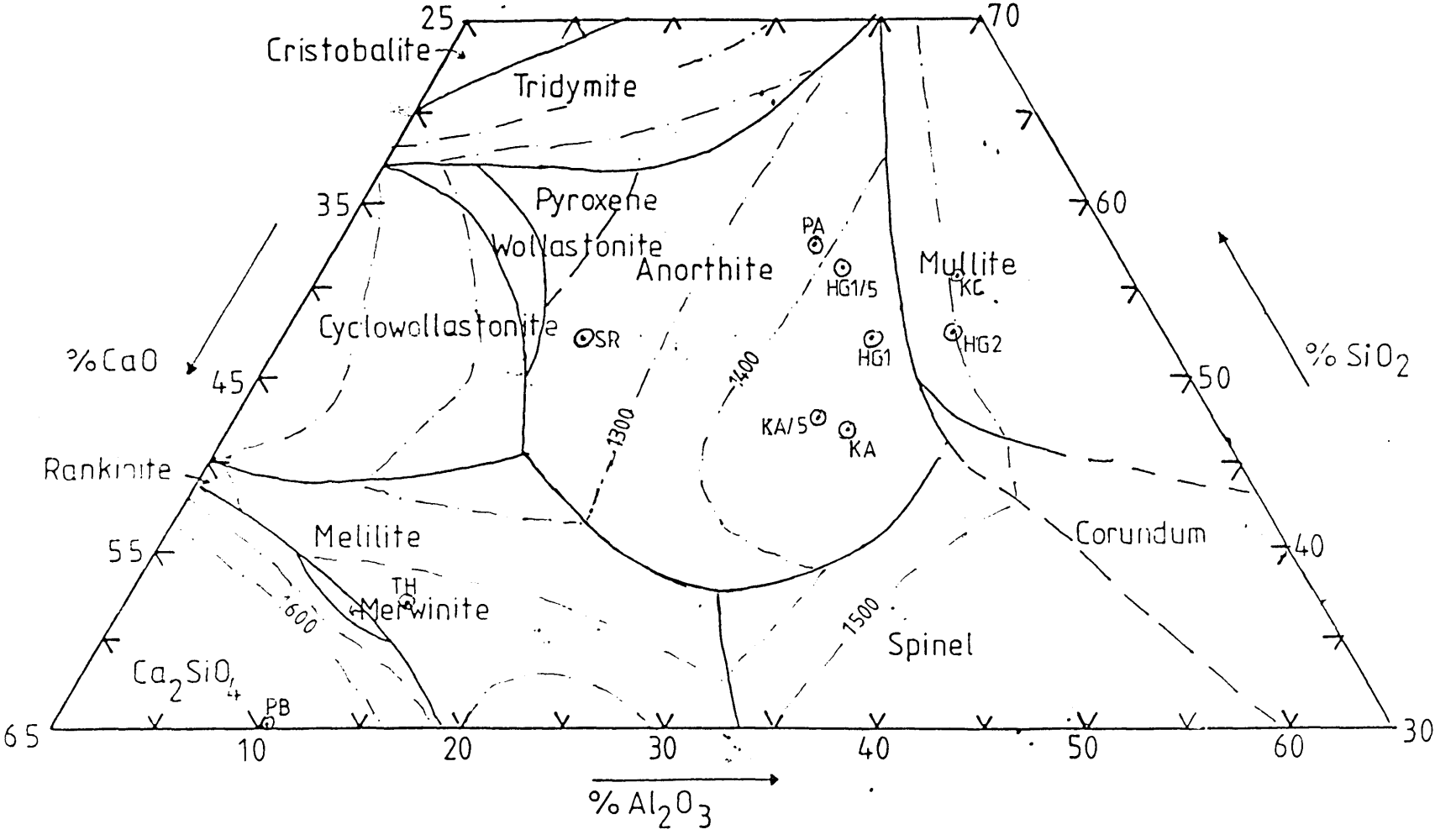


Fig.5.17. System $CaO-MgO-Al_2O_3-SiO_2$, 10% MgO plane. Crystallisation of lignitic ash melts.

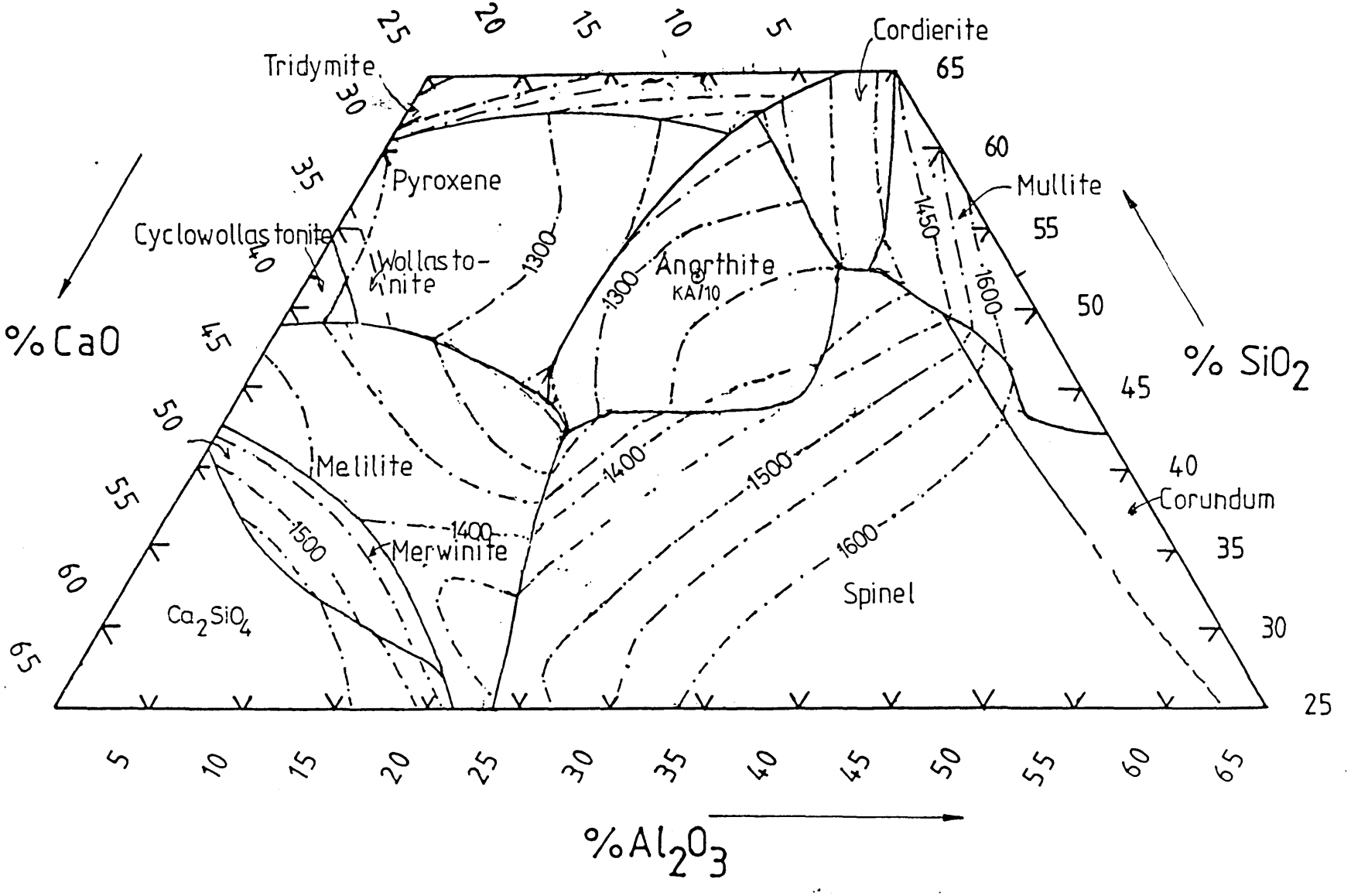
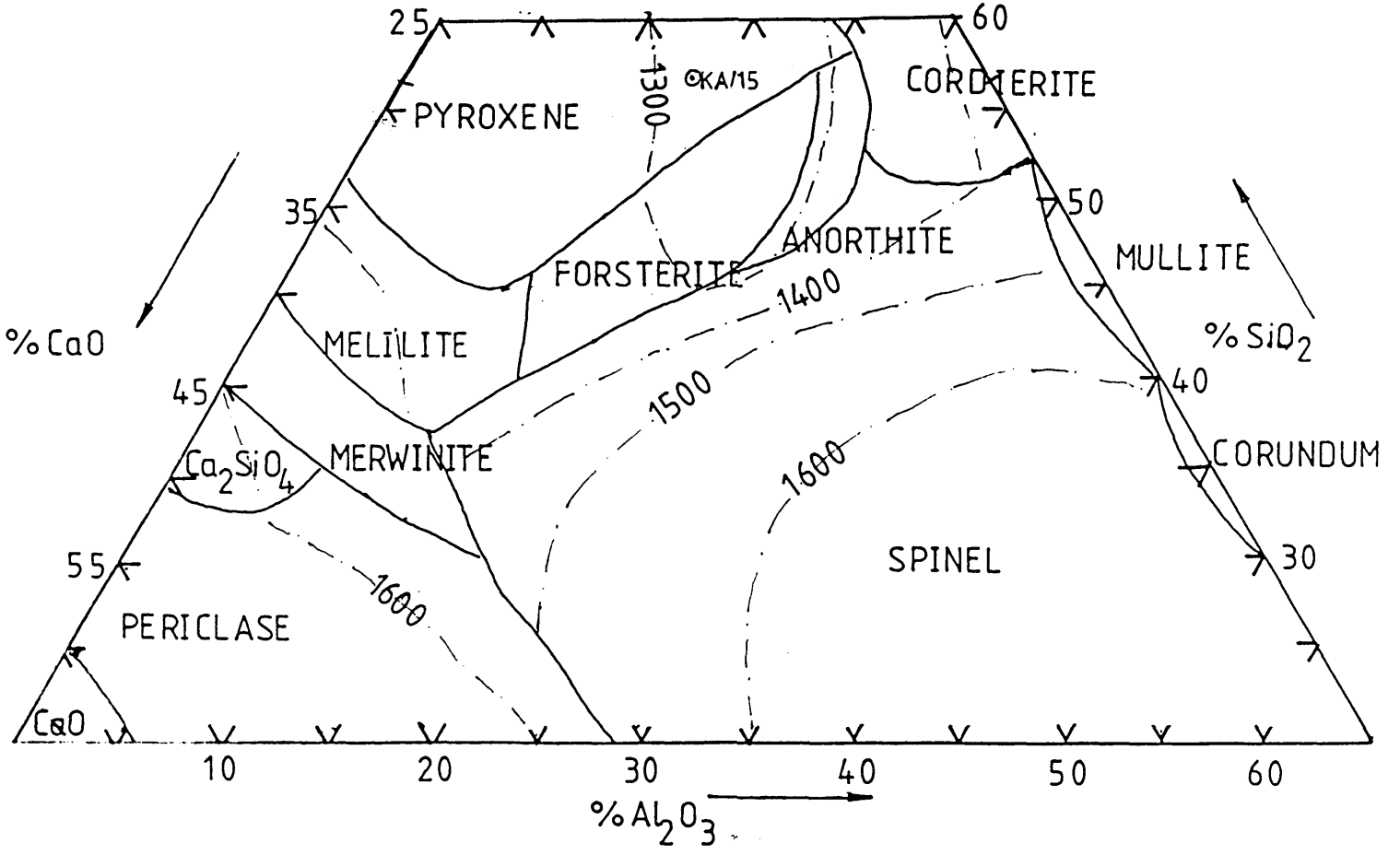


Fig.5.18. System $CaO-MgO-Al_2O_3-SiO_2$, 15% MgO plane. Crystallisation of lignitic ash melts.



appreciable iron oxide content and this naturally leads to a study of the system $CaO-Al_2O_3-SiO_2$-iron oxide. It will be shown that an appreciation of the latter system is of much greater value.

5.7 CRYSTALLISATION OF $CaO-Al_2O_3-SiO_2$-IRON OXIDE GLASSES

Two series of glasses were prepared, again based on the ternary compositions K1 - K5 with 5 and 10 wt % equivalent FeO. A further two series were prepared based on the glasses K1, K2 and K5 with 15 and 20 wt % equilvalent FeO. The crystallisation behaviour of each of the glasses was determined by quenching experiments in a mildly reducing atmosphere. The ferrous/total iron ratio observed in the quenched samples have been discussed previously in the results section.

The true representation of the system is as the quinary system $CaO-FeO-Al_2O_3-Fe_2O_3-SiO_2$ which would cause problems in analysis of crystallisation behaviour. The results of the experiments have been listed, along with the chemical composition in Table 5.9 and show that the crystalline phases present in the samples do not contain any iron in the Fe^{3+} state (although some Fe_2O_3 may be present in solid solution in the iron spinel phase). Therefore as the phase diagrams are to be used to describe the crystalline phases in equilibrium at a given temperature with a liquid phase the system can be described by the quaternary system $CaO-FeO-Al_2O_3-SiO_2$, though it must be remembered that the liquid phase will always contain some iron in the ferric state.

TABLE 5.9

Crystallisation behaviour of glasses of the system $CaO-Al_2O_3-SiO_2$-iron oxide

Glass	composition wt % SiO_2	Al_2O_3	CaO	FeO	Liquidus temp/°C	Primary phase	Temp.of appearance of 2° phase	Secondary phase	Temp.of appearance of 3° phase	Tertiary phase	Temp.of appearance of 4° phase	Quaternary phase
F1	47.0	30.0	18.0	5.0	>1480	anorthite	-	n.o.	-	n.o.	-	n.o.
F2	35.0	24.0	36.0	5.0	>1300	melilite	1200	anorthite	1200	calcium + silicate	-	n.o.
F3	39.0	26.0	30.0	5.0	>1450	anorthite	1200	melilite	1100	calcium + silicate	-	n.o.
F4	42.0	27.0	26.0	5.0	>1400	anorthite	1200	melilite	1100	calcium + silicate	-	n.o.
F5	47.0	33.0	15.0	5.0	<1500	anorthite	1200	iron spinel	-	n.o.	-	n.o.
F6	44.0	28.4	17.6	10.0	<1480	anorthite	1000	fayalite	-	n.o.	-	n.o.
F7	33.3	22.4	34.3	10.0	>1420	melilite	1200	anorthite	1100	calcium + silicate	-	n.o.
F8	37.4	24.2	28.4	10.0	<1420	anorthite	1200	melilite	1100	iron spinel	1000	olivine
F9	39.6	25.6	24.8	10.0	>1420	anorthite	1300	melilite	1000	olivine	-	n.o.
F10	44.0	31.6	14.4	10.0	>1400	anorthite	1200	iron spinel	1000	fayalite	-	n.o.
F11	41.6	26.8	16.6	15.0	>1400	anorthite	1400	fayalite	-	n.o.	-	n.o.
F12	31.5	21.2	32.2	15.0	>1300	melilite	1300	iron wollastonite	900	anorthite	900	iron spinel
F15	41.6	29.8	13.6	15.0	>1350	anorthite	1100	iron spinel	1000	fayalite	-	n.o.
F16	39.2	25.2	15.6	20.0	<1350	anorthite	1300	fayalite*	-	n.o.	-	n.o
F17+	29.6	20.0	30.4	20.0	>1300	melilite	1300	iron wollastonite	-	-		n.o.
F20	39.2	28.0	12.8	20.0	<1450	anorthite	1400	fayalite	1300	spinel	-	n.o.

+ see text

* determined as the secondary crystalline phase from the analysis of intensities of XRD pattern

n.o. = not observed

The method of representation of the quaternary system is the same as that used with the system $CaO-MgO-Al_2O_3-SiO_2$, that is planes of constant FeO content. The phase diagrams have not been previously published but it was possible to obtain the data necessary to construct the planes in regions of interest to coal ash studies from other published work. To be able to determine the extent of primary crystalline volumes and crystallisation paths not only have the 5, 10, 15 and 20% FeO planes been constructed but the study has been extended to include the 25, 30 and 50% planes. The method of preparation was as follows: the borders $CaO-SiO_2$ and $Al_2O_3-SiO_2$ were obtained from the ternary systems $CaO-FeO-SiO_2$[88] and $FeO-Al_2O_3-SiO_2$[88] by drawing a line of constant FeO content and determining the compositions at which the boundaries between primary crystalline fields and liquidus isotherms intersected this line. The boundaries, piercing points and liquidus isotherms within the plane were more difficult to obtain. The data available, that of Schairer[108] and Muan and Osborn[109] is of lines or planes through the tetrahedron between various compositional points. For example, planes of particular interest to this study were those of $FeO-SiO_2$-anorthite and $FeO-CaO.SiO_2$-anorthite. All the diagrams had an FeO apex and therefore a line could be drawn at constant FeO content. Where the lines intersected the boundaries and isotherms the composition was determined (in terms of the components) and the compositions were then recalculated in terms of component oxides. The data obtained from all the literature sources were plotted on the corresponding FeO levels and the boundaries and liquidus isotherms drawn. The data were not extensive and therefore the accuracy of the diagrams cannot be assured. Phases such as mullite, corundum, and rankinite ($3CaO.2SiO_2$) were not observed in the various

planes through the tetrahedron but were present in the border ternary systems ($CaO-FeO-SiO_2$ and $FeO.Al_2O_3.SiO_2$) and thus must be present at least to some extent within the quaternary system. In the case of the phase $CaO.6Al_2O_3$ included on the 5 and 10 wt % FeO planes there is no data but reference to the base ternary system ($CaO-Al_2O_3-SiO_2$) indicates that it may be present. (There is no phase diagram for the system $CaO-FeO-Al_2O_3$). Phase boundaries and liquidus isotherms were based on those of the base ternary systems, as in some cases only one or two datum points were achieved for each line. The basis for this was both the experimental data obtained in this study, as will be discussed subsequently, and the distinct similarities between the literature data and the base ternary system. The exception to this was the 50% FeO plane where the literature data, though severely limited, were distinctly different from that of the base ternary system. The planes prepared are illustrated in Figs 5.19 - 5.25.

Before discussion of the crystallisation behaviour of the glass studied it is worth describing the quaternary system and comparing it with the system $CaO-MgO-Al_2O_3-SiO_2$. The most striking observation is the little effect which addition of FeO has on the crystalline phase assemblages of the base ternary system. Unlike the magnesia system where the 5% MgO plane (Fig.5.9) contained magnesia-bearing phases (e.g. pyroxene) the lowest FeO plane at which an FeO-containing phase (excluding solid solution) was the 15% plane. While on the 15% MgO plane (Fig.5.11) the anorthite field is very small and the spinel field is dominant, the anorthite field on the 30% FeO plane (Fig.5.24) is still very much a major part of the system and hercynite is a relatively minor field. The anorthite primary volume actually extends up to the 50% FeO plane, the point A indicated in Fig.5.25 is the piercing

point at which the anorthite, olivine and hercynite primary volumes meet (the anorthite is below the plane). An important observation is the presence of the wollastonite solid solution primary phase which is stabilised by some substitution of FeO above the 10% plane.

The compositions studied have been plotted on the appropriate plane. Though the glasses contained appreciable amounts of ferric oxide (see Table 4.11) the composition used to enable plotting was the equivalent FeO content (i.e. the planned composition). With reference to Table 5.9 the primary phases observed for all the glasses studied agree with those of the corresponding planes of the quaternary system.

5.7.1 Crystallisation behaviour of glasses F1 - F20 containing 5-20 wt % FeO

The crystallisation behaviour of the glasses was observed to be quite complex but is sufficiently important to this study to necessitate a detailed description of each of the glasses. As with the quaternary system CaO-MgO-Al_2O_3-SiO_2 it is possible to calculate the initial crystallisation path for primary phases not exhibiting solid solution. The primary crystalline phase observed for all the glasses were those of the base ternary, i.e. anorthite and melilite (observed to be close to the composition of gehlenite). Thus the initial crystallisation paths will be towards higher FeO planes of the quaternary system. The compositions of the glasses and the compositions of the residual liquid phase on higher FeO planes (up to where a secondary phase is encountered or the 30% FeO plane) are listed in Table 5.10.

The glass F1 (based on the ternary composition K1 with 5% FeO) was observed to crystallise anorthite only. The composition of the residual liquid phase has been plotted on Figs 5.20, 5.21 and 5.22 (the 10, 15 and 20% FeO planes) and designated F1/10, F1/15 and F1/20 respectively. It can be seen that as anorthite crystallises, the residual liquid phase becomes increasingly enriched in silica and iron oxide. The secondary crystalline phase would be expected to be tridymite under equilibrium conditions. The crystallisation of tridymite is known to be exceedingly slow and would not have been expected to crystallise within the time-scale of the heat treatments used. As the composition of the residual liquid phase (F1/20) is just within the tridymite field on the 20% FeO plane about 75% of the glass must have crystallised before the secondary phase was encountered.

The glass F2 (based on the ternary composition K2 with 5% FeO) was in the primary phase melilite (solid solution between gehlenite and iron-akermanite). The initial crystallisation path was calculated assuming that the primary phase was gehlenite. The composition of the residual liquid phase on the 10% FeO plane (Fig.5.20), designated F2/10, lies in the primary field of cyclo-wollastonite. With reference to Table 4.11 both anorthite and a calcium metasilicate were observed with melilite at 1200 °C and thus the crystallisation path must have encountered the anorthite/melilite boundary before subsequent crystallisation of cyclo-wollastonite. The presence of wollastonite as the tertiary phase at lower temperatures (1100 °C and 1000 °C) may be due to the effects of viscosity and the presence of iron oxide. The observation of cyclowollastonite at 900 °C (Table 4.11) suggests that there is a peritectic point between the wollastonite, cyclo-

wollastonite, melilite and anorthite primary volumes. On cooling melt F2 from the liquidus temperature melilite and anorthite would crystallise out as the primary and secondary phase respectively. The tertiary phase of cyclowollastonite would be expected from the phase diagram and would crystallise until the peritectic point is reached where, from the observed behaviour, cyclowollastonite will react with the liquid phase to produce wollastonite. The presence of the cyclowollastonite at 900 °C may be due to the viscosity of the liquid phase inhibiting the peritectic reaction. It is important to note that the ternary phase assemblage (melilite, anorthite and calcium metasilicate) is the same as that which would be predicted from the compatibility triangle of the base ternary system ($CaO-Al_2O_3-SiO_2$) in which the composition K2 lies.

The glass F3 (based on the ternary glass K3 with 5% FeO) was observed to crystallise in the sequence anorthite, melilite, calcium metasilicate. The composition (F3/10) of the residual liquid phase on the 10% FeO plane has been plotted and lies in the melilite primary phase which agrees with the observed behaviour. Cyclowollastonite was determined to be the tertiary crystalline phase at 1200 °C whereas at lower temperatures wollastonite was observed. This gives further evidence for the existence of a peritectic point as indicated by the behaviour of glass F2. As with F2 the ternary phase assemblage for glass F3 was the same as that expected for the ternary glass K3.

The primary crystalline phase observed for the glass F4 (based on the ternary composition K4 with 5% FeO) was anorthite. The composition of the residual liquid phase on the 10% FeO plane (point F4/10) indicates a crystallisation path towards the melilite

boundary though the composition of the residual liquid phase (F4/15) on the 15% FeO plane lies in the cyclowollastonite field. The crystallisation behaviour observed, that of the sequence anorthite, melilite, wollastonite, agrees well with the initial crystallisation path. Cyclowollastonite was not observed but the wollastonite phase was only observed at temperatures below 1200 °C (i.e. at temperatures below the apparent peritectic point). As with the glass F2, and F3 the phase assemblage is the same as that expected for the ternary composition K4.

The composition of glass F5 was based on that of K5 with 5% FeO. Anorthite was observed as the primary crystalline phase with iron spinel (hercynite) appearing as the secondary phase at 1200 °C. The compositions of the residual liquid phase on the 10 and 15% FeO planes (F5/10 and F5/15) have been plotted on the corresponding planes. The crystallisation path indicates that with crystallisation of anorthite the residual liquid phase becomes increasingly enriched in alumina, iron oxide and to a lesser extent silica. Though the phase diagram would predict a secondary crystalline phase of mullite the observation of hercynite indicates that the presence of ferric oxide within the residual liquid phase reduces the solubility of iron spinel. With reference to the base glass K5 mullite was expected to be the secondary phase but was not observed despite lengthy treatment.

The primary crystalline phase observed for the glass K6 (based on the ternary glass K1 with 10% FeO) was anorthite with only the secondary phase of fayalite observed at 1000 °C. The crystallisation path as indicated by the composition of the residual liquid extends into the 30% FeO plane (Fig.5.24) without meeting a secondary phase (see points F6/15, F6/20, F6/25 and

F6/30 on the appropriate planes). The residual liquid phase becomes increasingly iron and silica rich and fayalite would be expected as the secondary phase. Analysis of the 50% FeO plane (Fig.5.25) shows that the olivine primary phase occupies the region that the crystallisation path of F6 is directed towards. The olivine primary field includes fayalite ($2FeO.SiO_2$) and thus this phase might be expected as the secondary phase from the crystallisation path.

The crystallisation behaviour of glass F7 (based on composition K2 with 10% FeO) was the same as that of the 5% analogue F2. The composition of the residual liquid phase on the 15% FeO plane, F7/15, lies in the anorthite primary field indicating this to be the secondary crystalline phase. The calcium metasilicate observed as the tertiary phase was that of wollastonite which is present on the 20% FeO plane (Fig.5.22). As with the glass F4 wollastonite was observed below 1200 °C (below the apparent peritectic). The ternary phase assemblage was the same as that observed for the ternary glass K2.

The glass F8 (based on composition K3 with 10% FeO) was observed to crystallise to four components at 1000 °C. The crystallisation sequence observed was anorthite, melilite, iron spinel (hercynite) and olivine ($CaO.FeO.SiO_2$). The composition of the residual liquid phase on the 15% FeO plane (point F8/15) is in the melilite phase indicating this to be the secondary phase (as observed). The presence of hercynite and olivine in the quenched samples indicates that the residual liquid phase on crystallisation of anorthite and melilite becomes initially alumina and iron oxide rich and after crystallisation of hercynite

calcium, iron oxide and silica rich. The olivine field (that of $CaO.FeO.SiO_2$) initially appears on the 30% FeO plane which indicates that the residual liquid phase must become very rich in FeO before crystallisation of olivine occurs.

The primary crystalline phase for the glass F9 (based on the ternary glass K4 with 10% FeO) was anorthite. Only the secondary and tertiary phases of melilite and olivine were observed. The crystallisation path (indicated by the points F9/15, F9/20 and F9/25 plotted on the 15, 20 and 25% planes) shows that the anorthite/melilite boundary would have been encountered before the 25% FeO plane. With reference to Fig.5.24 of the 30% FeO plane it can be seen that the olivine phase ($CaO.FeO.SiO_2$) is above the compositionF9/25. Therefore on crystallisation of anorthite and melilite the residual liquid phase becomes enriched in CaO, SiO_2 and iron oxide resulting in saturation and subsequent crystallisation of olivine.

The glass F10 was based on the composition K5 with 10% FeO. The sequence of crystallisation was anorthite, hercynite followed by fayalite with no quaternary phase observed. The crystallisation path (from the compositions of the residual liquid phases F10/15, F10/20 and F10/25) indicates an increasingly SiO_2, Al_2O_3 and FeO - rich liquid. As with the 5% FeO analogue (glass F5) the spinel phase (hercynite) crystallised instead of the expected mullite phase. It can be seen that the crystallisation path is directed towards the FeO apex and thus the residual liquid on crystallisation of hercynite will become enriched in iron oxide and SiO_2 and hence fayalite would be expected as the tertiary phase (as observed).

The glass F11 was based on the composition of K1 with 15% FeO and was observed to crystallise in the same sequence as the 10% FeO analogue (F6), that is anorthite followed by fayalite. The crystallisation path (F11/20, F11/25 and F11/30) indicates a residual liquid phase moving in the direction of the olivine primary field (50% FeO plane, Fig.5.25). What was unexpected was the small temperature range between the liquidus temperature and the temperature at which fayalite appeared. This may have been due to the effect of Fe_2O_3 present in the liquid phase.

The glass F12 (based on the ternary glass composition K2 with 15% FeO) was observed to have crystallised in the sequence melilite, iron wollastonite, anorthite, followed by hercynite. The crystallisation path indicates anorthite to be the secondary phase but the path may have met the wollastonite solid solution field between the two planes. It is apparent that iron oxide would have to be taken up by the wollastonite phase as the next phase to appear which contained iron was hercynite at 900 °C with crystallisation of anorthite.

Glass F15 (based on the ternary glass K5 with 15% FeO) crystallised in the same sequence as its 10% analogue (F10), that is anorthite, hercynite followed by fayalite. The crystallisation path is indicated by the composition of the residual liquid phase points F15/20, F15/25 and F15/30 on the appropriate diagrams.

The glass F16 was based on the ternary glass K1 with 20% FeO. Only anorthite (the primary crystalline phase) and fayalite were observed in quenched samples. The crystallisation behaviour was the same as that of the 10 and 15% analogues, glasses F6 and F11. The crystallisation path, indicated by compositions F16/25 and

F16/30 shows the residual liquid phase moving in the direction of the olivine field present on the 50% FeO plane.

The primary crystalline phase observed for the glass F17 (based on the ternary composition K2 with 20% FeO) was melilite with a complex subsequent crystallisation behaviour. The crystallisation path (compositions F17/25 and F17/30) indicates a secondary phase of anorthite, the behaviour observed initially was melilite present with iron wollastonite (between 1100 °C and 1300 °C). At lower temperatures a ternary phase assemblage of melilite, anorthite and olivine ($CaO.FeO.SiO_2$) was observed with no evidence of a wollastonite phase. This behaviour is difficult to explain from the data available but it appears that iron wollastonite is a metastable phase in an iron oxide and silica - rich liquid at temperatures below 1100 °C. With reference to the 30 and 50% FeO planes (Figs 5.24 and 5.25) the wollastonite solid solution field is present on the lower FeO plane but not on the 50% plane whereas olivine is. The primary phase volume is known to lie just underneath the plane (at point A) and thus the crystallisation path of glass F17 may have passed through a peritectic point.

The glass F20 (based on composition K5 with 20% FeO) was observed to crystallise in the sequence anorthite, fayalite followed by hercynite. The crystallisation path (compositions F20/25 and F20/30) indicates that hercynite would be expected as the secondary phase. The presence of fayalite suggests that under the experimental conditions the crystallisation of fayalite is thermodynamically more favourable. On crystallisation of anorthite the residual liquid phase becomes richer in alumina, silica and iron oxide. Therefore with crystallisation of fayalite the

TABLE 5.10

Composition of Residual Liquid Phase for F Series of Glasses

Glass	Composition Wt %				Primary Field
	SiO_2	Al_2O_3	CaO	FeO	
F1	47.0	30.0	18.0	5.0	Anorthite
F1/10	51.0	23.0	16.0	10.0	Anorthite
F1/15	55.0	15.9	14.1	15.0	Anorthite
F1/20	59.2	8.8	12.0	20.0	Tridymite
F2	35.0	24.0	36.0	5.0	Melilite
F2/10	49.0	11.0	30.0	10.0	Cyclowollastonite
F3	39.0	26.0	30.0	5.0	Anorthite
F3/10	35.0	15.0	40.0	10.0	Melilite
F4	42.0	27.0	26.0	5.0	Anorthite
F4/10	41.0	17.0	32.0	10.0	Anorthite
F4/15	40.0	6.9	38.1	15.0	Cyclowollastonite
F5	47.0	33.0	15.0	5.0	Anorthite
F5/10	51.0	29.0	10.0	10.0	Anorthite
F5/15	55.0	24.9	5.1	15.0	Mullite
F6	44.0	28.0	17.6	10.0	Anorthite
F6/15	44.5	24.1	16.4	15.0	Anorthite
F6/20	45.0	19.8	15.2	20.0	Anorthite
F6/25	45.5	15.5	14.0	25.0	Anorthite
F6/30	46.0	11.1	12.9	30.0	Anorthite
F7	33.3	22.4	34.3	10.0	Melilite
F7/15	39.0	15.1	30.9	15.0	Anorthite
F8	37.4	24.2	28.4	10.0	Anorthite
F8/15	34.7	17.8	17.5	15.0	Melilite
F9	39.6	25.6	24.8	10.0	Anorthite
F9/15	38.0	19.9	27.1	15.0	Anorthite
F9/20	36.2	14.2	29.6	20.0	Anorthite
F9/25	34.5	8.5	32.0	25.0	Melilite
F10	44.0	31.6	14.4	10.0	Anorthite
F10/15	44.5	29.0	11.5	15.0	Anorthite
F10/20	45.0	26.2	8.8	20.0	Anorthite
F10/25	45.5	23.5	6.0	25.0	Anorthite
F10/30	46.0	20.7	3.3	30.0	Mullite

... Continued ...

TABLE 5.10 ... Continued ...

Glass	Composition Wt %				Primary Field
	SiO_2	Al_2O_3	CaO	FeO	
F11	41.6	26.8	16.6	15.0	Anorthite
F11/20	41.0	23.5	15.5	20.0	Anorthite
F11/25	40.7	20.0	14.3	25.0	Anorthite
F11/30	40.2	16.6	13.2	30.0	Anorthite
F12	31.5	21.2	32.3	15.0	Melilite
F12/20	34.7	16.0	29.3	20.0	Anorthite
F15	41.6	29.8	13.6	15.0	Anorthite
F15/20	41.0	27.5	11.5	20.0	Anorthite
F15/25	40.7	25.0	9.3	25.0	Anorthite
F15/30	40.2	22.6	7.2	30.0	Anorthite
F16	39.2	25.2	20.0	20.0	Anorthite
F16/25	38.3	22.2	14.5	25.0	Anorthite
F16/30	37.4	19.3	13.3	30.0	Anorthite
F17	29.6	20.0	30.4	20.0	Melilite
F17/25	31.5	15.7	27.8	25.0	Melilite
F17/30	33.4	11.5	25.1	30.0	Melilite
F20	39.2	28.0	12.8	20.0	Anorthite
F20/25	38.3	25.7	11.0	25.0	Anorthite
F20/30	37.4	23.5	9.1	30.0	Anorthite

Fig.5.19.System $CaO-FeO-Al_2O_3-SiO_2$,5% FeO plane. Crystallisation of F series of glasses.

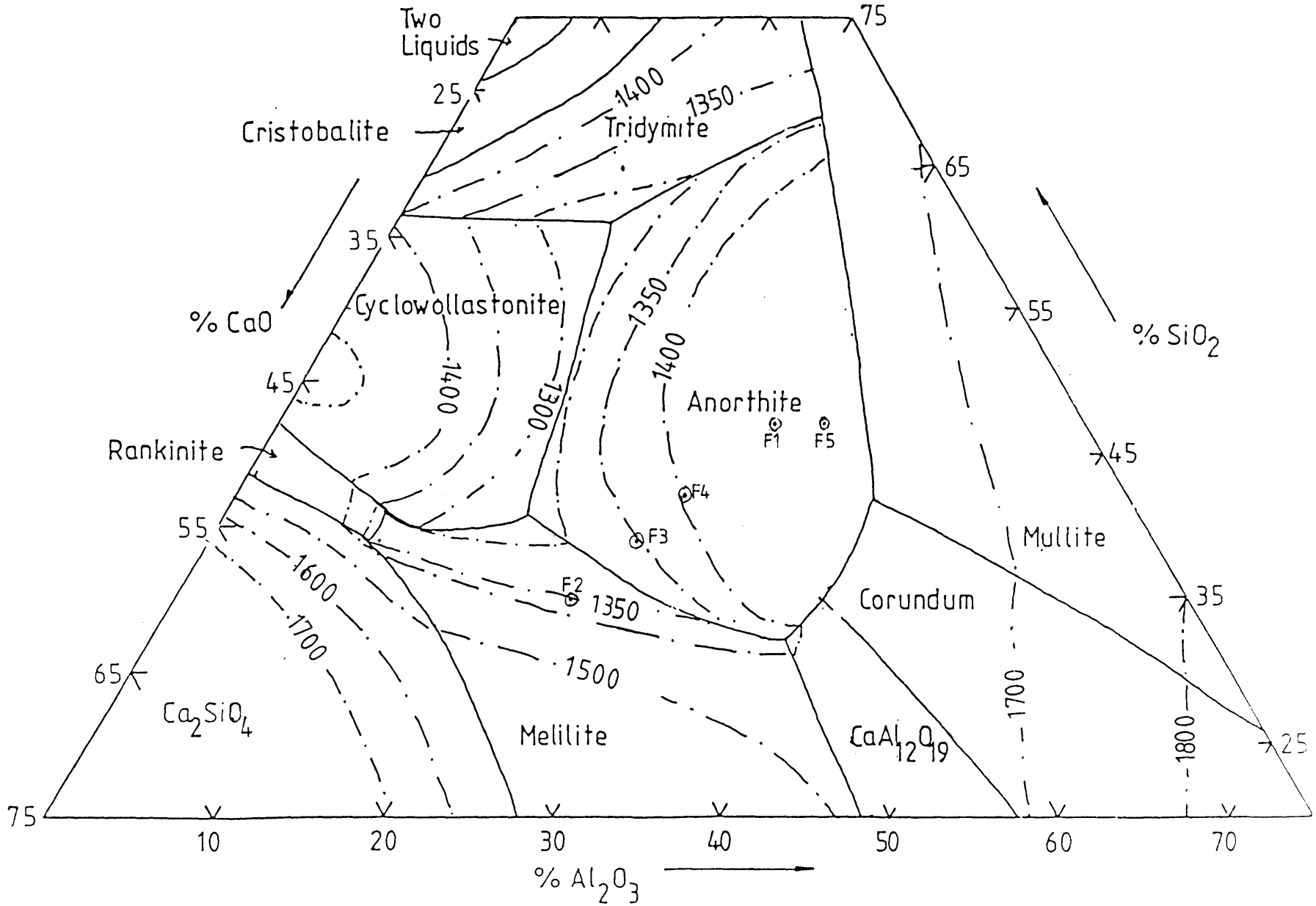


Fig. 5.20. System $CaO-FeO-Al_2O_3-SiO_2$, 10% FeO plane. Crystallisation of F series of glasses.

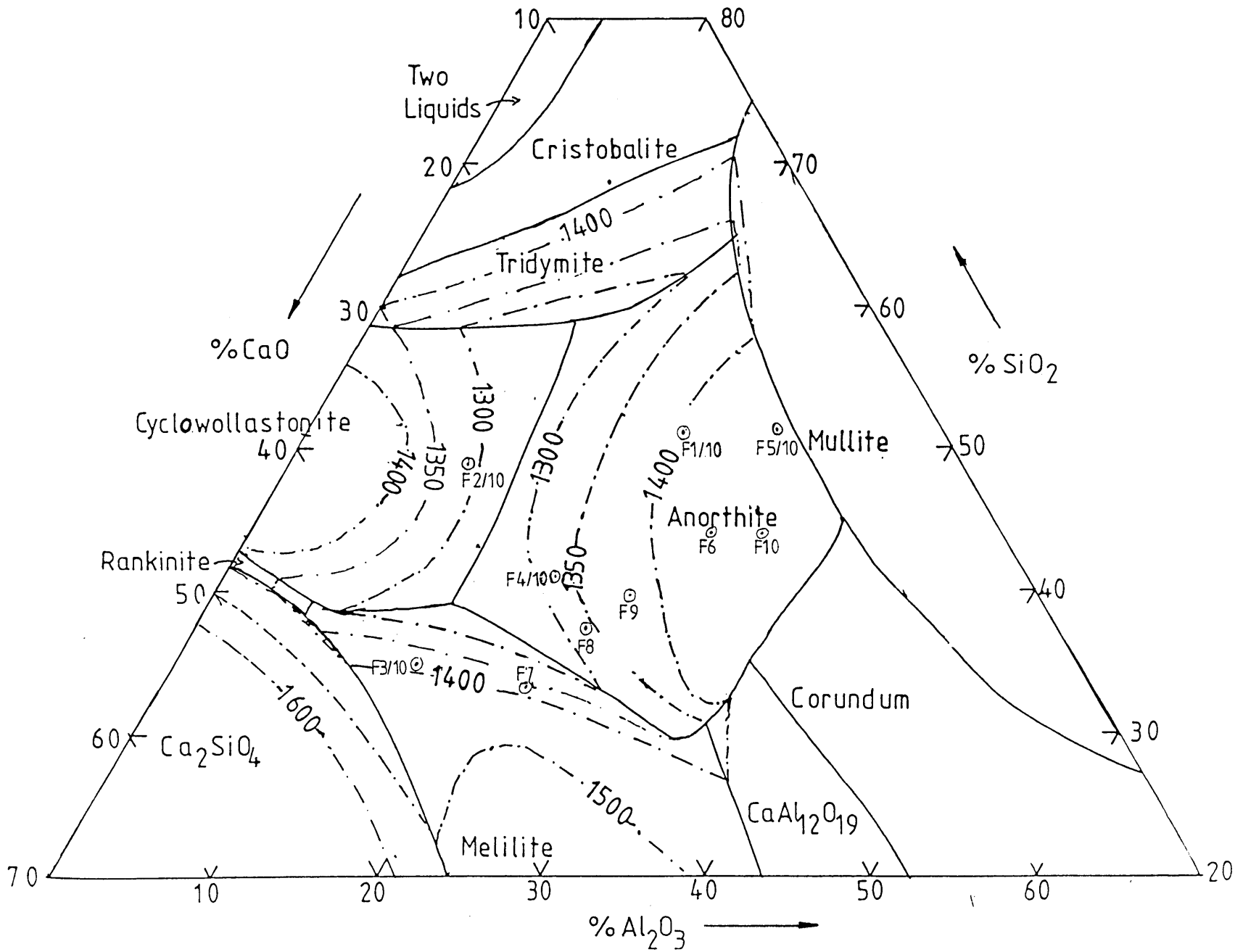


Fig. 5.21. System $CaO-FeO-Al_2O_3-SiO_2$, 15% FeO plane. Crystallisation of F series of glasses.

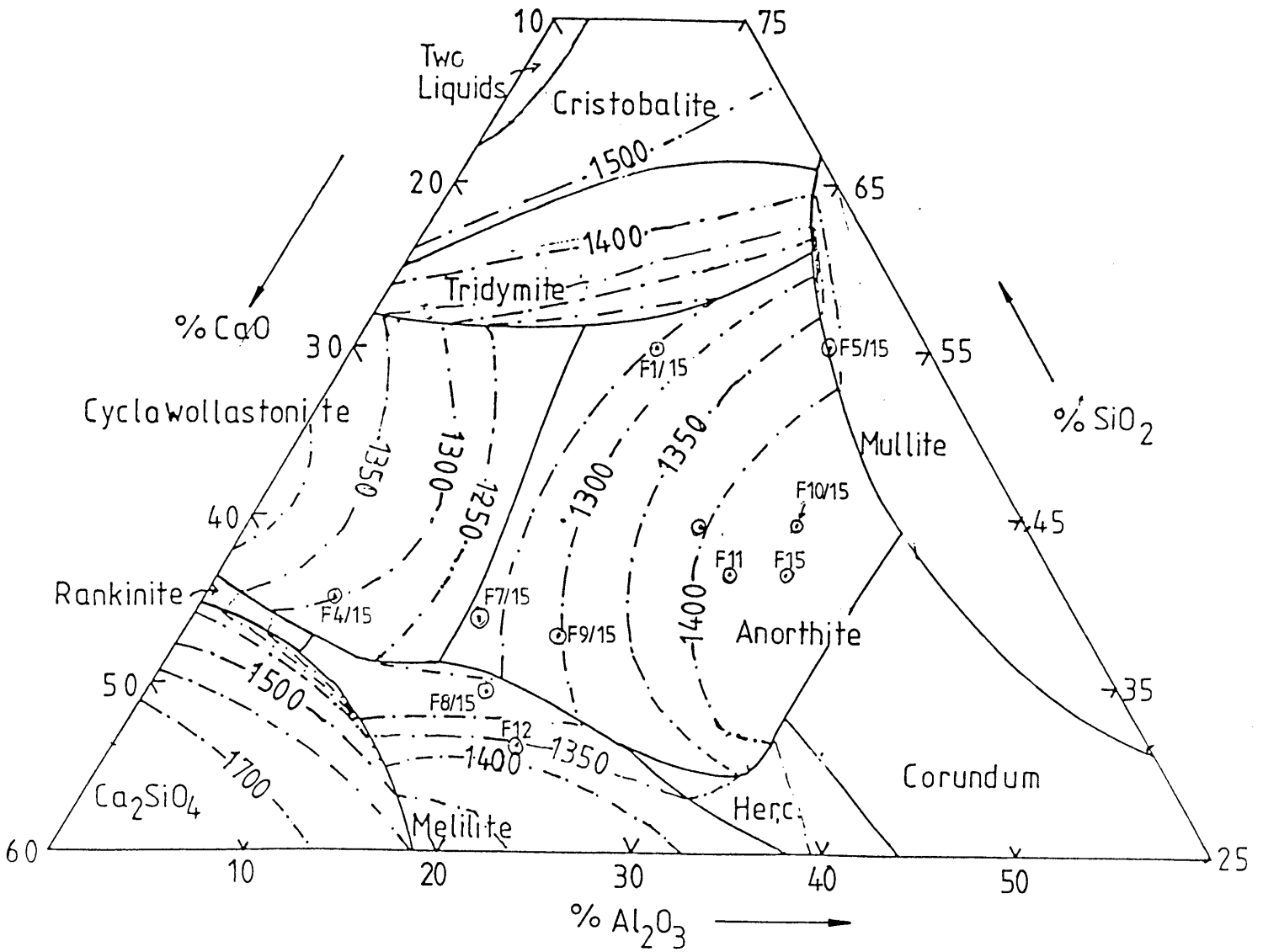


Fig.5.22. System $CaO-FeO-Al_2O_3-SiO_2$, 20% FeO plane. Crystallisation of F series of glasses.

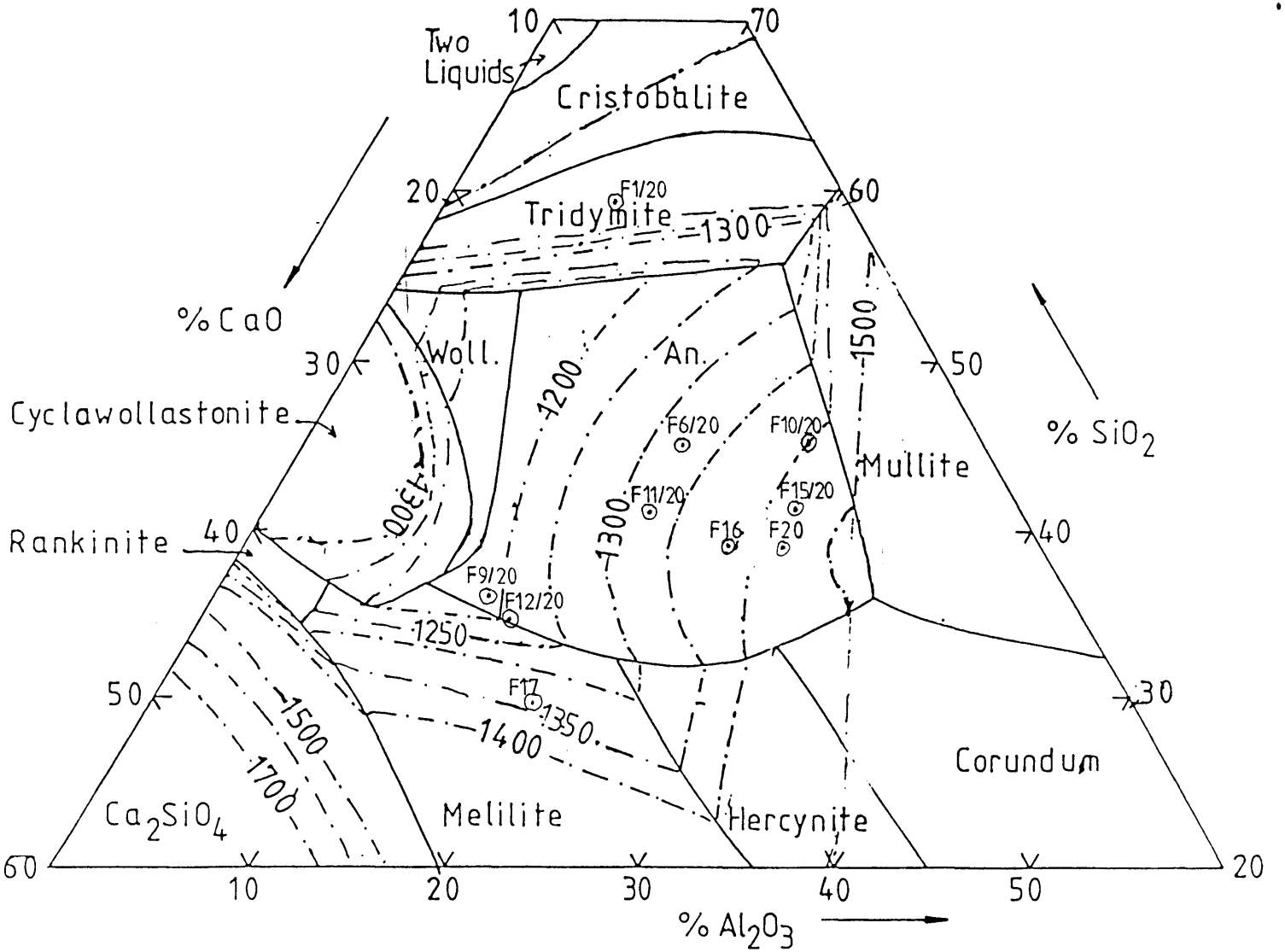


Fig.5.23.System $CaO-FeO-Al_2O_3-SiO_2$, 25% FeO plane. Crystallisation of F series of glasses.

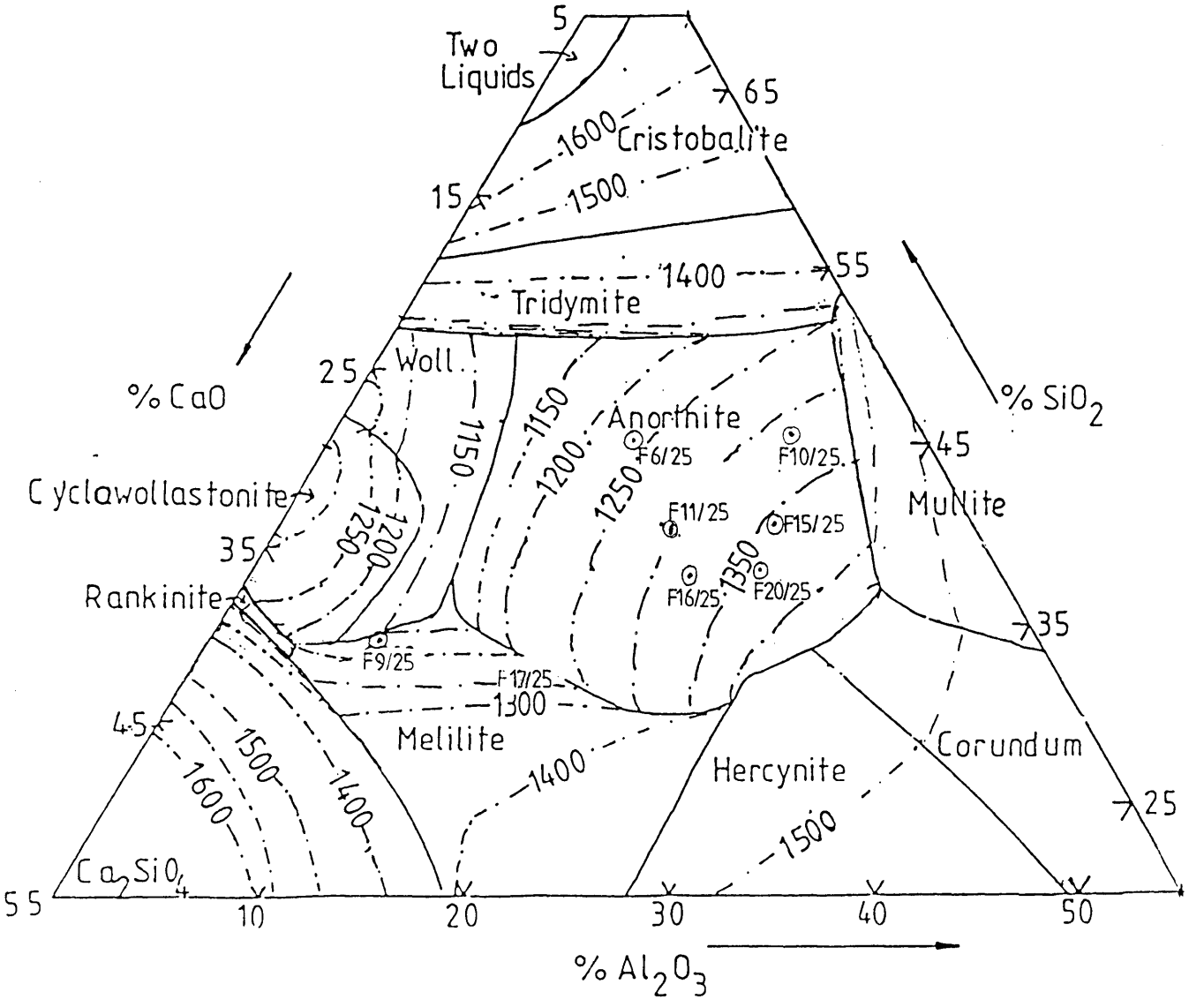


Fig.5.24. System $CaO-FeO-Al_2O_3-SiO_2$, 30% FeO plane. Crystallisation of F series of glasses.

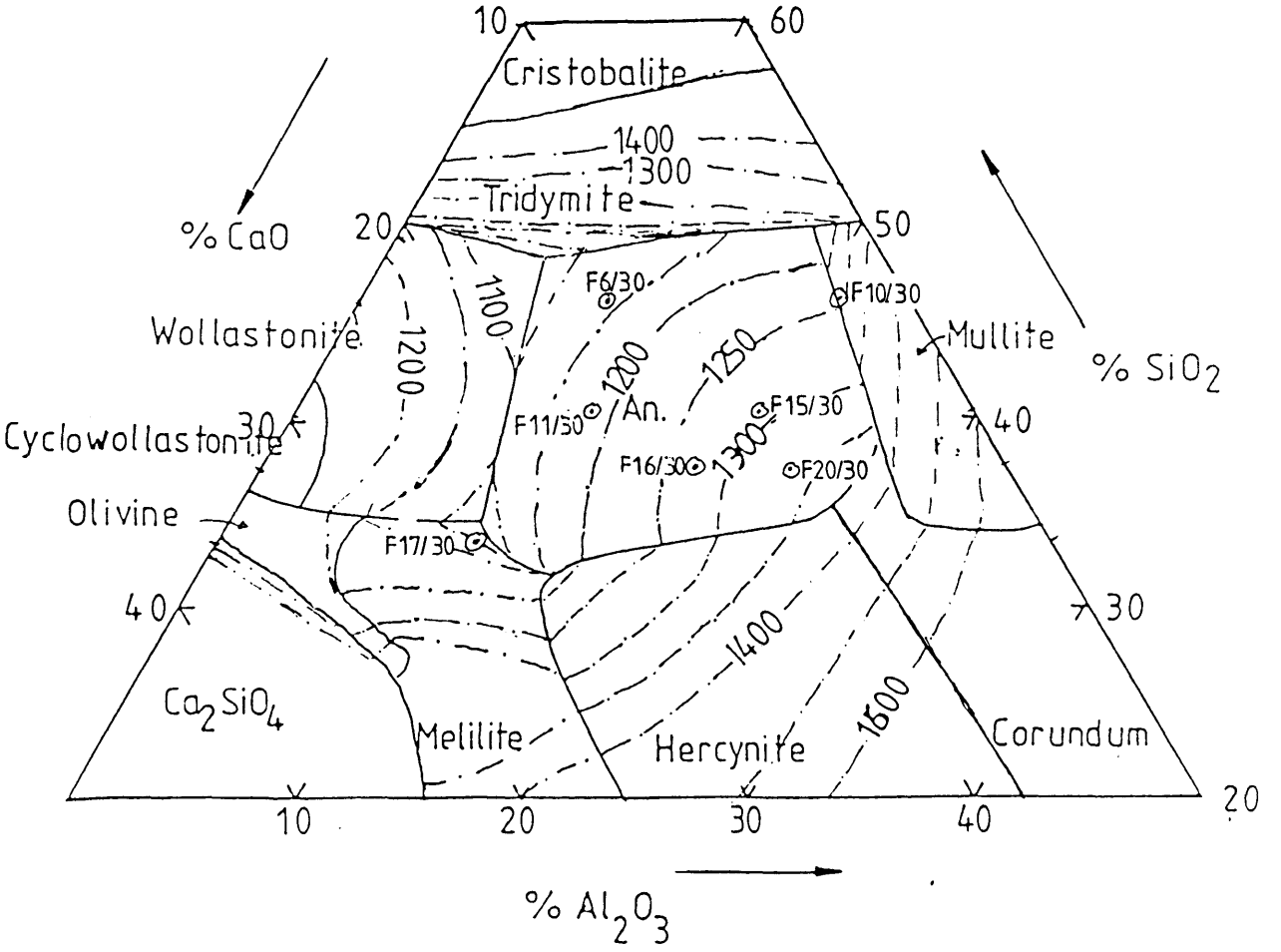
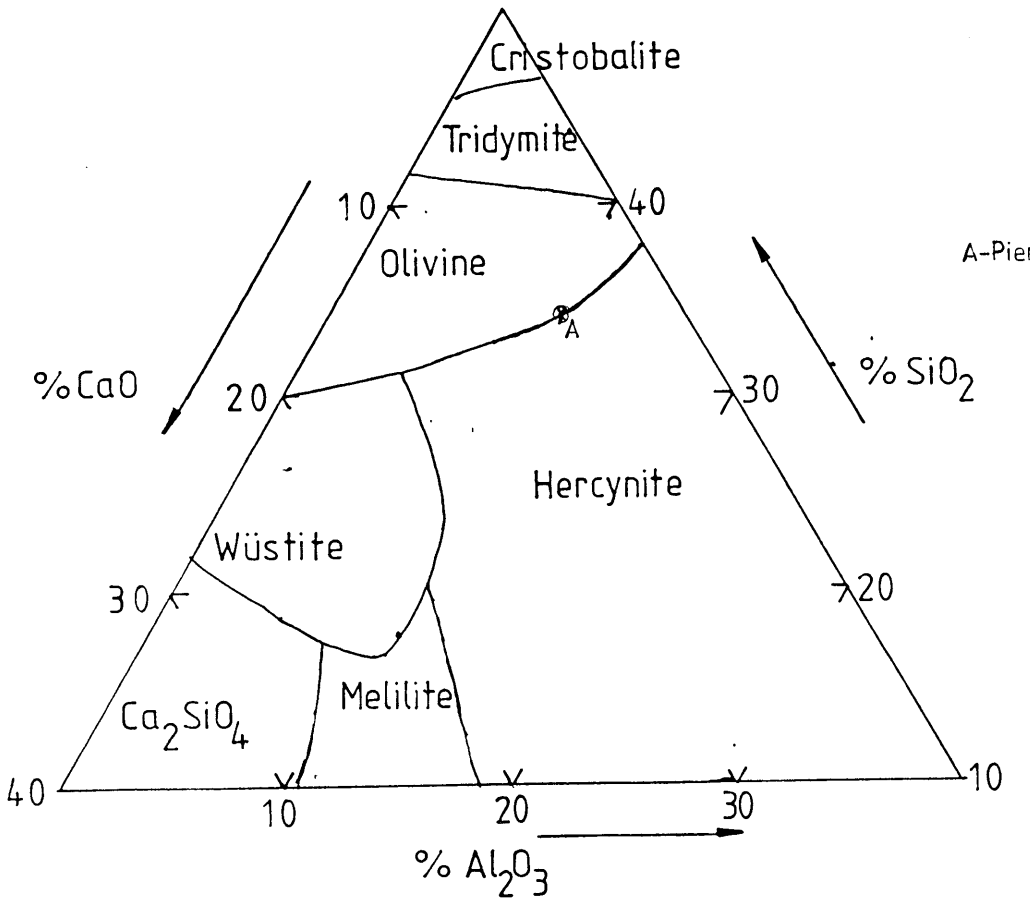


Fig.5.25. System $CaO-FeO-Al_2O_3-SiO_2$, 50% FeO plane.



A-Piercing point; anorthite-olivine-hercynite

residual liquid phase will be enriched in alumina and thus hercynite would be expected as the tertiary phase.

The relevance of the system $CaO-FeO-Al_2O_3-SiO_2$ to the crystallisation of coal ash melts will now be described.

5.8 CRYSTALLISATION OF MULTICOMPONENT GLASSES BASED ON ASH COMPOSITIONS

The series of glasses Mat 3, Mat 4 and Mat 5 were based on the composition of ash KA with compositions normalised to five, seven and eight components respectively. The compositions of the glasses and the results of the crystallisation study have been listed in Table 5.11. The glass Mat 5 was of the same composition as ash KA and was observed to have the same crystallisation behaviour determined for this ash; that is only anorthite was observed to crystallise.

The glass Mat 3 exhibited a secondary phase of magnetite. This was at first surprising but it appears that addition of magnesia to $CaO-FeO-Al_2O_3-SiO_2$ melts reduces the solubility of iron oxide. This effect is known in iron-making slags where magnesia is known to increase the activity of iron. The composition of the residual liquid phase for the normalised four-component composition ($CaO-FeO-Al_2O_3-SiO_2$) of the glass Mat 3 (designated M3) has been calculated and is listed in Table 5.12. The compositions have been plotted on the appropriate plane of the quaternary system (Figs 5.26 - 5.29). As can be seen the crystallisation behaviour expected would be precipitation of anorthite only as the crystallisation path

extends into the tridymite field on the 20% FeO plane. The crystallisation behaviour of the glass was determined in air and thus a significant amount of iron oxide present in the liquid phase would be in the ferric state, and with the effect of magnesia the liquid phase becomes saturated in iron oxide with crystallisation of anorthite. The effect of ferric oxide in the liquid phase of glasses studied in the mildly reducing atmosphere has been attributed to the crystallisation of an iron spinel phase (see the behaviour of glass F5, p.**228**).

The glass Mat 4 exhibited a secondary phase of iron wollastonite. The crystallisation path is the same as that of M3 (points M3/10, M3/15 and M3/20 on Figs 5.27, 5.28 and 5.29 respectively) and it appears that the presence of alkali oxides alters the crystallisation path. Though the glass contained only 1.0% total alkali oxide the residual liquid phase on the 20% FeO plane will contain 4% alkali oxide which may reduce the effect of the high silica content of the composition on that plane. The alkali oxides must also reduce the effect of magnesia observed for the glass Mat 3.

Only anorthite was observed to crystallise for the glass Mat 5. The behaviour can be explained from the crystallisation of the normalised four component composition shown by the crystallisation path of M3 (points M3/10 - M3/20). It appears that the presence of titania (1.9 wt %) in this composition negates the effect of magnesia and alkali oxides on the devitrification behaviour of the glass.

The glass D1 was of the same composition as the bituminous-type ash KB and showed the same crystallisation

behaviour. Mullite was observed as the primary crystalline phase with a secondary phase of iron spinel appearing below 1200 °C. The normalised four component composition ($CaO-FeO-Al_2O_3-SiO_2$) (DA) and the compositions of the residual liquid on the 10 and 15% planes (composition DA/10 and DA/15) have been listed in Table 5.13 along with the composition of the glass. The normalised composition has an FeO content of 9.6% and thus has been plotted on the 10% FeO plane (Fig.5.27) and lies in the mullite primary field and likewise the composition DA/10. The composition DA/15 has a high silica and low alumina content while relatively rich in FeO, and lies outside the SiO_2 limits of the diagram (Fig.5.28). The crystallisation of the iron spinel phase was analogous to the behaviour of glass F10 (p.230) that is, the enrichment of the residual liquid phase with silica and iron oxide reduced the solubility of iron oxide which lead to the precipitation of the spinel phase.

The quaternary system $CaO-FeO-Al_2O_3-SiO_2$ can therefore be used to describe the crystallisation behaviour of multicomponent glasses from the normalised composition. The diagrams predict the primary crystalline phase and from the observed behaviour of glasses of the system $CaO-Al_2O_3-SiO_2$-iron oxide studied and analysis of crystallisation paths the precipitation of secondary phases can be successfully accounted for.

The relevance of this study to the crystallisation of coal ash melts will now be described.

TABLE 5.11

Crystallisation behaviour of multicomponent glasses

Glass	Composition wt %								Primary phase	Temp. of appearance of secondary phase/^{o}C	Secondary phase
	SiO_2	Al_2O_3	Fe_2O_3	CaO	MgO	Na_2O	K_2O	TiO_2			
MAT 3	44.2	28.6	5.3	17.8	3.9	0.0	0.0	0.0	Anorthite	1400	Magnetite
MAT 4	43.9	28.3	5.2	17.7	3.9	0.7	0.3	0.0	Anorthite	1200	Iron wollastonite
MAT 5	43.1	27.8	5.1	17.3	3.8	0.7	0.3	1.9	Anorthite	-	n.o.
D1	54.6	26.5	9.3	1.5	1.6	1.2	4.2	1.1	Mullite	1200	Iron spinel

TABLE 5.12

Composition of Residual Liquid Phase for Glass MAT3* (Normalised Composition)

	Composition Wt %					
	SiO_2	Al_2O_3	CaO	MgO	Fe_2O_3	FeO
MAT3	43.1	27.8	17.3	3.8	5.1	4.6+
M3	46.4	30.0	18.6	0.0	-	5.0
M3/10	49.8	23.0	17.2	0.0	-	10.0
M3/15	53.2	16.0	15.8	0.0	-	15.0
M3/20	56.6	9.0	14.4	0.0	-	20.0

*Crystallisation of anorthite

+Equivalent FeO

TABLE 5.13

Composition of Residual Liquid Phase for Glass D1* (Normalised Composition)

	Composition Wt %								
	SiO_2	Al_2O_3	CaO	MgO	Na_2O	K_2O	TiO_2	Fe_2O_3	FeO
D1	54.6	26.5	1.5	1.6	1.2	4.2	1.1	9.3	8.4+
DA	60.0	29.1	1.7	0.0	0.0	0.0	0.0	-	9.2
DA/10	62.8	25.3	1.9	0.0	0.0	0.0	0.0		10.0
DA/15	80.5	1.7	2.8	0.0	0.0	0.0	0.0	-	15.0

*Crystallisation of mullite

+Equivalent FeO

Fig.5.26. System $CaO-FeO-Al_2O_3-SiO_2$, 5% FeO plane. Crystallisation of multicomponent glasses.

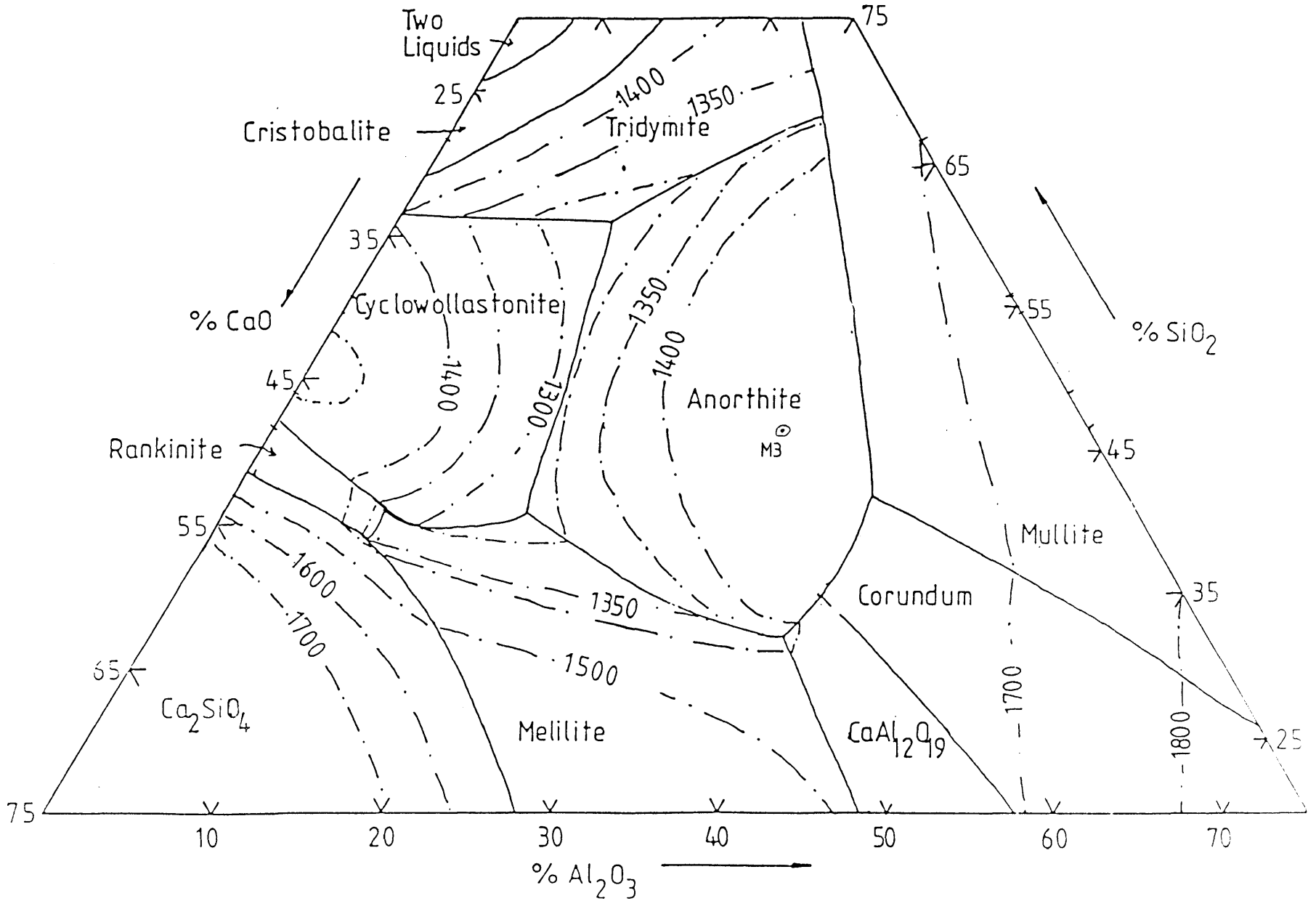


Fig.5.27. System $CaO-FeO-Al_2O_3-SiO_2$, 10% FeO plane. Crystallisation of multicomponent glasses.

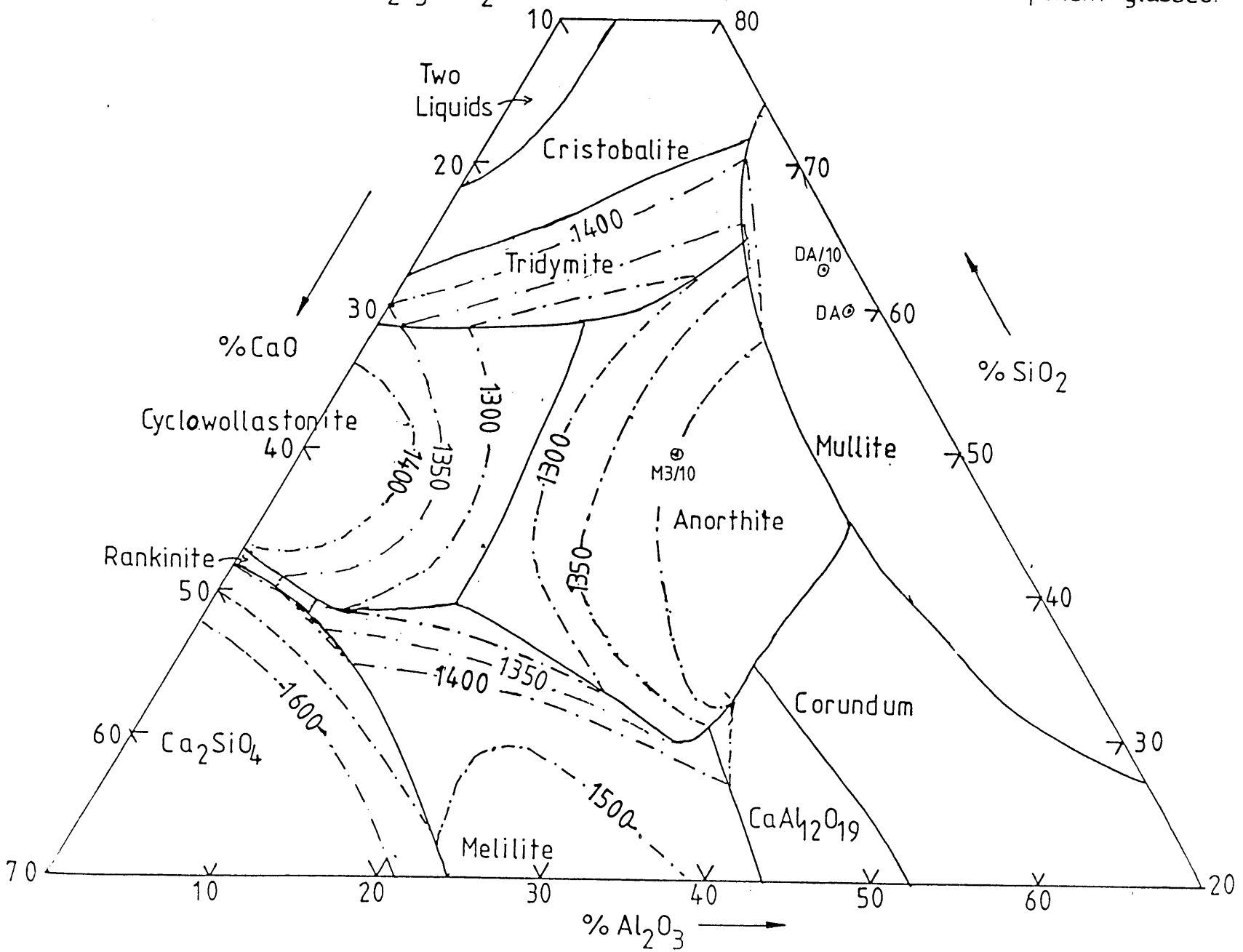


Fig. 5.28. System $CaO-FeO-Al_2O_3-SiO_2$, 15% FeO plane. Crystallisation of multicomponent glasses.

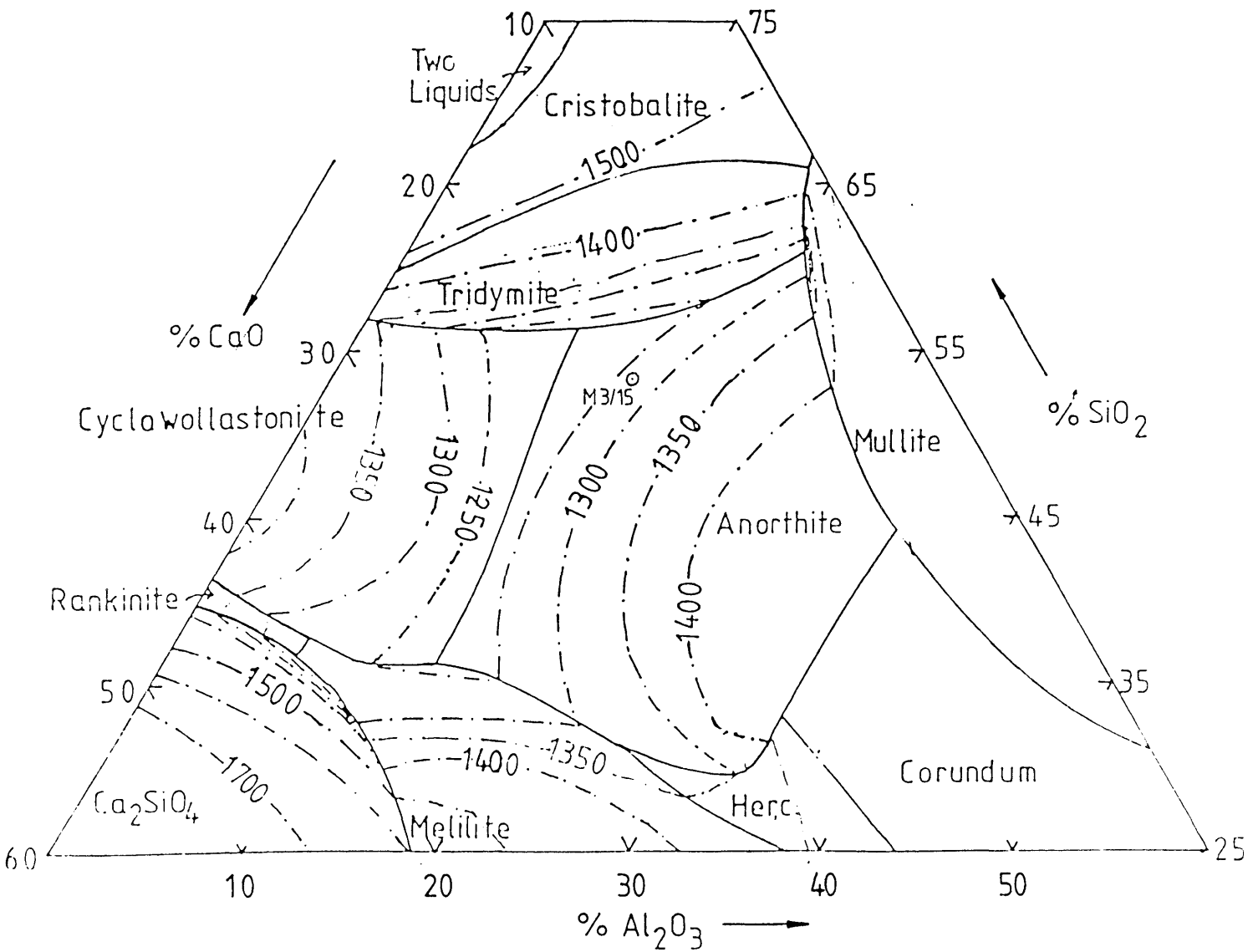
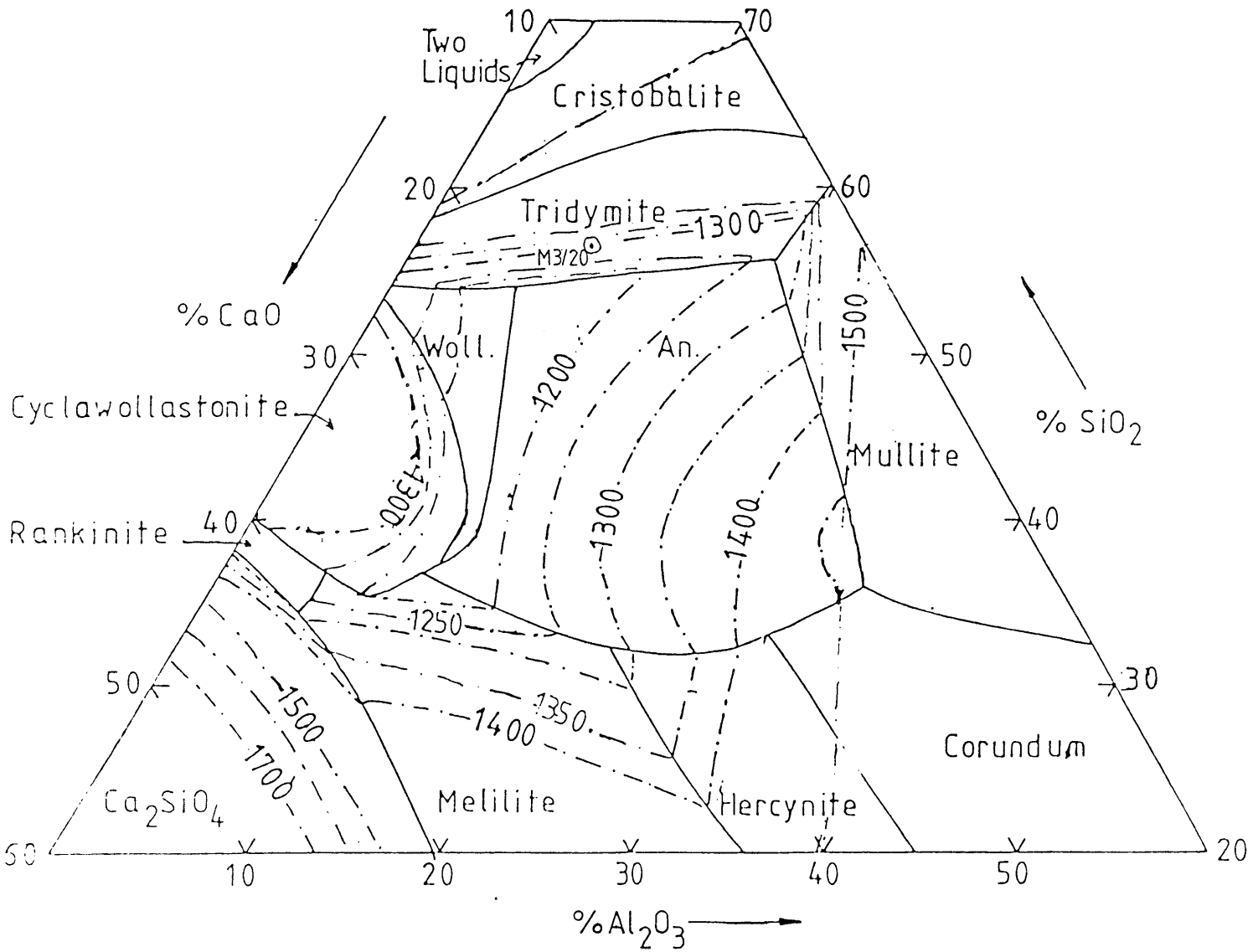


Fig. 5.29. System $CaO-FeO-Al_2O_3-SiO_2$, 20% FeO plane. Crystallisation of multicomponent glasses



5.9 COMPARISON OF COAL-ASH MELT CRYSTALLISATION WITH PREDICTIONS BASED ON THE SYSTEM $CaO-FeO-Al_2O_3-SiO_2$

High temperature phase equilibria data on the system $CaO-FeO-Al_2O_3-SiO_2$, together with the observations on crystallisation of glasses, made as part of this study, have been shown to account for the crystallisation behaviour of glasses with compositions based on a known lignitic-type ash and a bituminous-type ash (glasses Mat 5 and D1). To be able to relate the crystallisation behaviour of coal ashes to the formation and growth of boiler deposits, the crystallisation behaviour observed in various ash melts have been collected and compared with that predicted from the quaternary system. There have unfortunately been relatively few detailed mineralogical studies of bituminous-type deposits and any correlation obtained may be limited.

The chemical compositions of the bituminous melts, together with the crystalline phases reported, have been listed in Table 5.14. The normalised four component composition (obtained by converting Fe_2O_3 to equivalent FeO) have been plotted on the appropriate plane of the quaternary system (as indicated in the Table). The agreement between the primary crystalline phase observed and that predicted from the phase diagram is quite good, with 8 out of 10 in full agreement. The ashes GM, WA, BB and BU were removed from German wet bottom boilers as molten slag and studied optically by Rost and Ney;[107] the phases reported may not be characteristic of the whole sample.

The true boiler slags, i.e. vitreous deposits formed on the heat absorbing surfaces, IR, HA and KLR show excellent

TABLE 5.14

Crystallisation behaviour of bituminous-type melts and predictions based on the system $CaO-FeO-Al_2O_3-SiO_2$

Melt	Composition wt %									Crystalline Phases Observed	Normalised composition wt %				Primary phase	Fig.	Ref.
	SiO_2	Al_2O_3	Fe_2O_3	FeO^+	CaO	MgO	Na_2O	K_2O	TiO_2		SiO_2	Al_2O_3	CaO	FeO			
IRONBRIDGE IR	41.1	22.1	28.0	25.2	4.5	1.5	0.4	1.4	0.9	Ironspinel Anorthite Mullite	44.3	23.8	4.8	27.1	Anorthite	5.32	46
HANAASARI HA	47.2	20.1	10.2	9.2	7.0	3.9	0.8	2.4	1.0	Anorthite Ironspinel	56.5	24.1	8.4	11.0	Anorthite	5.30	46
PRATT PR	49.0	30.4	8.3	7.5	3.0	2.4	0.4	2.5	1.6	Mullite	54.5	33.8	3.3	8.4	Mullite	5.30	85
PITTSBURGH PI	52.8	25.9	12.4	11.2	2.4	0.5	1.9	1.9	1.2	Mullite	57.2	28.1	2.6	12.1	Mullite	5.30	85
SOMERSET SO	62.5	25.9	4.4	4.0	1.4	0.9	1.8	2.2	0.7	Mullite	66.6	27.6	1.5	4.3	Mullite	5.29a	85
KLR	52.9	31.9	9.1	8.2	2.0	1.0	2.4	2.3	n.d	Mullite	55.7	33.6	2.1	8.6	Mullite	5.30	110
GM	45.1	34.6	11.4	10.3	4.8	0.6	n.d	n.d	0.9	Mullite	47.5	36.5	5.1	10.9	Mullite	5.30	107
BB	35.8	30.5	21.0	18.9	10.6	1.2	n.d	n.d	0.6	Hercynite	37.4	31.8	11.1	19.7	Anorthite	5.31a	107
WA	41.6	15.8	28.0	25.2	10.3	1.8	n.d	n.d	0.4	Anorthite Ironwollastonite Ironspinel	44.8	17.0	11.1	27.1	Anorthite	5.32	107
BU	44.0	26.5	15.9	14.3	9.4	1.9	n.d	n.d	0.7	Anorthite Ironwollastonite	46.7	28.1	10.0	15.2	Anorthite	5.31	107

$^+$Equivalent FeO

n.d = not determined.

agreement with the quaternary system. Samples IR and HA have been studied by Livingston et al.[46] and were obtained from boilers at Ironbridge (UK) and Hanaasari (Finland) respectively. Though the authors examined many samples from different regions of the boiler, only a characteristic example has been chosen for correlation. The major phase observed for sample IR was an iron spinel with minor amounts of anorthite and to an even lesser extent mullite. The quaternary system would predict anorthite as the primary crystalline phase but with the high iron oxide content (28.0% Fe_2O_3) and the observed effect of similar iron oxide contents on the crystallisation of spinel from some iron glasses (see p.231) the behaviour would be expected. The composition of the residual liquid phase (IR/30, Table 5.15) still lies in the anorthite field of the 30% plane (Fig.5.33) but is near the mullite boundary and slight heterogeneity of the slag may lead to the crystallisation of mullite. The primary phase for the deposit HA was predicted to be anorthite, which was observed to be the major crystalline phase of the deposit, with minor amounts of iron spinel. The composition of the residual liquid phase on the 15% FeO plane has been calculated (HA/15, Table 5.15) and lies in the primary field of tridymite (Fig.5.31). The crystallisation behaviour is analogous to that observed for the glass F10 (p.**230**) which has a similar crystallisation path to composition HA.

The deposit KLR was studied by Kiss et al.[110] and was obtained from the CEGB Aberthaw (UK) boiler. Mullite was determined to be the major crystalline phase with minor amounts of iron spinel reported. The quaternary system would predict the primary phase observed. The composition of the residual liquid phase on the 10% plane has been plotted (composition KLR/10,

Table 5.15) and also lies in the mullite field. With crystallisation of mullite the residual liquid phase would become enriched in silica and to a lesser extent iron oxide, and the crystallisation of iron spinel would initially be unexpected. The presence of ferric oxide and the minor components may reduce the solubility of iron oxide and alumina in the liquid phase.

The ashes PR, PI and SO were studied under laboratory conditions by Huggins et al.[85] and were derived from American Eastern-type coals (Pratt, Pittsburgh and Somerset respectively). The investigators heated up cylinders of laboratory prepared ash (roasted at 750 °C) both in air and in a mildly reducing atmosphere and determined that only mullite was present in an iron rich liquid phase in all the samples treated above 1200 °C. The primary crystalline phase of mullite would be predicted from the normalised compositions of the ashes.

Of the slags studied by Rost and Ney,[107] only the samples which correspond to the predictions of the quaternary system will be discussed. Mullite only was observed in the sample GM which corresponds with that predicted from the composition. The phases anorthite, iron wollastonite were observed in the slag WA. The quaternary composition lies in the anorthite field on the 25% FeO plane. The composition of the residual liquid phase on the 30% FeO plane (WA/30, Table 5.15) also lies in the anorthite field. The crystallisation path indicates an iron-rich residual liquid phase and iron spinel would be expected to crystallise. The presence of iron wollastonite may be due to heterogeneity of the slag.

TABLE 5.15

Composition of Residual Liquid Phase of Bituminous Ash Melts

Melt	Normalised Composition Wt %				Primary Field
	SiO_2	Al_2O_3	CaO	FeO	
IR	44.3	23.8	4.8	27.1	Anorthite
IR/30	44.4	22.4	3.2	30.0	Anorthite
HA	56.5	24.1	8.4	11.0	Anorthite
HA/15	61.4	19.4	4.2	15.0	Tridymite
PR	54.5	33.8	3.3	8.4	Mullite
PR/10	59.5	26.5	4.0	10.0	Mullite
PI	57.2	28.1	2.6	12.1	Mullite
PI/15	64.3	17.5	3.2	15.0	Tridymite
SO	66.6	27.6	1.5	4.3	Mullite
SO/5	72.9	20.3	1.7	5.0	Mullite
KLR	55.7	33.6	2.1	8.6	Mullite
KLR/10	60.2	27.3	2.5	10.0	Mullite
GM	47.5	36.5	5.1	10.9	Mullite
GM/15	54.9	23.1	7.0	15.0	Anorthite
WA	44.8	17.0	11.1	27.1	Anorthite
WA/30	45.0	14.8	10.2	30.0	Anorthite
BU	46.7	28.1	10.0	15.2	Anorthite
BU/20	47.9	25.3	6.8	20.0	Anorthite
BU/25	49.0	22.4	3.6	25.0	Anorthite
BU/30	50.4	19.4	0.2	30.0	Mullite

Fig. 5.29a. System $CaO-FeO-Al_2O_3-SiO_2$, 5% FeO plane. Crystallisation of bituminous ash melts.

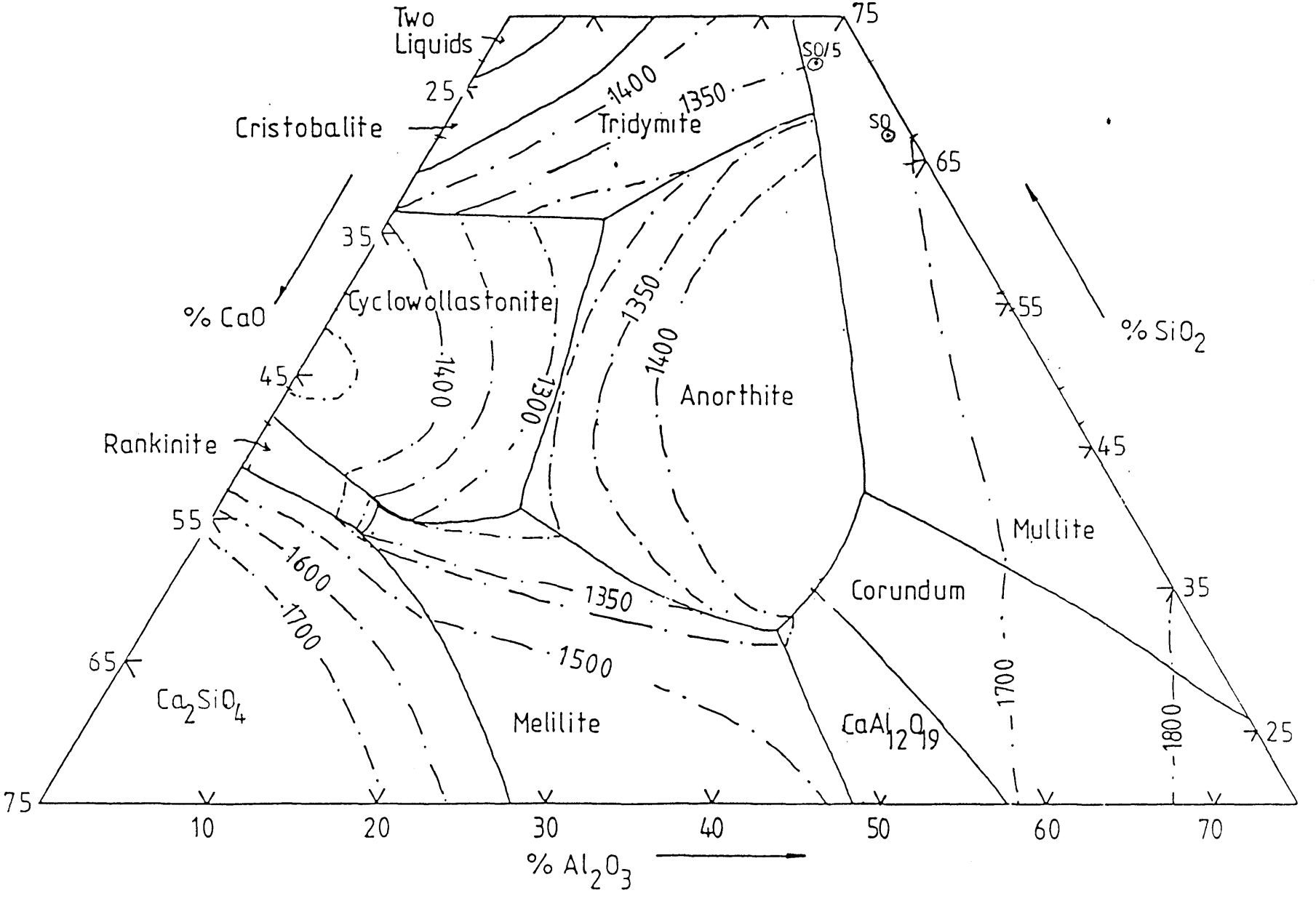


Fig.5.30. System $CaO-FeO-Al_2O_3-SiO_2$, 10% FeO plane. Crystallisation of bituminous ash melts.

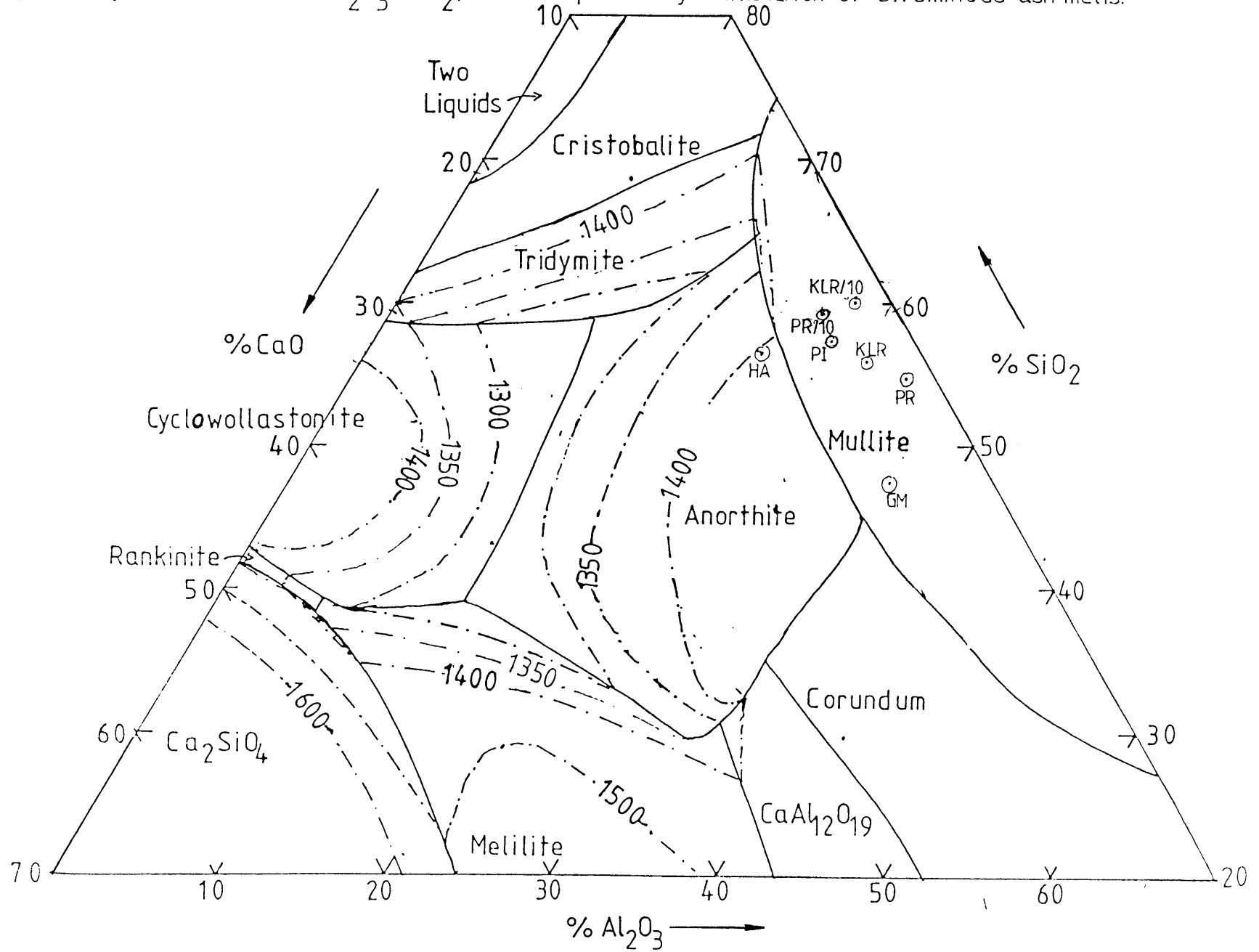


Fig.5.31. System $CaO-FeO-Al_2O_3-SiO_2$,15% FeO plane. Crystallisation of bituminous ash melts.

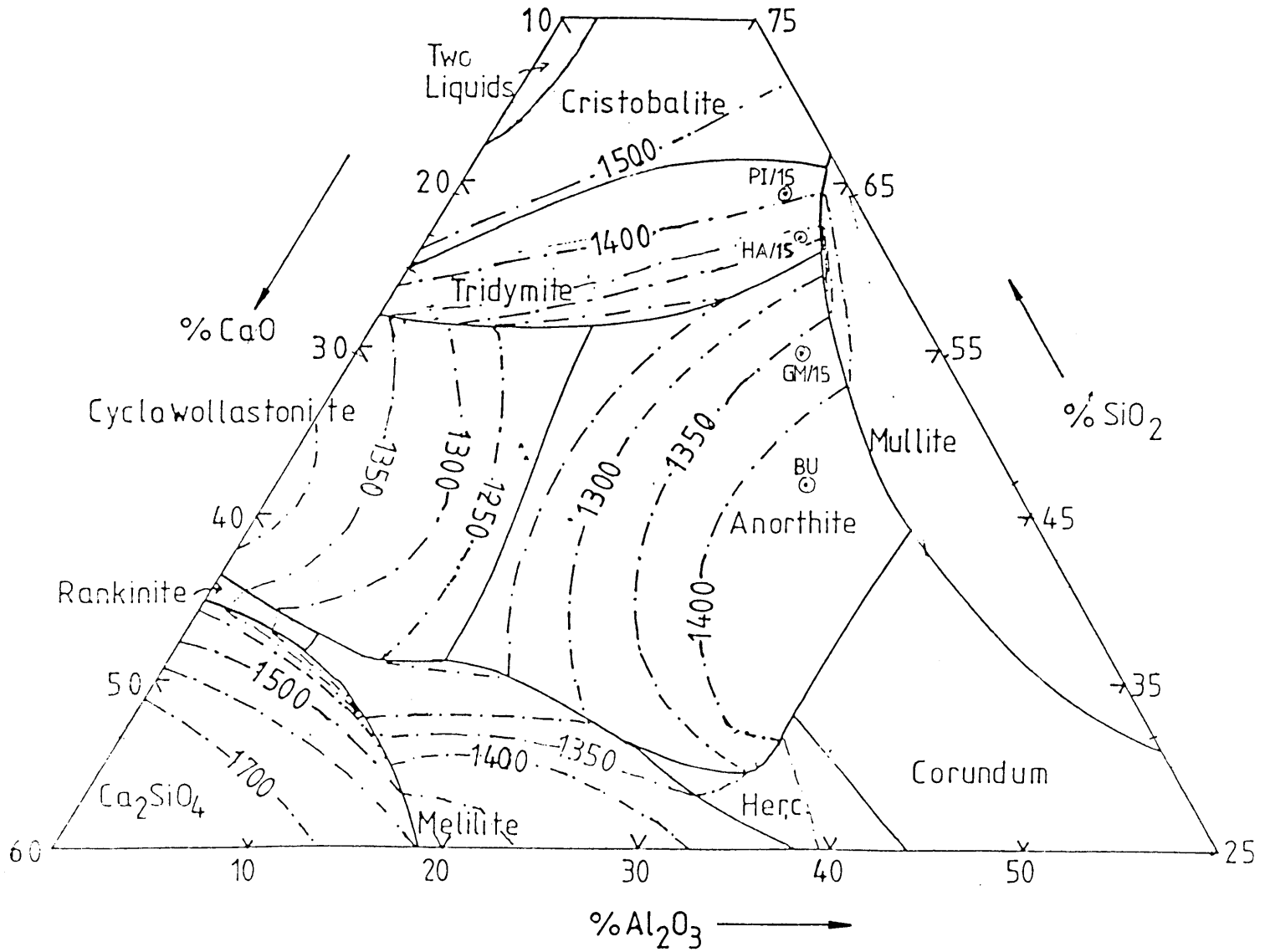


Fig.5.31a. System $CaO-FeO-Al_2O_3-SiO_2$, 20% FeO plane. Crystallisation of bituminous ash melts.

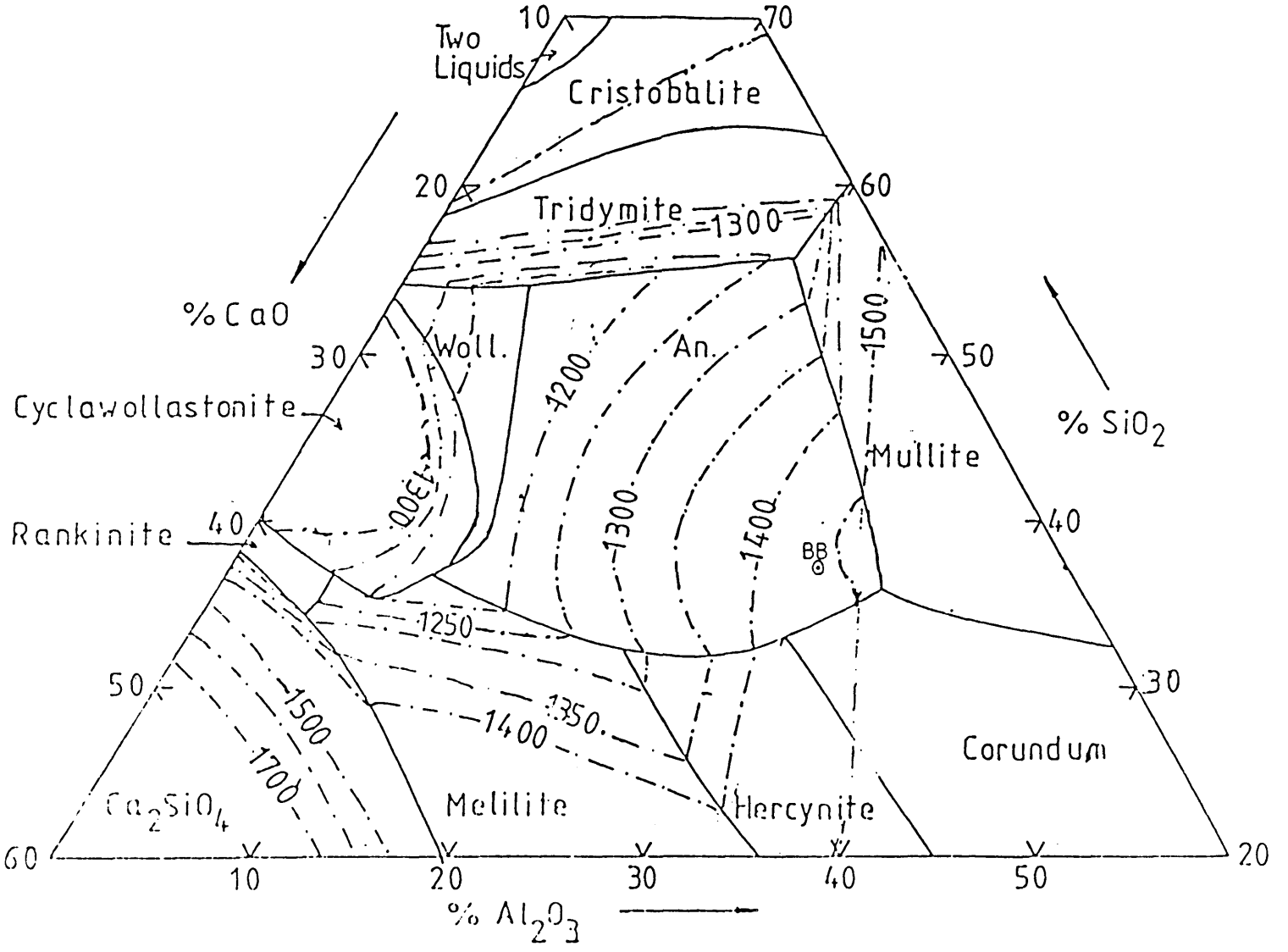


Fig.5.32. System $CaO-FeO-Al_2O_3-SiO_2$, 25% FeO plane. Crystallisation of bituminous ash melts.

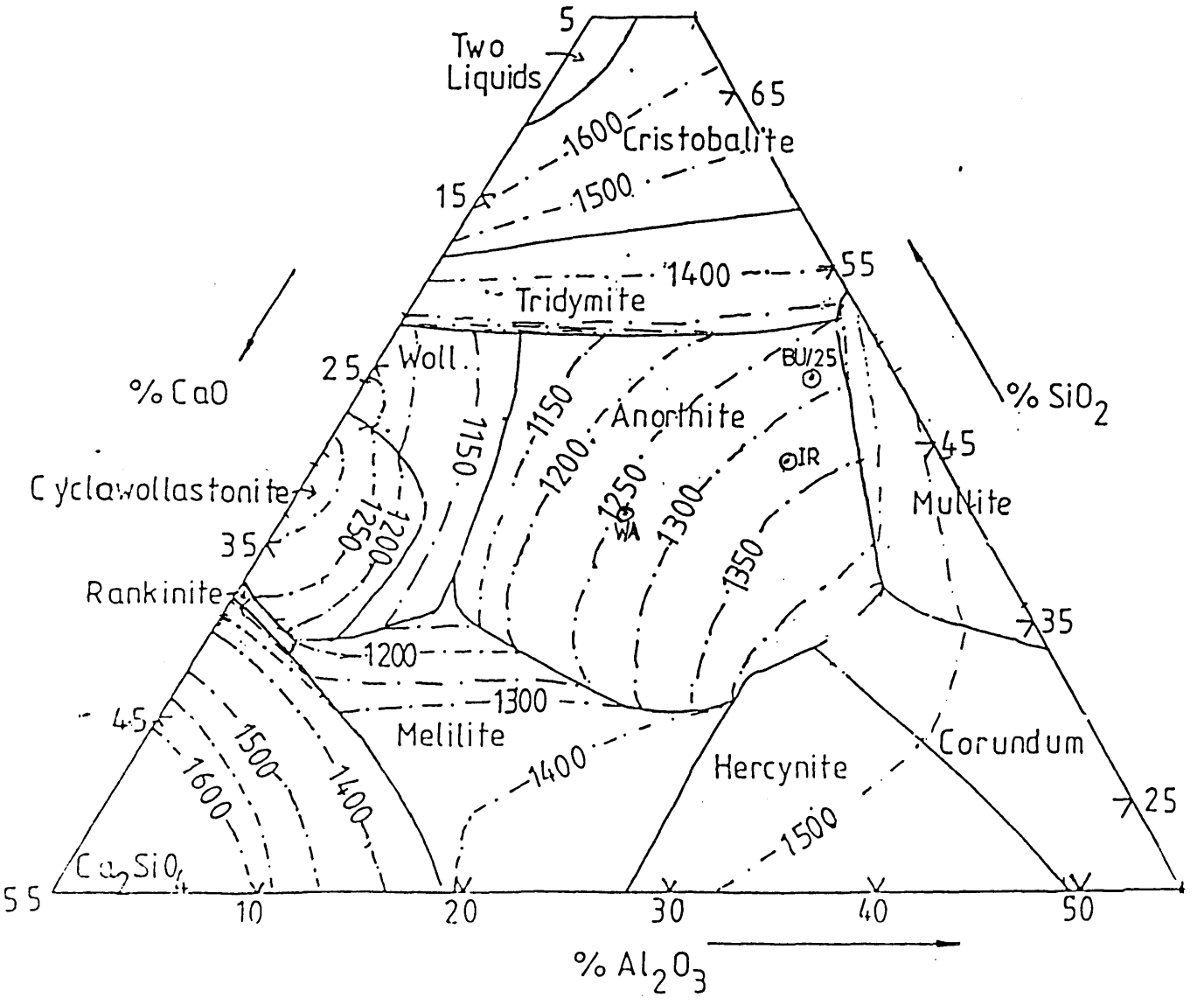
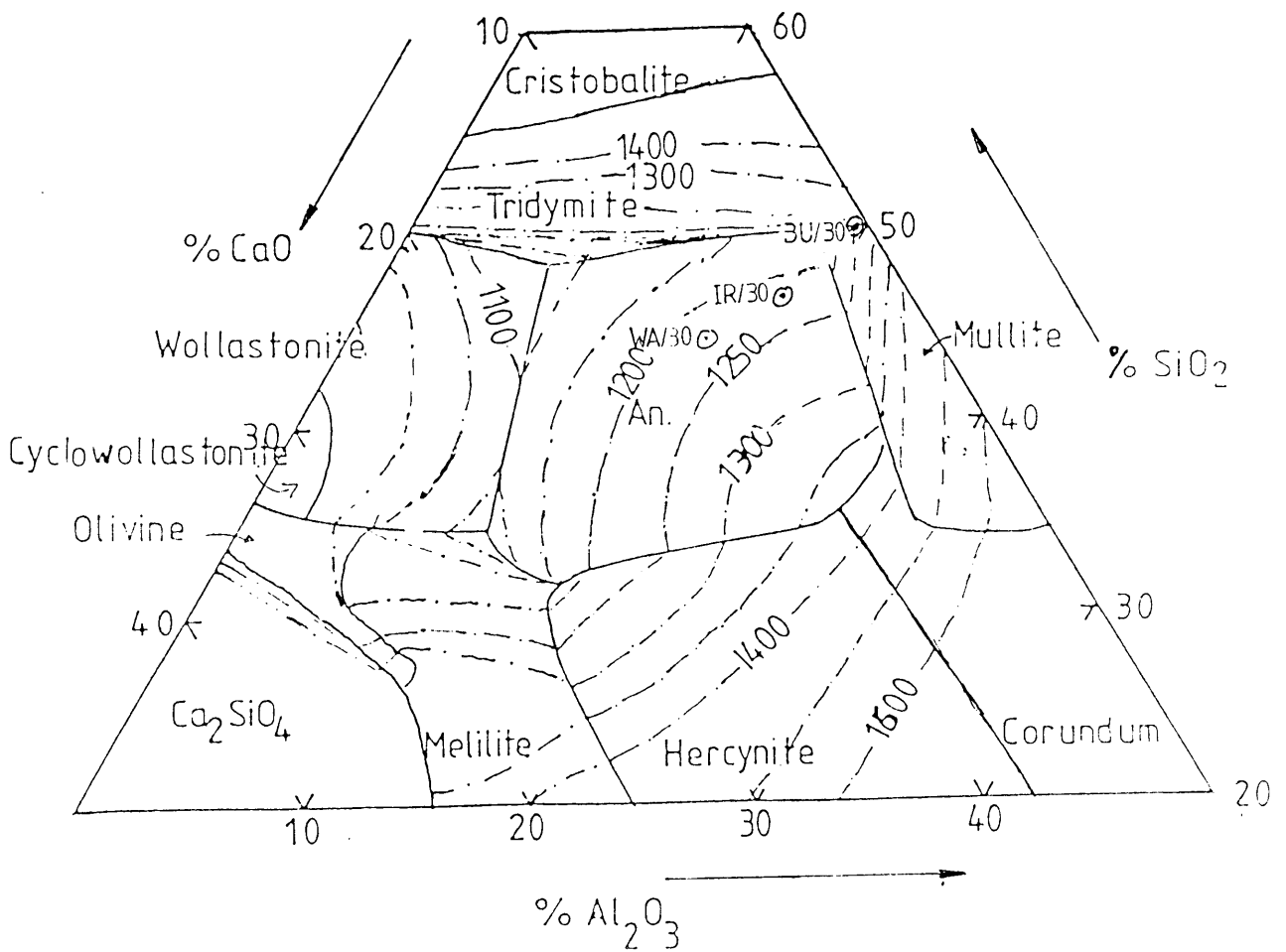


Fig.5.33. System $CaO-FeO-Al_2O_3-SiO_2$, 30% FeO plane. Crystallisation of bituminous ash melts.



The crystalline phases observed for slag BU were anorthite and iron wollastonite. The quaternary phase diagram predicts correctly the major phase for the composition (anorthite) but the crystallisation path (indicated by points BU/20, BU/25 and BU/30, Table 5.15) indicates an increasingly silica and iron rich residual liquid phase. The presence of iron wollastonite is presumably due to heterogeneity of the glass.

Thus, though there are relatively few studies with which to make a comparison, the quaternary system, CaO-FeO-Al_2O_3-SiO_2, together with observations made in this study, can be used to predict adequately the crystallisation of complex bituminous-type ash melts. The correlation of the crystallisation of the mullite component glasses based on the composition of the lignitic-type ash KA (Mat 3, Mat 4 and Mat 5) with the quaternary system CaO-FeO-Al_2O_3-SiO_2 (see Section 5.8) indicates that the system may be of more relevance to lignitic-type ashes than the system CaO-MgO-Al_2O_3-SiO_2.

The crystalline phases present in the various lignitic-type melts discussed previously and the chemical composition are listed in Table 5.16. The normalised CaO-FeO-Al_2O_3-SiO_2 composition and the primary phase for the sample is also listed in the Table. As the iron oxide contents of the samples were not the same as the planes of the system the compositions were plotted using the silica and alumina contents on the appropriate FeO plane and the primary phase determined. The results of the study of ash KC has also been included in the Table. Of the six samples only one (SR) does not compare well with the predictions from the phase diagram. The sample (along with TH) was studied by Rost and Ney[107] and, as mentioned previously, the observations reported

TABLE 5.16

Crystallisation behaviour of lignitic ash melts and predictions based on the system CaO-FeO-Al_2O_3-SiO_2

	Composition wt %										Normalised composition wt %					
Melt	SiO_2	Al_2O_3	Fe_2O_3	FeO	CaO	MgO	Na_2O	K_2O	TiO_2	Crystalline Phases Observed	SiO_2	Al_2O_3	FeO	CaO	Primary phase	Ref.
KC	51.2	29.0	4.8	4.3	9.5	2.6	0.6	1.0	1.3	Anorthite	54.5	30.8	4.6	10.1	Anorthite	
HG1	46.7	25.9	6.4	5.8	13.8	3.1	0.8	0.4	1.5	Anorthite Magnetite $CaSO_4$(tr.)	50.6	28.1	6.3	15.0	Anorthite	42
HG2	47.7	30.1	5.2	4.7	10.6	2.5	0.5	0.6	1.8	Anorthite Cordierite Cristobalite	51.2	32.3	5.1	11.4	Anorthite	43
PA	51.6	23.7	4.9	4.4	13.1	1.7	0.3	0.3	2.2	Anorthite	55.6	25.5	4.8	14.1	Anorthite	
SR	41.8	13.0	11.5	10.4	20.1	5.2	n.d	n.d	0.5	Melilite	49.0	15.2	12.2	23.6	Anorthite	107
TH	28.5	11.5	16.4	14.8	34.8	1.9	n.d	n.d	0.2	Hercynite Anorthite Melilite	31.8	12.8	16.5	38.9	Melilite	107

n.d = not determined.

may not be fully characteristic. The composition of the residual liquid phase for all the samples (except SR) on the plane or planes above the FeO content of the composition have been listed in Table 5.17 and plotted on the corresponding plane (Figs 5.34 - 5.37).

The composition of KC lies in the anorthite primary field near the mullite boundary. The crystallisation path indicated by composition KC/5 is towards the mullite boundary and the silica apex, i.e. a viscous, stable glass-forming region. Only anorthite was observed in the series of crystallisation experiments which corresponds to the crystallisation path determined. It should be mentioned that both the $CaO-Al_2O_3-SiO_2$ and $CaO-MgO-Al_2O_3-SiO_2$ predicted mullite as the primary crystalline phase. This indicates that system $CaO-FeO-Al_2O_3-SiO_2$ is of greater relevance to the crystallisation of lignitic-type ash melts.

Sample HG1 lies in the primary field of anorthite and the composition on the 10% plane (point HG1/10) also lies in the anorthite field. The crystallisation path is towards the tridymite field, as confirmed by composition HG1/15 and indicates an increasingly silica-rich residual liquid phase. The presence of magnetite (5.2%) reported by Hanusch and Grimshaw[42] may be due to the saturation of iron oxide (present as Fe_2O_3 and FeO) as observed for the glass Mat 3 or from slight heterogeneity of the deposit.

For the deposit HG2 the primary crystalline phase predicted was anorthite, as observed by Hanusch and Grimshaw[43]. The crystallisation path is towards the mullite boundary (see point HG2/10). The crystallisation of cordierite and cristobalite

TABLE 5.17

Composition of Residual Liquid Phase of Lignitic Ash Melts

Melt	Composition Wt %				Primary Field
KC	54.5	30.8	10.1	4.6	Anorthite
KC/5	55.5	30.2	9.2	5.0	Anorthite
HG1	50.6	28.1	15.0	6.3	Anorthite
HG1/10	55.1	22.8	12.1	10.0	Anorthite
HG1/15	61.2	15.7	8.1	15.0	Tridymite
HG2	51.2	32.3	11.4	5.1	Anorthite
HG2/10	59.0	27.9	3.1	10.0	Mullite
PA	55.6	25.5	14.1	4.8	Anorthite
PA/5	56.1	25.0	13.9	5.0	Anorthite
PA/10	69.2	13.1	7.7	10.0	Tridymite
TH	31.8	12.8	38.9	16.5	Melilite
TH/20	34.0	7.6	38.4	20.0	Melilite

Fig.5.34. System $CaO-FeO-Al_2O_3-SiO_2$, 5%FeO plane. Crystallisation of lignitic ash melts.

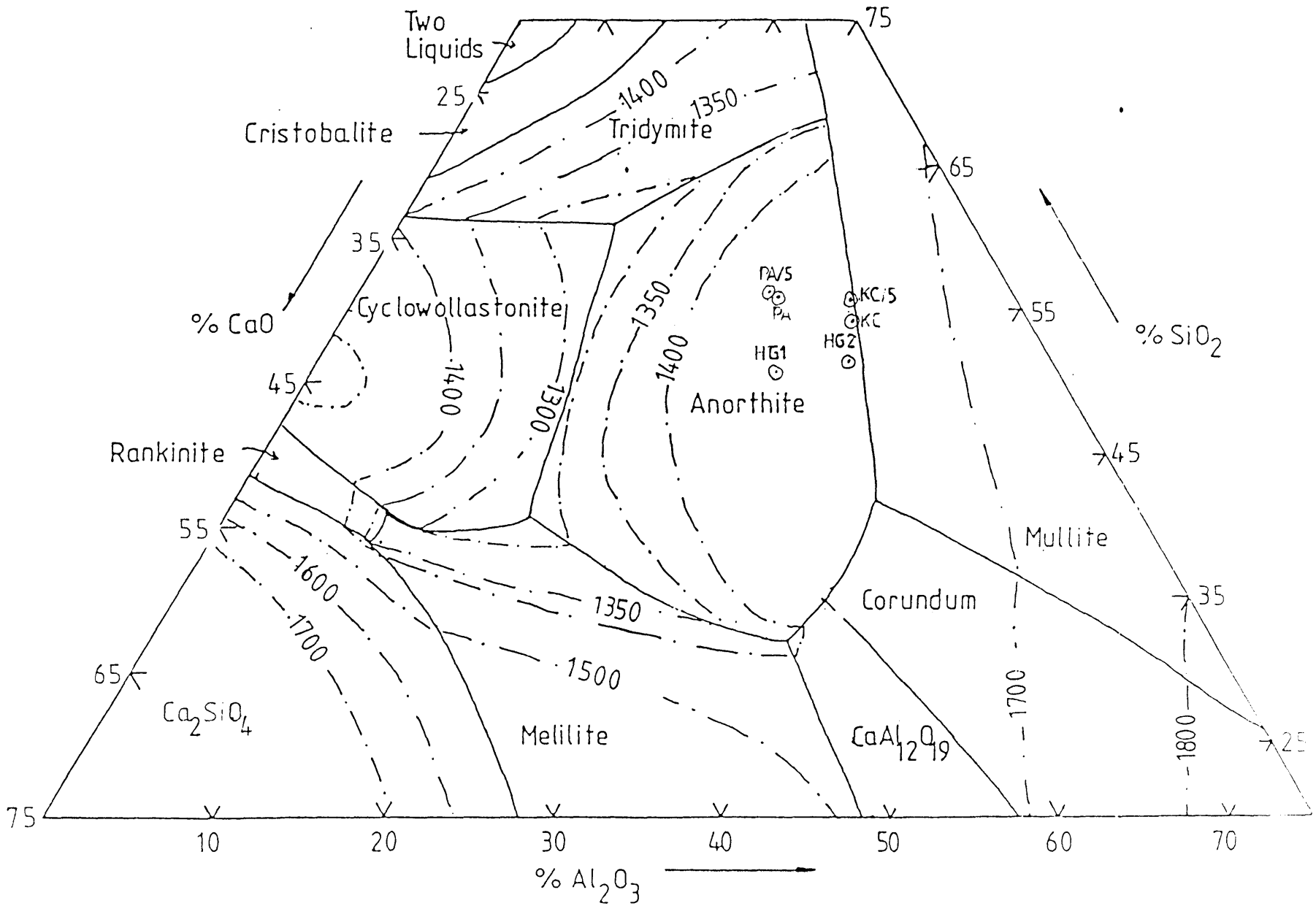


Fig.5.35. System $CaO-FeO-Al_2O_3-SiO_2$, 10% FeO plane. Crystallisation of lignitic ash melts.

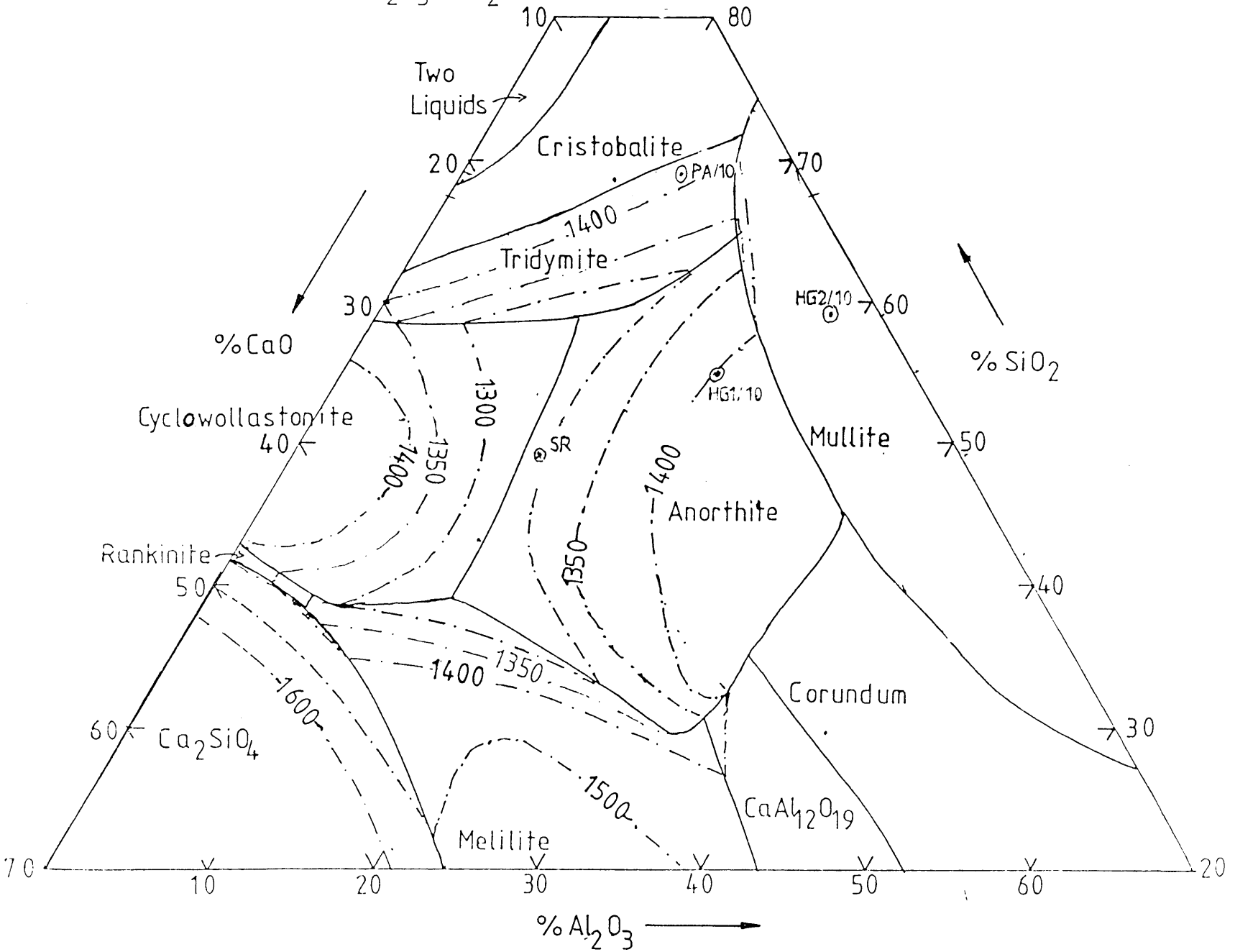


Fig. 5.36. System $CaO-FeO-Al_2O_3-SiO_2$, 15% FeO plane. Crystallisation of lignitic ash melts.

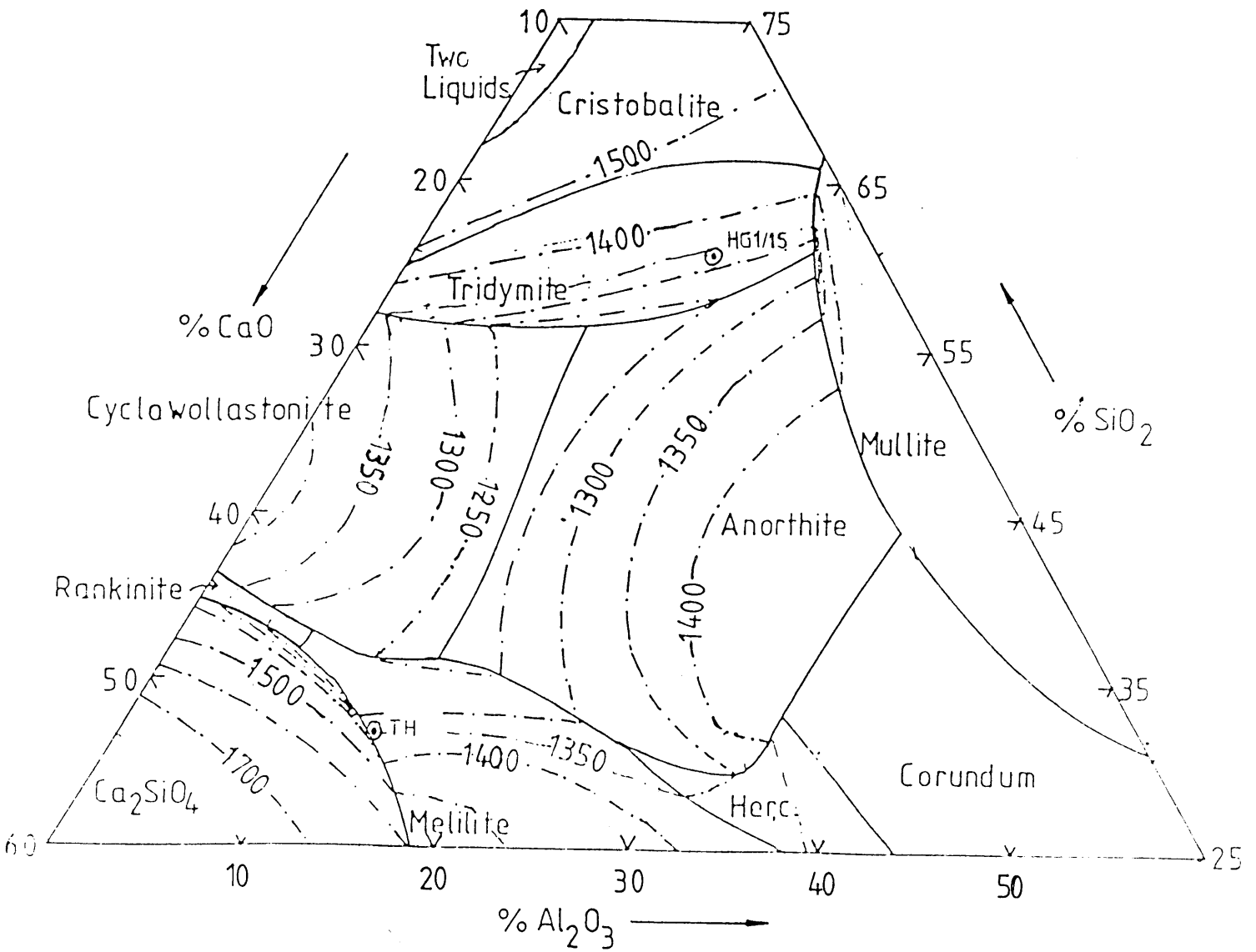
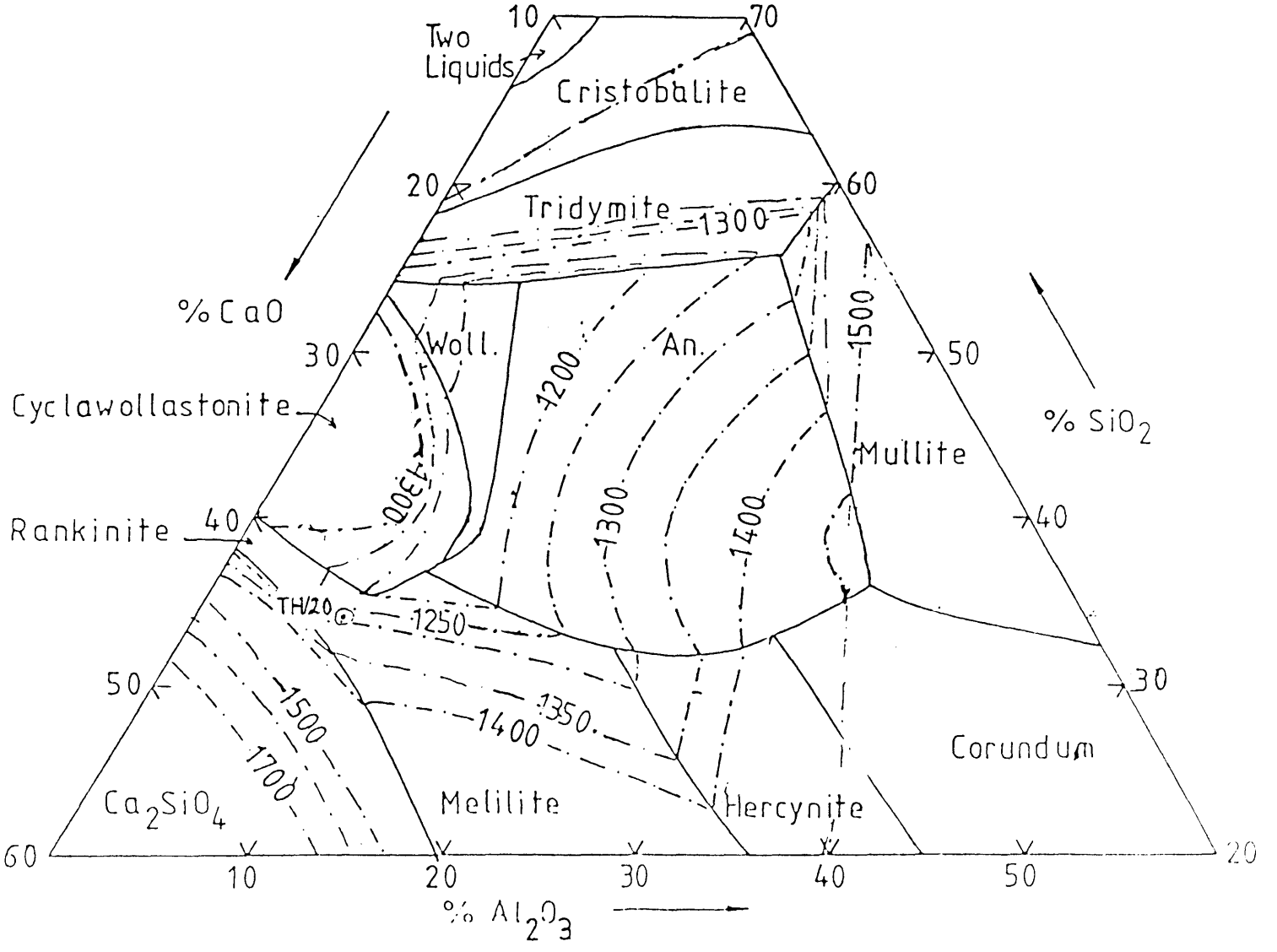


Fig.5.37. System $CaO-FeO-Al_2O_3-SiO_2$, 20% FeO plane. Crystallisation of lignitic ash melts.



reported has been discussed previously in relation to the quaternary system $CaO-MgO-Al_2O_3-SiO_2$.

The only crystalline phase observed in the slag PA was anorthite which would be predicted from the normalised quaternary composition. The crystallisation path was similar to that determined for the melt KC, i.e. towards the primary field of tridymite.

Melilite, anorthite and hercynite were observed in the lignitic-type ash slag TH by Rost and Ney.[107] The phase diagram predicted melilite as the primary phase and though the crystallisation path (crystallisation of gehlenite) indicated by points TH (Fig.5.36) and TH/20 is towards the rankinite primary volume the phase assemblage is similar to that observed for glass F12 (p.231) but without the presence of iron wollastonite.

Thus the quaternary system $CaO-FeO-Al_2O_3-SiO_2$ can be used, with qualifications observed in this study to predict the crystallisation of both lignitic- and bituminous-type ash melts.

5.10 PREDICTION OF SLAGGING PROPENSITY

The important part of this study is to relate the crystallisation behaviour of ashes in a boiler to the mechanism of growth and the development of strength in a boiler deposit. The model of the rate of increase in deposit strength (ds/dt) is based on the mechanism of sintering by viscous flow and is given by:

$$\frac{ds}{dt} = \frac{3k\gamma}{2\eta r} \qquad (k = \text{constant})$$

The surface tension (γ) and the initial radius of the particles (r) are both effectively constant compared with the variability of viscosity (η) and thus the factors which affect the latter will largely determine the value of ds/dt.

The fusion of a lignitic-type coal ash (KD) has been shown to be rapid with all the minerals present in coal, except quartz and in some circumstances iron minerals, fusing within 15 s at 1450 °C in air. Assuming that the ash is completely fused within the burner zone of a boiler to form a homogeneous melt, phase equilibria should be able to predict the crystallisation path of the melt and in consequence the composition of the residual liquid phase. The crystal growth rates of the primary phase for two glasses of compositions based on lignitic-type ashes (glasses Mat 8 and Mat 9) have been observed to be very rapid. The studies of the mineralogy of boiler deposits have clearly indicated that the crystallisation was from melts and that the system CaO-FeO-Al_2O_3-SiO_2 can describe the behaviour.

Thus it should be possible to predict the slagging propensity of a coal ash from a study of the quaternary system. To substantiate this theory the known deposit formation behaviour of coal ashes must be correlated with the predicted behaviour from the normalised composition.

The major factor which determines the rate of increase in strength of a boiler deposit at a given temperature is the degree of fluidity of the melt (inverse viscosity). This factor will depend on the composition and temperature of the liquid phase, and as has already been shown the quaternary system can describe the change in composition with crystallisation. The viscosity of ash

melts and the effects of crystallisation on the viscosity are discussed in detail in Appendix C. Generally if the residual liquid phase becomes enriched in silica the viscosity will increase and hence ds/dt will decrease, and if the residual liquid phase becomes enriched in modifying components (e.g. CaO and FeO) the viscosity will decrease with an increase in the value of ds/dt. These factors will be used in the following analysis of slagging behaviour.

Table 5.18 is a collection of the available data on the known slagging behaviour of coal ashes, in some cases only an example of the coal ashes reported in the reference is included. The chemical composition (excluding the oxides of sulphur and phosphorus), type of ash, flow temperature, FT (determined in a mildly reducing atmosphere), slagging behaviour and the normalised four component composition ($CaO-FeO-Al_2O_3-SiO_2$) are included in the Table. The normalised composition has been plotted on the appropriate plane of the quaternary system (Figs 5.38 - 5.43). The liquidus temperature (in some cases the lack of data necessitated only an approximate value to be assigned) and the primary crystalline phase were determined and included in Table 5.18. The ashes A to L are reported not to form slagging deposits when the coal is fired in a boiler whereas ashes M to W are known to cause slagging problems.

Analysis of Table 5.18 shows that all the ashes, both lignitic-type and bituminous-type, which do not form slagging deposits have relatively low FeO contents (13.7% or less) and low alkali oxide contents when compared to the slagging ashes. All the ashes A to M lie in the mullite primary field, with high liquidus temperatures with the exception of ashes G, J and K which

TABLE 5.18

Slagging behaviour of various ashes and predicted crystallisation behaviour.

Source	Type	Composition wt.% SiO_2	Al_2O_3	Fe_2O_3	FeO*	CaO	MgO	Na_2O	K_2O	TiO_2	F.T.+ /°C	Slagging	Normalised comp. wt.% SiO_2	Al_2O_3	CaO	FeO	Liq. Temp. /°C	Primary phase
A CLIFFSIDE[44]US	Bit.	55.0	26.5	10.4	9.4	1.2	1.4	0.5	3.6	1.3	1470	No	59.7	28.8	1.3	10.2	>1400	Mullite
B MORGANTOWN[44]US	Bit.	51.0	27.3	14.1	12.7	1.6	1.1	0.3	2.7	1.4	1450	No	55.1	29.5	1.7	13.7	>1400	Mullite
C MONTOUR[44]US	Bit.	54.3	27.8	8.0	7.2	4.1	1.1	0.3	2.7	1.4	1460	No	58.1	29.8	4.4	7.7	>1400	Mullite
D FRICKLEY[1]UK	Bit.	42.3	26.0	8.9	8.0	4.9	n.d	0.6	1.3	n.d	n.d	No	52.1	32.0	6.0	9.9	1500	Mullite
E MARKHAM-STAVELEY[1] UK	Bit.	50.3	26.9	11.5	10.4	1.6	n.d	0.9	2.2	n.d	n.d	No	56.4	30.2	1.8	11.6	>1400	Mullite
F KIRKBY[1] UK	Bit.	53.7	29.2	8.3	7.5	1.1	1.5	1.0	2.7	0.9	n.d	No	58.7	31.9	1.2	8.2	>1400	Mullite
G ONAKAWANA[45]CAN	Lig.	48.9	14.4	7.1	6.4	14.0	3.8	1.0	0.8	1.0	1150	No	58.5	17.2	16.7	7.6	1320	Anorthite
H CASTLE PEAK[5]UK	Lig.	59.6	21.3	2.5	2.3	4.7	1.1	0.2	0.7	1.3	>1500	No	67.8	24.2	5.4	2.6	>1400	Mullite
I EV3[5]	Lig.	41.4	31.0	4.3	3.9	10.4	1.8	0.6	0.6	1.6	1500	No	47.7	35.8	12.0	4.5	>1400	Mullite
J FINSVAERKET[5]	Lig.	41.4	28.9	6.6	5.9	10.0	2.3	0.5	0.6	1.3	1430	No	48.0	33.5	11.6	6.9	>1400	Anorthite
K MATLA S.A[5]	Lig.	36.9	26.8	5.4	4.9	17.6	3.4	0.8	0.6	1.6	n.d	No	42.8	31.1	20.4	5.7	>1400	Anorthite
L LIDDEL AUS[111]	Lig.	50.1	28.4	5.2	4.7	7.1	1.1	0.7	0.9	0.3	n.d	No	55.5	31.5	7.8	5.2	>1400	Mullite
M LABADIE1[44]US	Bit.	53.5	19.7	17.0	15.3	4.7	1.1	0.5	2.4	1.0	1260	Yes	57.6	21.2	5.1	19.2	1420	Mullite
N LABADIE4[44]US	Bit.	51.8	19.2	19.8	17.8	6.3	1.0	0.5	2.6	1.0	1240	Yes	55.7	20.7	4.4	19.2	1300	Mullite
O MILLCREEK[44]US	Bit.	45.5	18.5	24.5	22.1	6.3	1.0	0.4	2.6	0.9	1200	Yes	49.3	20.0	6.8	23.9	1260	Anorthite
P SILVERDALE[1]UK	Bit.	40.1	27.9	23.0	20.7	0.9	n.d	0.2	0.4	n.d	n.d	Yes	44.8	31.1	1.0	23.1	1500	Mullite
Q HANAASARI[46]POL	Bit.	47.2	20.1	10.2	9.2	7.0	3.9	0.8	2.4	1.0	1310	Yes	56.5	24.1	8.4	11.0	1410	Anorthite
R PLEM BUGGENUM[5] -	Bit.	48.1	21.8	15.1	13.6	5.2	1.5	0.5	2.7	0.9	1320	Yes	54.2	24.6	5.9	15.3	1390	Mullite
S IRON BRIDGE[46]UK	Bit.	41.1	22.1	28.0	25.2	4.5	1.5	0.4	1.4	0.9	n.d	Yes	44.2	23.8	4.8	27.1	1330	Anorthite
T BIENFAIT[45]CAN.	Lig.	22.4	18.1	5.7	5.1	22.0	7.1	7.6	0.0	0.6	1215	Yes	33.2	26.8	32.5	7.5	1300	An/Mel
U HAZELWOOD[5]US	Lig.	20.0	15.9	12.2	11.0	17.3	5.4	10.5	0.1	1.0	1300	Yes	31.2	24.8	26.9	17.1	1340	Mel
V LEIGH CREEK[111] AUS	Lig.	47.5	22.1	6.7	6.0	6.0	1.9	5.6	1.1	1.7	n.d	Yes	58.2	27.1	7.3	7.4	>1400	Mullite
W KRIEL[103]S.A	Lig.	51.6	23.7	4.9	4.4	13.1	1.7	0.3	0.3	2.2	1410	Yes	55.6	25.5	14.1	4.8	>1400	Anorthite

n.d = not determined. * equivalent FeO F.T.= Flow temperature (reducing conditions)

lie in the anorthite primary phase. Ash G has a relatively low liquidus temperature (1320 °C) which compares with the flow temperature determined (1150 °C).

Of the eleven slagging ashes only 5 lie in the mullite primary field, with liquidus temperatures relatively lower than non-slagging ashes in the same primary field. Comparison of flow temperature with the liquidus temperature shows quite good correlation, especially for the ashes in the anorthite and melilite primary fields. The bituminous slagging ashes M to W all have high FeO contents (except ash Q) compared with non-slagging ashes, and in addition some lignitic-type ashes have high alkali oxide contents.

With reference to the 10% FeO plane, ash D (non-slagging) and ash V (slagging) both lie in the mullite field and would be expected to have similar liquidus temperatures and thus may have similar crystallisation behaviour. As will be seen, not only is the primary crystalline phase and the liquidus temperature important but the crystallisation path of the ash melt must also be considered in the context of slagging performance.

The composition of the residual liquid phase on the planes above the original normalised composition has been listed in Table 5.19 along with the original four component composition and the primary phase in which the composition lies (determined from Figs 5.38 - 5.43). It can be seen that all the non-slagging ashes except ash K and J have a crystallisation path towards the tridymite boundary. With reference to the model of rate of growth of deposits, the viscosity of the residual liquid phase will increase substantially with crystallisation of the primary phase and thus the value of ds/dt will rapidly decrease. Though the

secondary crystalline phase predicted for ash J would be mullite the residual liquid phase will subsequently become enriched in silica as with the other ashes. The ash K is from the same coal seam as the lignitic-type ashes studied in this work and similar to the slagging ash W. Of all the non-slagging ashes K seems the most likely to form deposits from the viewpoint of crystallisation behaviour. The compositions of the residual liquid phase on planes above the original composition (Table 5.19) indicate that the crystallisation path is towards the FeO apex of the tetrahedron and the anorthite/wollastonite s.s. boundary. The residual liquid phase does not become richer in silica as with all the other non-slagging ashes. The crystallisation path of ash W on the other hand is towards the silica apex which would suggest non-slagging behaviour. The only explanation which can be offered is the difference in design between the two respective boilers; Matla (ash K) and Kriel (ash W). Ash K is known[5] to form fouling deposits which are easily removed by soot blowing (i.e. lightly sintered together) which would be expected from the crystallisation path.

The bituminous slagging ashes M, N, P and R which lie in the mullite primary field all have crystallisation paths towards the tridymite boundary, but have relatively low liquidus temperatures (the actual value will be lower due to the fluxing action of the other components). The slagging behaviour can be directly attributed to the mechanism of rate of increase in deposit strength. If some of the molten ash adheres to tube walls the outer surface may be soft or tacky and may therefore capture subsequent particles. On crystallisation of mullite the residual phase for these compositions will become enriched in iron oxide (FeO and

TABLE 5.19

Composition of Residual Liquid Phase for Melts of Known Slagging Behaviour

	SiO_2	Al_2O_3	CaO	FeO	Primary Field
A	59.7	28.8	1.3	10.2	Mullite
A/15	74.6	8.5	1.9	15.0	
B	55.1	29.5	1.7	13.7	Mullite
B/15	57.7	25.4	1.9	15.0	Mullite
B/20	67.6	9.9	2.5	20.0	Cristobalite
C	58.1	29.8	4.4	7.7	Mullite
C/10	67.1	17.1	5.7	10.0	Tridymite
D	52.1	32.0	6.0	9.9	Mullite
D/15	64.5	11.4	9.1	15.0	Tridymite
E	56.4	30.2	1.8	11.6	Mullite
E/15	64.7	18.0	2.3	15.0	Tridymite
F	58.7	31.9	1.2	8.2	Mullite
F/10	65.5	23.0	1.5	10.0	Mullite
G	58.5	17.2	16.7	7.6	Anorthite
G/10	63.4	10.9	15.7	10.0	Tridymite
H	67.8	24.2	5.4	2.6	Mullite
	(not present on 5% plane)				
I	47.7	35.8	12.0	4.5	Mullite
I/5	49.9	31.8	13.3	5.0	Anorthite
J	48.0	33.5	11.6	6.9	Anorthite
J/10	50.3	31.9	7.8	10.0	Mullite
K	42.8	31.1	20.4	5.7	Anorthite
K/10	42.6	26.7	20.7	10.0	Anorthite
K/15	42.4	21.6	21.0	15.0	Anorthite
K/20	42.4	16.2	21.4	20.0	Anorthite
K/25	42.1	11.0	21.9	25.0	Anorthite
K/30	42.1	5.8	22.1	30.0	Woll.
L	55.5	31.5	7.8	5.2	Mullite
L/10		n.d.			
M	57.6	21.2	5.1	19.1	Mullite
M/20	58.9	18.8	5.3	20.0	Tridymite

... Continued ...

TABLE 5.19 ... Continued ...

	SiO_2	Al_2O_3	CaO	FeO	Primary Field
N	55.7	20.7	4.4	19.2	Mullite
N/20	56.9	18.5	4.6	20.0	Tridymite
O	49.3	20.0	6.8	23.9	Anorthite
O/25	49.6	19.2	6.2	25.0	Anorthite
O/30	50.9	15.7	3.4	30.0	Tridymite
P	44.8	31.1	1.0	23.1	Mullite
P/25	46.2	27.7	1.1	25.0	Mullite
P/30	49.8	18.8	1.4	30.0	Mullite/Tridymite
Q	56.5	24.1	8.4	11.0	Anorthite
Q/15	61.4	19.4	4.2	15.0	Tridymite
R	54.2	24.6	5.9	15.3	Mullite
R/20	62.2	10.1	7.7	20.0	Tridymite
S	44.2	23.8	4.8	27.1	Anorthite
S/30	44.4	22.4	3.2	30.0	Anorthite/Mullite
T	33.2	26.8	32.5	7.5	Melilite/Anorthite
T/10	37.0	23.3	29.7	10.0	Anorthite
U	31.2	24.8	26.9	17.1	Melilite
U/20	32.8	22.6	24.6	20.0	Anorthite
V	58.2	27.1	7.3	7.4	Mullite
V/10	68.8	11.3	9.9	10.0	Tridymite
W	55.6	25.5	14.1	4.8	Anorthite
W/5	56.1	25.0	13.9	5.0	Anorthite
W/10	69.2	13.1	7.7	10.0	Tridymite

Fig.5.38. System $CaO-FeO-Al_2O_3-SiO_2$, 5% FeO plane. Crystallisation of slagging & non-slagging melts.

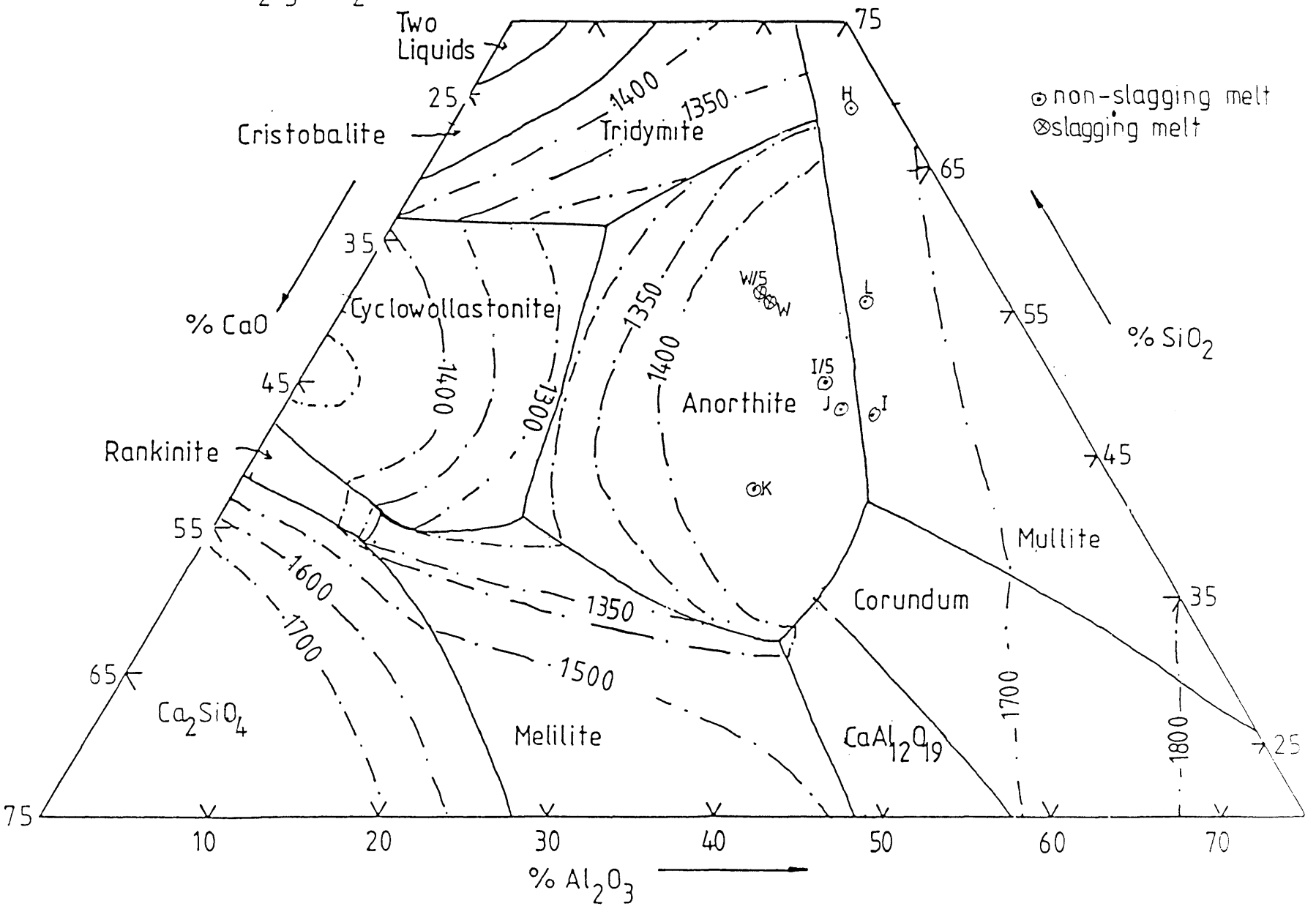


Fig.5.39. System $CaO-FeO-Al_2O_3-SiO_2$, 10% FeO plane. Crystallisation of slagging & non-slagging melts.

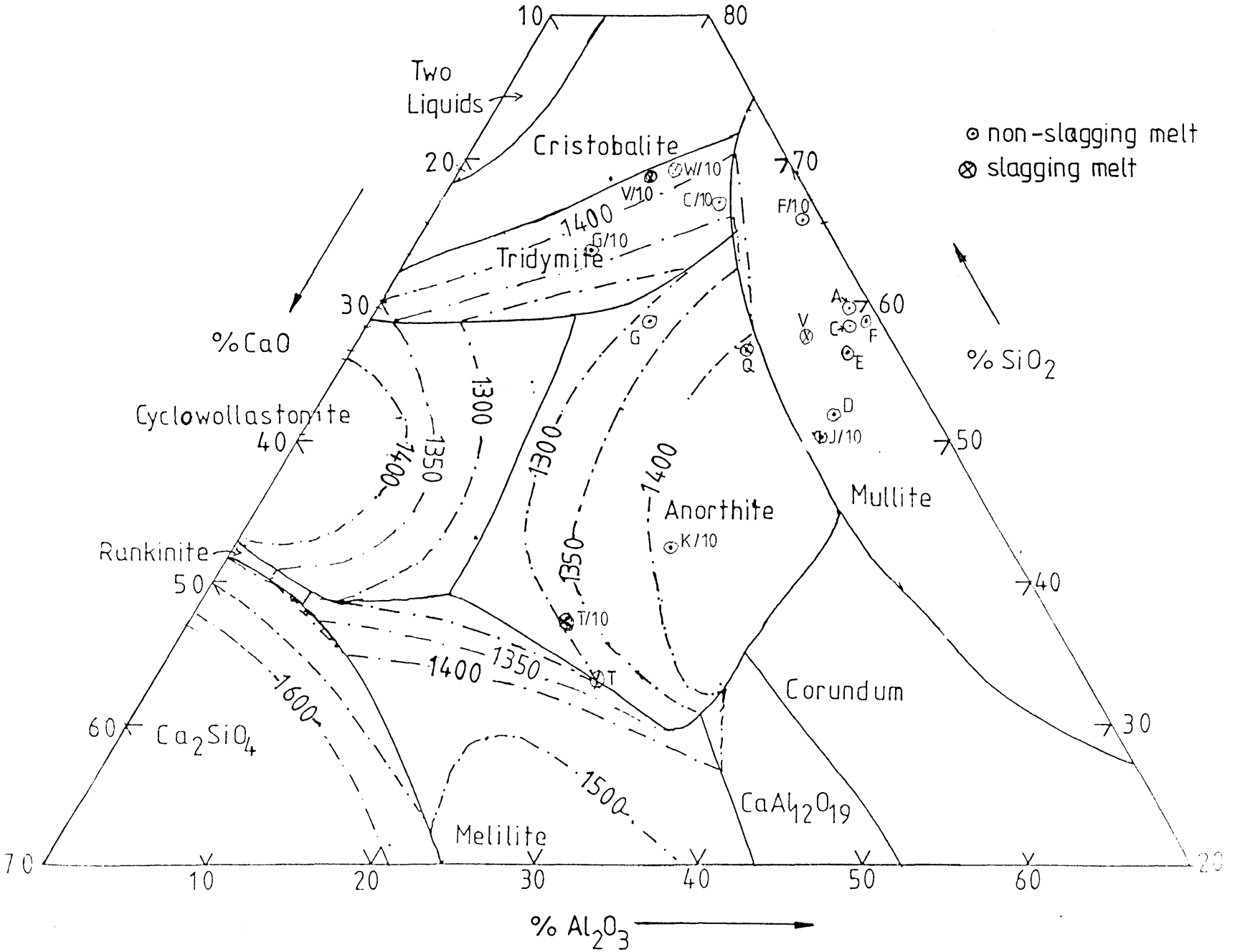


Fig.5.40. System $CaO-FeO-Al_2O_3-SiO_2$, 15% FeO plane. Crystallisation of slagging & non-slagging melts.

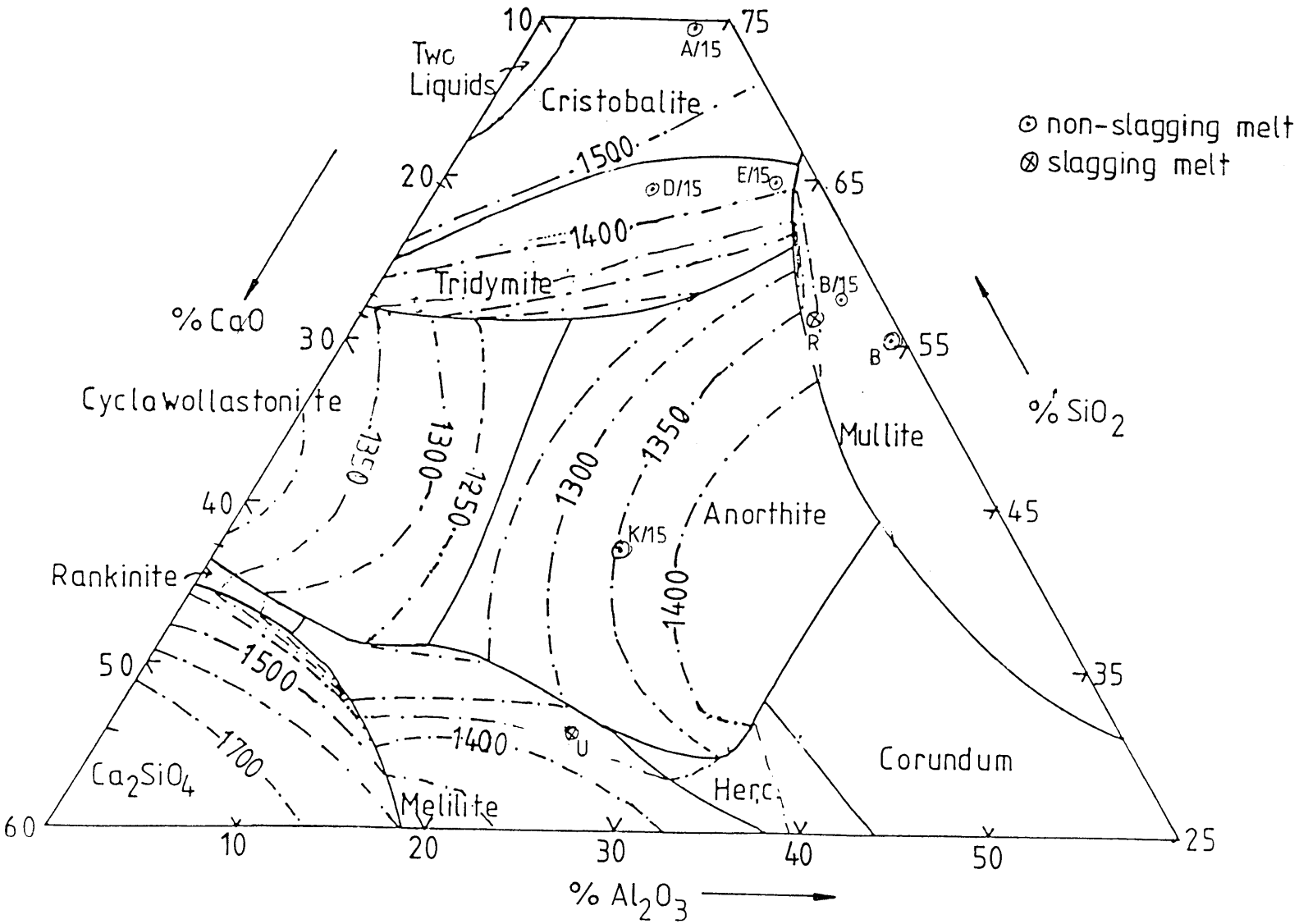


Fig. 5.41. System $CaO-FeO-Al_2O_3-SiO_2$, 20% FeO plane. Crystallisation of slagging & non-slagging melts.

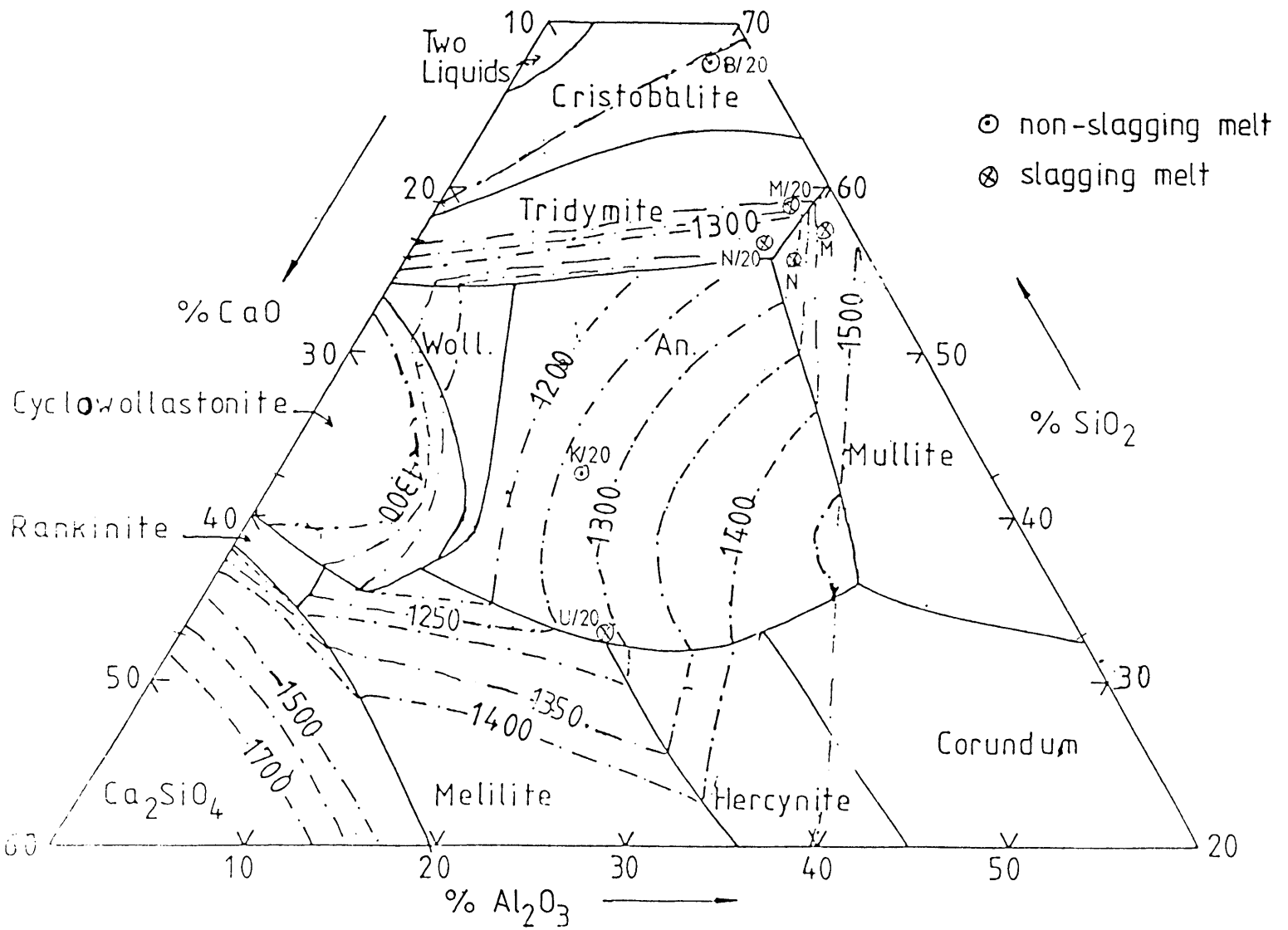


Fig. 5.42. System $CaO-FeO-Al_2O_3-SiO_2$, 25% FeO plane. Crystallisation of slagging & non-slagging melts

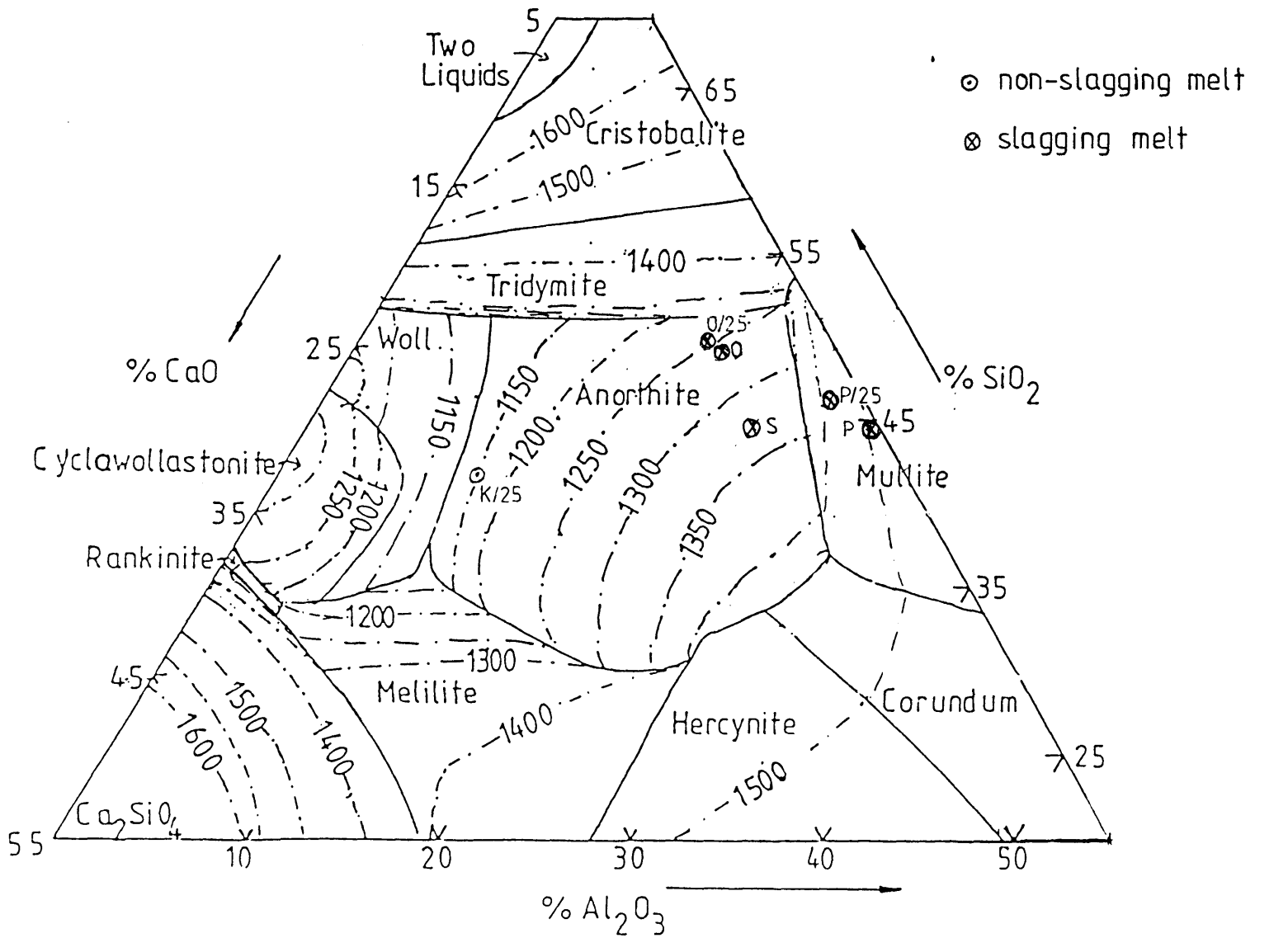
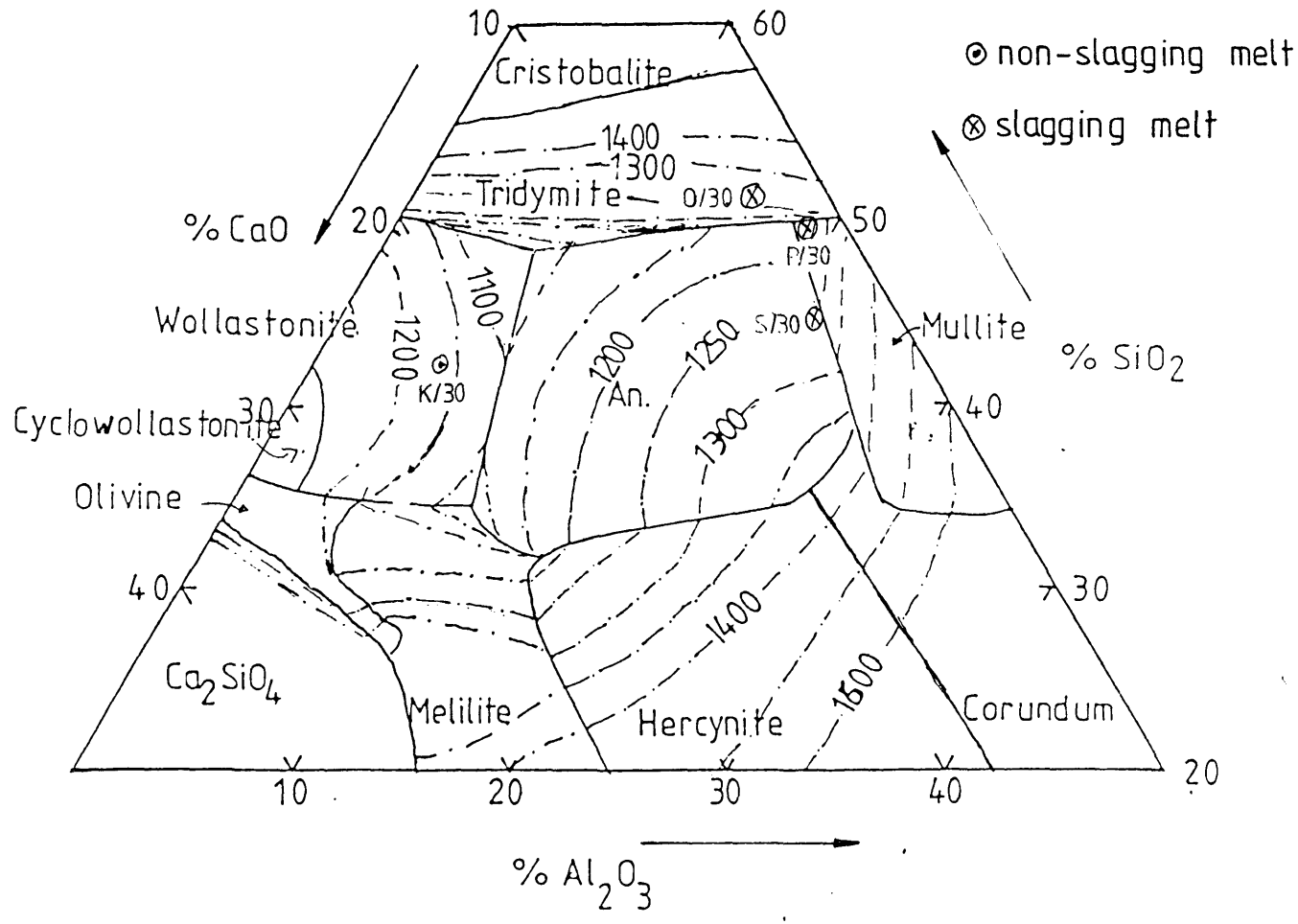


Fig.5.43. System $CaO-FeO-Al_2O_3-SiO_2$, 30% FeO plane. Crystallisation of slagging & non slagging melts.



Fe_2O_3) leading to a reduced viscosity, despite the high silica content. The lower liquidus temperature than the corresponding non-slagging ashes would indicate a greater amount of a liquid phase at a given temperature for the slagging ashes which would increase the amount of viscous flow. The slagging ashes O and S both lie in the anorthite field and while their crystallisation paths are towards the tridymite and mullite fields respectively, the high iron oxide content would be expected to lower the viscosity of the residual liquid phase which would account for the observed slagging behaviour. The EPRI[44] study reported that the normal slagging factors (see Table 2.9) predicted moderate slagging propensity for ashes M and N yet the analysis of the phase equilibria data and the effect of high iron oxide content on viscosity would indicate slagging behaviour, as observed.

Ash Q presents something of a problem. Analysis of the data would not suggest an ash which would give a troublesome slag. The relatively high liquidus temperature and a crystallisation path towards the tridymite boundary, and the low iron oxide content would not indicate slagging problems. It is known that the same coal when burnt in a boiler of different design does not cause slagging problems and this is a clear indication of yet another variable, i.e. the design of the boiler. Further analysis of this feature is outside the scope of the present thesis, but indicates an important area which needs further consideration.

The lignitic-type ash T lies on the anorthite melilite boundary. The composition has a relatively low liquidus temperature and the residual liquid phase would be expected to be fluid at temperatures at which slagging deposits form. With reference to

the complete chemical composition the presence of 7.1% MgO and 7.6% Na_2O would also cause both the ash melt and the residual liquid phase to be quite fluid and thus slagging problems would be predicted.

The liquidus temperature of ash U which lies in the melilite primary field is relatively high but with crystallisation of melilite the residual liquid phase will become quite fluid. The original composition contains a significant amount of Na_2O and MgO and FeO contents which would all reduce the viscosity of the residual liquid phase still further, leading to slagging problems.

The ash V lies in the primary crystalline field of mullite and has a relatively high liquidus temperature. The crystallisation path is similar to non-slagging coals, i.e. towards the tridymite boundary. Wibberly et al[111] have reported serious fouling problems for this lignitic-type ash which would be expected from the sodium oxide content and relatively high iron oxide levels. The authors proposed the formation of a sticky sodium silicate layer on the fly ash particles from the condensation of the alkali onto the surface as the cause of the growth of deposits. If the ash completely fused to a homogeneous melt, an assumption inherent in this study, the subsequent crystallisation of mullite would result in a silica and sodium oxide rich residual liquid phase which would account for the observations.

Thus in conclusion the analysis of the liquidus temperature data, crystallisation path of the normalised composition of a coal ash along with a knowledge of the viscosity of ash melts may be combined to give a clear indication of slagging propensity. An important observation is that the minor components such as the

alkali oxides and magnesia contents should be taken into consideration when determining the liquidus temperature, the viscosity of the residual liquid phase and hence the slagging propensity.

The proposed method to predict the slagging propensity of a coal ash can be summarised as a series of steps:

1) Composition of coal ash.
2) Conversion of Fe_2O_3 to equivalent FeO.
3) Normalisation of composition to four components CaO-FeO-Al_2O_3-SiO_2.
4) Selection of appropriate plane of quaternary system.
5) Determination of primary phase and estimation of liquidus temperature.
6) Calculation of compositions of residual liquid phases to determine the crystallisation path.

From the results, the observations of known slagging and non-slagging ash melt behaviour, and a knowledge of coal ash viscosity (as detailed in Appendix C) a prediction of slagging propensity may be obtained.

This method provides an entirely new approach towards the problems of predicting the slagging propensity of a coal ash. Previous methods, as discussed in the literature survey, were based on arbitrary or empirical derived relationships. These methods, though extensively used by both boiler designers and operators are known to give, in some circumstances, wrong or misleading indications resulting in costly boiler cleaning operations. Unlike previous studies this investigation has dealt with the thermodynamic behaviour of melts which enable the changes of state of an ash melt

to be reliably predicted. The laboratory study has included the extensive investigation of the crystallisation of synthetic ash melts under conditions approaching equilibrium. Compositions have covered both lignitic and bituminous-type ashes and kinetic factors such as fusion of a lignitic-type ash and crystal growth rates in synthetic ash melts have been studied. Both the phase equilibria studies and the experimental observations correlate extremely well with the observed mineralogy and microstructure of field samples.

The proposed method will be valuable to both designers and operators of p.f. boilers. The approach predicts the type of deposit (if any) which will be formed and to some extent the mechanical properties. This knowledge may enable the suitability of a coal for firing to be assessed and/or the operating requirements for reduction of deposit formation (e.g. the predicted effectiveness of soot blowing). The designers of a p.f. boiler may be able to use the predictions of the quaternary system as a guide to the maximum coal feed rates and hence temperatures which may be obtained in the boiler. At present the major parameters used are the ash fusion temperatures of a mean coal (calculated from the range of coals to be fired). The new method can make a detailed assessment of each of the coals to be fired and hence limiting values of design parameters can be determined.

CHAPTER 6

CONCLUSIONS AND SUGGESTIONS FOR FURTHER WORK

6.1 CONCLUSIONS

High-temperature microscopy of low-temperature coal ashes has shown that the fusion process commences at lower temperatures than that indicated by standard predictive techniques. A study of the fusion of a lignitic-type ash using a quenching technique has shown that the formation of liquid silicates and the precipitation of crystalline phases occurs simultaneously at 1450°C, while at 1550°C no formation of devitrification products was observed. Quartz was determined to be the only original coal mineral present in the treated samples. The rapid devitrification of the coal ash melt has been confirmed by a study of crystal growth rates of glasses with compositions similar to those of the ashes used in the fusion experiments. The study of the crystallisation of coal ash melts has been shown to involve the precipitation of phases comprising only the major components present in the melt (i.e. SiO_2, Al_2O_3, CaO and FeO).

Deposition of liquid silicate melts within the radiation and convection zones of a coal-fired boiler may be followed by crystallisation of the deposit, leaving a vitreous or semi-vitreous mass which may significantly reduce the thermal efficiency of the boiler. The results of the reactions of coal ash melts and a study of the high temperature phase equilibria of the systems CaO-MgO-Al_2O_3-SiO_2 and CaO-Al_2O_3-SiO_2-iron oxide, in a reducing atmosphere have shown that a

valuable technique to predict the phase assemblage of crystalline and vitreous phases within a deposit may be developed. The increase in strength of a boiler deposit is mainly due to sintering by viscous flow and hence the rate at which this occurs will be dependent primarily on the viscosity of the liquid phase. This model has been used as the basis of a new method to predict the slagging propensity of a coal ash from relevant phase equilibria data (predominantly that of the system $CaO-FeO-Al_2O_3-SiO_2$). The phase assemblages predicted by this technique have been compared with field samples of boiler deposits and found to agree extremely well. The method has been extended to the prediction of slagging propensity, from the coal ash composition, of various coal ashes and compared with the known behaviour of the ash within the boiler. Again the predicted behaviour agrees well with published data and reports from various utilities.

This approach will provide boiler designers and operators with an entirely new technique to estimate the likely slagging potential of a coal and represents a significant advance on the empirical assessments used at present.

6.2 SUGGESTIONS FOR FURTHER WORK

This study has involved predominantly the investigation and prediction of the phase assemblage of boiler deposits. An important factor in the efficiency of a coal-fired boiler is the nature of the deposit. The microstructure of a deposit would be expected to affect significantlythe heat transfer and the susceptibility of the deposit to physical/thermal shock

from soot/steam blowers. The design of a boiler and hence its geometry is also known to be a factor in the slagging behaviour of some coal ashes.

An investigation of the microstructure of boiler deposits and the relationship between boiler geometry and slagging behaviour would be expected to give further valuable insight into the behaviour of an ash. Such a study would be aimed at optimising the design of a boiler to obtain the most efficient operation of coal-fired utilities.

APPENDIX A

Components used for preparation of glasses

Component	Supplier, reagent	Grade	Drying temp/°C
SiO_2	Hi-Temp Materials Angolan crushed quartz	-	1000
Al_2O_3	BDH, Al_2O_3	Analar	1000
CaO	BDH, $CaCO_3$	Analar	150
MgO	BDH, MgO	Analar	1100
Fe_2O_3	BDH, Fe_2O_3	General purpose	not dried
FeO	BDH, $FeC_2O_4.2H_2O$	General purpose	not dried
Na_2O	BDH, Na_2CO_3	General purpose	not dried
K_2O	BDH, K_2CO_3	General purpose	not dried
TiO_2	BDH, TiO_2	General purpose	1000

APPENDIX B

Determination of oxygen partial pressure for an initial gas mixture of hydrogen and carbon dioxide

The equilibrium constant (K) for the water-gas reaction:

$$H_2 + CO_2 \overset{K}{\rightleftharpoons} CO + H_2O$$

may be expressed as

$$K = \frac{p_{H_2O}}{p_{H_2}} \cdot \frac{p_{CO}}{p_{CO_2}}$$

For an initial mixture of hydrogen and carbon dioxide the species present at equilibrium will be H_2, CO_2 CO and H_2O.

Therefore from the material balance

$$\frac{(p_{CO_2})_i}{(p_{H_2})_i} = \frac{p_{CO_2} + p_{CO}}{p_{H_2O} + p_{H_2}}$$

(i indicates initial quantities)

rearranging

$$\frac{(p_{CO_2})_i}{(p_{H_2})_i} = \frac{p_{CO_2}}{p_{H_2O}} \cdot \frac{(p_{CO}/p_{CO_2} + 1)}{(p_{H_2}/p_{H_2O} + 1)}$$

as $$\frac{p_{H_2}}{p_{H_2O}} = \frac{1}{K} \frac{p_{CO}}{p_{CO_2}}$$

and substituting

$$\frac{(p_{CO_2})_i}{(p_{H_2})_i} = \frac{p_{CO_2}}{p_{H_2O}} \cdot \frac{(p_{CO}/p_{CO_2} + 1)}{(p_{CO}/p_{CO_2}.1/K + 1)}$$

$$= \frac{p_{CO_2}}{p_{H_2O}} \cdot \frac{(1 + p_{CO_2}/p_{CO})}{(1/K + p_{CO_2}/p_{CO})}$$

from the reaction $p_{H_2} = p_{CO}$

$$\therefore \frac{(p_{CO_2})_i}{(p_{H_2})_i} = \frac{p_{CO_2}}{p_{CO}} \cdot \frac{(1 + p_{CO_2}/p_{CO})}{(1/K + p_{CO_2}/p_{CO})}$$

for an initial ratio 1:1

$$1 = \frac{p_{CO_2}}{p_{CO}} \cdot \frac{(1 + p_{CO_2}/p_{CO})}{(1/K + p_{CO_2}/p_{CO})}$$

rearranging

$$(1/K + p_{CO_2}/p_{CO}) = p_{CO_2}/p_{CO} \cdot (p_{CO_2}/p_{CO} + 1)$$

$$(1/K + p_{CO_2}/p_{CO}) = (p_{CO_2}/p_{CO})^2 + p_{CO_2}/p_{CO}$$

$$\therefore 1/K = (p_{CO_2}/p_{CO})^2$$

The oxygen partial pressure can be determined from the equilibrium constant for the reaction

$$2CO + O_2 \overset{K_1}{\rightleftharpoons} 2CO_2$$

where $K_1 = \dfrac{(p_{CO_2})^2}{(p_{O_2})(p_{CO})^2}$

$\therefore \quad K_1 \cdot p_{O_2} = \left(\dfrac{p_{CO_2}}{p_{CO}}\right)^2$

as $\quad 1/K = (p_{CO_2}/p_{CO})^2$

thus $1/K = p_{O_2} \cdot K_1$

and

$$p_{O_2} = 1/K.K_1$$

Thus the value of the oxygen partial pressure at a given temperature or an initial mixture of CO_2 and H_2 in the ratio of 1:1 will be dependent on the values of K and K_1. The partial pressure of oxygen has been plotted against temperature in Fig. B.1 for the ratio of CO_2:H_2O of 1:1.

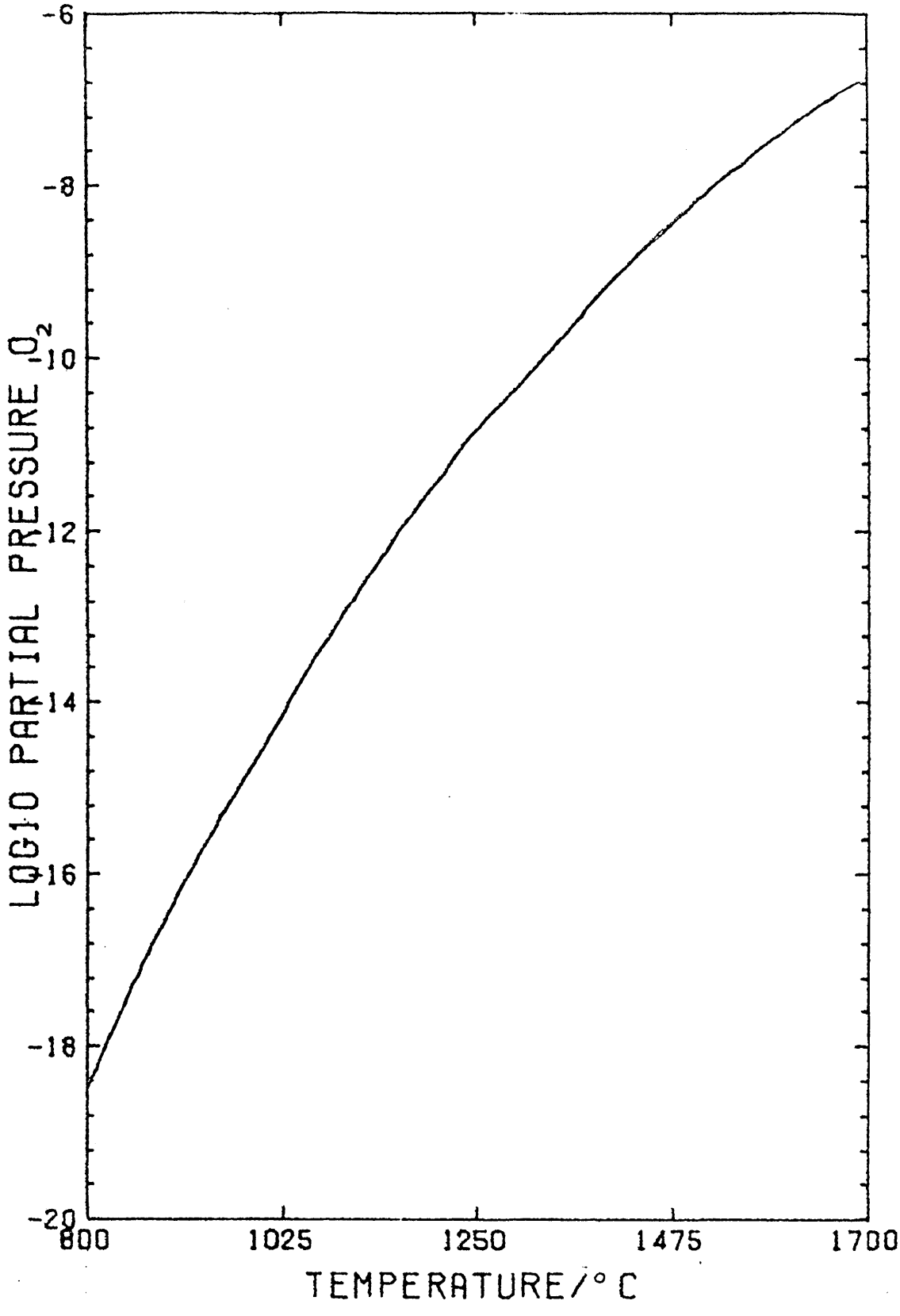


Fig.B. Graph of log partial pressure oxygen vs. temperature for an initial gas mixture of H_2 and CO_2 (ratio 1:1 by volume). From the data of Muan and Osborn.[112]

APPENDIX C

Viscosity of coal-ash melts

The viscosity of a coal ash melt and its variation with temperature has been shown in the text to be of great importance to the slagging behaviour of coal ashes. It is intended here to discuss succinctly the rheological behaviour of coal ash melts, both homogeneous and residual liquid phases.

Coal ash viscometry has been rarely undertaken and empirical relationships have been developed by a number of investigators notably Watt and Fereday,[52] and Nichols and Reid.[60] The relation derived by Watt and Fereday has been extensively used by fuel technologists. The method is based on the four major ash components (SiO_2, Al_2O_3, CaO, Fe_2O_3) and is only valid over certain compositional limits (given in Table C.1).

A method has recently been developed by Urbain et al.[101a] based on the theory of glass formation (i.e. the role of the component oxides as network formers, modifiers or intermediates). The relationship was determined from silicate melts of a wide range of compositions (geological samples) and thus may be of greater value than the Watt-Fereday method.

The $\log_{10}$ viscosity temperature curves for three ash melts have been determined using the two relationships discussed above and compared with the measured values for the three ash melts. The curves obtained for each melt are illustrated in Fig. C.1. The compositions of the melts (designated A, B and C) are listed in Table C.2. Melts A and B are lignitic-type compositions, the former is that of a coal ash (similar to

TABLE C.1

Compositional range for Watt-Fereday viscosity calculations

Component	Range Minimum wt %	Maximum wt %
SiO_2	30	60
Al_2O_3	15	35
Fe_2O_3	3	30
CaO	2	30
MgO	1	10

TABLE C.2

Composition wt%	Melt A	B	C
SiO_2	46.0	47.6	59.5
Al_2O_3	27.0	30.0	24.7
Fe_2O_3	3.5	5.2	6.8
CaO	9.3	10.6	3.8
MgO	3.1	2.5	1.4
Na_2O	0.7	0.5	0.6
K_2O	0.7	0.6	2.2
TiO_2	1.6	1.8	1.0
P_2O_5	1.1	0.9	n.d.
SO_3	7.0	0.3	n.d.
	100.0	100.0	100.0

Matla ashes KA, KC and KD) whereas B is that of a deposit formed from the ash A. The viscosity behaviour of the melts were determined for Babcock Power Ltd. Melt C is that of a bituminous-type ash and the viscosity-temperature curve was determined by Gibb.[102] The inflexions in the measured curve may be experimental error or indicate an effect due to crystallisation.

With reference to Fig. C.1 the curves calculated from the method of Urbain et al. fit the measured curves remarkably well and better than the corresponding Watt-Fereday calculations. For the lignitic-type melts the Watt-Fereday values are an order of magnitude greater than the measured viscosity. The two calculated curves for the bituminous melt B were similar and matched the measured behaviour reasonably closely.

Thus the method developed by Urbain et al. appears to predict, with remarkable accuracy, the viscosity temperature behaviour of a coal ash melt. Though the compositional limits of the method have not been investigated fully it would be expected that the relationship would be valid over a greater range than the Watt-Fereday method. The method will not be detailed here as it is clearly described in the original paper. The technique is designed for calculation by computer and the total chemical composition (excluding sulphate SO_3) is used in the calculation. The authors indicated that both the FeO and Fe_2O_3 contents should be used (values from chemical analysis) for the iron oxide content. The validity of this operation is questionable as the relative values of the FeO and Fe_2O_3 will vary considerably with temperature and will

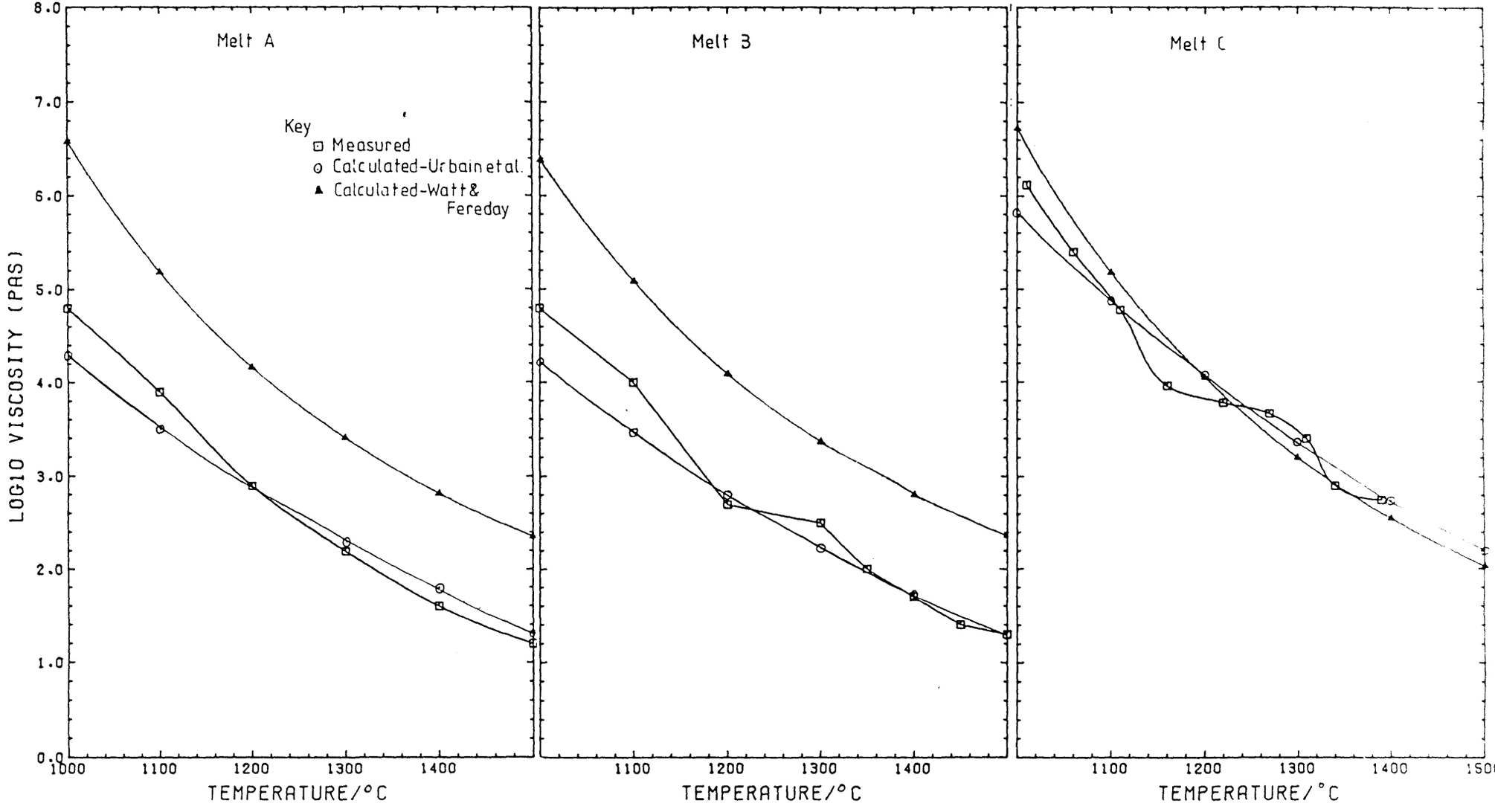


Fig. C1. Viscosity-temperature curves for three ash melts. Comparison of methods of calculating viscosity.

not be the same as the original sample. The present writer observed that the best match with the measured curve was obtained from assuming that all the iron oxide was present as Fe_2O_3. This may not be the case for higher (greater than 15%) iron oxide contents.

Both methods for calculating viscosity are only valid for melts which do not exhibit non-Newtonian flow. The results of the present study have shown that significant crystallisation can take place in the ash melt. The experimental techniques for evaluating ash melt viscosity can generally be described as the measure of the drag of the melt on an object. The results are those of the bulk viscosity and do not indicate the flow properties residual liquid phase. In the model of deposit growth the value of viscosity (η) indicated is that of the liquid phase involved in the sintering mechanism by viscous flow. Thus though the bulk viscosity-temperature relationship is of value the viscosity of the liquid phase at a given temperature will be the major factor in the increase in strength of a boiler deposit.

The Urbain et al. method has been used to calculate the viscosity of the residual liquid phase for two ash compositions after crystallisation has taken place (specifically 5, 10, 15 and 20% of the primary phase). Composition 1 is that of a coal ash from Frickley, U.K. field and lies in the mullite field whereas composition 2 is that of a composition chosen to have the same iron oxide and alkali oxide contents as 1 but to lie in the anorthite field. The compositions of the residual liquid phases with crystallisation of the primary

phases for both examples have been listed in Table C.3. The compositions were then used to determine the viscosity of the liquid phase at a given temperature (1100°C, 1200°C, 1300°C and 1400°C). The $\log_{10}$ viscosity values for each composition have been plotted against % crystallisation in Fig. C2.

As can be seen the viscosity of the residual liquid phase for composition 1 increases at a given temperature with crystallisation of mullite. With reference to Table C3 the silica content increases with crystallisation of mullite, and though the percentage of fluxing agents (e.g. CaO, Na_2O) also increases, the higher silica content would be expected to dominate and lead to an increase in the viscosity. An important note to make is that melts with a viscosity greater than 10^3 Pas are usually glassy and stable towards devitrification. A viscosity of 10^5 Pas is known to be the limit at which sintering by viscous flow occurs. The coal ash corresponding to composition 1 is known not to form slagging problems which would be expected from the crystallisation behaviour. The viscosity of the residual liquid phase at a given temperature for composition 2 decreases with crystallisation of anorthite. With reference to Table C.3 the relative contents of silica and alumina decrease whereas those of lime, iron oxide and alkali oxides increase with crystallisation. The residual liquid phase is relatively fluid at all the temperatures indicated and the composition would be expected to cause slagging problems.

Therefore from the crystallisation path of a normalised composition indicated by the composition of the residual liquid

TABLE C.3

Composition 1.

Component[+]	% Crystallisation of Mullite 0	5	10	15	20
SiO_2	50.4	51.6	52.9	54.4	56.0
Al_2O_3	31.0	28.8	26.4	23.7	20.7
Fe_2O_3	10.6	11.2	11.8	12.5	13.3
CaO	5.8	6.1	6.4	6.8	7.2
Na_2O	0.7	0.7	0.8	0.8	0.9
K_2O	1.5	1.6	1.7	1.7	1.9
	100.0	100.0	100.0	100.0	100.0

Composition 2

Component	% Crystallisation of Anorthite 0	5	10	15	20
SiO_2	35.4	34.9	34.5	34.0	33.5
Al_2O_3	21.0	20.2	19.2	18.2	17.0
Fe_2O_3	10.6	11.2	11.8	12.5	13.3
CaO	30.8	31.4	32.0	32.7	33.5
Na_2O	0.7	0.7	0.8	0.8	0.9
K_2O	1.5	1.6	1.7	1.8	1.8
	100.0	100.0	100.0	100.0	100.0

[+]MgO and TiO_2 contents not determined.

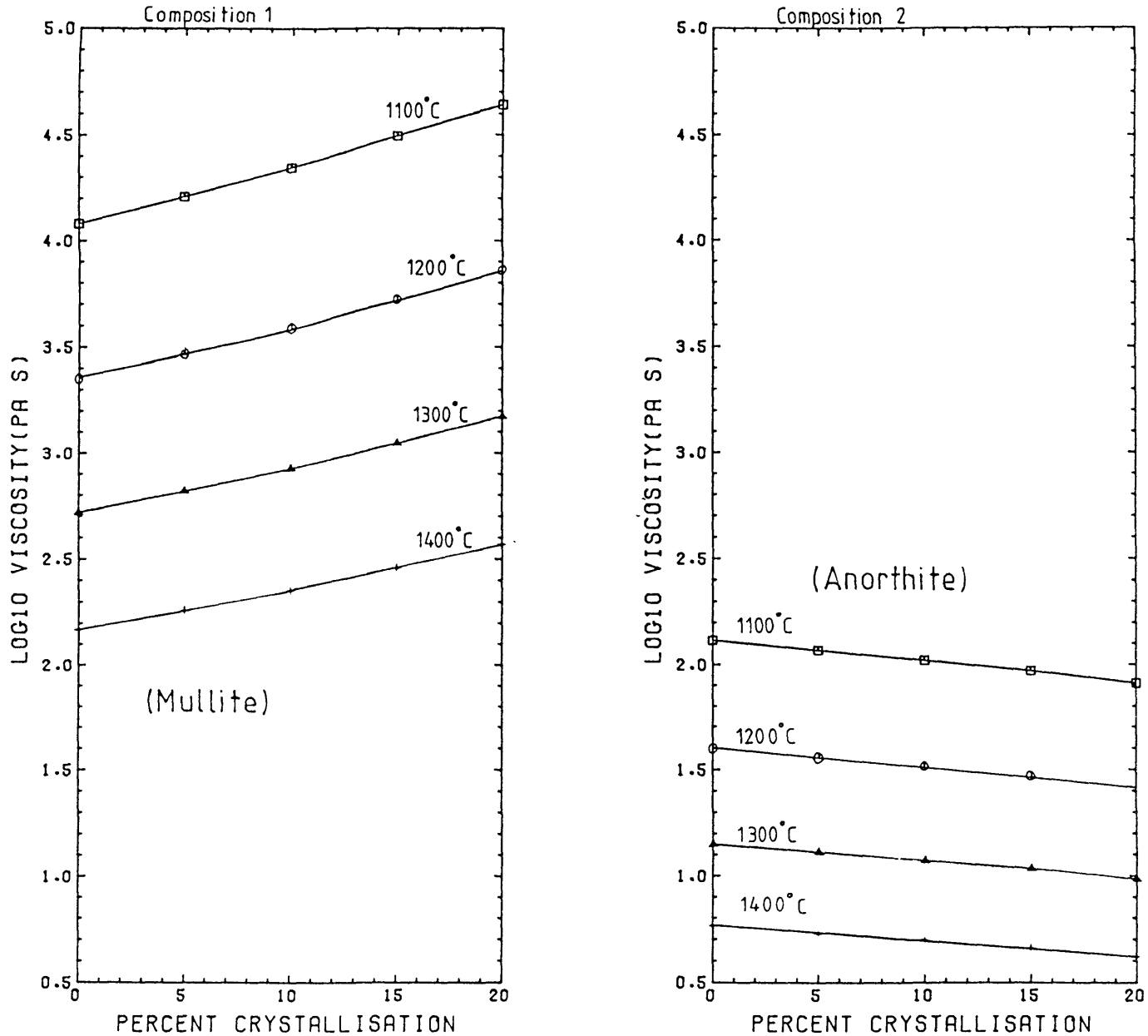


Fig C 2. Viscosity of residual liquid phase for two compositions with crystallisation at various temperatures.

phase an indication of the viscosity of the liquid can be obtained from the method of Urbain et al.. Generally if the residual liquid phase becomes enriched in silica the viscosity will increase and vice versa. Though the effect of high iron oxide contents on the viscosity have not been investigated it is known that the coal ashes with high iron oxide contents (greater than 20%) generally do cause slagging problems due presumably to the fluidity of the residual liquid phase.
In assessing the slagging propensity and in particular the viscosity of the liquid phase the total chemical composition should be taken into account. For example, the ash U (main text) contained 10.5% Na_2O which though not included in the normalised composition would cause the ash melt and residual liquid phase to be significantly fluid at elevated temperatures.

REFERENCES

1. P.J. Jackson, private communication.

2. C.L. Wilson, Ed., "Coal - Bridge to the Future", Ballinger, 1980 p.242.

3. W.T. Reid, "Chemistry of coal utilization", 2nd supp. vol. Ed. M.A. Elliot, 2nd Supp. Vol., John Wiley & Sons, 1981, Ch.21.

4. Babcock and Wilcox, "Steam - its generation and use" 38th Ed. various chapters.

5. A. Sanyal, Babcock Power Ltd., private communication.

6. M.F.R. Mulcahy, J. Boow and P.R.C. Goard, "Fireside deposits and their effect on heat transfer in a pulverised-fuel-fired boiler, Pt.I: The thermal radiance emittance and effective thermal conductance of the deposits" J. Inst. Fuel, 37, 1966, pp.385-94.

7. Chemical Rubber Co. "Handbook of Chemistry and Physics", 60th Ed., Table F9-8.

8. A. Sanyal & C.R. Coleman, "The control of slagging in coal fired utility furnaces: A case history of the use of copper oxychloride as a fireside additive", ASME paper 82-JPGC-Fu-1. (1982).

9. R. Lessing, "Studies in the distribution of mineral matter in coal". Trans IME, 60, 1921, pp.288-309.

10. H.J. Glubskoter, "Ash deposits and corrosion due to impurities in combustion gases" Ed. R.W. Bryers, Hemisphere, 1978, pp.3-20.

11. C.P. Rao & H.J. Gluskoter, "Occurrence and distribution of minerals in Illinois coals". Illinois State Geological Survey Circular 476, 56pp.

12. British Standard 1016, Pt.14, 1963. "Methods for the analysis and testing of coal and coke, analysis of coal ash and coke ash" pp.34.

13. R.N. Miller, R.F. Yarzab & P.H. Given, "Determination of the mineral matter contents of coal by low-temperature ashing" Fuel, 58, 1978, pp.4-11.

14. H.J. Gluskoter, "Electronic low-temperature ashing of bituminous coal". Fuel, 44, 1965, pp.285-91.

15. J.V. O'Gorman & P.L. Walker, Jnr., "Thermal behaviour of mineral fractions separated from selected American coals". Fuel, 52,1973, pp.71-9.

16. P.A. Estep, J.J. Kovach & C. Karr, Jnr., "Quantitative infra-red multicomponent determination of minerals occurring in coal". Anal. Chem., 40, 1968, pp.358-63.

17. R.R. Dutcher, E.W. White & W. Spackman, "Elemental ash distribution in coal components - use of the electron probe" Proc. 22nd Iron making Conf., Iron and Steel Div., Metallurgical Soc., American Inst. of Mining Engineers, N.Y., 1964, pp.463-83.

18. H.J. Gluskoter & R.R. Duch, "Iron sulfide minerals in Illinois coals". Geological Society of America, 3(7), 1971, p.582.

19. F.E. Huggins, D.A. Kosmack, G.P. huffman & R.J. Lee. "Coal Mineralogies by SEM Automatic Image Analysis". S.E.M., 1, 1980, p.531-

20. J.D. Watt, "The physical and chemical behaviour of the mineral matter in coal under the conditions met in combustion plant. Pt. II; 1969.

B.C.U.R.A. Lit. Survey.

21. G.M. Schwab & J. Philinis, "Reactions of iron pyrite: Its thermal decomposition, reduction by hydrogen and air oxidation". J. Am. Chem. Soc., 69, 1947, pp.2589-98.

22. D. Flint & A.J. Copson, B.C.U.R.A., see 20.

23. P. Murray & H.C. Fischer, Trans. Am. Soc. Test. Mat., 51, 1951, p.1197.

24. T.L. Webb & H. Heystek, "The Carbonate Minerals", 1957.

25. H. Lehmann & K.H. Muller, "Differentialthermoanalyse von Dolomit im Vakuum und bei normalem Luftdruck". Tonind-Ztg.u.Keram; 84, 1960, pp.200-1.

26. H.E. Powell, U.S. Bur. Mines, R.I., 6643, 1965. "Thermal decomposition of sederite and consequential reaction" pp.33.

27. J.L. Kulp, P. Kent & P.F. Kerr, "Thermal study of the Ca-Mg-Fe carbonate minerals". Am. Min., 36, 1951, pp.643-70.

28. G. Kohn, "Reactions in the solid state" Chem. Rev., 42, 1948, pp.527-79.

29. M.E. Pozin & A.M. Ginstling, J. App. Chem. (U.S.S.R.), 1951, p.37. Consult. Bur. Chem. Coll. No.2, Basic Sci. I, pp.111-22.

30. W.D. Kingery, H.K. Bowen & D.R. Uhlmann, "Introduction to Ceramics", 2nd Ed., Wiley, 1976, p.492.

31. J.D. Watt & D.M. Wikins, B.C.U.R.A, I.C. No.319, 1967.

32. R.S. Mitchell & H.J. Gluskoter, "Mineraology of ash of some American coals: Variations with temperature and source" Fuel, 55, 1976, pp.90-6.

33. A.S. Padia, "The behaviour of ash in pulverised coal under simulated combustion conditions" D.Sc. Thesis, M.I.T., 1976.

34. A.R. Cooper, Jnr., "Dissolution kinetics in glass making". Advances in Glass Technology, Vol. I, Plenum Press, New York, 1962, pp.215-30.

35. H.E. Crossley, Report of the Pulverised Fuel Conference (1968) 1, p.322.

36. J.H. Carlile, "Boiler availability: Some factors affecting the formation of deposits on the external heating surfaces of coal-fired boilers". J. Inst. Fuel, 25, 1952, pp.252-60.

37. H.E. Crossley, "A special study of ash and clinker in industry, 4: External boiler deposits", J. Inst. Fuel, 25, 1952, pp.221-5.

38. P.J. Jackson & J.M. Ward, "Relationship between coal constituents and boiler fouling". J. Inst. Fuel, 29, 1956, pp.154-64.

39. D. Ounsted & J. Schoen, "The release of sodium aerosols during the combustion of pulverised coal: A laboratory investigation". J. Inst. Fuel, 33, 1960, pp.199-206.

40. P.H. Crumley, A.W. Fletcher & D.S. Wilson, "The formation of bonded deposits in pulverised-fuel-fired boilers", J. Inst. Fuel, 28, 1955, pp.117-20.

41. J.D. Watt, "Coal-ash slags Pt. I: Formation and mineralogy", B.C.U.R.A., Mon. Bull., 23, 1959, pp.49-70.

42. A. Hanusch & R. Grimshaw, "Matla slags" Univ. Leeds Report to Babcock Power Ltd., 1981.

43. A. Hanusch & R. Grimshaw, "Matla slags - 2nd series" Univ. Leeds Report to Babcock Power Ltd., 1981.

44. Electric Power Research Institute "Influence of coal mineral matter on slagging of utility boilers". Report 736, 1981.

45. F.D. Friedrich, G.K. Lee & E.R. Mitchell, "Combustion and fouling characteristics of two Canadian lignites" J. Eng. Power, 94, 1972, pp.127-32.

46. W.R. Livingston, A. Sanyal & J. Williamson, "The role of copper oxychloride to alleviate slagging in coal fired boilers." The Effectiveness of Fuel Additives, Conf., Leatherhead, Surrey, Oct. 1983.

47. E.J. D. Smith, "The sintering of fly-ash", J. Inst. Fuel, 29, 1956, pp.253-60.

48. E. Raask. "Flame imprinted characteristics of ash relevant to boiler slagging, corrosion, and erosion", J. Eng. Power, 104, 1982, pp.858-66.

49. A.K. Moza & L.G. Austin, "Studies on slag deposit formation in pulverised coal combustors. 1. Results on the wetting and adherence of synthetic coal ash drops on steel." Fuel, 60, 1981, pp.1057-64.

50. R.J. Lauf, "Cenospheres in fly ash and conditions favouring their formation". Fuel, 60, 1981, pp.1177-79.

51. J.D. Watt & F. Fereday, "The flow properties of slags formed from the ashes of British Coals. Pt. I. Viscosity of homogeneous slags in relation to slag composition". J. Inst. Fuel, 42, 1969, pp.99-103.

52. W.T. Reid, Method given in ref. 44 p.D-1-4.

53. British Standard 1016, Pt.15. 1970. "Methods for the analysis of coal and coke. Fusibility of coal ash and coke ash", p.14.

54. American Society for Testing of Materials D.1857, 1968. "Standard method of test for fusibility of coal and coke ash", p.4.

55. E.G. Bailey & F.G. Ely, "Significance of coal-ash fusing temperatures in the light of recent furnace studies". Trans. A.S.M.E., 57, 1941, pp.465-77.

56. G.P. Huffman, F.E. Huggins & G.R. Dunmyre, "Investigation of the high temperature behaviour of coal ash in reducing and oxidising atmospheres". Fuel, 60, 1981, pp.585-97.

57. E.C. Winegartner, "Coal fouling and slagging parameters", A.S.M.E. Special Publication, 1974.

58. W.L. Sage & J.B. McIlroy, "Relationship of coal ash viscosity to chemical composition". J. Eng. Power, 82, 1960, pp.145-55.

59. R.C. Attig & A.F. Duzy, American Power Conference, 1967.

60. P. Nicholls & W.T. Reid, "Viscosity of coal ash slags", Trans. A.S.M.E., 56, 1940, pp.141-53.

61. W.T. Reid, "External corrosion and deposits: Boilers and gas turbines", Elsevier, 1971.

62. W.T. Reid & P. Cohen, "The flow characteristics of coal-ash slags in the solidification range". Trans. A.S.M.E., 66, 1944, pp.83-97.

63. H.R. Hoy, A.G. Roberts & D.M. Wikins. American Engineers Comm: 672, London, 1964.

64. W.H. Gibb, "The slagging and fouling characteristics of coals - I: Ash viscosity measurements for the determination of slagging propensity". Power. Ind. Res. 1, 1981, pp.29-42.

65. J.H. Welch, "A simple microscope attachment for observing high-temperature phenomena". J. Sci. Instrum., 31. 1954, pp.458-62.

66. F. Ordway, "Techniques for growing and mounting small single crystals of refractory compounds." J. Res. Nat. Bur. Stand. 48, 1952, p.48.

67. M.C.K. Jones, H. Farmer, J.E. Brewer & H.C. Porter "Observations of the micropyrometer and the gas furnace method for the determination of fusion point of coal ash". Ind. Eng. Chem. Anal. Ed., 2, 1930, pp.325-8.

68. H.S. Vasser, Proc. Am. Gas Ass. 1929, pp.1099-102.

69. J. Nolan, P.S. Rogers, A. Sanyal & J. Williamson, "A laboratory study of the thermal behaviour of coal minerals". Proc. 13th An. Meeting. Int. Metalog. Soc., Brighton, 1980, pp.99-108.

70. J.W. Cumming, "The electrical resistance of coal ash at elevated temperatures". J. Inst. Energy, 53, 1980, pp.153-4.

71. G. Thiessen, C.G. Ball & P.E. Grotts, "Coal ash and coal mineral matter". Ind. & Eng. Chem., 28, 1936, pp.355-61.

72. G.B. Gould & H.L. Brunjes, "Proportions of free fusible material in coal ash as an index of clinker and slag formation". Trans. A.I.M.E., 139 (COAL), 1940, pp.364-83.

73. T.G. Estep, H. Seltz, H. Bunker & H.S. Strickler, "The effect of mixing coals on the ash fusion temperature of the mixture". Carnegie Inst. of Tech., Mining and Metallurgical Investigations Co-op. Bull., 62, 1934, pp.7-48.

74. T.G. Estep, H. Seltz & W.J. Osborn, "Determination of the effects of oxides of sodium, calcium and magnesium on ash fusion temperatures by the use of synthetic coal ash." Carnegie Inst. of Tech., Mining and Metallurgical Investigations Co-op. Bull., 74, 1937, pp.1-15.

75. E.P. Barrett, "The fusion, flow and clinkering of coal ash. A survey of the chemical background." Chemistry of Coal Utilization, Ed. E. Lowry, Vol. 1, 1945, Ch.15, pp.496-576.

76. R. Rieke, Sprechsaal, 16, 1910, pp.229-32 cited in "A compilation of phase-rule diagrams of interest to the ceramist and silicate technologist". F.P. Hall & H. Insley, J. Am. Ceram. Soc., 16, 1933, pp.463-567.

77. E. Prost, "The relation between composition and fusibility in coal ashes." Colliery Guardian, 74, 1897, pp.602-3.

78. Nicholls & W.A. Selvig, U.S. Bur. Mines, Bull. 364. "Clinker formation as related to the fusibility of coal ash", p.71.

79. R.L. Schaefer & Demorest, see ref. 75, p.521.

80. D.J. Jones & E.C. Buller, "Analyses and softening temperatures of coal ash". Ind. & Eng. Chem. Anal. Ed., 8, 1936, pp.25-7.

81. B.K. Dutta, B. Rai & K.R. CHakravorty, "A study of the fusion characteristics of coal ashes: softening temperature of coal ashes in oxidizing atmosphere". J. Sci. & Ind. Res. 19b, 1966, pp.206-12.

82. B.K. Dutta. B. Rai. & K.R. Chakravorty, "A study of the fusion characteristics of coal ashes: softening temperature of coal ashes in mild reducing atmosphere". J. Sci. & Ind. Res., 21d, 1962, pp.44-8.

83. E.C. Winegartner & B.T. Rhodes, "An empirical study of the relation of chemical properties to ash fusion temperatures". J. Eng. Power, 97, 1975, pp.395-406.

84. See ref. 56.

85. F.E. Huggins, D.A. Kosmack & G.P. Huffman, "Correlation between ash-fusion temperatures and ternary phase diagrams". Fuel, 60, 1981, pp.577-97.

86. J.W. Gibbs, "On the equilibrium of heterogeneous substances". Trans. of the Conneticut Academy of Science, a series of papers between 1875-76.

87. G.A. Rankin & F.E. Wright, "The ternary system $CaO-Al_2O_3-SiO_2$." Am. J. Sci., 39, 1914, pp.1-73.

88. E.M. Levins, C.R. Robbins & H.F. McMurdie, "Phase Diagrams for Ceramists". Amer. Ceram. Soc., Columbus, Ohio, 1964.

89. A. Sanyal & J. Williamson, "Slagging in boiler furnaces: an assessment technique based on the thermal behaviours of coal minerals". J. Inst. Energy, 54, 1981, pp.158-62.

90. J.S. Machin & T.B. Yee, "Viscosity studies of the system $CaO-MgO-Al_2O_3-SiO_2$: II. $CaO-Al_2O_3-SiO_2$". J. Amer. Ceram. Soc., 31, 1948, pp.200-4.

91. J.W. Cahn,"On the morphological stability of growing crystals". Crystal Growth, Ed. H.S. Peiser, Pergamon Press, Oxford, 1967.

92. J.W. Christian, "The theory of transformations in metals and alloys". Pergamon Press, Oxford, 1967.

93. J. Williamson, A.J. Tipple & P.S. Rogers, "Influence of iron oxides on kinetics of crystal growth in $CaO-MgO-Al_2O_3-SiO_2$ glasses". J. Iron & Steel Inst., 206, 1968, pp.898-903.

94. J.H. Welch, "The system $CaO-MgO-Al_2O_3-SiO_2$: Phase equilibrium relationships along the join anorthite-spinel". J. Iron and Steel Inst., 183, 1956, pp.275-83.

95. J.C.P.D.S. - International Centre for Diffraction Data.

96. J.W. Cumming, private communication.

97. M.H. Hey, "Determination of ferrous iron in resistant silicates", Min. Mag. 26, 1941, pp 116-8.

98. A. Paul. "Chemistry of Glasses". Ch.5. pp.148-68; Chapman & Hall. 1982.

99. W.R. Livingston, private communication.

100. B. Keyworth. "Crystallisation phenomena in glasses containing chromium". Ph.D. Thesis, Univ. London, 1969.

101. H. Rawson, "Inorganic Glass-forming Systems". Academic Press, 1967, pp.35-7.

101a. G. Urbain, F. Cambier, M. Deletter & M.R. Anseau, "Viscosity of silicate melts". Trans. J. Br. Ceram. Soc., 80, 1981, pp.139-41.

102. W. Gibb, private communication to Babcock Power Ltd.

103. S. Pollman & W. Albrecht, "Investigations of the slagging behaviour of bituminous coals in large dry-bottom steam generators". Cont. Experimental Research into Fouling and Slagging resulting from Impurities in Combustion Gases, 1981, Henniker, New Hampshire, pp.85-9.

104. W. Gutt & A.D. Russell, "Studies of the system $CaO-SiO_2-Al_2O_3-MgO$ in relation to the stability of blast furnace slag". Jnl. Mat. Sci., 12, 1977, 1869-78.

105. G. Cavalier & M. Sandrea-Deudon, "Laitiers quaternaires $CaO-MgO-Al_2O_3-SiO_2$: Temperature de crystallisation commencante et champs de crystallisation surplans a magnesia constant". Rev. de Metallurgie, 57, 1960, pp.1143-57.

106. A.T. Prince, "Liquidus relationships on the 10% MgO plane of the system lime-magnesia-alumina-silica". J. Am. Ceram. Soc., 37, 1954, pp.402-9.

107. F. Rost & P. Ney, "Zur Kenntnis der Kesselschlaken." Brennstoff Chemie, 37, 1956, pp.201-10.

108. J.F. Schairer, "The system $CaO-FeO-Al_2O_3-SiO_2$: I Results of quenching experiments on five joins". J. Am. Ceram. Soc., 25, 1942, pp.241-74.

109. A. Muan & E.F. Osborn in "Phase Diagrams for Ceramists" (ref. 88) p.288.

110. L.T. Kiss, B. Lloyd & E. Raask, "The use of copper oxychloride to alleviate boiler slagging", J. Inst. Fuel. 45, 1972, pp.213-23.

111. L.J. Wibberley & T.F. Wall, "Alkali-ash reactions and deposit formation in pulverised-coal-fired boilers: The thermodynamic aspects involving silica sodium, sulphur and chlorine". Fuel, 60, 1982, pp.87-92.

112. A. Muan & E.F. Osborn, "Phase Equilibria among Oxides in Steelmaking", Addison Wesley, Reading, Mass., 1965, p.50.

ACKNOWLEDGEMENTS

The author would like to take this opportunity to thank the members of the Nuffield Research Group for their encouragement and assistance throughout this project. Great debt is owed to Dr. W.R. Livingston for his friendship and criticism. For the encouragement and help given by Dr. Sanyal and his colleagues at Babcock Power Ltd. (London) and staff at the Research Centre (Renfrew) for the preparation of coal ashes and other valuable data pertinent to this study, the author is greatly thankful. This study would not have been possible without the invaluable patience and guidance of my supervisor, Dr. J. Williamson. To my wife, Mary, I thank her for the love and support given to me throughout this project.

Finally, the author acknowledges the financial assistance given by Babcock Power Ltd. and the studentship awarded by the Science and Engineering Research Council.